Biofilm Formation of *Vibrio parahaemolyticus*

A thesis presented in partial fulfilment of the requirements for the degree of

Doctor of Philosophy

In

Food Microbiology

At Massey University, Campus Manawatū, New Zealand

Dan Wang

2024

Highlights

- *Vibrio parahaemolyticus* uses multiple pathways to form biofilms. These include UDP-glucose metabolism, cellulose biosynthesis, rhamnose metabolism, O antigen biosynthesis, CRISPR-Cas system and MSHA pilus-led attachment believed to contribute to robust biofilm formation in *V. parahaemolyticus*.
- Cellulose production is important for strong biofilm formation in *V. parahaemolyticus*. The cellulose synthase operon, consisting of *bcsG*, *bcsE*, *bcsQ*, *bcsA*, *bcsB*, *bcsZ*, *bcsC,* was present in 15.94% (22/138) of *V. parahaemolyticus*.
- Biofilm communities of strong biofilm-forming *V. parahaemolyticus* showed higher resistance to sodium hypochlorite and peroxyacetic acid than the weak biofilm formers. *V. parahaemolyticus* biofilms indicated ~75 times more resistant to sodium hypochlorite than planktonic counterparts, while ~4 times more resistant to PAA. PAA is an effective alternative to sodium hypochlorite when treating *V. parahaemolyticus* biofilms.
- RNA-seq and differential gene expression analysis revealed *V. parahaemolyticus* biofilm cells rearranged nucleotide and energy metabolism. Biosynthesis of secondary metabolites, purine and pyrimidine metabolism, propanoate metabolism, and valine, leucine and isoleucine degradation appear to be required in the young biofilm cells. The genes *purH*, *purF*, *pdhA* are potential genetic targets for biofilm prevention and control of *V. parahaemolyticus*.

Abstract

Vibrio parahaemolyticus in seafood can cause food poisoning. There is increasing concern with the increase in reports of illness globally believed to be due to climate change affecting sea temperatures. Biofilm formation of *V. parahaemolyticus* is an additional concern as biofilms are more resistant to cleaning and sanitation than planktonic cells. However, little is known about the biofilm formation of *V. parahaemolyticus.* Strain variation and the factors determining biofilm formation were investigated in this study with the aim to provide information that can be used to design more effective control strategies.

This study identified two robust biofilm forming strains (PFR30J09 and PFR34B02) from nine *V. parahaemolyticus* seafood isolates. Comparative genome analysis unveiled 136 unique accessory genes in robust biofilm formers. Protein-protein-interaction analysis showed interactions between UDP-glucose metabolism (Gene ontology (GO): 0006011), cellulose biosynthesis (GO: 0030244), rhamnose metabolism (GO: 0019299) and O antigen biosynthesis (GO: 0009243). Cellulose contributed to robust biofilm formation. Cellulose biosynthesis was identified as being acquired from within the order *Vibrionales*. The cellulose synthase operons consisting of genes *bcsG*, *bcsE*, *bcsQ*, *bcsA*, *bcsB*, *bcsZ*, *bcsC* were present in 15.94% (22/138) of *V. parahaemolyticus*.

Strong biofilm-forming *V. parahaemolyticus* showed greater resistance to sanitizers of biofilm cells than the weaker biofilm forming cells. The effective concentrations of sodium hypochlorite for inactivating most *V. parahaemolyticus* biofilm cells were higher than the recommended concentration. Available chlorine of 1176 mg/L inactivated 1.74-2.28 $\log_{10}$ CFU/cm^2 of biofilm on stainless steel surfaces and 4704 mg/L inactivated > 7.00 $\log_{10}$

CFU/cm^2 of biofilm (to undetectable levels, < 10 CFU/cm^2), except for biofilms formed by the strong biofilm formers. Peracetic acid (PAA) at 200 ppm (89.56 mg/L PAA, 471.64 mg/L hydrogen peroxide) inactivated > 5.00 $\log_{10}$ CFU/cm^2 of biofilm from stainless steel surfaces (except for those the strong biofilm formers, see Figure 4.4).

RNA sequencing (RNA-seq) identified 74 differentially expressed genes when comparing planktonic and biofilm cells of *V. parahaemolyticus*. These represented the rearrangement of nucleotide and energy metabolism in biofilm cells. Biosynthesis of secondary metabolites, purine and pyrimidine metabolism, propanoate metabolism, and valine, leucine and isoleucine degradation were deemed essential in the young *V. parahaemolyticus* biofilms. Genes of *purH*, *purF*, *pdhA* are potential genetic targets for biofilm prevention and control of *V. parahaemolyticus*.

Understanding *V. parahaemolyticus* biofilm formation will help to design strategies to overcome the limitations of chemical sanitizers, improving product safety and quality in the seafood industry.

Acknowledgements

Deeply grateful and appreciative for Massey University giving me this position, enabling the chance to undertake this wonderful journey. Great thanks for Massey offering me a Doctoral Scholarship to finance this research. Thanks to Massey and the School of Food and Advanced Technology staff, for their kind help and support, allowing me to navigate this journey smoothly.

I express appreciations for my main supervisor Steve Flint, for his valuable feedback and patient guidance during this study. I would like to thank Steve for his in-depth knowledge and expertise, his efforts in improving me as an international Ph.D. student. Thanks to the Massey University Biofilm Research Team, for the resources and opportunities provided by this lovely group. Thanks also go to Jon Palmer, who patiently offered feedback and suggestions during each of my weekly report meetings. Many thanks to Dragana Gagic, without whom, I could not have started molecular research for *V. parahaemolyticus*. Thanks to Graham Fletcher, for providing isolates and sequences of *V. parahaemolyticus*, as well as his valuable expertise on *V. parahaemolyticus* and the seafood industry. Thanks to Stephen On, for valuable feedback and inspiration he provided for this study. It has been my giant honor to work with my supervisory committee.

Many thanks to the staff from the Food Microbiology Lab. Thanks to Ann-Marie, Kylie Evans, Baizura Zain, Emmanuel Kyere, Tianyang Wang and Haoran Wang. Thanks for their maintenance of equipment and reagents, and their warm and generous support when I encountered difficulties at the lab.

Thanks to my office mates at the PD Hut; Ramandeep, Yiying, Zheng, Abilasha, Kent, Maru, Linda, Farah and Sujirtha. Thanks for the company and moral support. Thanks to the lovely new Ph.D. students joining the PD Hut family. Thanks for the happiness, gatherings, and discussions from mates in the Biofilm Research Team - Yiying, Emmanuel, Tianyang, David, Murali, Thu, Farah, Srinithi, Ili, Krisha, Yining, Hasani, Van and Diluthi.

Thanks so much to all of you, for helping me get to the completion of my PhD thesis.

Poster and Oral Presentations

Efficacy of commercial peroxyacetic acid on *Vibrio parahaemolyticus* planktonic cells and biofilms on stainless steel and Greenshell™ mussel (*Perna canaliculus*) surfaces. Poster Presentation, 2022 NZMS Conference, 21-14th November, Wellington, New Zealand.

Genome analysis of strong biofilm-forming *Vibrio parahaemolyticus*. Oral Presentation, 2022 NZMS Conferencem 21-24th November, Wellington, New Zealand.

Publications

Wang, D., Flint, S. H., Palmer, J. S., Gagic, D., Fletcher, G. C., & On, S. L. (2022). Global expansion of *Vibrio parahaemolyticus* threatens the seafood industry: Perspective on controlling its biofilm formation. *LWT*, 158, 113182.

Wang, D., Fletcher, G. C., On, S. L., Palmer, J. S., Gagic, D., & Flint, S. H. (2023). Biofilm formation, sodium hypochlorite susceptibility and genetic diversity of *Vibrio parahaemolyticus*. *International Journal of Food Microbiology*, *385*, 110011.

Wang, D., Fletcher, G. C., Gagic, D., On, S. L., Palmer, J. S., & Flint, S. H. (2023). Comparative genome identification of accessory genes associated with strong biofilm formation in *Vibrio parahaemolyticus*. *Food Research International*, 166, 112605.

Wang, D., Palmer, J. S., Fletcher, G. C., On, S. L., Gagic, D., & Flint, S. H. (2023). Efficacy of commercial peroxyacetic acid on *Vibrio parahaemolyticus* planktonic cells and biofilms on stainless steel and Greenshell™ mussel (*Perna canaliculus*) surfaces. *International Journal of Food Microbiology*, *405*, 110372.

Wang, D., Flint, S. H., Gagic, D., Palmer, J. S., Fletcher, G. C., & On, S. L. (2021). *In silico* analysis revealing CsrA roles in motility-sessility switching and tuning VBNC cells in *Vibrio parahaemolyticus*. *Biofouling*, 37(6), 680-688.

Table of Contents

List of Figures

List of Tables

Chapter 1. Introduction

1.1 Background

Vibrio parahaemolyticus causes food poisoning, often associated with seafood. This pathogen survives temperatures of 5-45 °C with an optimal growth temperature in seawater between 14-19 °C (Cruz et al., 2015; Han et al., 2017; Konrad et al., 2017; MPI, 2001; Ndraha & Hsiao, 2021). This pathogen is prevalent in summer and autumn. Global warming is believed to be responsible for an increasing frequency of *V. parahaemolyticus* infections in more countries. Food poisonings and outbreaks have been reported in areas where there were previously no or only sporadic cases (FAO, 2021). *V. parahaemolyticus*, like most microorganisms, is believed to gain advantages through biofilm formation.

Biofilm communities are dynamic and complicated biological systems. The life cycle involves cells for attachment, microcolony formation, matrix production and dispersion. Mature biofilms are comprised of sessile microbial communities adhering to a surface inside a self-produced matrix made up of extracellular polymeric substances (EPS) including polysaccharides, proteins, glycoproteins, glycolipids and extracellular DNA (e-DNA) (Brooks & Flint, 2008). Cells deploy multiple genetic strategies to form biofilms. In nature, multi-species biofilms are prevalent with distinct regulatory pathways and greater complexity than planktonic cells.

Understanding *V. parahaemolyticus* biofilm formation will help develop strategies to control biofilm and reduce risks of *V. parahaemolyticus* infections. This research aims to identify and overcome the limitations of current chemical disinfectant treatments, applying phenotypic screening, whole genome sequencing (WGS) and RNA sequencing (RNA-seq) to illustrate the mechanisms of *V. parahaemolyticus* persistence in the food industry. This knowledge will help develop novel control strategies to safety and quality in the seafood industry.

1.2 Research questions

A. Does *V. parahaemolyticus* form biofilms in the seafood processing plants and will biofilm formation pose risks to food safety? Are current chemical disinfectants effective in reducing *V. parahaemolyticus* biofilm cells?

B. What genotypes of *V. parahaemolyticus* are responsible for biofilm formation and virulence? What genes are responsible for biofilm formation in isolates from seafood environments, how do they compare with the reference strain RIMD2210663? What genes are responsible for robust biofilm formation and strong sanitizer resistance?

C. Can gene expression provide information to help design an improved strategy for the control of *V. parahaemolyticus* biofilms?

1.3 Research objectives

A. Explore biofilm forming activities of *V. parahaemolyticus* from the New Zealand seafood industry and their susceptibility to widely used sanitizers in the food industry.

B. Determine the similarities and differences in genome sequences from strong and weak biofilm forming *V. parahaemolyticus* candidates.

C. Determine variations in gene expression between biofilm forming cells and planktonic cells.

1.4 Research hypothesis

Genomic characteristics that are responsible for biofilm formation, can help to provide a strategy for the control of *V. parahaemolyticus* in seafood.

1.5 Reference

Brooks, J. D., & Flint, S. H. (2008). Biofilms in the food industry: problems and potential solutions. *International Journal of Food Science & Technology*, 43(12), 2163-2176.

Cruz, C., Hedderley, D., & Fletcher, G. (2015). Long-term study of *Vibrio parahaemolyticus* prevalence and distribution in New Zealand shellfish. *Applied and environmental microbiology*, *81*(7), 2320-2327.

FAO. (2021). Advances in science and risk assessment tools for *Vibrio parahaemolyticus* and *V. vulnificus* associated with seafood: meeting report (9240024875).

Han, F., Gu, R.-R., Shen, X.-S., Chen, Y.-G., Tian, L.-L., Zhou, W.-F., & Cai, Y.-Q. (2017). Detection of total and pathogenic *Vibrio parahaemolyticus* in shellfish growing along the south yellow sea and the East China sea. *Journal of Food protection*, *80*(11), 1882-1889.

Konrad, S., Paduraru, P., Romero-Barrios, P., Henderson, S. B., & Galanis, E. (2017). Remote sensing measurements of sea surface temperature as an indicator of *Vibrio parahaemolyticus* in oyster meat and human illnesses. *Environmental Health*, *16*(1), 1-11.

MPI. (2001). Microbial Pathogen Data Sheets: *Vibrio Parahaemolyticus*. https://www.mpi.govt.nz/dmsdocument/11033-Vibrio-parahaemolyticus-Microbial-pathogen-data-sheet

Ndraha, N., & Hsiao, H.-I. (2021). Influence of climatic factors on the temporal occurrence and distribution of total and pathogenic *Vibrio parahaemolyticus* in oyster culture environments in Taiwan. *Food Microbiology*, *98*, 103765.

Chapter 2. Literature review: global expansion of *Vibrio parahaemolyticus* threatens the seafood industry - perspective on controlling its biofilm formation

This chapter contains material that was published (published article reproduced in Appendix VI) as a peer-reviewed article:

Wang, D., Flint, S. H., Palmer, J. S., Gagic, D., Fletcher, G. C., & On, S. L. (2022). Global expansion of *Vibrio parahaemolyticus* threatens the seafood industry: Perspective on controlling its biofilm formation. *LWT*, 158, 113182.

2.1 Introduction

Seafood is a sustainable food predicted to increase to 12-25% of all meat sources by 2050 (Costello et al., 2020). *V. parahaemolyticus* is a curved rod, Gram-negative bacterium that naturally exists in the marine environment (Robinson, 2014). It can be prevalent in oysters, clams, fish, shrimps, mussels, scallop and periwinkle (Odeyemi, 2016), and food poisoning is associated with the consumption of raw or undercooked seafood. *V. parahaemolyticus* survives at 5-45 °C and grows when seawater temperatures are between 14-19 °C (Cruz et al., 2015; F. Han et al., 2017; Konrad et al., 2017; MPI, 2001; Ndraha & Hsiao, 2021). This explains why this pathogen is prevalent in summer and autumn seasons. Global warming has caused an increased geographical range and frequency of *V. parahaemolyticus* infections. Repeated cases of infection and outbreaks have been reported in unexpected areas where there were previously no or only sporadic cases (FAO, 2021; Martinez-Urtaza et al., 2010) (Table 2.1).

Biofilm formation provides *V. parahaemolyticus* bacterial communities protection for survival and colonization (Yildiz & Visick, 2009). *V. parahaemolyticus* forms biofilm assisted by a dual flagellar system - polar and lateral flagella (Kim & McCarter, 2000). This dual flagellar system allows *V. parahaemolyticus* to move under various conditions, thereby adjusting to different environments and attaching onto surfaces. Biofilm formation starts after bacterial cells attach onto a surface. *V. parahaemolyticus* colonizes and forms biofilms on biotic (shrimp, crab, mussel, etc.) and abiotic surfaces (stainless steel, polystyrene, glass, etc.) according to published studies by Han et al. (2016), Ashrafudoulla et al. (2019) and Wong (2002). EPS is a self-secreted polysaccharide covering bacterium, and it is required for mature biofilm formation (Yildiz & Visick, 2009). Biofilm formation process is affected by various factors, including temperature, contact surface, cell surface, strain variants and so on (Brooks & Flint, 2008; Palmer et al., 2007).

Table 2. 1 *Vibrio* food poisoning in unexpected regions.

Region	Year	No. of cases	Infection route	Reference
France	2010-2019	91	Seafood	(FAO, 2021)
Canada	2020	21	Oysters	
Canada	2015	82	Oysters	
England	2010-2020	22	Seafood	(Pattis, 2020, 2022)
New Zealand	2019-2021 (till January)	~ 40	Mussels	

Understanding *V. parahaemolyticus* biofilm formation will help develop measures to control biofilm in seafood and reduce risks of *V. parahaemolyticus* outbreaks. This chapter reviews new findings and conclusions about *V. parahaemolyticus* biofilm formation in seafood and processing plants, as well as describes recent advances in understanding the mechanisms of *V. parahaemolyticus* biofilm formation. It will contribute to overcoming the limitations of current chemical disinfectant treatments and help develop novel cost-effective control strategies to improve product safety and quality in the seafood industry.

2.2 Overview of *V. parahaemolyticus* biofilm formation in seafood related environments

2.2.1 Fundamentals of *V. parahaemolyticus* biofilm formation in seafood related environments

V. parahaemolyticus forms biofilms on marine biotic surfaces and abiotic surfaces under appropriate incubation conditions, functioning as a source of pathogenic bacteria with protection (Takahashi et al., 2016). Table 2.2 summarizes published methods for detecting and enumerating *V. parahaemolyticus* biofilms. While these methods have contributed to a deeper understanding of *V. parahaemolyticus* biofilms, each method has limitations. Certain techniques may concentrate exclusively on a single or a few aspects of biomass, cell viability, viable but non-culturable cell (VBNC) population, matrix structure or biofilm composition. Researchers commonly employ a combination of methods to detect and describe biofilm characteristics.

Odeyemi (2016) examined the prevalence of *V. parahaemolyticus* based on 48 published studies, the prevalence in oysters, clams, fish, shrimp, and mussels was 63.4%, 52.9%, 51.0%, 48.3%, and 28.0%, respectively. *V. parahaemolyticus* can form biofilms on these surfaces

(Table 2.3), especially uneven seafood surfaces that provide protection for biofilm communities from biocidal treatments (Guo et al., 2020; Han et al., 2016). *V. parahaemolyticus* biofilms were identified on crab and shrimp surfaces by Han et al. (2016), and on shrimp and mussel surfaces by Ashrafudoulla et al. (2019). However, Rosa et al. (2018) discovered that *V. parahaemolyticus* did not form biofilms on shrimp shells. This may be explained by different isolates examined. Several studies have documented that *V. parahaemolyticus* forms biofilms on abiotic surfaces (Table 2.3). Stainless steel, polystyrene, fiberboard, polypropylene boxes, and glass are among materials that have the potential to support biofilm production.

2.2.2 Biofilm life cycle

2.2.2.1 Surface attachment

V. parahaemolyticus forms biofilms using polar and lateral flagella. Polar flagella (driven by sodium ions) are ulitized for swimming, while lateral flagella (driven by protons) are used for swarming (Kimbrough et al., 2020). Polar flagella function via the *fla* gene system, which is highly regulated and comprises three distinct types of gene clusters. The polar flagella function as a mechano-sensor, resulting in a reduction in flagellar rotation and activation of the *laf* gene-encoded lateral flagella expression (Kimbrough et al., 2020). Swarming via lateral flagella requires bacterial cells to reach certain numbers, and the morphology of *V. parahaemolyticus* becomes elongated as it transitions from swimming to swarming cells (Freitas et al., 2020). However, it is unknown whether the flagella are lost and/or degraded following surface attachment, or whether flagella serve as structural components of the biofilm, and little is understood about how the various forms of motility interact and initiate biofilm development in *V. parahaemolyticus*.

Table 2. 2 Different methods to determine *V. parahaemolyticus* biofilm.*

Method	Application	Limitations
Colony formation Units (CFU)	Enumeration of culturable cells in the biofilm matrix	Only detects culturable biofilm populations, but not dormant, viable but non culturable communities. Underestimates biofilm populations due to cell aggregation. Time consuming.
Microtiter plate assay - crystal violet dye & biofilm formation index (BFI)	Quantification of biomass through crystal violet stain	Lack of sensitivity. Lack of consistency. Dead cells will be stained and included as the biomass volume.
Microtiter plate assay - Calgary device	Quantification of biomass	Calgary device lid and bottom plate are needed. CFU assay to enumerate cell numbers inside biofilm matrix still needs to be performed.
PMA-qPCR method	Quantification of viable cell numbers in the biofilm matrix	Expensive. Need to use CFU assay to enumerate cultivable cell population to obtain viable but non-culturable cell (VBNC) cell population.
Fluorescence microscopy	Enumeration of living and dead cell numbers through living and dead cells stains	Expensive use of fluorescence dye. Cell number counts are limited by microscopic view scopes.

Confocal laser scanning microscopy (CLSM) imaging	Biofilm matrix observation, structural detection	High price of fluorescence dye. Interference of self-fluorescence from the matrix.
Scanning electron microscopy (SEM) imaging	Observe the biofilm morphology	General observation of biofilm morphology, not useful if used to compare biofilms with limited differences.
XTT [2, 3-bis (2-methoxy-4-nitro-5-sulfophenyl)-2H-tetrazolium-5-carboxanilide] method	Determination of biofilm metabolic activity	Detection limit of 10^3-10^8 CFU/biofilm. Comparing the metabolic activity within the biofilm formed by same strain, strain variations may induce differences of metabolic activity.
Phenol-sulfuric acid method	Chemical method to quantify extracellular polymeric substance (EPS) production	Can only detect extracellular polysaccharides. Low accuracy. Quantification of EPS requires standard curves, or EPS production can only be compared by OD value.
RT-qPCR	Quantifies expression levels of biofilm relative genes	Expensive. Multiple steps to extract clean RNA.

* This table was referred from published studies (Chen et al., 2020; Guo et al., 2020; Han et al., 2016; Q. Han et al., 2017; Li et al., 2020; Mougin et al., 2019; Ning et al., 2021; Roy et al., 2021; Sun et al., 2019; Tan et al., 2021).

Table 2. 3 Biofilm formulation of *V. parahaemolyticus* on biotic and abiotic surfaces.

Surface	Strain	Inoculum size	Incubation parameters	Biofilm formulation results	References
Biotic -crab -shrimp Abiotic -Stainless steel	Cocktail of *V. parahaemolyticus* K CTC 2471, KCTC 2729, ATCC 33844	Crab & shrimp: 1: 2500 dilution of OD 1.0 cell suspension SS: 1:50 dilution of OD 1.0 cell suspension	Time: 24 h Temperature: 4, 10, 15, 20, 25, 30, 35, and 37 °C	The higher CFU levels were observed on the crab surfaces (almost 8 log CFU/cm^2) than on the shrimp surfaces (7 log CFU/cm^2) at 25-37 °C. 30 °C was the optimum condition for biofilm formation (> 8 log CFU/cm^2).	Han et al. (2016)
Biotic -shrimp -mussel	*V. parahaemolyticus* clinical isolates *(*ATCC17802, ATCC27969) and 8 other environmental isolates	10^5 CFU/mL, 10mL	Time: 24 h Temperature: 30 °C	For shrimp surfaces, environmental isolates formed 6.21-6.89 $\log_{10}$ CFU/cm^2, clinical isolates formed 5.59-6.19 $\log_{10}$ CFU/cm^2. For mussel surfaces, environmental isolates formed 5.91-6.40 $\log_{10}$ CFU/cm^2, clinical isolates formed 5.29-5.72 $\log_{10}$ CFU/cm^2.	Ashrafudoulla et al. (2019)
Biotic -shrimp -Fish, white mouth croaker	*8 V. parahaemolyticus* environmental isolates	Original concentration of overnight culture	Time: 240 h (replace inoculum broth each 48 h) Temperature: 37 °C	No biofilms on shrimp shells, but on operculum of fish (5-6 $\log_{10}$ CFU/cm^2).	Rosa et al. (2018)

Abiotic -Stainless steel	*V. parahaemolyticus* ANSES collection 14-B3PA-0046	10^8 CFU/mL, 11mL	Time: 24 h, 48 h Temperature: 3 h, 24 h and 48 h	No big difference of biofilm formation at 8 and 37 °C, ranging from 6-9 $\log_{10}$ CFU/cm^2.	Mougin et al. (2019)
Abiotic -Stainless steel -glass	*V. parahaemolyticus* ST55, 16 clinical and 12 environmental isolates	1:2 dilution of OD 1.5 cell suspension	Time: 1-8 h Temperature: 25 °C	Clinical strains attached better on stainless steel surface than did environmental strains. The cell density reached a peak at 6 or 8 h (6-8*10^5 CFU/mL) on stainless steel and glass surfaces and declined thereafter.	Wong (2002)
Abiotic - glass	*V. parahaemolyticus* V P-C7	1:100 dilution of OD 0.4 cell suspension	Time: 2 h, 8 h, 12 h, 24 h and 48 h Temperature: 15, 25 and 37 °C	When cultured at 15 °C, a mature biofilm only forms after 48 h (biofilm thickness of 19.73 μm), while a mature biofilm forms between 12 to 24 h at 25 C° (biofilm thickness of 18.94-19.80 μm).	Song et al. (2017)

2.2.2.2 Microcolony formation and the matrix

Microcolonies are aggregates of 50 or fewer cells that form as a forerunner to biofilm formation; small colony variants promote biofilm aggregate production and antimicrobial tolerance, acting as a survival strategy with a low reproduction rate (Steenackers et al., 2016). Following microcolony development, the cells become stronger and more stable due to the secretion of structural components, exopolysaccharides, matrix proteins, and eDNA that work as a "molecular glue" to aid attachment. The mechanism by which individual cells transform into cell aggregates, on the other hand, is not completely understood.

Biofilm maturation results in cells buried deep within biopolymer layers with a variety of mature matrix structures, including: 1) monolayer biofilms - *V. parahaemolyticus* was reported to form this structure at 4 and 10 °C (Han et al., 2016); 2) multilayer biofilms with large aggregates of bacterial cells; 3) a matrix structure previously described for other species but not yet been observed for *V. parahaemolyticus*, consisting of multi-layered biofilms with small aggregates at the base and motile cells covering the surface, and associated with a late mature biofilm and dispersion (Houry et al., 2012). Chemical components contained within the *V. parahaemolyticus* biofilm matrix, such as polysaccharides, proteins and eDNA, shape the biofilm architecture by changing the biovolume, porosity and mean thickness of the three-dimensional matrix (Tan et al., 2018), but the mechanisms are poorly understood.

2.2.2.3 Dispersion

Dispersion is the final stage of the biofilm life cycle; cells inside the biofilm actively escape from the extracellular matrix, resulting in eroded biofilm matrices and bacterial cells that can migrate to new nutrition and resource-rich environments (Steenackers et al., 2016). While it is

well established that dispersion is associated with cell death and lysis, little is known about this in *V. parahaemolyticus*.

2.2.3 Environmental factors influencing biofilm formation

Attachment and biofilm formation of *V. parahaemolyticus* to biotic and abiotic surfaces is a complicated process influenced by a variety of factors including temperature, composition of the attachment medium, substrate surface, cell surface and strain variants.

Temperature. Temperature influences *V. parahaemolyticus* biofilm formation. Song et al. (2017) reported that *V. parahaemolyticus* produced better biofilm at 25 °C than at 15 °C and 37 °C. According to Han et al. (2016), *V. parahaemolyticus* develops multi-layered biofilms at 15 and 37 °C, but monolayers at 4 and 10 °C. Biofilm formation of *V. parahaemolyticus* at high temperatures, such as 25-37 °C, could be the main cause of food safety problems due to this pathogen (Han et al., 2016).

Sodium chloride and glucose. Sodium chloride (NaCl) and glucose influence adhesion and maturation of *V. parahaemolyticus* biofilms. Salinity in open ocean seawater is approximately 3.5%. *V. parahaemolyticus* forms the best biofilm in tryptic soy broth (TSB) containing 2% NaCl and the least biofilm in TSB containing 5% NaCl (NaCl concentrations of 0.5%, 1%, 2%, 3%, 4%, 5% examined). Glucose concentrations of 0.005-0.015% in TSB promote whereas high glucose concentrations of 0.05% inhibit biofilm formation (Mizan et al., 2018).

Contact surface (charge, hydrophobicity, roughness). The charge on the cell surface varies under different physiological conditions, influencing bacterial attachment to surfaces. Cells of *V. parahaemolyticus* are frequently negatively charged, and thus attach to positively charged surfaces (Chaiyakosa et al., 2007). *V. parahaemolyticus* biofilm formation is positively correlated with cell surface hydrophobicity and is associated with the flagellar and proteins on

the bacterial cell outer membrane (Mizan et al., 2016). The hydrophobicity of the substrate surface (stainless steel, polystyrene, and glass) shows a negative correlation with the amount of eDNA, extracellular protein and biofilm biomass in *V. parahaemolyticus* biofilms (Guo et al., 2020). Instead of hydrophobic stainless steel, *V. parahaemolyticus* grows a better biofilm on surfaces such as polystyrene and glass and is believed to relate to survival adaptation mechanisms on these surfaces (Guo et al., 2020; Wong, 2002).

2.3 Molecular mechanisms of *V. parahaemolyticus* biofilm formation

The mechanisms by which *V. parahaemolyticus* biofilms form are regulated by a systemic and integrated regulatory network. Though there are numerous genes responsible for EPS biosynthesis and production, the *cps* locus has been extensively studied and will be discussed under Positive regulators and Negative regulators (Figure 2.1).

2.3.1 Positive regulators

CpsQ can activate the expression of the capsular polysaccharide genes *cpsA-cpsJ* (*vpa1403-1412*) in *V. parahaemolyticus*, thereby regulating biofilm production. CpsQ is a c-di-GMP binding protein that is regulated by intracellular c-di-GMP concentrations, and has been demonstrated to be a positive, regulator of capsular polysaccharide CPSA expression. It was reported that quorum sensing regulators OpaR and AphA bind to the promoter region of the *mfpABC* operon to enhance and repress *mfpABC* transcription, as well as repress and enhance *cpsQ-mfpABC* operon expression, and influence biofilm development (Zhou et al., 2013). Due to their accumulation at high cell density, it was hypothesised that CpsQ and MfpABC might play a role in the middle/late stages of growth and pathogenesis. CpsQ contributes to capsule expression when c-di-GMP levels are elevated, but it is not solely

responsible for biofilm formation, therefore, deletion of CpsQ does not eliminate biofilm formation (Kimbrough et al., 2020).

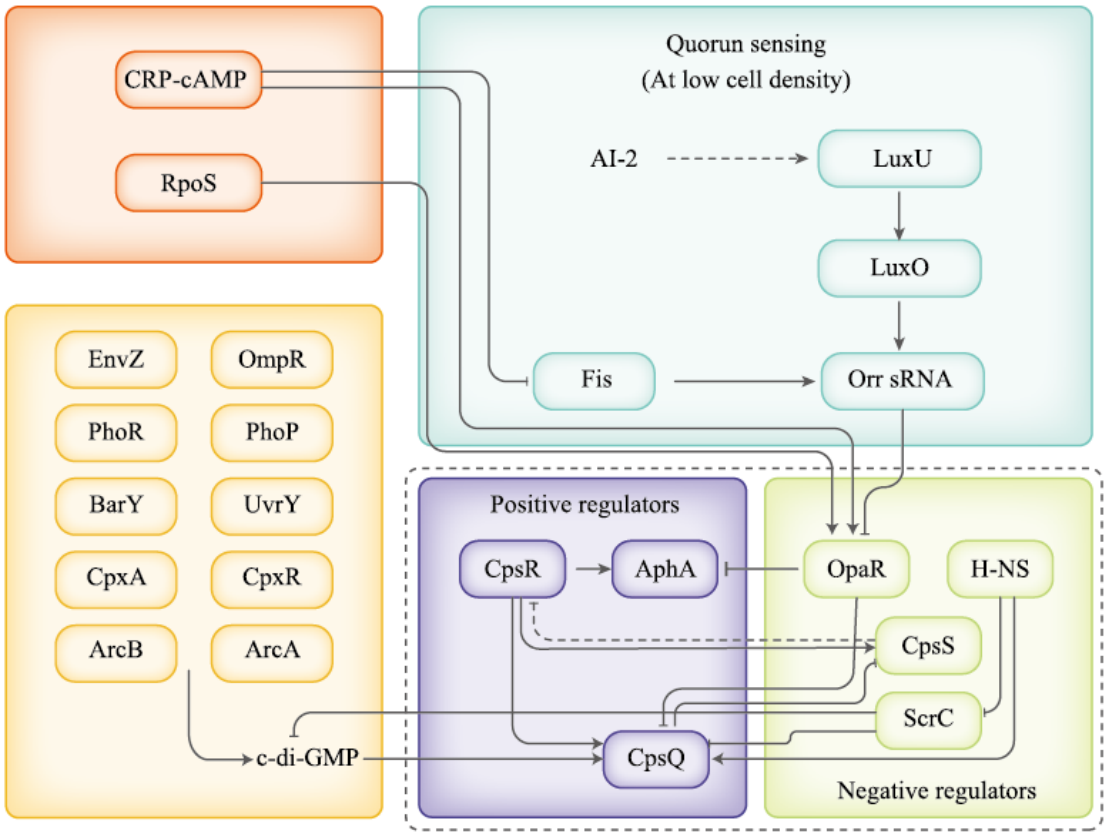

Figure 2. 1 The transcriptional network of *V. parahaemolyticus* biofilm formation.
This figure was depicted according to published articles about transcriptional control of EPS production genes in *V. parahaemolyticus*.

CpsR is another transcription regulator that regulates the formation of the biofilm matrix. CpsR is also not solely required for biofilm formation in *V. parahaemolyticus,* but it is critical for the increased CPSA expression elicited by c-di-GMP (Yildiz & Visick, 2009). It is required in the ScrABC-dependent pathway to regulate swarming and EPS production. Introduction of the *cpsR1*::Tn*5* allele into the rugose *scrA* mutant resulted in the transformation of a rugose colony to smooth colony, the elimination of exopolysaccharide production, and a decreased

capacity for biofilm formation (Guvener & McCarter, 2003). CpsR acts prior to CpsQ and can activate CpsQ and CpsS. The CpsS-CpsR-CpsQ regulatory cascade is responsible for the EPS production (Guvener & McCarter, 2003).

Quorum sensing governs sets of cellular pathways, including motility, virulence, and biofilm formation through its master regulators-AphA and OpaR. AphA is a small PadR family expression regulator with an N-terminal winged-helix DNA-binding domain. AphA is activated at low cell density, to promote the transcription of virulence, flagella-mediated motility and biofilm formation (Zhou et al., 2013). In the presence of low cell density, redundant Qrr_{1-4} sRNAs regulated by LuxQ-LuxU-LuxO pathway inhibit *opaR* and *cpsQ-mfpABC* transcription, thereby influencing the formation of *V. parahaemolyticus* biofilms (Liu et al., 2021; Zhou et al., 2013).

2.3.2 Negative regulators

Signaling via chemotaxis ScrABC is involved in competitive colonization and the development of the biofilm matrix. ScrA is encoded by *scrA*, which is part of the *scrABC* operon, and promotes the expression of *laf* genes (Boles & McCarter, 2002). ScrC functions as a diguanylate cyclase (DGC), contains GGDEF and EAL domains and is regulated by ScrA and ScrB at translation level, and can promote CpsQ repression and c-di-GMP degradation (Kimbrough et al., 2020). A *scrABC* operon mutation has a profound effect on gene expression, resulting in decreased swarming activity, increased cellular c-di-GMP levels, overproduced CPSA, crinkly colonies and enhanced biofilm formation (Kimbrough et al., 2020).

CpsS is the dominant negative regulator in *V. parahaemolyticus* (Yildiz & Visick, 2009). It is another member of the CsgD family and contains a DNA-binding domain similar to that of CsgD. CpsS can inhibit cpsR expression, while *cpsR* activates *cpsQ*, and CpsQ inhibits *cpsS.*

CpsS represses CpsQ, but it is unknown whether it directly or indirectly regulates CpsQ. Deletion of *cpsS* results in capsule overexpression and wrinkly colonies (Enos-Berlage et al., 2005).

OpaR governs biofilm formation through regulating CpsQ (Zhou et al., 2013). The histone-like nucleoid structuring protein H-NS is a "transcriptional silencer". It is involved in the transcription of genes and the folding of DNA and an expression activator of the *cpsA-cpsJ* operon (Enos-Berlage et al., 2005). Mutants of *hns* fail to trigger CPSA production and polar flagellar activity, thereby resulting in decreased biofilm formation in *V. parahaemolyticus* (Enos-Berlage et al., 2005).

2.3.3 Extracellular polymeric substances (EPS) synthesis genes

Numerous genes have been identified as being involved in the formation of the extracellular matrix of *V. parahaemolyticus* biofilms. *cpsA-J* (*vpa1403-1412*) is required for the synthesis of capsular polysaccharide A (CPSA), a major component of the *V. parahaemolyticus* biofilm (Yildiz & Visick, 2009). *cpsA-J* is also required for the formation of opaque colonies, rugose phase transmission of the colony and biofilm development (Enos-Berlage & McCarter, 2000). *vp1476-1458* is an ortholog of the *syp* locus that is conserved in *V. fischeri*. This locus was reported to be responsible for wrinkled colonies, pellicle formation and matrix production in *V. fischeri* (Yildiz & Visick, 2009). *V. parahaemolyticus* shares 85.9 and 75.8% similarities with the glycosyltransferase gene *sypQ* from *V. alginolytious* 12G01 and *V. harveyi* ATCC BAA-1116 respectively (Ye et al., 2014), indicating the relatedness with poly-N-acetylglucosamine (PNAG) biosynthesis. Cellulose is typically found in Gram-negative bacteria, but in *V. parahaemolyticus*, the cellulose synthase gene cluster is unknown. Another locus involved in *V. parahaemolyticus* biofilm formation is *vp0214*-0237, which results in translucent colonies, decreased adherence to surfaces, inhibition of swarming motility and

interruption of biofilm maturation (Enos-Berlage et al., 2005). Proteins and eDNA in the extracellular matrix contribute to the structure and stability, but they are poorly studied in *V. parahaemolyticus*.

2.3.4 Does pathogenicity influence biofilm formation?

Virulence factors are typically associated with bacterial pathogenicity. Song et al. (2017) concluded that the pathogenicity of a strain and its ability to form biofilms are related properties as pathogenic *V. parahaemolyticus* accumulates more biofilm matrix than non-pathogenic strains. Similarly, Wong (2002) found that clinical strains adhered more readily to stainless steel than environmental strains, and that decreased c-di-GMP levels within cells can promote biofilm formation and pathogenicity in *V. parahaemolyticus*. Zhang et al. (2019) revealed that the transcription factor QsvR works in conjunction with a QS system to regulate the expression of virulence genes, T3SS1 and pathogenicity islands (PAI, T3SS2 and thermostable direct hemolysin (TDH)), in *V. parahaemolyticus*. AphA has a role in the initial colonization stage, activating T3SS1 gene expression but inhibiting the expression of PAI genes, thus boosting *V. parahaemolyticus* cytotoxicity. OpaR and QsvR act at a higher cell density by activating PAI transcription, thereby enhancing enterotoxicity and causing severe gastroenteritis. QsvR can also maintain basal levels of T3SS1 expression despite OpaR negatively regulating it.

2.4 Limitation of chemical disinfectants and promising mitigation strategies

2.4.1 Limitation of chemical disinfectants

Chemical disinfectant treatment is a simple, cost-effective, and widely used strategy for pathogen contamination control in the food industry. Numerous studies to determine the efficacy of various chemical disinfectants against *V. parahaemolyticus* biofilms have been conducted (Table 2.4). While cleaning chemicals and disinfectants remove soils and inactivate

biofilm cells from seafood and plant surfaces, using disinfectants alone at recommended concentrations makes it difficult to control biofilm effectively, as recurrence and recolonization of pathogen communities with increased acquired resistance may occur (Rosa et al., 2018). Increased disinfectant concentrations are discouraged, as they may corrode plant surfaces, influence seafood sensory and produce chlorine and/or other by-products that are hazardous to human health. Additionally, routine exposure of biofilm populations to chemical disinfectants may also result in an increase in VBNC state cells, which aids in the persistence of biofilm communities on seafood processing plants. For instance, the routine use of chemical disinfectants in cleaning and sanitation in smoked salmon processing plants has resulted in the development of *Listeria monocytogenes* VBNC populations that are resistant to environmental stress and difficult to eradicate (Brauge et al., 2020).

2.4.2 Promising strategies

As chemical disinfectant treatments fail to remove *V. parahaemolyticus* biofilms effectively, alternative strategies for mitigating these risks are required (Figure 2.2).

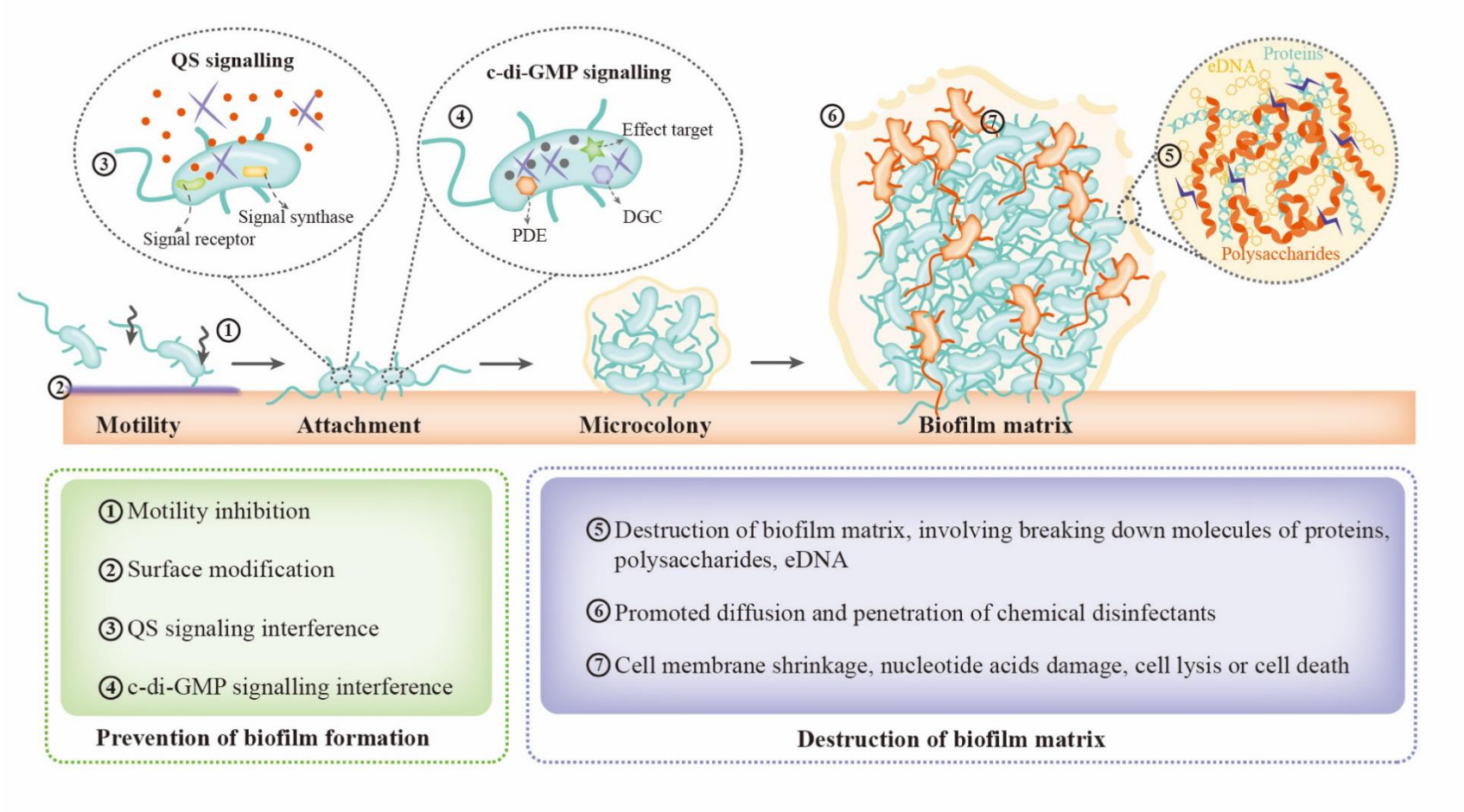

Figure 2. 2 Promising inactivation forms of *V. parahaemolyticus* biofilm communities.

This picture displays dynamic procedure of biofilm formation, points in the rectangular box indicate promising ways to prevent biofilm formation and destruct biofilm matrix, respectively. PDE stands for c-di-GMP-specific phosphodiesterase, DGC stands for diguanylate cyclase.

2.4.2.1 Plant surface modification

Processing plant surface modifications have been studied to inhibit biofilm colonisation and development. For example, sol-gel modification, modified stainless steel surfaces using Thermolon, reduced biomass during pasteurization of milk. This investigation indicated that the biomass weight on stainless steel 316L and sol-gel-modified coupons in a benchtop plate heat exchanger was 19.21 mg/cm^2 and 0.37 mg/cm^2, respectively (Liu et al., 2017).

Biosurfactants are surface-interactive molecules that exhibit both hydrophobic and hydrophilic properties. BS-SLSZ2 is a biosurfactant derived from the marine bacterium *Staphylococcus lentus*, which has been shown to hinder bacterial attachment, impair bacteria-bacteria interactions, and prevent the formation of biofilms. At a dose of 20 μg, *V. harveyi* and *Pseudomonas aeruginosa* biofilm formation were inhibited by 80% and 82%, respectively (Hamza et al., 2017).

2.4.2.2 Physical treatment

Bubbles. The use of bubbles is being developed for antibiofilm applications. Laser-induced vapour bubbles are used to enhance the distance between sessile cells. Millimetre-sized air bubbles in water significantly removed *Pseudomonas* biofilm cells attached to stainless steel and polypropylene surfaces by 1.6 and 0.9 $\log_{10}$, respectively, and also removed the carbohydrate, protein and fat residues from stainless steel surfaces (Burfoot et al., 2017). Shiroodi et al. (2021) employed bubbles to treat *V. parahaemolyticus* biofilms on plastic and stainless-steel coupons, achieving reductions of 2.5 and 1.4 $\log_{10}$ colony forming units (CFU)/cm^2 biofilm cells respectively in 2 min, and > 7 $\log_{10}$ CFU/cm^2 in 5 min.

Table 2. 4 The effect of chemical disinfectant treatment on *V. parahaemolyticus* biofilm.

Disinfectants	Biofilm	Reduction	Reference
Sodium hypochlorite -20 ppm chlorine (~ 20 mg/L chlorine), 10min	240 h old biofilms formed on biotic and abiotic surfaces	*V. parahaemolyticus* biofilm communities of 2-5 log_{10} CFU/cm^2 were remained after treatment (~ 6 log_{10} CFU/cm^2 biofilm as control).	Rosa et al. (2018)
Sodium hypochlorite -4 mg/L chlorine, 1h	72 h old biofilm on glass slides	The bacterial density dropped from 7.90 to 3.97 log_{10} CFU/cm^2;	Shikongo-Nambabi et al. (2010)
Hydrogen peroxide (H_2O_2) -0.08%, 1h		Inactivated cells to non-detectable levels from over 7 log_{10} CFU/cm^2;	
Ozone -1.6 mg/L, 1h		Reduced ~ 2 log_{10} CFU/cm^2 biofilm cell densities.	
Sodium hypochlorite -50-300ppm, 6% w/v chlorine, 5min Strong acidic electrolyzed water (SAEW) -30 ppm chlorine (~ 30 mg/L chlorine), 1-15 min	24 h old biofilm on shrimp and crab surfaces	Sodium hypochlorite rendered maximum reductions of 3.78 and 3.32 log_{10} CFU/cm^2 on shrimp and crab surfaces (6.87 and 7.37 log_{10} CFU/cm^2 as control); SAEW achieved reductions of 1.42-3.05 and 1.14 to 2.56 log_{10} CFU/cm^2 on shrimp and crab surfaces.	Roy et al. (2021)
Strong acidic electrolyzed water (SAEW) -pH 2.3, 136.33 mg/L chlorine, 30s	48 h old biofilm	Decreased viable *V. parahaemolyticus* from 6.90 to 3.33 log_{10} CFU/cm^2.	Han et al. (2017)
Acidic electrolyzed water -pH 2.28, 52.26 mg/mL chlorine, 10 min	48 h old biofilms on polystyrene surfaces	The biovolume, eDNA, protein and polysaccharide content of *V. parahaemolyticus* matrix was significantly reduced.	Li et al. (2020)

Cold Plasma. Cold plasma has received much attention for biofilm control due to its non-thermal, rapid, green and waterless properties. The reactive species generated have antibiofilm activity through destroying the biofilm matrix and penetrating biofilm structures leading to death of the bacterial cells. High-voltage cold plasma (80 kV) treatment for 60 s reduced *L. monocytogenes*, *Salmonella enterica* and *Pseudomonas fluorescens* biofilm cells by 3.76, 4.14 and 2.6 $\log_{10}$ CFU/mL respectively from an initial cell concentration of 5.4 ± 0.4 $\log_{10}$ CFU/mL (Patange et al., 2019). Dielectric barrier discharge plasma treatment (1.1 kV, 30 min) reduced *Escherichia coli* in fresh oysters by 1.01 $\log_{10}$/g, while having no effect on the glycogen content or texture of oyster meat (Choi et al., 2022), demonstrating the potential for cold plasma application in seafood environments. However, there is little information on the effect of cold plasma for the inactivation of *V. parahaemolyticus* biofilms.

Low-frequency and high-intensity ultrasound treatment. Ultrasound with a low frequency and a high intensity has been proposed to be effective at inactivating biofilm cells. Biofilm removal is based on mechanical oscillation, free radicals (H· and .OH) and hydrogen peroxide (H_2O_2) generated, as well as localized heating. 10 s treatment of 40 kHz with a flat ultrasonic transducer removed *E. coli* and *S. aureus* dairy biofilms from stainless steel surfaces (Yu et al., 2021). The high-intensity ultrasound has been examined for its application on fish, including salmon (*S. salar*), mackerel (*S. scombrus*), cod (*G. morhua*) and hake (*M. merluccius*) fillets. The microorganism on fish surfaces were significantly reduced, but there were no significant changes in lipid content, and the moisture level remained stable except in hake (Pedrós-Garrido et al., 2017). Additional research using low-frequency and high-intensity ultrasound treatment on *V. parahaemolyticus* biofilm cells is needed.

Ultraviolet-C (UV-C) treatment. UV-C (250-270 nm) is lethal to a wide range of microorganisms, including bacteria, yeasts, and viruses. UV-C (5, 10 min) combined with 50-

500 μg/mL peroxyacetic acid reduced *S.* Enteritidis biofilm cells from stainless-steel and silicone rubber surfaces by 3.10-6.41 $\log_{10}$ CFU/mL and, UV-C (5, 10 min) in combination with 0.5-2.0% lactic acid reduced biofilm by 3.35-6.41 $\log_{10}$ CFU/mL (Byun et al., 2022). UV-C treatment of 5-60 mW*s/cm^2 (examined treatment of 5, 10, 30, 60 mW*s/cm^2) decreased *V. parahaemolyticus* biofilm communities by 1.37-2.53 and 0.75-1.94 $\log_{10}$ CFU/cm^2 from shrimp and crab surfaces, respectively. UV-C (60 mW*s/cm^2) along with sodium hypochlorite (300 ppm) decreased biofilm cells by 3.78 and 3.32 $\log_{10}$ CFU/cm^2 on these same two surfaces respectively. UV-C (60 mW*s/cm^2) combined with slightly acidic electrolyzed water reduced *V. parahaemolyticus* biofilm cells by 4.41 and 4.06 $\log_{10}$ CFU/cm^2, from these surfaces respectively (Roy et al., 2021).

High hydrostatic pressure (HHP) treatment. HPP is another nonthermal approach that is effective in inactivating *V. parahaemolyticus* in the seafood industry. 400 MPa HHP (20 ℃, 3 min) decreased *V. parahaemolyticus* in oysters to an undetectable level from ~5 $\log_{10}$ CFU/g, and the characteristic taste of oyster meat was retained for up to 15 days if refrigerated at - 20 ℃ (Liu et al., 2022). However, little is known about HPP efficacy on *V. parahaemolyticus* biofilm cells in seafood, despite reports of its use against other food pathogens. For example, *Cronobacter sakazakii* biofilm at 24 h was reduced by 45% when treated with 400 MPa HHP (Liao et al., 2021).

Lighting Photodynamic inactivation (PDI). PDI involves use of a photosensitizer activated by visible light, leading to the production of reactive oxygen species (ROS) and consequently inactivation of microbial cells. Inactivation of microbes is caused by ROS which has potential to deconstruct EPS, proteins, lipids and nucleic acids in the biofilm matrix (Tan et al., 2021). Chen et al. (2020) found that PDI treatment (5 min, 1.14 J/cm^2) with 1.0 μM curcumin as the photosensitizer decreased *V. parahaemolyticus* (~ 8 $\log_{10}$ CFU/mL) to non-detectable levels. It

downregulated genes associated with the virulence (*tdh* and *toxR*) and biofilm formation (*oxyR*, *aphA*, *luxR* and *opaR*) thereby controlling *V. parahaemolyticus* biofilm. They also found that 20.0 μM curcumin PDI treatment (60 min, 13.68 J/cm^2) almost removed 48 h old *V. parahaemolyticus* biofilm on polystyrene surfaces.

2.4.2.3 Chemical strategies

Essential oils. Essential oils are plant-based extracts that contain a variety of antibacterial and antibiofilm components. Citrus peel essential oils inhibit *V. parahaemolyticus* biofilm formation by repressing flagella gene transcription, T3SS effector function and quorum sensing activities (Sun et al., 2019). At concentrations of 3.125 and 6.25 μg/mL, citral reduced 42 and 58% autoinducer-2 quorum sensing activity, respectively. Concentrations of 6.25 and 12.5 μg/mL of citral decreased *V. parahaemolyticus* swimming and swarming by 20-47% and 35-50%, respectively. Citral at a concentration of 12.5 μg/mL disrupted the three-dimensional *V. parahaemolyticus* biofilm matrix and dispersed the cells (Sun et al., 2019).

2.4.2.4 Biocontrol strategies

Small-molecule signal blocker. Interference with biofilm formation by small molecules is a novel strategy. For example, DGC has been identified as a critical target for modulating the c-di-GMP process and biofilm formation phenotypes. Christen et al. (2019) demonstrated that 4-(2,5-dimethylphenoxy)-N-(4-morpholin-4-ylphenyl) butanamide and six other small molecules at low μM concentration, inhibited c-di-GMP signaling and biofilm formation via regulation of the DGC in a non-competitive manner. Similarly, 2,6-Di-*tert*-butyl-4-methylphenol (DTBMP) from *Chroococcus turgidus* was found to inhibit initial *V. parahaemolyticus* biofilm formation by interfering with hydrophobic activity, swarming motility and quorum sensing. A concentration of 250 μg/mL of DTBMP reduced EPS

production by 74%. DTBMP was examined *in vivo* on pacific white shrimp and demonstrated anti-adherence efficacy without killing the shrimp (Santhakumari et al., 2018).

Enzymes. Enzymes are an alternative for biofilm control in the food industry. For example, endolysins are peptidoglycan hydrolases that can deconstruct biofilm matrix and hydrolyse bacterial cell wall peptidoglycan. The combination of endolysin Lysqdvp001 (60 U/g) and ε-PL (ε-poly-lysine, 0.20 mg/g) can significantly reduce *V. parahaemolyticus* in *Gadus macrocephalus*, *Penaeus orientalis* and oyster by 3.75, 4.16 and 2.50 $\log_{10}$ CFU/g, respectively. Using ε-PL alone reduced biofilms of *V. parahaemolyticus* by 28.67%, 14.27% and 12.67%, respectively, from polystyrene, glass and stainless-steel surfaces. Lysqdvp001 had no substantial effect. A cocktail of these two enzymes removed 55.13%, 44.43% and 68.00% of the biofilms, indicating the synergistic effect of enzyme treatment may be due to the attack of different *V. parahaemolyticus* target sites (Ning et al., 2021).

Bacteriophages. Bacteriophages can destroy biofilms by inducing bacterial cell death and breaking down the biofilm matrix. For example, phage cocktails were prepared by mixing phage isolated from cattle faeces. The phage cocktails had the potential to inhibit *E. coli* O177 biofilm formation at 25 ℃ within 24 h, and the possibility to reduce pre-formed biofilms to undetectable levels within 5 h (Montso et al., 2021). Bacteriophage OMN was reported to kill 90% and 99% of *V. parahaemolyticus* communities on oyster meat surfaces after 48 and 72 h of treatment, respectively, showing the potential of bacteriophage application in seafood (Zhang et al., 2018). However, as much of the bacteriophage studies are limited to laboratory conditions, additional work is required to apply in the industry.

2.5 Conclusion and perspectives

The persistence of the *V. parahaemolyticus* biofilm in the seafood plant may result in pathogen recurrence and complicate hygienic treatment. It is necessary to understand the mechanism by which *V. parahaemolyticus* biofilms form. However, genes responsible for *V. parahaemolyticus* strong biofilm formation are unknown. This study will uncover *V. parahaemolyticus* biofilm formation, revealing insights into biofilm control strategies for *V. parahaemolyticus* in the food industry.

2.6 Recent published studies of related fields

In addition to Section 2.2.3: Yu and Rhee (2023) reported that *V. parahaemolyticus* biofilms formed on fish skin were significantly higher than stainless steel surfaces, indicated that surface roughness influenced attachment of *V. parahaemolyticus*.

In addition to Section 2.4.2.4: Zhu et al. (2023) identified that Laurel essential oil interfered with swimming motility, inhibited hydrophobicity and reduced attachment to food contact surfaces (stainless steel, silicone and glass) of *V. parahaemolyticus*, indicating that this essential oil can be a potential alternative to the biofilm control strategy.

In addition to Section 2.4.2.4: Li et al. (2022) used enzymes consisting 22 U/mL lipase, 3 U/mL cellulase and 45 U/mL proteinase (pH 5.4) to inhibit biofilm formation and remove biofilm cells of *V. parahaemolyticus*. The combined enzymes reached inhibition of 68.79%, 89.65% and 57.04% for biofilms at 6^{th}, 24^{th}, and 48^{th} h (biofilms were incubated at conditions of 30 ℃, 180 rpm, TSB containing 3% NaCl), removed 57.62%, 67.65%, and 54.87% of 6-h old, 24-h old and 48-h old biofilms, respectively.

In addition to Section 2.2.3 Contact surface: Stainless steel coupons of 316L, 304, 430 with 2B finish and 304 with BA finish were studied for *V. parahaemolyticus* biofilm formation. The roughest surface was 316L/2B, the least roughness was 430/2B and 304/BA. V. parahaemolyticus attached better on rougher surfaces (Tantratian et al., 2022).

In addition to Table 2.4:

Disinfectants	Biofilms	Reduction	Reference
Benzalkonium chloride (BAC) -0.02%	24-h and 72-h old biofilms	5-min exposure reduced biofilm cells to non-detectable levels	(Tantratian et al., 2022)

In addition to Section 2.4.2.4: Engineering Lysqdvp001 with outer membrane destabilizing peptides assisted in improving antibiofilm efficacy, sTHA-Lysqdvp001 at MIC (50 μg/mL) removed 82% of mature *V. parahaemolyticus* biofilms (10-h old, 37℃) (Ning et al., 2023).

2.7 Reference

Ashrafudoulla, M., Mizan, M. F. R., Park, H., Byun, K. H., Lee, N., Park, S. H., & Ha, S. D. (2019). Genetic Relationship, Virulence Factors, Drug Resistance Profile and Biofilm Formation Ability of *Vibrio parahaemolyticus* Isolated From Mussel [Original Research]. *Frontiers in Microbiology*, *10*(513), 513. https://doi.org/10.3389/fmicb.2019.00513

Boles, B. R., & McCarter, L. L. (2002). *Vibrio parahaemolyticus scrABC*, a novel operon affecting swarming and capsular polysaccharide regulation. *Journal of Bacteriology*, *184*(21), 5946-5954. https://doi.org/10.1128/JB.184.21.5946-5954.2002

Brauge, T., Faille, C., Leleu, G., Denis, C., Hanin, A., & Midelet, G. (2020). Treatment with disinfectants may induce an increase in viable but non culturable populations of *Listeria monocytogenes* in biofilms formed in smoked salmon processing environments. *Food Microbiology*, *92*, 103548. https://doi.org/10.1016/j.fm.2020.103548

Brooks, J. D., & Flint, S. H. (2008). Biofilms in the food industry: problems and potential solutions. *International Journal of Food Science & Technology*, *43*(12), 2163-2176.

Burfoot, D., Limburn, R., & Busby, R. (2017). Assessing the effects of incorporating bubbles into the water used for cleaning operations relevant to the food industry. *International Journal of Food Science & Technology*, *52*(8), 1894-1903. https://doi.org/10.1111/ijfs.13465

Byun, K.-H., Na, K. W., Ashrafudoulla, M., Choi, M. W., Han, S. H., Kang, I., Park, S. H., & Ha, S.-D. (2022). Combination treatment of peroxyacetic acid or lactic acid with UV-C to control *Salmonella* Enteritidis biofilms on food contact surface and chicken skin. *Food Microbiology*, *102*, 103906.

Chaiyakosa, S., Charernjiratragul, W., Umsakul, K., & Vuddhakul, V. (2007). Comparing the efficiency of chitosan with chlorine for reducing *Vibrio parahaemolyticus* in shrimp. *Food Control*, *18*(9), 1031-1035.

Chen, B., Huang, J., Li, H., Zeng, Q.-H., Wang, J. J., Liu, H., Pan, Y., & Zhao, Y. (2020). Eradication of planktonic *Vibrio parahaemolyticus* and its sessile biofilm by curcumin-mediated photodynamic inactivation. *Food Control*, *113*, 107181. https://doi.org/10.1016/j.foodcont.2020.107181

Choi, M.-S., Jeon, E. B., Kim, J. Y., Choi, E. H., Lim, J. S., Choi, J., & Park, S. Y. (2022). Application of dielectric barrier discharge plasma for the reduction of non-pathogenic *Escherichia coli* and *E. coli* O157:H7 and the quality stability of fresh oysters (*Crassostrea gigas*). *LWT*, *154*, 112698.

Christen, M., Kamischke, C., Kulasekara, H. D., Olivas, K. C., Kulasekara, B. R., Christen, B., Kline, T., & Miller, S. I. (2019). Identification of Small-Molecule Modulators of Diguanylate Cyclase by FRET-Based High-Throughput Screening. *Chembiochem*, *20*(3), 394-407. https://doi.org/10.1002/cbic.201800593

Costello, C., Cao, L., Gelcich, S., Cisneros-Mata, M. A., Free, C. M., Froehlich, H. E., Golden, C. D., Ishimura, G., Maier, J., Macadam-Somer, I., Mangin, T., Melnychuk, M. C., Miyahara, M., de Moor, C. L., Naylor, R., Nostbakken, L., Ojea, E., O'Reilly, E., Parma, A. M., Plantinga, A. J., Thilsted, S. H., & Lubchenco, J. (2020). The future of food from the sea. *Nature*, *588*(7836), 95-100. https://doi.org/10.1038/s41586-020-2616-y

Cruz, C., Hedderley, D., & Fletcher, G. (2015). Long-term study of *Vibrio parahaemolyticus* prevalence and distribution in New Zealand shellfish. *Applied and environmental microbiology*, *81*(7), 2320-2327.

Enos-Berlage, J. L., Guvener, Z. T., Keenan, C. E., & McCarter, L. L. (2005). Genetic determinants of biofilm development of opaque and translucent *Vibrio parahaemolyticus*. *Molecular Microbiology*, *55*(4), 1160-1182. https://doi.org/10.1111/j.1365-2958.2004.04453.x

Enos-Berlage, J. L., & McCarter, L. L. (2000). Relation of capsular polysaccharide production and colonial cell organization to colony morphology in *Vibrio parahaemolyticus*. *Journal of Bacteriology*, *182*(19), 5513-5520. https://doi.org/10.1128/JB.182.19.5513-5520.2000

FAO. (2021). Advances in science and risk assessment tools for *Vibrio parahaemolyticus* and *V. vulnificus* associated with seafood: meeting report (9240024875).

Freitas, C., Glatter, T., & Ringgaard, S. (2020). The release of a distinct cell type from swarm colonies facilitates dissemination of *Vibrio parahaemolyticus* in the environment. *The ISME Journal*, *14*(1), 230-244. https://doi.org/10.1038/s41396-019-0521-x

Guo, L., Wang, J., Gou, Y., Tan, L., Liu, H., Pan, Y., & Zhao, Y. (2020). Comparative proteomics reveals stress responses of *Vibrio parahaemolyticus* biofilm on different surfaces: Internal adaptation and external adjustment. *Science of the Total Environment*, *731*, 138386. https://doi.org/10.1016/j.scitotenv.2020.138386

Guvener, Z. T., & McCarter, L. L. (2003). Multiple regulators control capsular polysaccharide production in *Vibrio parahaemolyticus*. *Journal of Bacteriology*, *185*(18), 5431-5441. https://doi.org/10.1128/JB.185.18.5431-5441.2003

Hamza, F., Satpute, S., Banpurkar, A., Kumar, A. R., & Zinjarde, S. (2017). Biosurfactant from a marine bacterium disrupts biofilms of pathogenic bacteria in a tropical aquaculture system. *FEMS Microbiology Ecology*, *93*(11). https://doi.org/10.1093/femsec/fix140

Han, F., Gu, R.-R., Shen, X.-S., Chen, Y.-G., Tian, L.-L., Zhou, W.-F., & Cai, Y.-Q. (2017). Detection of total and pathogenic *Vibrio parahaemolyticus* in shellfish growing along the south yellow sea and the East China sea. *Journal of Food protection*, *80*(11), 1882-1889.

Han, N., Mizan, M. F. R., Jahid, I. K., & Ha, S.-D. (2016). Biofilm formation by *Vibrio parahaemolyticus* on food and food contact surfaces increases with rise in temperature. *Food Control*, *70*, 161-166. https://doi.org/10.1016/j.foodcont.2016.05.054

Han, Q., Song, X., Zhang, Z., Fu, J., Wang, X., Malakar, P. K., Liu, H., Pan, Y., & Zhao, Y. (2017). Removal of Foodborne Pathogen Biofilms by Acidic Electrolyzed Water. *Frontiers in Microbiology*, *8*, 988. https://doi.org/10.3389/fmicb.2017.00988

Houry, A., Gohar, M., Deschamps, J., Tischenko, E., Aymerich, S., Gruss, A., & Briandet, R. (2012). Bacterial swimmers that infiltrate and take over the biofilm matrix. *Proceedings of the National Academy of Sciences of the United States of America*, *109*(32), 13088-13093. https://doi.org/10.1073/pnas.1200791109

Kim, Y. K., & McCarter, L. L. (2000). Analysis of the polar flagellar gene system of *Vibrio parahaemolyticus*. *Journal of Bacteriology*, *182*(13), 3693-3704.

Kimbrough, J. H., Cribbs, J. T., & McCarter, L. L. (2020). Homologous c-di-GMP-Binding Scr Transcription Factors Orchestrate Biofilm Development in *Vibrio parahaemolyticus*. *Journal of Bacteriology*, *202*(6). https://doi.org/10.1128/JB.00723-19

Konrad, S., Paduraru, P., Romero-Barrios, P., Henderson, S. B., & Galanis, E. (2017). Remote sensing measurements of sea surface temperature as an indicator of *Vibrio parahaemolyticus* in oyster meat and human illnesses. *Environmental Health*, *16*(1), 1-11.

Li, Y., Dong, R., Ma, L., Qian, Y., & Liu, Z. (2022). Combined Anti-Biofilm Enzymes Strengthen the Eradicate Effect of *Vibrio parahaemolyticus* Biofilm: Mechanism on *cpsA-J* Expression and Application on Different Carriers. *Foods*, *11*(9), 1305. https://www.mdpi.com/2304-8158/11/9/1305

Li, Y., Tan, L., Guo, L., Zhang, P., Malakar, P. K., Ahmed, F., Liu, H., Wang, J. J., & Zhao, Y. (2020). Acidic electrolyzed water more effectively breaks down mature *Vibrio parahaemolyticus* biofilm than DNase I. *Food Control*, *117*, 107312. https://doi.org/10.1016/j.foodcont.2020.107312

Liao, Q., Tao, H., Li, Y., Xu, Y., & Wang, H. L. (2021). Evaluation of Structural Changes and Molecular Mechanism Induced by High Hydrostatic Pressure in *Enterobacter sakazakii* [Original Research]. *Frontiers in Nutrition*, *8*(669), 739863. https://doi.org/10.3389/fnut.2021.739863

Liu, C., Gu, Z., Lin, X., Wang, Y., Wang, A., Sun, Y., & Shi, Y. (2022). Effects of high hydrostatic pressure (HHP) and storage temperature on bacterial counts, color change, fatty acids and non-volatile taste active compounds of oysters (*Crassostrea ariakensis*). *Food Chemistry*, *372*, 131247. https://doi.org/10.1016/j.foodchem.2021.131247

Liu, D. Z., Jindal, S., Amamcharla, J., Anand, S., & Metzger, L. (2017). Short communication: Evaluation of a sol-gel-based stainless steel surface modification to reduce fouling and biofilm formation during pasteurization of milk. *Journal of Dairy Science*, *100*(4), 2577-2581. https://doi.org/10.3168/jds.2016-12141

Liu, M., Zhu, X., Zhang, C., & Zhao, Z. (2021). LuxQ-LuxU-LuxO pathway regulates biofilm formation by *Vibrio parahaemolyticus*. *Microbiological Research*, *250*, 126791. https://doi.org/10.1016/j.micres.2021.126791

Martinez-Urtaza, J., Bowers, J. C., Trinanes, J., & DePaola, A. (2010). Climate anomalies and the increasing risk of *Vibrio parahaemolyticus* and *Vibrio vulnificus* illnesses. *Food Research International*, *43*(7), 1780-1790.

Mizan, M. F., Jahid, I. K., Kim, M., Lee, K. H., Kim, T. J., & Ha, S. D. (2016). Variability in biofilm formation correlates with hydrophobicity and quorum sensing among *Vibrio parahaemolyticus* isolates from food contact surfaces and the distribution of the genes involved in biofilm formation. *Biofouling*, *32*(4), 497-509. https://doi.org/10.1080/08927014.2016.1149571

Mizan, M. F. R., Ashrafudoulla, M., Sadekuzzaman, M., Kang, I., & Ha, S.-D. (2018). Effects of NaCl, glucose, and their combinations on biofilm formation on black tiger shrimp (*Penaeus monodon*) surfaces by *Vibrio parahaemolyticus*. *Food Control*, *89*, 203-209. https://doi.org/10.1016/j.foodcont.2017.12.004

Montso, P. K., Mlambo, V., & Ateba, C. N. (2021). Efficacy of novel phages for control of multi-drug resistant *Escherichia coli* O177 on artificially contaminated beef and their potential to disrupt biofilm formation. *Food Microbiology*, *94*, 103647. https://doi.org/10.1016/j.fm.2020.103647

Mougin, J., Copin, S., Bojolly, D., Raguenet, V., Robert-Pillot, A., Quilici, M.-L., Midelet-Bourdin, G., Grard, T., & Bonnin-Jusserand, M. (2019). Adhesion to stainless steel surfaces and detection of viable but non cultivable cells of *Vibrio parahaemolyticus* and *Vibrio cholerae* isolated from shrimps in seafood processing environments: Stayin' alive? *Food Control*, *102*, 122-130. https://doi.org/10.1016/j.foodcont.2019.03.024

MPI. (2001). Microbial Pathogen Data Sheets: *Vibrio Parahaemolyticus*. https://www.mpi.govt.nz/dmsdocument/11033-Vibrio-parahaemolyticus-Microbial-pathogen-data-sheet

Ndraha, N., & Hsiao, H.-I. (2021). Influence of climatic factors on the temporal occurrence and distribution of total and pathogenic *Vibrio parahaemolyticus* in oyster culture environments in Taiwan. *Food Microbiology*, *98*, 103765.

Ning, H., Zhang, J., Wang, Y., Lin, H., & Wang, J. (2023). Development of highly efficient artilysins against *Vibrio parahaemolyticus* via virtual screening assisted by molecular docking. *Food Control*, *146*, 109521.

Ning, H. Q., Lin, H., & Wang, J. X. (2021). Synergistic effects of endolysin Lysqdvp001 and epsilon-poly-lysine in controlling *Vibrio parahaemolyticus* and its biofilms. *International Journal of Food Microbiology*, *343*, 109112. https://doi.org/10.1016/j.ijfoodmicro.2021.109112

Odeyemi, O. A. (2016). Incidence and prevalence of *Vibrio parahaemolyticus* in seafood: a systematic review and meta-analysis. *Springerplus*, *5*(1), 464. https://doi.org/10.1186/s40064-016-2115-7

Palmer, J., Flint, S., & Brooks, J. (2007). Bacterial cell attachment, the beginning of a biofilm. *Journal of Industrial Microbiology and Biotechnology*, *34*(9), 577-588. https://doi.org/10.1007/s10295-007-0234-4

Patange, A., Boehm, D., Ziuzina, D., Cullen, P. J., Gilmore, B., & Bourke, P. (2019). High voltage atmospheric cold air plasma control of bacterial biofilms on fresh produce. *International Journal of Food Microbiology*, *293*, 137-145. https://doi.org/10.1016/j.ijfoodmicro.2019.01.005

Pattis, I. H., Beverley; Armstrong, Bridget; Cressey, Peter; Lopez, Liza;. (2020). Annual Report Concerning Foodborne Disease in New Zealand 2019. https://www.mpi.govt.nz/dmsdocument/42874-Annual-report-concerning-foodborne-disease-in-New-Zealand-2019

Pattis, I. H., Beverley; Cressey, Peter; Armstrong, Bridget; Lopez, Liza; Soboleva, Tanyz;. (2022). Annual report concerning foodborne diseases in New Zealand 2021. https://www.mpi.govt.nz/dmsdocument/53872-Annual-report-concerning-Foodborne-Diseases-in-New-Zealand-2021-

Pedrós-Garrido, S., Condón-Abanto, S., Beltrán, J. A., Lyng, J. G., Brunton, N. P., Bolton, D., & Whyte, P. (2017). Assessment of high intensity ultrasound for surface decontamination of salmon (*S. salar*), mackerel (*S. scombrus*), cod (*G. morhua*) and hake (*M. merluccius*) fillets, and its impact on fish quality. *Innovative Food Science & Emerging Technologies*, *41*, 64-70. https://doi.org/10.1016/j.ifset.2017.02.006

Robinson, R. K. (2014). *Encyclopedia of food microbiology*. Academic press.

Rosa, J. V., Conceição, N. V., Conceição, R. C. S., & Timm, C. (2018). Biofilm formation by *Vibrio parahaemolyticus* on different surfaces and its resistance to sodium hypochlorite. *Ciência Rural*, *48*.

Roy, P. K., Mizan, M. F. R., Hossain, M. I., Han, N., Nahar, S., Ashrafudoulla, M., Toushik, S. H., Shim, W.-B., Kim, Y.-M., & Ha, S.-D. (2021). Elimination of *Vibrio parahaemolyticus* biofilms on crab and shrimp surfaces using ultraviolet C irradiation coupled with sodium hypochlorite and slightly acidic electrolyzed water. *Food Control*, *128*, 108179. https://doi.org/10.1016/j.foodcont.2021.108179

Santhakumari, S., Jayakumar, R., Logalakshmi, R., Prabhu, N. M., Abdul Nazar, A. K., Karutha Pandian, S., & Veera Ravi, A. (2018). *In vitro* and *in vivo* effect of 2,6-Di-tert-butyl-4-methylphenol as an antibiofilm agent against quorum sensing mediated biofilm formation of *Vibrio* spp. *International Journal of Food Microbiology*, *281*, 60-71. https://doi.org/10.1016/j.ijfoodmicro.2018.05.024

Shikongo-Nambabi, M. N. N. N., Kachigunda, B., & Venter, S. N. (2010). Evaluation of oxidising disinfectants to control *Vibrio* biofilms in treated seawater used for fish processing. *Water SA*, *36*, 215-220. http://www.scielo.org.za/scielo.php?script=sci_arttext&pid=S1816-79502010000300003&nrm=iso

Shiroodi, S., Schwarz, M. H., Nitin, N., & Ovissipour, R. (2021). Efficacy of Nanobubbles Alone or in Combination with Neutral Electrolyzed Water in Removing *Escherichia coli* O157:H7, *Vibrio parahaemolyticus*, and *Listeria innocua* Biofilms. *Food and Bioprocess Technology*, *14*(2), 287-297. https://doi.org/10.1007/s11947-020-02572-0

Song, X. Y., Ma, Y. J., Fu, J. J., Zhao, A. J., Guo, Z. R., Malakar, P. K., Pan, Y. J., & Zhao, Y. (2017). Effect of temperature on pathogenic and non-pathogenic *Vibrio parahaemolyticus* biofilm formation. *Food Control*, *73*, 485-491.

Steenackers, H. P., Parijs, I., Dubey, A., Foster, K. R., & Vanderleyden, J. (2016). Experimental evolution in biofilm populations. *FEMS Microbiology Reviews*, *40*(3), 373-397. https://doi.org/10.1093/femsre/fuw002

Sun, Y., Guo, D., Hua, Z., Sun, H., Zheng, Z., Xia, X., & Shi, C. (2019). Attenuation of Multiple *Vibrio parahaemolyticus* Virulence Factors by Citral. *Frontiers in Microbiology*, *10*, 894. https://doi.org/10.3389/fmicb.2019.00894

Takahashi, K., Tanaka, R., & Fukuzaki, S. (2016). Inactivation of *Vibrio parahaemolyticus* Unattached and Attached to a Solid Surface in pH-Controlled Sodium Hypochlorite Solutions. *Biocontrol Science*, *21*(4), 265-268. https://doi.org/10.4265/bio.21.265

Tan, L., Li, H., Chen, B., Huang, J., Li, Y., Zheng, H., Liu, H., Zhao, Y., & Wang, J. J. (2021). Dual-species biofilms formation of *Vibrio parahaemolyticus* and *Shewanella*

putrefaciens and their tolerance to photodynamic inactivation. *Food Control*, *125*, 107983. https://doi.org/10.1016/j.foodcont.2021.107983

Tan, L., Zhao, F., Han, Q., Zhao, A. J., Malakar, P. K., Liu, H. Q., Pan, Y. J., & Zhao, Y. (2018). High correlation between structure development and chemical variation during biofilm formation by *Vibrio parahaemolyticus*. *Frontiers in Microbiology*, *9*, 1881.

Tantratian, S., Srimangkornkaew, N., Prakitchaiwattana, C., & Sanguandeekul, R. (2022). Effect of different stainless steel surfaces on the formation and control of *Vibrio parahaemolyticus* biofilm. *LWT*, *166*, 113788.

Wong, H. (2002). Attachment and inactivation of *Vibrio parahaemolyticus* on stainless steel and glass surface. *Food Microbiology*, *19*(4), 341-350. https://doi.org/10.1006/fmic.2002.0478

Ye, L., Zheng, X., & Zheng, H. (2014). Effect of *sypQ* gene on poly-N-acetylglucosamine biosynthesis in *Vibrio parahaemolyticus* and its role in infection process. *Glycobiology*, *24*(4), 351-358. https://doi.org/10.1093/glycob/cwu001

Yildiz, F. H., & Visick, K. L. (2009). *Vibrio* biofilms: so much the same yet so different. *Trends in Microbiology*, *17*(3), 109-118. https://doi.org/10.1016/j.tim.2008.12.004

Yu, H., Liu, Y., Yang, F., Xie, Y., Guo, Y., Cheng, Y., & Yao, W. (2021). Combined an acoustic pressure simulation of ultrasonic radiation and experimental studies to evaluate control efficacy of high-intensity ultrasound against *Staphylococcus aureus* biofilm. *Ultrasonics Sonochemistry*, *79*, 105764.

Yu, H., & Rhee, M. S. (2023). Characterization of ready-to-eat fish surface as a potential source of contamination of *Vibrio parahaemolyticus* biofilms. *Food Research International*, *169*, 112890.

Zhang, H., Yang, Z., Zhou, Y., Bao, H., Wang, R., Li, T., Pang, M., Sun, L., & Zhou, X. (2018). Application of a phage in decontaminating *Vibrio parahaemolyticus* in oysters. *International Journal of Food Microbiology*, *275*, 24-31. https://doi.org/10.1016/j.ijfoodmicro.2018.03.027

Zhang, Y., Hu, L., Qiu, Y., Osei-Adjei, G., Tang, H., Zhang, Y., Zhang, R., Sheng, X., Xu, S., Yang, W., Yang, H., Yin, Z., Yang, R., Huang, X., & Zhou, D. (2019). QsvR integrates into quorum sensing circuit to control *Vibrio parahaemolyticus* virulence. *Environmental Microbiology*, *21*(3), 1054-1067. https://doi.org/10.1111/1462-2920.14524

Zhou, D., Yan, X., Qu, F., Wang, L., Zhang, Y., Hou, J., Hu, Y., Li, J., Xin, S., Qiu, J., Yang, R., & Mao, P. (2013). Quorum sensing modulates transcription of *cpsQ-mfpABC* and *mfpABC* in *Vibrio parahaemolyticus*. *International Journal of Food Microbiology*, *166*(3), 458-463. https://doi.org/10.1016/j.ijfoodmicro.2013.07.008

Zhu, W., Liu, J., Zou, Y., Li, S., Zhao, D., Wang, H., & Xia, X. (2023). Anti-Biofilm Activity of Laurel Essential Oil against *Vibrio parahaemolyticus*. *Foods*, *12*(19), 3658. https://www.mdpi.com/2304-8158/12/19/3658

Chapter 3. Biofilm forming abilities of *V. parahaemolyticus*

This chapter is an adaptation of material that was published (published article reproduced in Appendix VII) as a peer-reviewed article:

Wang, D., Fletcher, G. C., On, S. L., Palmer, J. S., Gagic, D., & Flint, S. H. (2023). Biofilm formation, sodium hypochlorite susceptibility and genetic diversity of *Vibrio parahaemolyticus*. *International Journal of Food Microbiology*, *385*, 110011.

3.1 Introduction

V. parahaemolyticus is a cause of food poisoning associated with consuming raw or undercooked seafood. It grows well between 14-19 ℃ and is prevalent during summer and autumn (Cruz et al., 2015; Han et al., 2017; Konrad et al., 2017; MPI, 2001; Ndraha & Hsiao, 2021). The average annual number of *Vibrio* infections in the United States increased by 54% between 2006 and 2017, and by 79% in 2019 (Abanto et al., 2020). The "Cholera and Other *Vibrio* Illness Surveillance System" in the United States received 4116 reports of *V. parahaemolyticus* infections between 2010 and 2018 (CDC, 2021). In China, they experienced an average of 523.5 recorded cases each year during 2010 and 2020 (FAO, 2021). Climate change has been proposed as an explanation for the global spread of *V. parahaemolyticus* infections (FAO, 2021). Outbreaks have been regularly reported in countries with no or sporadic incidence such as Canada, the United Kingdom, France, North Europe, New Zealand and Australia (Baker-Austin et al., 2020; Baker-Austin et al., 2018; FAO, 2021), raising concerns in the food industry.

There were 5149 *V. parahaemolyticus* isolates submitted to the Molecular Typing and Microbial Genome Diversity (PubMLST) Database by February 2022 (Jolley et al., 2018). Some pandemic clones are more virulent than others and have been implicated in several previous outbreaks. Sequence type 3 (ST3) emerged in Asia in the mid-1990s and spread throughout the world, becoming the most common pandemic clone by 2012 (Nair et al., 2007). Sequence type 36 (ST 36) strains were present at the Pacific Northwest and Canada (Daniels et al., 2000), but have spread further into Europe, involving the largest known food-borne *Vibrio* outbreak reported in Spain in 2012 (Martinez-Urtaza et al., 2018). ST 36, according to Abanto et al. (2020), can disperse intercontinentally due to its highly pathogenic and persistent nature, posing a threat to the safety of seafood products and human health. The

epidemiology of *V. parahaemolyticus* infections has shifted from the dominance of domestically redistricted strains to the transcontinental spread of new clones. However, the relationship between ST and biofilm-forming ability of *V. parahaemolyticus* is unknown.

Biofilm formation is a dynamic life cycle involving motility, attachment, biofilm production and dispersion; once biofilm develops, the endurance and environmental adaptability enable cells to survive environmental stress. *V. parahaemolyticus* as a biofilm has advantages in seafood environments. *V. parahaemolyticus* biofilms form on stainless steel, polystyrene, glass, and other abiotic surfaces in food processing equipment and packaging materials, showing a higher resistance than their planktonic counterparts, to cleaning and sanitation that may lead to recurring contamination (Rosa et al., 2018). Along with widespread awareness of *V. parahaemolyticus* control in seafood, it is required to understand biofilm formation of *V. parahaemolyticus*. Using *V. parahaemolyticus* strains from New Zealand, this part of study is to assess that whether *V. parahaemolyticus* form biofilms on seafood processing plant surfaces and the potential risks for seafood safety.

3.2 Methods

3.2.1 Cultures

There were ten strains used in this study, seven of them were kindly offered by Plant and Food Research Ltd., New Zealand, there were another two clinical isolates, PFR37D08 (National Health Index (NHI) No. 75/0294) and PFR37E03 (NHI No. CHE2822), which were provided by Institute of Environmental Science and Research (ESR), New Zealand. The reference strain incorporated in this study was RIMD2210633, that was imported from Research Institute for Microbial Disease, OSAKA University. Detailed information of strain number, collection date, isolation source, country of origin, pathogenicity and where cited is in Table 3.1.

Cultures were received either on agar slopes or freeze-dried ampoules. They were initially cultured in 3% NaCl TSB (Difco™, Becton, Dickson and Company, France), at 37 ℃ for 24 h. To indicate the purity, each culture was plated on Thiosulfate-Citrate-Bile Salts-Sucrose (TCBS, Difco™, Becton, Dickson and Company, France) agar, the growth of *V. parahaemolyticus* was indicated by a green colony due to the inability to ferment sucrose in the agar.

Strains were stored at -80 ℃ using a bead system (Protection, Thermo Fisher, USA). To revive a culture, one bead was inoculated into 3% NaCl TSB and incubated at 37 ℃ for 5-8 h, allowing it to enter stationary phase. Cultures were centrifuged (8427× *g*, 5 min) and washed using sterilized saline, harvested for further use.

3.2.2 Crystal violet (CV) assay

A CV assay was used to screen the isolates for the ability to form biofilm. A cell suspension was diluted to obtain an OD_{595} (Absorbance measurements at 595 nm) of 0.15 ± 0.05 using a microplate reader (Varioskan Lux 3020-1333, Thermo Fisher, USA), 200 µL of each culture was added into the well of a 96-well flat-bottom microtiter plate (6 biological replicates, 3 technical replicates; FALCON®, Corning Incorporated, Durham, USA). The plate was incubated at 37℃ for 72 h, then the OD_{595} was examined. The plate was inverted to remove the cultures, and each well was washed three times using 230 µL of distilled water, followed by 230 µL of ethanol for 10 min to fix the cells. The ethanol was removed, and the plate was allowed to dry. Then, each well was stained with 230 µL of 2% CV for 10 min, washed three times using distilled water, followed by 210 µL of 33% acetic acid added into each well to dissolve the CV stain. The absorbance of resulting solution in each well was measured at 570

Table 3. 1 Information of *V. parahaemolyticus* candidate strains used in this study.

No.	Strain	Source	Pathogenicity	Collection date	Country of origin	Reference
1	PFR21C03	Pacific oyster	Non-pathogenetic	16/02/2009	New Zealand	
2	PFR24B07	Greenshell™ mussel	Non-pathogenetic	2/03/2010	New Zealand	
3	PFR29A04	Pacific oyster	Non-pathogenetic	22/11/2010	New Zealand	
4	PFR30G02	Pacific oyster	Non-pathogenetic	8/03/2011	New Zealand	
5	PFR30J09	Pacific oyster	Non-pathogenetic	21/03/2011	New Zealand	(Cruz et al., 2015)
6	PFR34B02	Pacific oyster	Non-pathogenetic	27/03/2012	New Zealand	
7	PFR37C06	Pacific oyster	Non-pathogenetic	17/01/2013	New Zealand	
8	PFR37D08	Clinical	Pathogenetic	1/01/2013	New Zealand	
9	PFR37E03	Clinical NZRM 3391	Pathogenetic	1/01/1975	New Zealand	
10	RIMD2210633	Clinical	Pathogenetic	1996	Japan	(Makino et al., 2003)

Table 3. 2 Multi-locus sequence typing (MLST) information of *V. parahaemolyticus* candidate strains used in this study.

Strains	MLST ST	Nearest ST match (loci hits)	*dnaE*	*gyrB*	*recA*	*dtdS*	*pntA*	*pyrC*	*tnaA*
PFR21C03	2632	-	*dnaE (226)*	*gyrB (25)*	*recA (97)*	*dtdS (19)*	*pntA (26)*	*pyrC (49)*	*tnaA (26)*
PFR24B07	New ST	2651(6)	*dnaE (175)*	*gyrB (235)*	*recA(3)*	*dtdS (85)*	*pntA (65)*	*pyrC (~68)*	*tnaA (23)*
PFR29A04	1357	-	*dnaE (162)*	*gyrB (399)*	*recA (80)*	*dtdS (150)*	*pntA (11)*	*pyrC (158)*	*tnaA (51)*
PFR30G02	1772	-	*dnaE (47)*	*gyrB (287)*	*recA (19)*	*dtdS (252)*	*pntA (245)*	*pyrC (18)*	*tnaA (217)*
PFR30J09	New ST	2650(3)	*dnaE (60)*	*gyrB (406)*	*recA (366)*	*dtdS (390)*	*pntA (18)*	*pyrC (94)*	*tnaA (47)*
PFR34B02	New ST	2648(6)	*dnaE (36)*	*gyrB (4)*	*recA (81)*	*dtdS (27)*	*pntA (26)*	*pyrC (82)*	*tnaA (225)*
PFR37C06	New ST	2650(5)	*dnaE (60)*	*gyrB (406)*	*recA (257)*	*dtdS (390)*	*pntA (~156)*	*pyrC (221)*	*tnaA (47)*
PFR37D08	36	-	*dnaE (21)*	*gyrB (15)*	*recA (1)*	*dtdS (23)*	*pntA (23)*	*pyrC (~21)*	*tnaA (16)*
PFR37E03	1140	-	*dnaE (19)*	*gyrB (295)*	*recA (295)*	*dtdS (223)*	*pntA (136)*	*pyrC (11)*	*tnaA (13)*

*In this table, *dnaE*, *gyrB*, *recA*, *dtdS*, *pntA*, *pyrC* and *tnaA* are housekeeping genes in *V. parahaemolyticus*, and distinct parameters reflect their varied multi-locus sequence typing (MLST) information. All 7 housekeeping loci matched with the PubMLST database otherwise, nearest match and loci hit numbers were shown above.

nm, and the biofilm forming index (BFI) of each strain was evaluated using the following equation:

$$BFI = \frac{(OD_{570} - OD_{570con})}{(OD_{595} - OD_{595con})}$$

OD_{570} and OD_{595} represent the absorbance value of sample wells at 570 nm and 595 nm, respectively. OD_{570con} and OD_{595con} represent the absorbance value of wells with only TSB containing 3% NaCl as a blank. The degree of biofilm formation was classified according to Naves et al. (2008): strong (BFI ≥ 1.10), moderate (1.09 ≥ BFI ≥ 0.70), weak (0.69 ≥ BFI ≥ 0.35) and none (BFI < 0.35).

3.2.3 Growth dynamic of *V. parahaemolyticus* biofilms

3.2.3.1 Coupon preparation

Coupon preparation was to remove leftover biofilms and pathogens. Stainless steel coupons (10 mm^2, 1 mm thick, 304 grade with a 2B finish; Advanced Sheetmetals, New Zealand) were used in this study to represent surfaces used for processing seafood. Coupons had previously been passivated and used in other experiments. Coupons were soaked in NaOH (1%, w/v; pH ~13.0; Merck KGaA, Darmstadt, Germany) for 35-40 min, then sonicated with mild heat (DT52; BANDELIN, Berlin, Germany) for 60 min. The coupons were rinsed with ~ 250 mL distilled water, then left to dry at 45 ℃ overnight. The cleaned coupons were then ready for dry cycle autoclaving at 121 ℃ for 15 min. Coupons were freshly prepared for each set of experiments.

3.2.3.2 Biofilm development

Each stainless steel coupon was placed flat in a well of a 48-well plastic plate (FALCON®, Corning Incorporated, Durham, USA) with 1 mL of *V. parahaemolyticus* cell culture (cell

concentration: ~ 4 $\log_{10}$ CFU/mL) in 3% NaCl TSB and incubated under a static condition at 25 ℃ to allow for biofilm formation.

3.2.3.3 Detachment of biofilm cells from stainless steel surfaces

The number of culturable cells in the biofilm matrix was determined using a bead vortex mixing method reported previously with minor modifications (Hayrapetyan et al., 2015). In short, each coupon was rinsed three times using sterile distilled water to remove planktonic cells and transferred it into a 25 mL glass bottle filled with 10 mL of 0.1% peptone buffered water (GranuCult™, Merck KGaA, Billerica MA, USA) including 1% NaCl and 5 g of sterile glass beads (~5 mm diameter, Sigma-Aldrich®, Merck, Darmstadt, Germany), followed by 1 min vortex mixing to disrupt the biofilm matrix from the stainless steel surface and obtain individual cells.

3.2.3.4 Biofilm cell enumeration using agar plate counting

Detached biofilm cell cultures were vortexed at 6000 × *g*. Serial 10-fold dilutions were prepared in 0.1% buffered peptone water with 1% NaCl, used to inoculate on 3% NaCl TSA plates, and incubated at 37 ℃ for 18 h before counting.

3.2.4 Fluorescence microscope screen

To visualize the biofilm, coupons with cultured biofilms (media: TSB containing 3% NaCl; temperature: 25 ℃; time: 6 h) were rinsed with sterile distilled water three times and allowed to half dry on a glass microscope slide. To stain, 1 drop of calcofluor white stain (Calcofluor white M2R 1g/L, Sigma-Aldrich®, Merck KGaA, Darmstadt, Germany) was placed on each coupon and left for 1 min before washing with sterile distilled water, allowing to partially dry. The stained samples were examined using an epifluorescent microscope (BX53; Olympus

Corp., Japan) equipped with a DAPI filter (excitation at 340–360 nm, emission at 410 nm), the images were captured by the cellSense Dimension program.

3.2.5 Statistical analysis

All experiments were performed with two or three biological replicates and three technical replicates. One-way variance analysis (ANOVA) was generated to evaluate the significant differences among experimental results using Duncan's multiple range test with a p value below 0.05 considered as statistically significant. Data analysis was implemented using SPSS Statistics software (version 29.0.2.0; IBM®, New York, United States).

3.3 Results

3.3.1 CV assay

The CV assay revealed that PFR30J09 and PFR34B02 formed the best biofilms, with CV values of 2.56 ± 1.28 and 2.47 ± 0.63, respectively. See Figure 3.1(a). Least biomass was observed from results of PFR21C03, PFR24B07, PFR37C06 and PFR37E03, with CV values of 1.42 ±0.45, 1.19 ± 0.18, 1.53 ± 0.11 and 1.32 ± 0.12, respectively. Results of BFI indices were consistent with those of CV values, see Figure 3.1(b). Highest BFI values were 1.21 ± 0.63 and 1.10 ± 0.20 observed in strain PFR30J09 and PFR34B02. Lowest values were obtained in PFR21C03, PFR24B07, PFR37C06 and PFR37E03, they were 0.64 ± 0.21, 0.51 ± 0.07, 0.61 ± 0.02 and 0.56 ± 0.06, respectively. According to classification criteria of biofilm-forming degree based on BFI values (See Section 3.2.2), strong biofilm forming strains are PFR30J09 and PFR34B02, weak biofilm forming strains are PFR21C03, PFR24B07, PFR37C06 and PFR37E03.

3.3.2 Biofilm growth dynamic within 24 h

Biofilm formation by *V. parahaemolyticus* on stainless steel coupons is shown in Figure 3.2. In general, viable cell numbers in *V. parahaemolyticus* biofilms increased from ~ 4 $\log_{10}$ CFU/cm^2 to ~ 7 $\log_{10}$ CFU/cm^2 at 25 °C within 24 h incubation. In the first 6-h incubation, cell population on stainless steel coupons was increasing. Biofilm cell numbers reached a maximum of 6.63 ± 0.11 (PFR21C03, at 6th hour), 6.87 ± 0.10 (PFR24B07, at 12th hour), 6.89 ± 0.18 (PFR29A03, at 6th hour), 6.91 ± 0.08 (PFR30G02, at 6th hour), 7.20 ± 0.15 (PFR30J09, at 6th hour), 7.08 ± 0.15 (PFR34B02, at 6th hour), 6.92 ± 0.17 (PFR37C06, at 6th hour), 6.41 ± 0.56 (PFR37D08, at 11th hour) and 6.98 ± 1.13 (PFR37E03, at 11th hour) $\log_{10}$ CFU/cm^2, respectively. For PFR24B07, PFR37D08 and PFR37E03, cell population in *V. parahaemolyticus* matrix at 6th hour was 6.63 ± 0.13, 5.88 ± 0.18 and 5.23 ± 0.52 $\log_{10}$ CFU/cm^2, respectively. Biofilm cell numbers encountered a mild decrease or remained stable after 6 h.

3.3.3 Epifluorescence microscopy screen of biofilm cells

Calcofluor white can stain 1-3 β and 1-4 β polysaccharides of biofilms. And polysaccharide content was visualized using epifluorescence microscopy following calcofluor white staining. *V. parahaemolyticus* on stainless steel coupons was stained after 6-h incubation at 25 °C. According to Figure 3.3, the most biomass was produced by PFR30J09 and PFR34B02 with dense and strong blue fluorescence. Other samples had a flat and loose sessile cell distribution with fewer cell clusters.

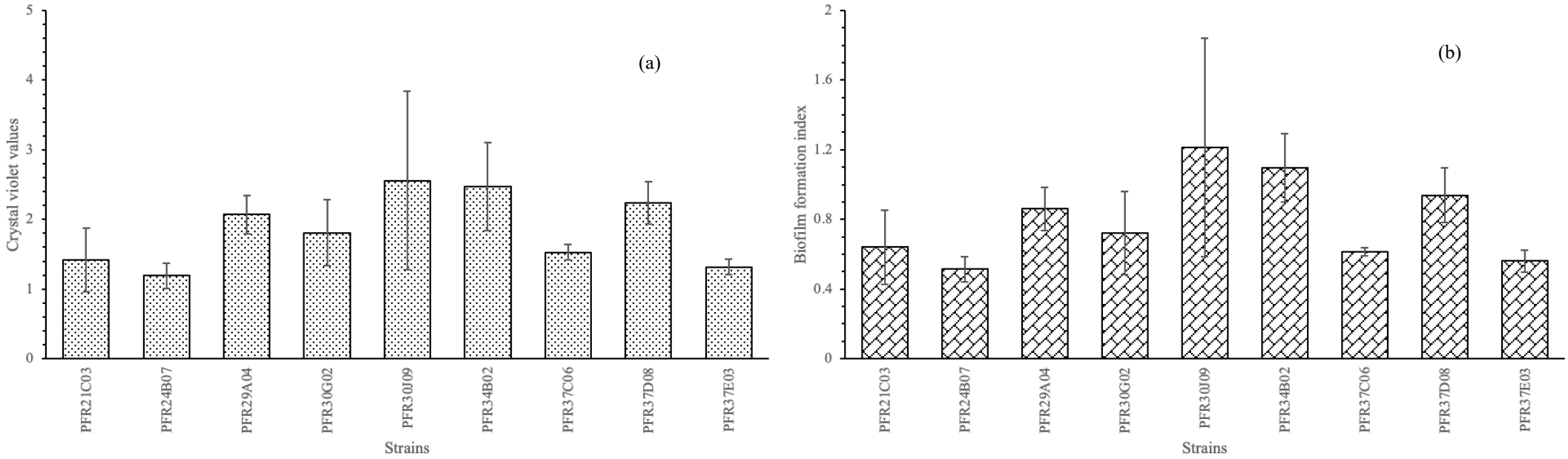

Figure 3. 1 Biofilm forming ability of *V. parahaemolyticus* strains.

Biofilms were formed at 37 °C for 72 h in medium of TSB containing 3% NaCl. (a) presents the OD readings of crystal violet staining. (b) shows their biofilm formation index results. Results are represented as Mean ± SD.

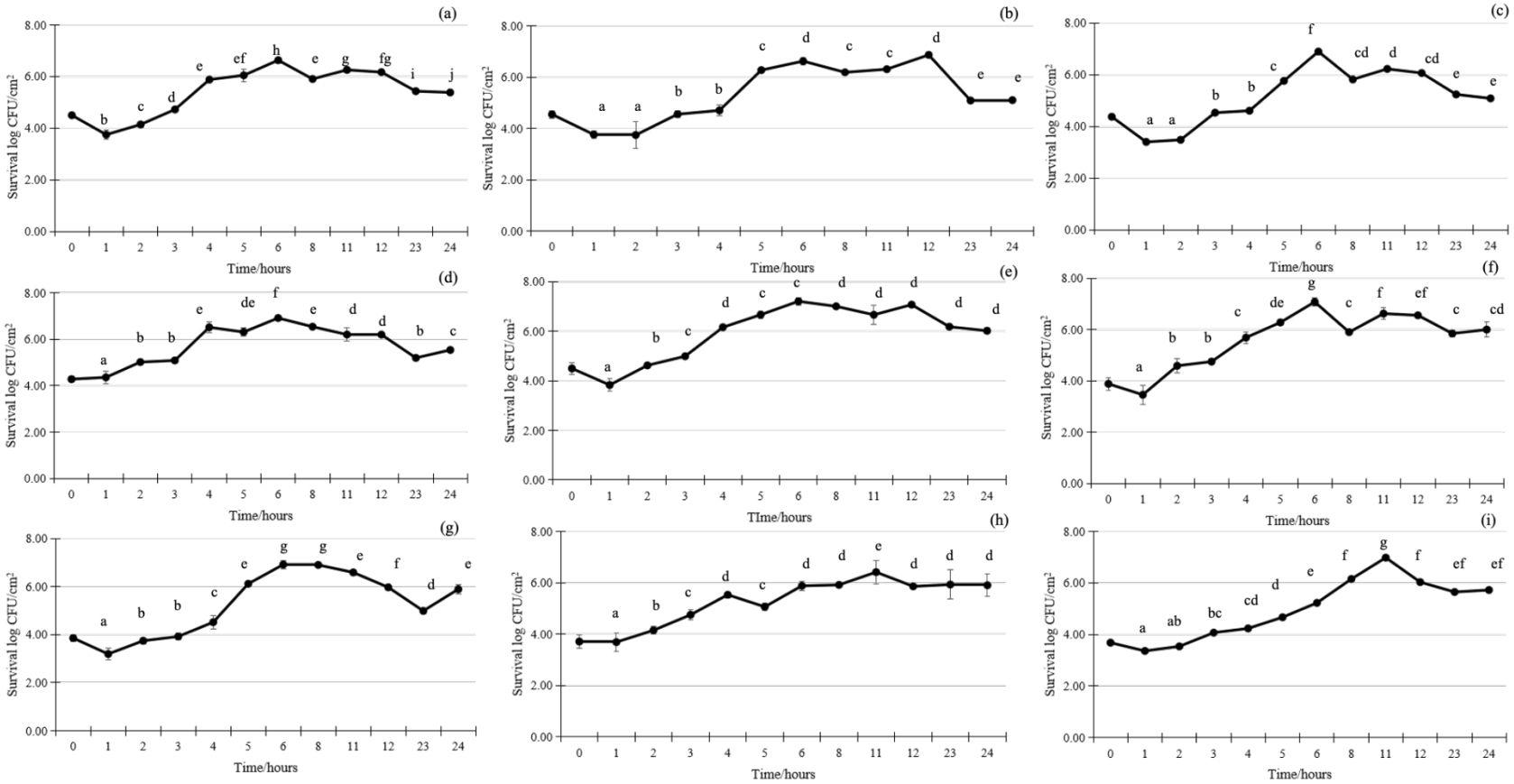

Figure 3. 2 *V. parahaemolyticus* growth on stainless steel coupons at 25 °C within 24 h.

The indications for strains are as follows: (a) PFR21C03, (b) PFR24B07, (c) PFR29A04, (d) PFR30G02, (e) PFR30J09, (f) PFR34B02, (g) PFR37C06, (h) PFR37D08 and (i) PFR37E03. Different letters indicate significant difference ($p < 0.05$) according to Duncan's multiple range test.

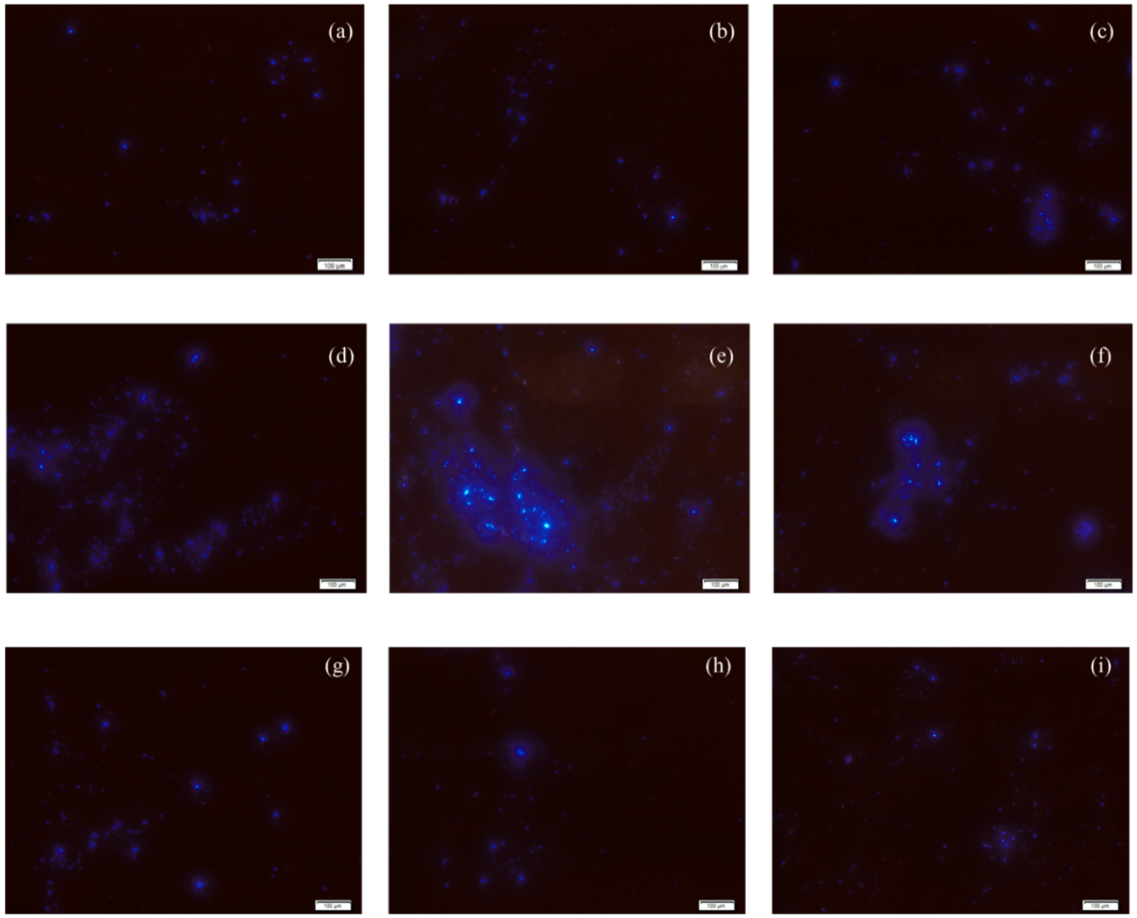

Figure 3. 3 Epifluorescence microscope screen of sessile *V. parahaemolyticus* on stainless steel.

Blue fluorescence was emitted from calcofluor white stain when binding with polysaccharides in biofilms. The indications for strains are as follows:

(a) PFR21C03, (b) PFR24B07, (c) PFR29A04, (d) PFR30G02, (e) PFR30J09, (f) PFR34B02, (g) PFR37C06, (h) PFR37D08 and (i) PFR37E03.

3.4 Discussion

Using the microtiter plate assay, CV staining of cell biomass and BFI determination have been commonly used to reveal biofilm forming abilities of bacteria (Naves et al., 2008). There are limitations of the CV assay. Kragh et al. (2019) concluded that this method cannot identify live cells, EPS and dead cells, meanwhile this method lacks reproducibility. Determining growth dynamics of biofilm communities in the present study contributed to indicate live cell numbers in the biofilm matrix. As stainless steel is one of the most frequently used surfaces in the food industry, determining biofilm formation of *V. parahaemolyticus* on stainless steel is critical for the food industry. Calcofluor white stain can bind to β-linked polysaccharides and emit blue fluorescence. In the present study, the epifluorescence microscopy screen using calcofluor white as the stain provided a direct, visual approach to define microbial biofilm forming ability, and distinct variations in EPS production were observed in this study using this stain.

In the present study, strains PFR30J09 and PFR34B02 produced the highest CV readings, indicating these two strains produced the most biomass on the surface of the 96-well flat-bottom microtiter plate at 37 °C. The least amount of biomass using CV as a stain was observed in PFR21C03, PFR24B07, PFR37C06 and PFR37E03 (Figure 3.1). The use of the BFI as outlined in section 3.3.2 classified Strain PFR30J09 and PFR34B02 as strong biofilm formers according the classification criteria by Naves et al. (2008). Based on the BFI results, weak biofilms on polystyrene surfaces were produced by PFR21C03, PFR24B07, PFR37C06 and PFR37E03, intermediate biofilms were produced by PFR29A04, PFR30G02 and PFR37D08. Strain variability in biofilm formation has been reported in other studies, for example, Song et al. (2017) reported the biofilm formation of 39 *V. parahaemolyticus* isolates at 15, 25 and 37 °C after incubation for 2, 8, 12, 24, and 48 h, using the CV assay. The biofilm formation abilities of strains varied with different culture conditions, the ratio of strong biofilm forming strains

were 51.3%, 97.4% and 41.0% when incubated for 24 h at 15, 25 and 37 °C, respectively. The criteria to classify weak, moderate, and strong biofilm formers were based on optical density of crystal violet stained samples (OD_{570nm}) and negative controls (ODc): non-biofilm producer ($OD_{570nm} \leq$ ODc), weak biofilm producer (ODc < $OD_{570nm} \leq$ 2-times ODc), moderate biofilm producer (2-times ODc < $OD_{570nm} \leq$ 4-times ODc), and strong biofilm producer (OD_{570nm} > 4-times ODc). The results exhibited variations when biofilms were cultured at different temperatures, with an increase in the variability when the temperature favors *V. parahaemolyticus* growth. This might be due to strain specific properties and the survival state of bacteria. Strain variability of biofilm forming ability was also studied in *S. enterica*, using the CV assay, with variation in biofilm formation under different culture conditions (pH, NaCl concentrations and temperatures) (Lianou & Koutsoumanis, 2012).

By determining viable biofilm cell numbers on stainless steel surfaces during biofilm incubation within 24 h, a dynamic biofilm growth curve was prepared, showing the peak of biofilm growth curve with the highest cell numbers for each strain. In the present study *V. parahaemolyticus* reached ~7.0 $\log_{10}$ CFU/cm^2 from an initial ~ 4.0 $\log_{10}$ CFU/cm^2 within 6 h at 25°C (Figure 3.2). Wong et al. (2002) investigated biofilm formation of 7 clinical (TDH-), 9 clinical (TDH+) and 12 environmental *V. parahaemolyticus* on stainless steel surfaces, with the cell density reaching maximum levels of 3.20×10^6, 3.00×10^6, and 1.66×10^6 cells/cm^2, respectively, after incubation at 25 °C for 6 h. In another study, incubation of *V. parahaemolyticus* at 30 °C for 24 h on stainless steel surfaces resulted in biofilm cell numbers of > 8.00 $\log_{10}$ CFU/cm^2 (Han et al., 2016). These results suggest that *V. parahaemolyticus* is able to rapidly grow on stainless steel and produce a biofilm within 6 h, highlighting the risk this microorganism poses to the food industry. The lowest viable biofilm cell numbers at the peak of the dynamic biofilm growth curve were observed in strains PFR21C03 and PFR37D08 (Figure 3.2). In the present study, PFR37D08 produced weak cell growth on stainless steel

(Figure 3.2) but showed a relatively high crystal violet value on polystyrene (Figure 3.1). This may be a result of the surface used with polystyrene rather than stainless steel favoring PFR37D08. Ideally a CV test should also be done on the stainless steel surfaces to determine if the observation is due to the nature of the substrate or the difference in test methods. Biofilm cell numbers varied in these studies, because the biofilm formation can be influenced by multiple factors such as strain variants, growth medium, surface roughness and surface conditioning (Brooks & Flint, 2008; Palmer et al., 2007).

3.5 Conclusion

V. parahaemolyticus grows rapidly on stainless steel, reaching maximum cell numbers within 6 hours. *V. parahaemolyticus* will be examined for its biofilms formed at 25 °C for 6 h on stainless steel surfaces for the following study, with PFR30J09 and PFR34B02 identified as strong biofilm-forming strains and PFR21C03 and PFR37D08 as weak biofilm-forming, with the others showing intermediate biofilm-forming ability. However, if current chemical disinfectants used in the seafood industry are not effective in reducing *V. parahaemolyticus* biofilm cells, what genes are responsible for the strong biofilm formation?.

3.6 Reference

Abanto, M., Gavilan, R. G., Baker-Austin, C., Gonzalez-Escalona, N., & Martinez-Urtaza, J. (2020). Global Expansion of Pacific Northwest *Vibrio parahaemolyticus* Sequence Type 36. *Emerging Infectious Diseases*, *26*(2), 323-326. https://doi.org/10.3201/eid2602.190362

Baker-Austin, C., Jenkins, C., Dadzie, J., Mestanza, O., Delgado, E., Powell, A., Bean, T., & Martinez-Urtaza, J. (2020). Genomic epidemiology of domestic and travel-associated *Vibrio parahaemolyticus* infections in the UK, 2008–2018. *Food Control*, *115*, 107244. https://doi.org/10.1016/j.foodcont.2020.107244

Baker-Austin, C., Oliver, J. D., Alam, M., Ali, A., Waldor, M. K., Qadri, F., & Martinez-Urtaza, J. (2018). *Vibrio* spp. infections. *Nature Reviews Disease Primers*, *4*(1), 8. https://doi.org/10.1038/s41572-018-0005-8

Brooks, J. D., & Flint, S. H. (2008). Biofilms in the food industry: problems and potential solutions. *International Journal of Food Science & Technology*, *43*(12), 2163-2176.

CDC. (2021). The Cholera and Other *Vibrio* Illness Surveillance (COVIS) System. https://www.cdc.gov/vibrio/surveillance.html

Cruz, C. D., Hedderley, D., & Fletcher, G. C. (2015). Long-Term Study of *Vibrio parahaemolyticus* Prevalence and Distribution in New Zealand Shellfish. *Applied and Environmental Microbiology*, *81*(7), 2320-2327.

Daniels, N. A., Ray, B., Easton, A., Marano, N., Kahn, E., McShan, A. L., 2nd, Del Rosario, L., Baldwin, T., Kingsley, M. A., Puhr, N. D., Wells, J. G., & Angulo, F. J. (2000). Emergence of a new *Vibrio parahaemolyticus* serotype in raw oysters: A prevention quandary. *JAMA*, *284*(12), 1541-1545. https://doi.org/10.1001/jama.284.12.1541

FAO. (2021). Advances in science and risk assessment tools for *Vibrio parahaemolyticus* and *V. vulnificus* associated with seafood: meeting report (9240024875).

Han, F., Gu, R.-R., Shen, X.-S., Chen, Y.-G., Tian, L.-L., Zhou, W.-F., & Cai, Y.-Q. (2017). Detection of total and pathogenic *Vibrio parahaemolyticus* in shellfish growing along the south yellow sea and the East China sea. *Journal of Food protection*, *80*(11), 1882-1889.

Han, N., Mizan, M. F. R., Jahid, I. K., & Ha, S.-D. (2016). Biofilm formation by *Vibrio parahaemolyticus* on food and food contact surfaces increases with rise in temperature. *Food Control*, *70*, 161-166.

Hayrapetyan, H., Muller, L., Tempelaars, M., Abee, T., & Nierop Groot, M. (2015). Comparative analysis of biofilm formation by *Bacillus cereus* reference strains and undomesticated food isolates and the effect of free iron. *International Journal of Food Microbiology*, *200*, 72-79. https://doi.org/10.1016/j.ijfoodmicro.2015.02.005

Jolley, K. A., Bray, J. E., & Maiden, M. C. J. (2018). Open-access bacterial population genomics: BIGSdb software, the PubMLST.org website and their applications. *Wellcome Open Research*, *3*, 124. https://doi.org/10.12688/wellcomeopenres.14826.1

Konrad, S., Paduraru, P., Romero-Barrios, P., Henderson, S. B., & Galanis, E. (2017). Remote sensing measurements of sea surface temperature as an indicator of *Vibrio parahaemolyticus* in oyster meat and human illnesses. *Environmental Health*, *16*(1), 1-11.

Kragh, K. N., Alhede, M., Kvich, L., & Bjarnsholt, T. (2019). Into the well—A close look at the complex structures of a microtiter biofilm and the crystal violet assay. *Biofilm*, *1*, 100006.

Lianou, A., & Koutsoumanis, K. P. (2012). Strain variability of the biofilm-forming ability of *Salmonella enterica* under various environmental conditions. *International Journal of Food Microbiology*, *160*(2), 171-178.

Makino, K., Oshima, K., Kurokawa, K., Yokoyama, K., Uda, T., Tagomori, K., Iijima, Y., Najima, M., Nakano, M., Yamashita, A., Kubota, Y., Kimura, S., Yasunaga, T., Honda, T., Shinagawa, H., Hattori, M., & Iida, T. (2003). Genome sequence of *Vibrio parahaemolyticus*: a pathogenic mechanism distinct from that of *V cholerae*. *Lancet*, *361*(9359), 743-749. https://doi.org/10.1016/S0140-6736(03)12659-1

Martinez-Urtaza, J., Trinanes, J., Abanto, M., Lozano-Leon, A., Llovo-Taboada, J., Garcia-Campello, M., Pousa, A., Powell, A., Baker-Austin, C., & Gonzalez-Escalona, N. (2018). Epidemic Dynamics of *Vibrio parahaemolyticus* Illness in a Hotspot of Disease Emergence, Galicia, Spain. *Emerging Infectious Diseases*, *24*(5), 852-859. https://doi.org/10.3201/eid2405.171700

MPI. (2001). Microbial Pathogen Data Sheets: *Vibrio Parahaemolyticus*. https://www.mpi.govt.nz/dmsdocument/11033-Vibrio-parahaemolyticus-Microbial-pathogen-data-sheet

Nair, G. B., Ramamurthy, T., Bhattacharya, S. K., Dutta, B., Takeda, Y., & Sack, D. A. (2007). Global dissemination of *Vibrio parahaemolyticus* serotype O3:K6 and its serovariants. *Clinical Microbiology Reviews*, *20*(1), 39-48. https://doi.org/10.1128/CMR.00025-06

Naves, P., del Prado, G., Huelves, L., Gracia, M., Ruiz, V., Blanco, J., Rodriguez-Cerrato, V., Ponte, M. C., & Soriano, F. (2008). Measurement of biofilm formation by clinical isolates of *Escherichia coli* is method-dependent. *Journal of Applied Microbiology*, *105*(2), 585-590. https://doi.org/10.1111/j.1365-2672.2008.03791.x

Ndraha, N., & Hsiao, H.-I. (2021). Influence of climatic factors on the temporal occurrence and distribution of total and pathogenic *Vibrio parahaemolyticus* in oyster culture environments in Taiwan. *Food Microbiology*, *98*, 103765.

Palmer, J., Flint, S., & Brooks, J. (2007). Bacterial cell attachment, the beginning of a biofilm. *Journal of Industrial Microbiology and Biotechnology*, *34*(9), 577-588. https://doi.org/10.1007/s10295-007-0234-4

Rosa, J. V., Conceição, N. V., Conceição, R. C. S., & Timm, C. (2018). Biofilm formation by *Vibrio parahaemolyticus* on different surfaces and its resistance to sodium hypochlorite. *Ciência Rural*, *48*.

Song, X., Ma, Y., Fu, J., Zhao, A., Guo, Z., Malakar, P. K., Pan, Y., & Zhao, Y. (2017). Effect of temperature on pathogenic and non-pathogenic *Vibrio parahaemolyticus* biofilm formation. *Food Control*, *73*, 485-491.

Wong, H.-C., Chung, Y.-C., & Yu, J.-A. (2002). Attachment and inactivation of *Vibrio parahaemolyticus* on stainless steel and glass surface. *Food Microbiology*, *19*(4), 341-350.

Chapter 4. Efficacy of sodium hypochlorite and peracetic acid (PAA) on *V. parahaemolyticus* planktonic cells and biofilms

This chapter is an adaptation of material that was published (published article reproduced in Appendix VII & VIII) as a peer-reviewed article:

Wang, D., Fletcher, G. C., On, S. L., Palmer, J. S., Gagic, D., & Flint, S. H. (2023). Biofilm formation, sodium hypochlorite susceptibility and genetic diversity of *Vibrio parahaemolyticus*. *International Journal of Food Microbiology*, *385*, 110011.

Wang, D., Palmer, J. S., Fletcher, G. C., On, S. L., Gagic, D., & Flint, S. H. (2023). Efficacy of commercial peroxyacetic acid on *Vibrio parahaemolyticus* planktonic cells and biofilms on stainless steel and Greenshell™ mussel (*Perna canaliculus*) surfaces. *International Journal of Food Microbiology*, *405*, 110372.

4.1 Introduction

V. parahaemolyticus biofilms form on stainless steel, polystyrene, glass, and other abiotic surfaces in food processing equipment and packaging materials, showing a higher resistance to cleaning and sanitization than their planktonic counterparts. This may lead to recurring contamination (Rosa et al., 2018). Chemical sanitizers are widely used for cleaning and disinfection in the food industry due to low cost, easy-use and broad-spectrum bactericidal activities. However, gaps remain in the response of *V. parahaemolyticus* biofilm cells to sodium hypochlorite and peracetic acid (peroxyacetic, PAA) used in the seafood processing environment (Wang et al., 2022).

Sodium hypochlorite at recommended concentrations is inadequate to inactivate *V. parahaemolyticus* in biofilms so optimization of treatment with sodium hypochlorite is required (Rosa et al., 2018). Shikongo-Nambabi et al. (2010) found that when exposing mature *V. parahaemolyticus* biofilms to sodium hypochlorite (4 mg/L free available chlorine, pH not specified), for 1 h, the bacterial density decreased from 7.90 to 3.97 $\log_{10}$ CFU/cm^2. Another study examined the efficacy of sodium hypochlorite in reducing the bacterial population of *V. parahaemolyticus* in mature biofilms formed on stainless steel, glass, and polystyrene, and discovered that a 10-minute treatment with sodium hypochlorite (20 mg/L available chlorine, pH not specified) could reduce cell populations by as much as 3.0 $\log_{10}$ CFU/cm^2 from 5.5 $\log_{10}$ CFU/cm^2 (Rosa et al., 2018). However, information gaps remain in these studies, in particular with reference to the pH and temperatures used. Firstly, sodium hypochlorite dissolved in water will raise the pH and reduce its antimicrobial efficacy. In the food industry, it has been recommended to adjust the pH of sodium hypochlorite solution to 6.5-7.0 before the use on food contact surfaces. However, the pH of sodium hypochlorite solution was overlooked when killing biofilm cells in the above studies. Additionally, sodium hypochlorite

efficacy for removing biofilm cells will depend on the amount and nature of biofilm formation of *V. parahaemolyticus*.

PAA has been proposed as a green alternative to sodium hypochlorite because it does not produce disinfection by-products and imparts no taste or odor (Wang et al., 2020). Sodium hypochlorite dissociates into hypochlorite ions in water, while PAA exists in aqueous equilibrium as acetic acid and hydrogen peroxide, producing further oxidative effects (Sharma et al., 2016). Several PAA commercial formulations are available, including SaniDate® 5.0, VigorOx® 15 F&V, BioSide® HS-15%, and Tsunami™ 100. PAA is approved for use as a sanitizer in the United States on food contact surfaces (Code of Federal Regulations 21 part 178.1010) and for direct food contact with meat, poultry and seafood (Code of Federal Regulations 21 part 173.310) at maximum concentrations of 80 and 110 ppm, respectively. In 2007, the U.S. Food and Drug Administration certified PAA for use as sanitizers in ice and wash water during the commercial preparation of fish and seafood, with a maximum allowed presence of PAA not exceeding 190 ppm (Food Contact Substance Notification FCN 000699). Since 2009, PAA permitted by Food Standards Australia New Zealand, with a limit of 0.7 mg/kg PAA allowed in food products (Australia New Zealand Food Standards F2009C00360). Similarly, the European Food Safety Agency (EFSA) accepts the use of PAA on poultry meat as effective against *E. coli*, *Salmonella* and *Campylobacter* spp., with potential for use in seafood environments (EFSA, 2014).

Despite widespread awareness of *V. parahaemolyticus* control in seafood, there is a lack of understanding around *V. parahaemolyticus* biofilm development and the effective concentrations of sodium hypochlorite and PAA. Thus, the objective of this study was to assess the susceptibility of *V. parahaemolyticus* planktonic and biofilm cells to sodium hypochlorite and PAA.

4.2 Methods

4.2.1 Bacterial isolates and culture conditions

Details were provided in Section 3.2.1, Chapter 3.

4.2.2 Biofilm development on stainless steel surfaces

Stainless steel coupons (10 mm^2, 1 mm thick, 304 grade with a 2B finish; Advanced Sheetmetals, New Zealand) were prepared by soaking in 99.5 % acetone for 12 h, rinsing with distilled water, followed by immersion in alkaline detergent 1 % NaOH (w/v, pH ~13.0; Merck KGaA, Darmstadt, Germany) for 1 h and rinsing again with distilled water. The coupons were cleaned using an ultrasonic cleaner (DT52; BANDELIN, Berlin, Germany) for 60 min, rinsed with distilled water, left to dry and sterilized by dry cycle autoclaving at 121 ℃ for 15 min. Coupons were freshly prepared for each set of experiments.

Prepared cell culture (1mL, ~ 4 log_{10} CFU/mL) was pipetted into each well of 48-well flat-bottom polystyrene plates, along with one pre-cleaned and sanitized stainless-steel coupon. Biofilms were statically incubated at 25 ℃, using medium of TSB containing 3% NaCl.

4.2.3 Preparing sodium hypochlorite solutions and measuring their concentrations

Sodium hypochlorite solution was prepared aseptically and used within 20 min. In brief, commercial concentrated sodium hypochlorite (XY-12®, ECOLAB, New Zealand) containing around 140 g/L available chlorine (147 g/L sodium hypochlorite) was diluted in distilled water and the pH was adjusted to a range of 6.7 to 6.9 using 1 M HCl. The amount of free chlorine in the sodium hypochlorite solution was determined using titration (Zheng & Brook, 2021).

4.2.4 Preparing PAA solutions and measuring their concentrations

Commercial PAA (ECOLAB, Hamilton, New Zealand), which contains hydrogen peroxide (H_2O_2, 10-30%, CAS-No. 7722-84-1), acetic acid (5-10%, CAS-No. 64-19-7) and peracetic acid (PAA, 1-5%, CAS-No. 79-21-0), was used in this study. The information supplied with the product stated that the recommended dilution ranges are from 0.2% to 2.0%. PAA solution was prepared and used within 20 min.

The actual PAA and H_2O_2 concentrations in the commercial preparation were determined using iodometric titrations. For PAA, H_2O_2 was first degraded with catalase (Terminox®, Novozymes A/S, Denmark), followed by titration with sodium thiosulfate. Specifically, a 10 µL PAA sample was diluted with 10 mL of distilled water and kept at 4 ℃. After adding 10 mL of Buffer solution A (5.014 g of $Na_2HPO_4 \cdot 12H_2O$, ScharLab®, Spain; 4.627 g of KH_2PO_4, Merck, Germany; 0.061 g of EDTA in 1000 mL H_2O) at pH 5.5, the sample was vortexed for 60 s. Next, 15 mL of 12 N sulfuric acid (97%; J.T. Baker®, Avantor, UK) and 15 mL of 166g/L potassium iodide (Merck, Darmstadt, Germany) solution were added, and the solution was kept in the dark for 20 min. The solution was titrated with 1% w/v sodium thiosulfate (AnalaR®, BDH, UK) using starch as an indicator, titrating until the blue color disappeared. The consumption of sodium thiosulfate solution corresponds to the concentration of PAA according to the following equation.

$$C_{PAA} = \frac{N_{Na_2SO_3} \times V_{Na_2SO_3} \times EW_{PAA} \times 1000}{V_{PAA}}$$

Where C_{PAA} is the PAA concentration in the product (mg/L); $N_{Na_2SO_3}$ is the normality of the thiosulfate solution; $V_{Na_2SO_3}$ is the titration volume of sodium thiosulfate solution required (mL); EW_{PAA} is the PAA equivalent weight; V_{PAA} is the volume of PAA diluted solution (mL).

To determine the H_2O_2 concentrations, 10 mL of 10% chilled sulfuric acid was added to 10 µL of the PAA sample and then diluted with 10 mL of distilled water. Next, 3 drops of 0.025 mol/L Ferroin solution were added to the mixture and titrated using a 0.1 mol/L Ce^{+4} sulphate (UNIVAR®, Ajax Finechem, Australia) solution until the color turned from orange to blue.

The determination of residual PAA and H_2O_2 was based on the N, N-diethyl-p-phenylenediamine sulfate salt (DPD; BDH, UK) photometric method, as reported by Liu et al. (2015) with minor modifications. PAA (100 µL) was mixed with 50 µL of Buffer solution B (30.25 g of $Na_2HPO_4 \cdot 12H_2O$; 23 g of KH_2PO_4; 0.01 g of NaCl; and 0.5 g of KI, UNIVAR®, Ajax Finechem, Australia in 1,000 mL of H_2O), and then 50 µL of DPD solution (1.6 g of DPD; 200 µL of 97% H_2SO_4; and 0.02 g of EDTA in 100 mL of H_2O) was added. The absorption at 550 nm was measured after 30 s using a spectrophotometer (SpectrostarNano, BMG Labtech, Ortenberg, Germany). To measure residual H_2O_2, the same procedure was used, but Buffer solution C, with 5 mg of peroxidase from horseradish, was applied instead of Buffer solution B to determine total peroxide. The absorption at 550 nm was measured after 30 s using a spectrophotometer.

4.2.5 Sanitizer treatment using sodium hypochlorite

To determine the sodium hypochlorite susceptibility of planktonic *V. parahaemolyticus* cells, each well of 96-well polystyrene plates was loaded with 180 µL of cell suspension (~ 8 $\log_{10}$ CFU/mL) and 20 µL of sodium hypochlorite solution. The reaction was neutralized with 50 µL of 1% sodium thiosulfate after 5 min exposure to sodium hypochlorite. Each set of experiments included a positive control (180 µL of inoculum and 20 µL distilled water) as well as a negative control (180 µL of saline and 20 µL of sodium hypochlorite). 10-fold serial dilutions of cells were prepared and CFU enumeration was examined on 3% NaCl TSA plates. To determine the sodium hypochlorite susceptibility of *V. parahaemolyticus* biofilm cells, coupons containing

pre-formed biofilm were placed into 48-well flat-bottom polystyrene plates. One mL of sodium hypochlorite solution was pipetted into each well, containing a coupon for 5 min, and then the coupon was aseptically transferred to another well containing 1% sodium thiosulfate to neutralize the sodium hypochlorite.

4.2.6 Sanitizer treatment using PAA

To determine the susceptibility of planktonic *V. parahaemolyticus* cells to PAA, sterilized 96-well polystyrene plates were loaded with a cell suspension (100 µL, ~ 8.00 $\log_{10}$ CFU/ml, cell culture concentration was based on OD value at 595 nm, that has been studied for its relationship with its corresponding viable cell numbers) in saline (0.85%), along with 100 µL of PAA solution. After a 5-minute exposure, the solution was neutralized with 50 µL of 1% sodium thiosulfate. To test the susceptibility of biofilms, stainless steel coupons with pre-formed biofilm were placed into 1 mL of PAA solution. After 5 min, they were transferred to 1% sodium thiosulfate to neutralize the sanitizer.

4.2.7 Detachment of biofilm populations and cell enumeration

The number of culturable cells in the biofilm matrix was determined using a bead vortex mixing method reported previously with minor modifications (Hayrapetyan et al., 2015). In short, each coupon was rinsed three times using sterilized distilled water to remove the planktonic cells and transferred into a 25 mL glass bottle filled with 10 mL of 0.1% peptone buffered water (containing 1% NaCl) and 5 g of glass beads (5-8 mm diameter), followed by 1 min vortex mixing to disrupt the biofilm matrix from the stainless steel surface and obtain individual cells. Serial 10-fold dilutions of the biofilm cell solution were prepared and CFU enumeration was examined on 3% NaCl TSA plates after incubation at 37 ℃ for 18 h.

4.2.8 Identification of potential functional genes for biofilm resistance

Raw reads were kindly offered by Plant and Food Research Ltd. (New Zealand), which sequencing was conducted by Centre for Fisheries, Environment and Aquaculture Science (CEFAS, UK) using MiSeq with a coverage of 40-120X. Raw reads were processed to clean low-quality reads, low-quality sequences, trim adapters, estimate genome size and quality control using Bactopia (version 2.1.0, involving built-in tools of BBTools, fastq-scan, Lighter, Mash, and fastQC) (Petit III & Read, 2020). Cur-offs for reads quality check are minimum sequencing coverage of 20, per read sequencing quality of Q12, minimum mean read length of 49 bp. Sequencing data for continued steps used standard of maximum coverage per genome of 100 X, estimated genome size of between 100000 bp and 18040666 bp. *De novo* assembly using the assemblers SPAdes (version 3.15.2) and Velvet (version 1.2.10) were generated for each genome. SPAdes used k-mers (21, 33, 55) to build *de Brujin* graphs and generate contigs. The mismatch careful mode and error correction procedure were used to improve the assembly (Bankevich et al., 2012). *De novo* assembly was also performed via *de Brujin*-based Velvet and Velvet Optimizer, sizes of the k-mer (substrings of length k contained within a biological sequence) applied were of 31, 51, 71, 91, 121 (Zerbino & Birney, 2008) respectively. The quality of the draft assembly was evaluated using QUAST (version 5.0.2) and CheckM (version 1.1.3) (Gurevich et al., 2013; Parks et al., 2015), criteria to assess the assemblies involves contig numbers, N50, total length, misassembled contigs length, GC depth, genome completeness.

The amino acid sequences of all *V. parahaemolyticus* candidates were analyzed using Roary version 3.13.0 with MAFFT as the alignment tool. Comparative analysis of these genomes was presented using a Flower plot. Kyoto Encyclopedia of Genes and Genomes (KEGG) pathway analysis was conducted using BlastKOALA (https://www.kegg.jp/blast koala/). The variances in KEGG pathways across strong biofilm-forming strains (PFR30J09 and PFR34B02) and the

reference strain (RIMD2210633) of *V. parahaemolyticus* were visualized using ggplot2 (version 3.4.0).

4.2.9 Data analysis

Viable colony counts were enumerated and transformed as $\log_{10}$ CFU/mL or $\log_{10}$ CFU/cm^2. The mean and standard deviation (SD) for *V. parahaemolyticus* cell counting was based on three biological replicates and three technical replicates. One-way analysis of variance (ANOVA) with a Duncan's multiple range test ($p < 0.05$) indicated significance of the results, analysis was conducted using SPSS Statistics software (version 29.0.2.0; IBM®, New York, United States). Principle component analysis (PCA) was used to compare biofilm cell resistance against commercial PAA, the analysis was conducted using XLSTAT-Premium software (version 19.3).

4.3 Results

4.3.1 Susceptibility of *V. parahaemolyticus* to sodium hypochlorite

4.3.1.1 Susceptibility of *V. parahaemolyticus* planktonic cells to sodium hypochlorite

Planktonic cells were reduced by approximately 0.9 $\log_{10}$ CFU/mL with 16 mg/L chlorine and they were reduced by 1.49-2.79 $\log_{10}$ CFU/mL with 35 mg/L chlorine (Figure 4.1). There was variation in the chlorine sensitivity of different strains with 35 mg/L chlorine, with PFR30J09 and PFR37E03 producing low reductions of 1.76 and 1.49 $\log_{10}$ CFU/mL, respectively, whereas PFR21C03, PFR37C06, and PFR37D08 were reduced by 2.33, 1.81, and 2.24 $\log_{10}$ CFU/mL, respectively. Following exposure to 63 mg/L chlorine, all *V. parahaemolyticus* planktonic cells decreased to undetectable levels on agar plates, a reduction of > 7 $\log_{10}$ CFU/mL.

4.3.1.2 Susceptibility of *V. parahaemolyticus* biofilm cells to sodium hypochlorite

Biofilms of *V. parahaemolyticus* required a chlorine concentration roughly 75 times greater than that needed for planktonic cells, to decrease the culturable cells to undetectable levels (< 10 CFU/cm^2) using the CFU counting method (Figure 4.2). A concentration of 1176 mg/L chlorine was required to lower the *V. parahaemolyticus* culturable cell populations on stainless steel coupons by 1.74-2.28 $\log_{10}$ CFU/cm^2. The smallest declines were observed in the PFR30J09 and PFR34B02 biofilms, with cell populations decreasing by 1.78 and 1.91 $\log_{10}$ CFU/cm^2, respectively. When biofilms were treated with 4704 mg/L chlorine, the cell populations of all strains except PFR30J09 and PFR34B02 were reduced to undetectable levels (< 10 CFU/cm^2).

4.3.2 Susceptibility of *V. parahaemolyticus* to PAA

4.3.2.1 Efficacy of PAA against planktonic *V. parahaemolyticus* cells

Figure 4.3 displays the effect of PAA on planktonic *V. parahaemolyticus* cells. The untreated control cells of planktonic *V. parahaemolyticus* ranged from 7.27 $\log_{10}$ CFU/mL to 7.84 $\log_{10}$ CFU/mL. The concentrations of PAA ranged from 5 to 50 ppm. A concentration of 5 ppm produced a < 2.00 $\log_{10}$ CFU/mL reduction. At 15 ppm, there was an average cell decrease of 2.70 ± 0.40 (mean ± SD) $\log_{10}$ CFU/mL. PAA of 35 ppm resulted in an average cell reduction of 4.76 ± 0.38 $\log_{10}$ CFU/mL. At 50 ppm PAA, there were no viable cells detected, indicating a cell reduction of > 7.00 $\log_{10}$ CFU/mL (with a 1.00 $\log_{10}$ CFU/mL detection limit, Figure 4.3).

4.3.2.2 Efficacy of PAA against *V. parahaemolyticus* on stainless steel coupons

Figure 4.4 illustrates the effectiveness of PAA in inactivating *V. parahaemolyticus* biofilms

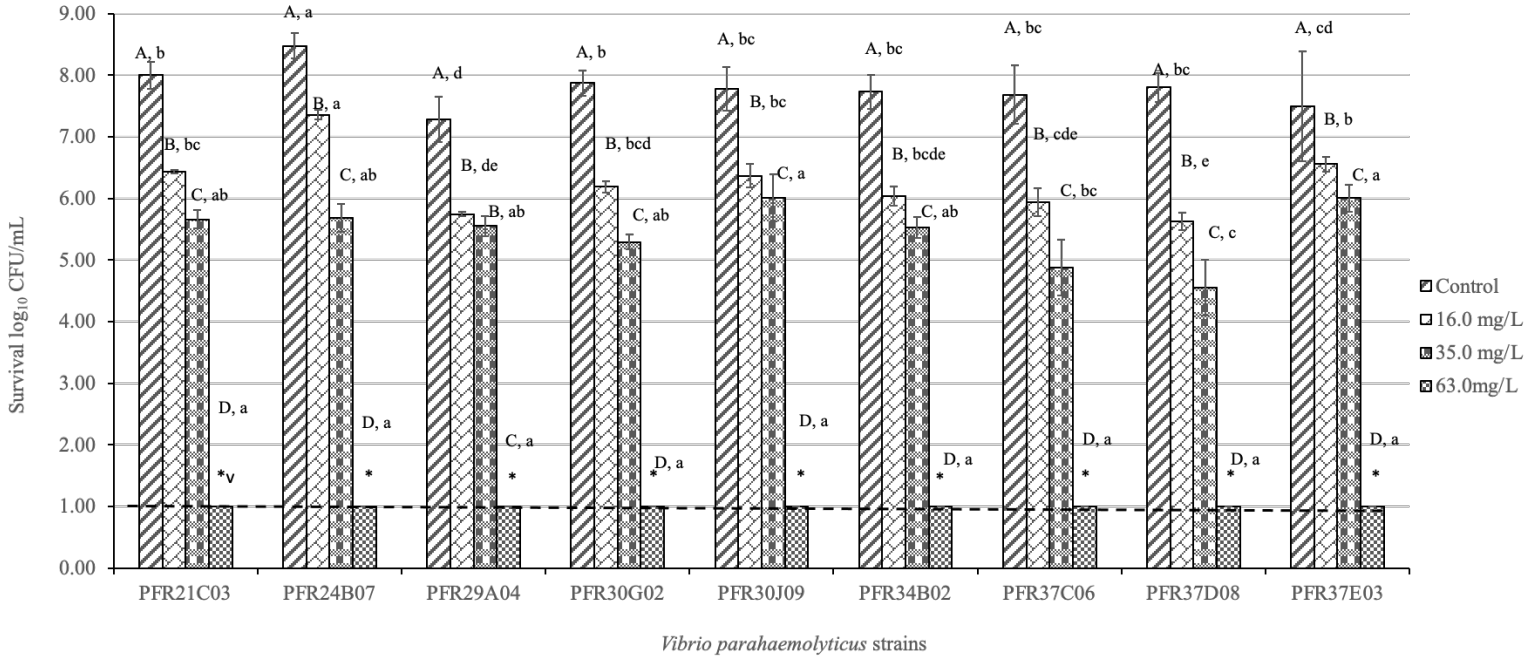

Figure 4. 1 Susceptibility of planktonic *V. parahaemolyticus* to sodium hypochlorite.

* indicates the limit of CFU detection (< 1.0 $\log_{10}$ CFU/mL, the dash line). Data results present as mean ± standard error (SD). Different letters signify are significantly different means ($p < 0.05$), the upper-case letters reflect significant difference between the strains, the lower-case letters reflect significant difference after treatment using sodium hypochlorite of different concentrations within the strain.

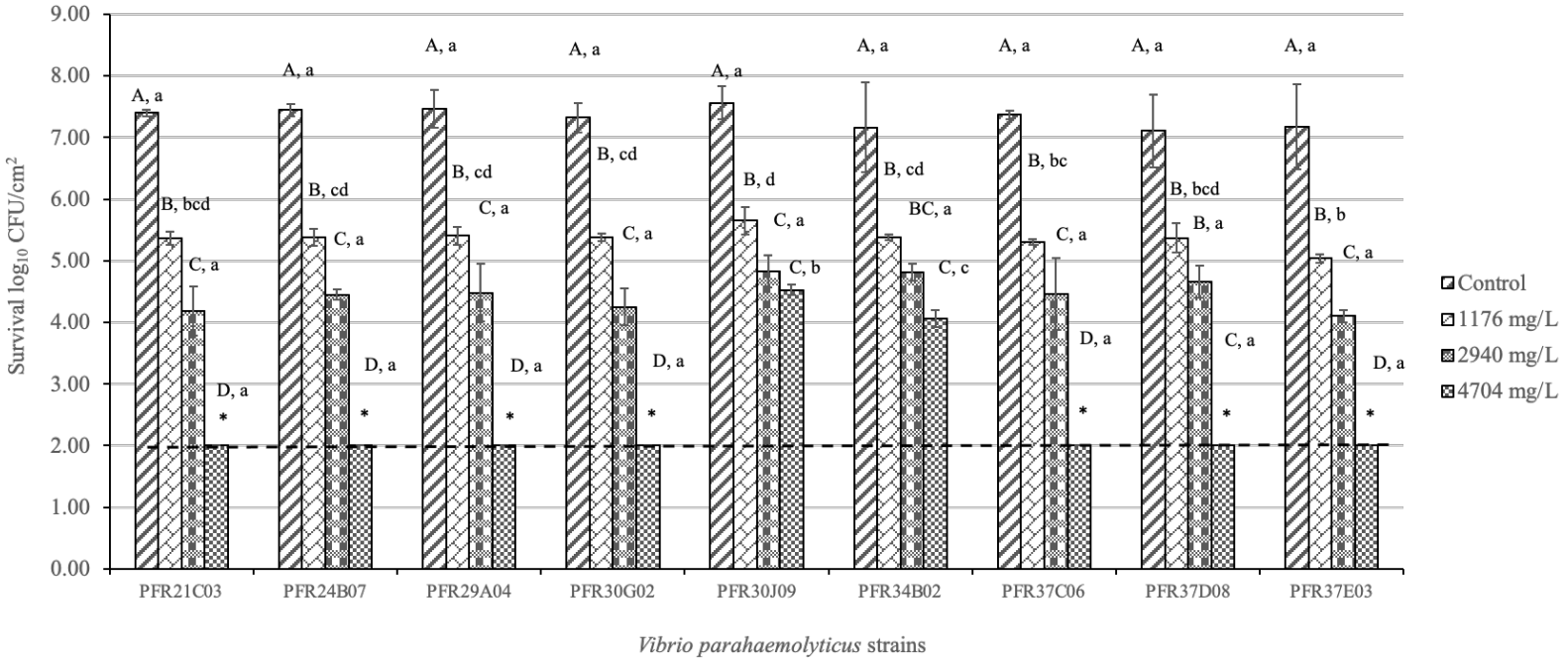

Figure 4. 2 Susceptibility of *V. parahaemolyticus* biofilms to sodium hypochlorite.

* indicates the limit of CFU detection (< 2.0 $\log_{10}$ CFU/cm^2, the dash line). Data results present as mean ± standard error (SD). Different letters signify are significantly different mean`s ($p < 0.05$), the upper-case letters reflect significant difference between the strains, the lower-case letters reflect significant difference after treatment using sodium hypochlorite of different concentrations within the strain.

grown on stainless steel surfaces. *V. parahaemolyticus* biofilm cells averaged 7.50 ± 0.21 $\log_{10}$ CFU/cm^2 in the untreated control. PAA of 10 ppm, produced log reductions ranging from 1.86 to 2.06 $\log_{10}$ CFU/cm^2. The average cell numbers decreased by 2.80 ± 0.52 $\log_{10}$ CFU/cm^2 after treatment with 50 ppm of PAA. Higher biofilm cell reduction was recorded for 100 ppm of PAA treatment, averaging of 3.19 ± 0.44 $\log_{10}$ CFU/cm^2. Cell reductions after PAA treatment using 200 ppm, were over 5.00 $\log_{10}$ CFU/cm^2 (undetectable) for most strains. However, the two strongest biofilm formers (PFR30J09 and PFR34B02) still showed average cell numbers of 2.60 and 2.52 $\log_{10}$ CFU/cm^2, respectively, indicating that concentrations exceeding 200 ppm of PAA are required to inactivate their biofilm communities.

4.3.3 Evaluation of PAA as a chlorine alternative sanitizer considering PAA residues

The original concentrations of peracetic acid and hydrogen peroxide in commercial PAA were titrated as 44.78 ± 6.01 g/L and 235.82 ± 6.37 g/L, respectively. The photometric method applied to the diluted commercial PAA gave a linear relationship between peracetic acid concentration (x axis) and OD_{550} (y axis) of $y = 0.0373x + 0.0694$ ($R^2 = 0.9436$), while the one between H_2O_2 (x axis) and OD_{550} (y axis) was $y = 0.1032x + 0.2655$ ($R^2 = 0.998$). The residues of peracetic acid and hydrogen peroxide in different dilutions of commercial PAA following biofilm treatment are listed in Table 4.1. The residue concentrations were higher for the PAA treatment of robust biofilm communities of PFR30J09 and PFR34B02, indicating less diffusion into these biofilm matrices and lower effectiveness of the sanitizers.

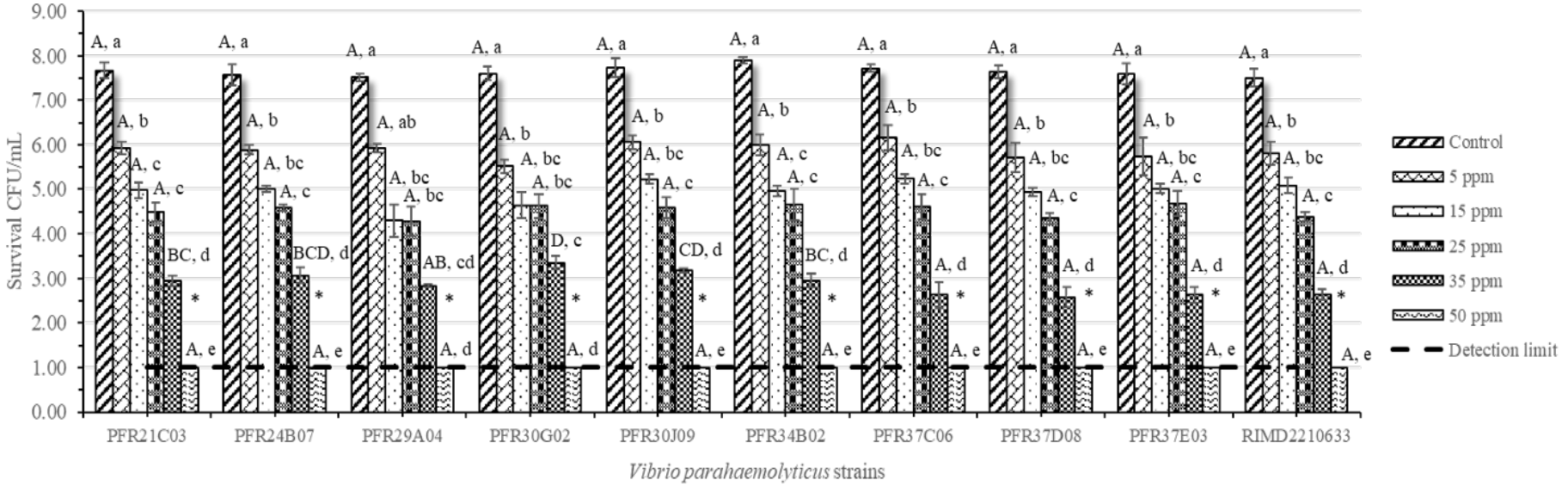

Figure 4. 3 Susceptibility of planktonic *V. parahaemolyticus* to peracetic acid (PAA).

The bars represent means with SD as error bars (three biological replicates each with three technical replicates). The detection limit was 1.00 $\log_{10}$ colony forming units (CFU)/mL. * indicates no detectable cells after exposure of *V. parahaemolyticus* to 50 ppm PAA for 5 min. Different letters signify are significantly different means ($p < 0.05$), the upper-case letters reflect significant difference between the strains, the lower-case letters reflect significant difference after treatment using PAA of different concentrations within the strain.

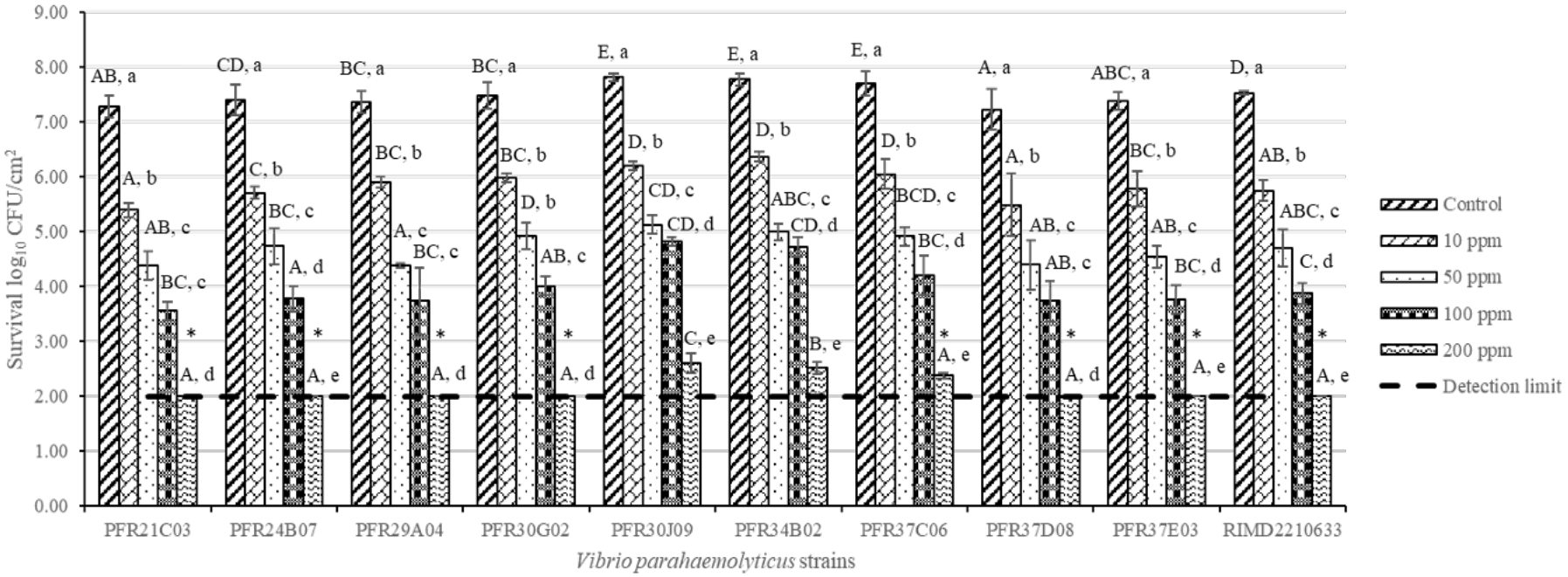

Figure 4. 4 Susceptibility of *V. parahaemolyticus* biofilm cells to PAA.

The detection limit was 2.00 $\log_{10}$ colony forming units (CFU)/cm^2. * indicates no detectable cells after exposure of *V. parahaemolyticus* to 200 ppm PAA for 5 min. Different letters signify are significantly different means ($p < 0.05$), the upper-case letters reflect significant difference between the strains, the lower-case letters reflect significant difference after treatment using PAA of different concentrations within the strain.

Table 4. 1 Residues of peracetic acid (PAA) and hydrogen peroxide (H_2O_2) after treating biofilms formed by different *V. parahaemolyticus* strains.

	PAA residue (mg/L) *				H_2O_2 residue (mg/L) *			
PAA dilution	200 ppm	100 ppm	50 ppm	10 ppm	200 ppm	100 ppm	50 ppm	10 ppm
PFR21C03	1.88 $^{AB, a}$ ± 0.16	1.77 $^{A, a}$ ± 0.17	1.29 $^{AB, b}$ ± 0.16	0.25 $^{ABC, c}$ ± 0.16	18.27 $^{BC, a}$ ± 0.37	17.9 $^{A, b}$ ± 0.61	6.79 $^{A, c}$ ± 0.08	1.7 $^{A, d}$ ± 0.08
PFR24B07	2 $^{AB, a}$ ± 0.17	1.8 $^{A, ab}$ ± 0.18	1.61 $^{B, b}$ ± 0.35	0.16 $^{ABC, c}$ ± 0.17	21.6 $^{BC, a}$ ± 0.62	18.93 $^{A, b}$ ± 0.49	6.47 $^{AB, c}$ ± 0.34	1.66 $^{AB, d}$ ± 0.07
PFR29A03	2.75 $^{C, a}$ ± 0.44	2.35 $^{B, ab}$ ± 0.28	2.01 $^{C, b}$ ± 0.2	0.09 $^{ABC, c}$ ± 0.15	21.51 $^{D, a}$ ± 0.61	18.74 $^{C, b}$ ± 0.12	6.52 $^{AB, c}$ ± 0.23	1.48 $^{ABC, d}$ ± 0.06
PFR30G02	3.29 $^{D, a}$ ± 0.17	2.8 $^{C, b}$ ± 0.25	2.07 $^{C, c}$ ± 0.16	0.3 $^{BC, d}$ ± 0.15	21.1 $^{CD, a}$ ± 1.9	18.49 $^{A, a}$ ± 1.17	6.13 $^{BC, b}$ ± 0.07	1.46 $^{BCD, d}$ ± 0.17
PFR30J09	4.16 $^{E, a}$ ± 0.33	3.36 $^{D, b}$ ± 0.3	2.48 $^{D, c}$ ± 0.22	0.4 $^{D, d}$ ± 0.16	23.85 $^{AB, a}$ ± 0.87	19.22 $^{B, b}$ ± 4.53	6.12 $^{BC, c}$ ± 0.15	1.22 $^{EF, d}$ ± 0.05
PFR34B02	5.4 $^{F, a}$ ± 0.21	5.33 $^{E, a}$ ± 0.16	3.04 $^{E, b}$ ± 0.4	0.71 $^{E, c}$ ± 0.14	24.49 $^{A, a}$ ± 0.98	19.09 $^{A, b}$ ± 0.17	6.44 $^{AB, c}$ ± 0.18	1.48 $^{ABC, d}$ ± 0.05
PFR37C06	2.03 $^{AB, a}$ ± 0.18	1.62 $^{A, b}$ ± 0.15	1.23 $^{AB, c}$ ± 0.15	0.38 $^{C, d}$ ± 0.19	19.46 $^{CD, a}$ ± 0.77	17.27 $^{B, b}$ ± 0.15	5.23 $^{D, c}$ ± 0.2	1.5 $^{ABC, d}$ ± 0.06
PFR37D08	1.79 $^{A, a}$ ± 0.13	1.63 $^{A, a}$ ± 0.15	0.99 $^{A, b}$ ± 0.14	0 $^{A, c}$ ± 0.14	18.83 $^{CD, a}$ ± 3.02	17.82 $^{A, a}$ ± 1.18	5.99 $^{BC, b}$ ± 0.4	1.06 $^{F, d}$ ± 0.25
PFR37E03	2.21 $^{B, a}$ ± 0.16	1.71 $^{A, b}$ ± 0.14	1.23 $^{AB, c}$ ± 0.14	0.13 $^{ABC, d}$ ± 0.16	17.41 $^{D, a}$ ± 0.96	18.09 $^{A, a}$ ± 0.84	5.78 $^{CD, b}$ ± 0.32	1.36 $^{CDE, d}$ ± 0.06
RIMD2210633	2.11 $^{AB, a}$ ± 0.16	1.53 $^{A, b}$ ± 0.22	1.15 $^{A, c}$ ± 0.19	0.03 $^{AB, d}$ ± 0.21	17.33 $^{D, a}$ ± 2.07	16.55 $^{AB, a}$ ± 2.59	6.45 $^{AB, b}$ ± 0.63	1.24 $^{DEF, d}$ ± 0.14

*Within the same examined strains, means not followed by the same letter are significantly different ($p < 0.05$). The upper-case letters reflect significant difference between the strains, the lower-case letters presented significant difference after treatment using PAA of different concentrations within the strain.

4.3.4 Genotype characteristics for biofilm resistance of strong biofilm-forming strains

PCA analysis revealed that PFR30J09 and PFR34B02 had distinct biofilm communities in terms of PAA resistance compared to the other strains (Figure 4.4). This is in accordance with the results from Section 4.3.1. According to PCA analysis in Figure 4.5a, PFR30J09 and PFR34B02 formed a distinct group; these two strains were strong biofilm formers as we discussed in Chapter 3 above, while 3 clinical strains (including RIMD2210633) and other environmental strains own lower biofilm-forming abilities. In Figure 4.5b, there are 3854 core genes shared by these ten *V. parahaemolyticus* candidate strains, with PFR30J09 having 778 shell genes and 282 unique genes, while PFR34B02 had 765 shell genes and 239 unique genes and the reference strain RIMD2210633 had 481 shell genes and 240 unique genes. KEGG analysis was used to compare functional variances based on the shell genes and unique genes in *V. parahaemolyticus*. Figure 4.5c shows that PFR30J09 and PFR34B02 had more genes in certain functional pathways, such as for microbial metabolism in diverse environments, degradation of aromatic compounds, pentose and glucuronate interconversions, amino sugar and nucleotide sugar metabolism, fructose and mannose metabolism, benzoate degradation, xylene degradation, dioxin degradation and mismatch repair. RIMD2210633, being the pathogenetic strain, had more gene counts in the pathway of polyketide sugar unit biosynthesis, bacterial secretion system and flagellar assembly than those of PFR30J09 and PFR34B02.

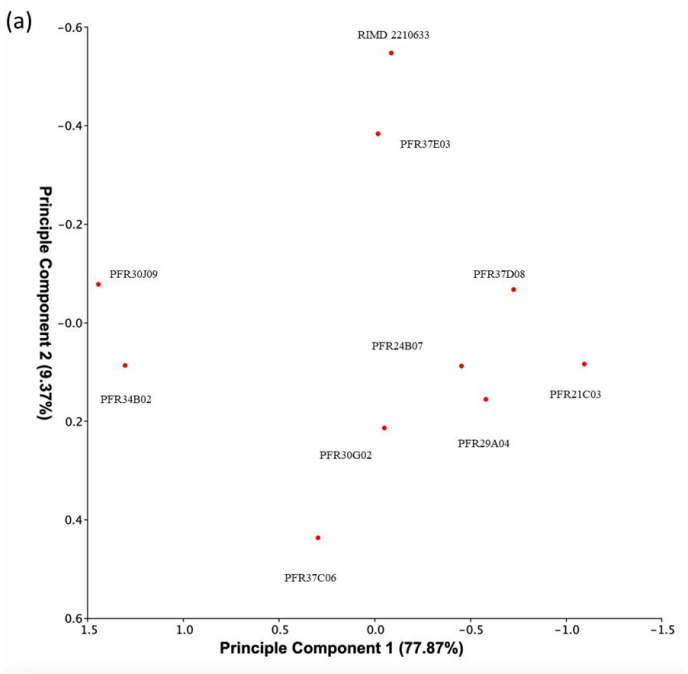
(a)
RIMD 2210633
PFR37E03
PFR30J09
PFR37D08
PFR24B07
PFR34B02
PFR21C03
PFR29A04
PFR30G02
PFR37C06
Principle Component 2 (9.37%)
Principle Component 1 (77.87%)
-0.6
-0.4
-0.2
-0.0
0.2
0.4
0.6
1.5
1.0
0.5
0.0
-0.5
-1.0
-1.5

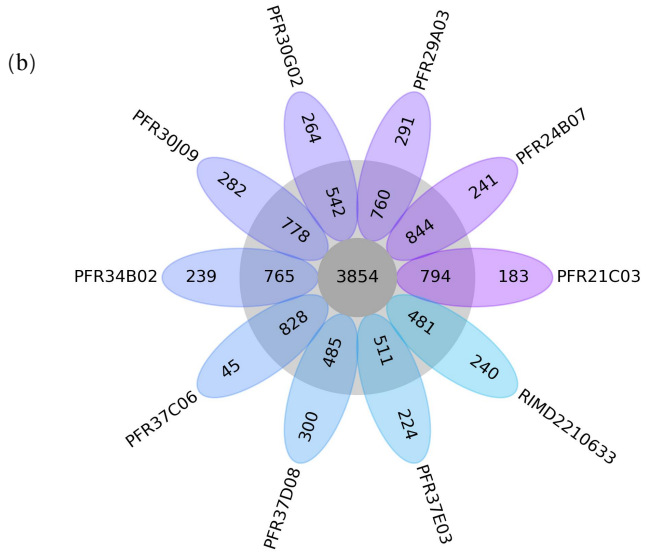
(b)
PFR30G02
PFR29A03
PFR30J09
PFR24B07
PFR34B02
PFR21C03
PFR37C06
RIMD2210633
PFR37D08
PFR37E03
264
291
282
241
542
760
778
844
239
765
3854
794
183
828
481
485
511
45
240
300
224

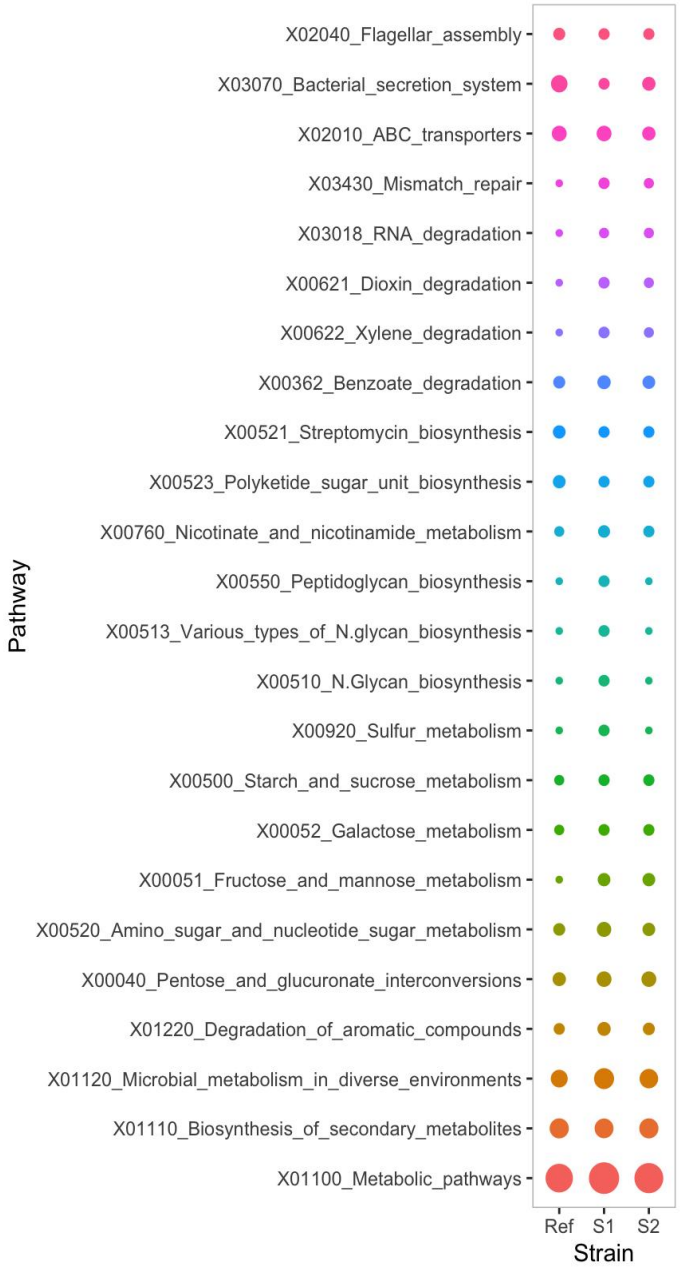
(c)
X02040_Flagellar_assembly
X03070_Bacterial_secretion_system
X02010_ABC_transporters
X03430_Mismatch_repair
X03018_RNA_degradation
X00621_Dioxin_degradation
X00622_Xylene_degradation
X00362_Benzoate_degradation
X00521_Streptomycin_biosynthesis
X00523_Polyketide_sugar_unit_biosynthesis
X00760_Nicotinate_and_nicotinamide_metabolism
X00550_Peptidoglycan_biosynthesis
X00513_Various_types_of_N.glycan_biosynthesis
X00510_N.Glycan_biosynthesis
X00920_Sulfur_metabolism
X00500_Starch_and_sucrose_metabolism
X00052_Galactose_metabolism
X00051_Fructose_and_mannose_metabolism
X00520_Amino_sugar_and_nucleotide_sugar_metabolism
X00040_Pentose_and_glucuronate_interconversions
X01220_Degradation_of_aromatic_compounds
X01120_Microbial_metabolism_in_diverse_environments
X01110_Biosynthesis_of_secondary_metabolites
X01100_Metabolic_pathways
Pathway
Ref
S1
S2
Strain

Figure 4. 5 Distinctive patterns of PAA resistance of *V. parahaemolyticus* biofilm and determination of the functional genes in resistant cells.

(a) PCA analysis results of PAA resistance in various *V. parahaemolyticus* biofilm cells. (b) Pangenome analysis of *V. parahaemolyticus* candidate strains. (c) KEGG annotation for shell and unique genes from strong biofilm forming strains (S1: PFR30J09, S2: PFR34B02) and reference strain RIMD2210633, respectively. Multiple colors represent different KEGG pathways. The round shapes represent gene count values.

4.4 Discussion

In this study, the effective chlorine concentration required to kill biofilm cells of *V. parahaemolyticus* on stainless steel coupons was approximately 75-fold higher (4704 mg/L free available chlorine, > 5 $\log_{10}$ CFU/cm^2 cells reduction) than that required to kill planktonic counterparts (63 mg/L, > 5 $\log_{10}$ CFU/mL cells reduction). In a previous published study, *V. parahaemolyticus*, a planktonic culture was reduced by 2.2 $\log_{10}$ CFU/mL from 7.6 $\log_{10}$ CFU/mL by a 30s treatment with sodium hypochlorite (35 mg/L available chlorine concentration, pH not specified) (Quan et al., 2010). In another study, the planktonic cells were treated with sodium hypochlorite (81 mg/L available chlorine concentration, pH 10.8) for 3 min, with no cells detectable from an initial cell concentration of 7.85 $\log_{10}$ CFU/mL (Chen et al., 2016). In determining sodium hypochlorite efficacy for killing biofilm cells on biotic surfaces, Roy et al. (2021) assessed a 5 min sodium hypochlorite treatment (50, 100, 200, and 300 mg/L, pH not specified), reducing *V. parahaemolyticus* biofilm cells from 0.54 to 2.59 and 0.64 to 2.32 $\log_{10}$ CFU/cm^2 on shrimp and crab surfaces, respectively, from initial concentrations of 6.87 and 7.37 $\log_{10}$ CFU/cm^2. The concentrations of sodium hypochlorite required to eliminate biofilm cells have been determined in many other species. Corcoran et al. (2014) reported 500 mg/L sodium hypochlorite was not effective against a *Salmonell*a biofilm, with a reduction of 1.11 $\log_{10}$ CFU/coupon after 90 min treatment. Cruz and Fletcher (2012) reported 3600 mg/L chlorine as the minimal effective concentration (99.999% reduction) against *L. monocytogenes* biofilm cells. For *E. coli* O157:H7 attached to cantaloupe rind surfaces for 2 h, a > 5 $\log_{10}$ reduction occurred after treatment with 2000 mg/L of sodium hypochlorite. For 12 h old biofilms, 2000 mg/L could only achieve a 1.86 $\log_{10}$ reduction (Fu et al., 2017). The effect of sodium hypochlorite on biofilms is dependent on a range of variants, the age of the biofilm, the structure of the biofilm matrix, the chlorine concentrations, pH and treatment time (Yuan et al., 2021).

In this PAA trial, PAA of 50 ppm resulted in a planktonic cell reduction of > 7.00 $\log_{10}$ CFU/mL when initial *V. parahaemolyticus* cells averaged 7.64 $\log_{10}$ CFU/mL. Wong et al. (2018) reported PAA at a concentration above 5 ppm (65.75 μM) was bactericidal to the wild-type *V. parahaemolyticus* strain, KX-V231, and using 5, 7.5 or 15 ppm of PAA resulted in the killing of 1.00, 2.00 or 4.50 $\log_{10}$ CFU/mL of planktonic cells, respectively. However, the exposure time of PAA in the current study was only 5 min, which is much shorter than the one-hour exposure time reported by Wong et al. (2018). This may explain why different effective PAA concentrations for killing planktonic *V. parahaemolyticus* strains were reported between the two studies. Little has been reported about PAA treatment of *V. parahaemolyticus* biofilm communities. In this study, the difference in sensitivity between planktonic and biofilm cells to PAA treatments demonstrated a likelihood that the biofilm matrices lowered the cell susceptibility to the sanitization.

Microorganisms of different species are known to vary in their sensitivity to sanitizers. Wang et al. (2020) reported that *Mycobacterium psychrotolerans* was reduced to undetectable levels (< 1.70 $\log_{10}$ CFU/mL) with 20 ppm of PAA treatment for 5 min, while 40 ppm for 1 min also inactivated the cells to undetectable levels (inoculum concentration of ~ 5.2 × 10^5 CFU/mL). In another study, 80 ppm of PAA exposure for 5 min was reported to inactivate *E. coli* O157:H7 cells by 1.5 and 1.5 $\log_{10}$ CFU/g from sliced apple and shredded lettuce surfaces, respectively (Rodgers et al., 2004). PAA at 90 ppm is the minimum inhibitory concentration for planktonic *S.* Thompson (Nahar et al., 2022). Melchior et al. (2007) indicated inactivation of cells in a biofilm depends on the sensitivity of each strain in the biofilm. For *L. monocytogenes* biofilms formed on polystyrene and stainless steel, PAA of 2000 ppm reduced the biofilm cells by 2.80 $\log_{10}$ CFU/cm^2 and 3.50 $\log_{10}$ CFU/cm^2, respectively (Poimenidou et al., 2016). The use of a wide collection of strains for the assessment of the bactericidal activity of sanitizers seems to

be necessary to ensure the optimal concentration is used, and the precise concentrations of PAA and H_2O_2 should be detailed.

PAA has shown potential for use in seafood or other meat related environments. For example, Thi et al. (2015) reported that 50 ppm of PAA (240 s exposure) decreased *E. coli* (3.8 $\log_{10}$ CFU/mL) levels below the detection level (< 1.00 $\log_{10}$ CFU/g) on *Pangasius* fillets. Wang et al. (2020) reported that 80 ppm PAA on saury (*Cololabis saira*) surfaces, for 1 min led to a 0.50 $\log_{10}$ CFU/cm^2 reduction in *M. psychrotolerans*, while a 5 min exposure time decreased the biofilm by 2.23 $\log_{10}$ CFU/cm^2 (initial inoculum size of ~ 10^6 CFU/ cm^2). PAA treatment also has the potential to extend shelf life of stored fish at 4 ℃ (Wang et al., 2020). Similar results have been reported in poultry and the treatment of beef with 200 ppm PAA delayed the onset of spoilage by 7, 21, and 54 days at 4, 2, and -1 °C, respectively (Yang et al., 2021).

PAA has generally been found to be a more effective sanitizer than sodium hypochlorite against planktonic cells of various microorganisms (Vázquez-Sánchez et al., 2014). However, Alasri et al. (1992) investigated the biocidal activity of some sanitizers against *E. coli, P. aeruginosa* and *S. aureus*, and found that chlorine (sodium hypochlorite) was more effective than PAA, even when the latter was considered in combination with H_2O_2. Comparing the sodium hypochlorite effective concentration in inactivating *V. parahaemolyticus* biofilm cells in Section 4.3.1, PAA at 200 ppm was more effective in reducing cells to non-detectable levels for 80% of strains from stainless steel coupons whereas sodium hypochlorite could not achieve this result, though it depends on the concentration of effective chlorine in the sodium hypochlorite. In a similar research, exposure to 100 ppm of sodium hypochlorite and PAA reduced biofilms cells of three food borne pathogens (*E. coli*, *Salmonella* Typhimurium and *L. monocytogenes*) by 0.50 to 3.63 and 2.83 to 5.78 $\log_{10}$ CFU/coupon (5 cm × 2 cm), respectively (Park et al., 2012).

Cleaning is essential before use of the sanitizers to remove food soils and/or EPS of biofilms, for example, Li et al. (2014) studied effect of food residues (milk, beef gravy and tuna gravy) on benzalkonium chloride and alkyldiaminoethylglycine hydrochloride in removing biofilms (*E. coli* O26, *P. aeruginosa*, *S. aureus*, *B. cereus*, and *B. cereus* spores) from polystyrene and ceramic dishes, pointed out food residues protect pathogens from dehydration and disinfectant treatment, and highlighted a proper cleaning process is a must before disinfectant treatment. Krysinski et al. (1992) reported that presence of milk reduced inactivation efficacy of *L. monocytogenes* biofilms on stainless steel and plastic conveyor belt surfaces, pointing out that cleaning must precede sanitization. Previous studies reported sanitizers of quaternary ammonium chloride, chlorine dioxide, and peracetic acid/hydrogen peroxide gave 7 log cycle kills of thermophilic *Bacillus* species, but residues of glycocalyx was left on stainless steel surfaces after treatment of quaternary ammonium chloride and chlorine dioxide (Flint et al., 1999; Parkar et al., 2004). Using sanitizers to treat biofilms may reduce cell numbers in biofilms, but it will not achieve removal of the glycocalyx (Brooks & Flint, 2008; Flint et al., 1999). The remained glycocalyx on surfaces by unproper cleaning and sanitization, will lead to recolonization of the bacteria and recurred contamination.

Oxidizing sanitizers kill pathogens by oxidizing the cell wall and causing lysis, or by diffusing through the cell wall and oxidizing the intracellular material (United States Environmental Protection Agency EPA 832-F-12-030). PAA treatment of *M. psychrotolerans* cells was found to cause damage to the cell membrane and cell surface without damaging chromosomal DNA or protein profiles, suggesting a mechanism involving oxidative damage (Wang et al., 2020). Although the mechanisms of planktonic *V. parahaemolyticus* resistance to PAA are not fully understood, it is believed that the accumulation of reactive oxygen species and the presence of catalase genes *katE1* and *katE2* contribute to resistance (Wong et al., 2018).

In this study, the resistance of robust biofilm matrices and physiological heterogeneity across strains may have contributed to variances in biofilm resistance. The variations in metabolic pathways identified within robust biofilm-forming strains could explain the resistance to sanitization in *V. parahaemolyticus*. Related results have been reported in recent studies. Wang et al. (2023) identified that chlorine sanitization induced *E. coli* on pea sprouts into a VBNC state with differentiated metabolic pathways and metabolite contents (culturable counterparts as the control). The metabolic pathways for amino acids, organic acids, sugars, alcohol, and nucleotide derivatives contributed to dormancy and resistance against sanitizers. Electrolyzed water acts as a sanitizer containing high oxidative and chlorine components. Electrolyzed water (4 mg/L free available chlorine) in addition to 50 ℃ heat treatment reduced *E. coli* by 2.31 $\log_{10}$ CFU/mL. Liu et al. (2020), through metabolomic analysis, demonstrated discriminative metabolic pathways of amino acid metabolism, nucleotide synthesis as well as lipid biosynthesis resulting in cell adaptation and stress response against the electrolyzed water and mild heat treatment in *E. coli* O157:H7.

This study pointed out a potential relationship between the metabolism of biofilm cells and sanitizer resistance. However, how metabolite patterns vary with sanitization treatment time is not clear. Inactivation kinetics is a predictive approach to determine the efficacy of sanitizers over time on biofilm cells. Zhao et al. (2022) reported the inactivation kinetics against electrolyzed water combined with ultrasound treatment. A modified Weibull model (R^2: 0.81–0.97; RMSE: 0.04–0.71) was a good fit, providing detailed information during the decontamination process. This study also screened metabolite profiles of *E. coli* biofilm cells, showing that the ultrasound treatment disrupted nucleotide metabolism and the electrolyzed water suppressed pathways of nucleotide biosynthesis, amino acid biosynthesis and energy-associated metabolism, suggesting a decreasing presence of nucleotide-related compounds (e.g., uridine, ATP, ADP) and most carbohydrates.

The present study provides hypotheses for understanding biofilm resistance based on whole genome sequencing. Integrated omics may provide more detailed information to understand antimicrobial and antibiofilm activities of various sanitizers (Lin et al., 2023; Liu et al., 2023; Mao et al., 2022). A combination of transcriptomics, proteomics, and metabolomics will help the verification of results from whole genome sequencing. Further exploration is needed to understand how the genes cooperate in *V. parahaemolyticus* and how they are quantitatively regulated.

4.5 Conclusion

This research evaluated the efficacy of the most widely used sanitizer, sodium hypochlorite, to eliminate *V. parahaemolyticus* cells, confirming the ineffectiveness of its recommended concentrations on inactivating biofilm cells on food contact surfaces. This study also evaluated the efficacy of using commercial PAA to sanitize *V. parahaemolyticus* planktonic cells and biofilm cells formed on stainless steel surfaces, mimicking the scenarios in the seafood industry. PAA of 50 ppm resulted in total inactivation (>7.00 $\log_{10}$ CFU/mL) of planktonic cells. PAA of 200 ppm reduced > 5.00 $\log_{10}$ CFU/cm^2 biofilm cells from stainless steel surfaces for 80% of *V. parahaemolyticus* strains. Strong biofilm-forming strains showed decreased efficacy owing to robust biofilm matrices and metabolism heterogeneity in the cells. Cleaning is an essential step prior to sanitization, considering sanitizers enable to reduce cell numbers in biofilms but can not achieve in removing glycocalyx.

4.6 Reference

Alasri, A., Roques, C., Michel, G., Cabassud, C., & Aptel, P. (1992). Bactericidal properties of peracetic acid and hydrogen peroxide, alone and in combination, and chlorine and formaldehyde against bacterial water strains. *Canadian Journal of Microbiology*, *38*(7), 635-642.

Australia New Zealand Food Standards F2009C00360, Processing aids. https://www.legislation.gov.au/Details/F2009C00360

Bankevich, A., Nurk, S., Antipov, D., Gurevich, A. A., Dvorkin, M., Kulikov, A. S., Lesin, V. M., Nikolenko, S. I., Pham, S., & Prjibelski, A. D. (2012). SPAdes: a new genome assembly algorithm and its applications to single-cell sequencing. *Journal of Computational Biology*, *19*(5), 455-477.

Brooks, J. D., & Flint, S. H. (2008). Biofilms in the food industry: problems and potential solutions. *International journal of food science & technology*, *43*(12), 2163-2176.

Chen, T. Y., Kuo, S. H., Chen, S. T., & Hwang, D. F. (2016). Differential proteomics to explore the inhibitory effects of acidic, slightly acidic electrolysed water and sodium hypochlorite solution on *Vibrio parahaemolyticus*. *Food Chemistry*, *194*, 529-537. https://doi.org/10.1016/j.foodchem.2015.08.019

Code of Federal Regulations 21 part 173.310, Secondary direct food additives permitted in food for human consumption: boiler water additives.

Code of Federal Regulations 21 part 178.1010, Substances utilized to control the growth of microorganisms: sanitizing solutions.

Corcoran, M., Morris, D., De Lappe, N., O'Connor, J., Lalor, P., Dockery, P., & Cormican, M. (2014). Commonly used disinfectants fail to eradicate *Salmonella enterica* biofilms

from food contact surface materials. *Applied Environmental Microbiology*, *80*(4), 1507-1514. https://doi.org/10.1128/AEM.03109-13

Cruz, C. D., & Fletcher, G. C. (2012). Assessing manufacturers' recommended concentrations of commercial sanitizers on inactivation of *Listeria monocytogenes*. *Food Control*, *26*(1), 194-199. https://doi.org/10.1016/j.foodcont.2012.01.041

EFSA. (2014). Scientific Opinion on the evaluation of the safety and efficacy of peroxyacetic acid solutions for reduction of pathogens on poultry carcasses and meat. *EFSA Journal*, *12*(3), 3599.

Flint, S. H., van den Elzen, H., Brooks, J. D., & Bremer, P. J. (1999). Removal and inactivation of thermo-resistant streptococci colonising stainless steel. *International Dairy Journal*, *9*(7), 429-436.

Food Contact Substance Notification FCN 000699, 190 ppm PAA in water and ice for seafood.

Fu, Y., Deering, A. J., Bhunia, A. K., & Yao, Y. (2017). Biofilm of *Escherichia coli* O157:H7 on cantaloupe surface is resistant to lauroyl arginate ethyl and sodium hypochlorite. *International Journal of Food Microbiology*, *260*, 11-16. https://doi.org/10.1016/j.ijfoodmicro.2017.08.008

Gurevich, A., Saveliev, V., Vyahhi, N., & Tesler, G. (2013). QUAST: quality assessment tool for genome assemblies. *Bioinformatics*, *29*(8), 1072-1075.

Hayrapetyan, H., Muller, L., Tempelaars, M., Abee, T., & Nierop Groot, M. (2015). Comparative analysis of biofilm formation by *Bacillus cereus* reference strains and undomesticated food isolates and the effect of free iron. *International Journal of Food Microbiology*, *200*, 72-79. https://doi.org/10.1016/j.ijfoodmicro.2015.02.005

Krysinski, E., Brown, L., & Marchisello, T. (1992). Effect of cleaners and sanitizers on *Listeria monocytogenes* attached to product contact surfaces. *Journal of food protection*, *55*(4), 246-251.

Li, R., Kuda, T., & Yano, T. (2014). Effect of food residues on efficiency of surfactant disinfectants against food related pathogens adhered on polystyrene and ceramic surfaces. *LWT-Food Science and Technology*, *57*(1), 200-206.

Lin, Z., Wang, G., Zhang, K., Jiang, S., Li, S., & Yang, H. (2023). Metabolomics investigation of global responses of *Cronobacter sakazakii* against common sanitizing in infant formula processing environments. *Food Research International*, *172*, 113162. https://doi.org/10.1016/j.foodres.2023.113162

Liu, D., Straus, D. L., Pedersen, L.-F., & Meinelt, T. (2015). Comparison of the toxicity of Wofasteril peracetic acid formulations E400, E250, and Lspez to *Daphnia magna*, with emphasis on the effect of hydrogen peroxide. *North American Journal of Aquaculture*, *77*(2), 128-135.

Liu, J., Zhao, H., Yin, Z., Dong, H., Chu, X., Meng, X., Li, Y., & Ding, X. (2023). Application and prospect of metabolomics-related technologies in food inspection. *Food Research International*, *171*, 113071. https://doi.org/10.1016/j.foodres.2023.113071

Liu, Q., Chen, L., Laserna, A. K. C., He, Y., Feng, X., & Yang, H. (2020). Synergistic action of electrolyzed water and mild heat for enhanced microbial inactivation of *Escherichia coli* O157:H7 revealed by metabolomics analysis. *Food Control*, *110*, 107026. https://doi.org/10.1016/j.foodcont.2019.107026

Mao, X., Xia, L., Yang, L., You, Y., Luo, P., Li, Y., Wu, Y., & Jiang, G. (2022). Data mining of natural hazard biomarkers and metabolites with integrated metabolomic tools.

Journal of Hazardous Materials, *427*, 127912. https://doi.org/10.1016/j.jhazmat.2021.127912

Melchior, M. B., Fink-Gremmels, J., & Gaastra, W. (2007). Extended antimicrobial susceptibility assay for *Staphylococcus aureus* isolates from bovine mastitis growing in biofilms. *Veterinary Microbiology*, *125*(1-2), 141-149. https://doi.org/10.1016/j.vetmic.2007.05.019

Montso, P. K., Mlambo, V., & Ateba, C. N. (2021). Efficacy of novel phages for control of multi-drug resistant *Escherichia coli* O177 on artificially contaminated beef and their potential to disrupt biofilm formation. *Food Microbiology*, *94*, 103647. https://doi.org/10.1016/j.fm.2020.103647

Nahar, S., Jeong, H. L., Cho, A. J., Park, J. H., Han, S., Kim, Y., Park, S. H., & Ha, S. D. (2022). Efficacy of ficin and peroxyacetic acid against *Salmonella enterica* serovar Thompson biofilm on plastic, eggshell, and chicken skin. *Food Microbiology*, *104*, 103997. https://doi.org/10.1016/j.fm.2022.103997

Park, S. H., Cheon, H. L., Park, K. H., Chung, M. S., Choi, S. H., Ryu, S., & Kang, D. H. (2012). Inactivation of biofilm cells of foodborne pathogen by aerosolized sanitizers. *International Journal of Food Microbiology*, *154*(3), 130-134. https://doi.org/10.1016/j.ijfoodmicro.2011.12.018

Parkar, S. G., Flint, S. H., & Brooks, J. D. (2004). Evaluation of the effect of cleaning regimes on biofilms of thermophilic bacilli on stainless steel. *Journal of Applied Microbiology*, *96*(1), 110-116. https://doi.org/10.1046/j.1365-2672.2003.02136.x

Parks, D. H., Imelfort, M., Skennerton, C. T., Hugenholtz, P., & Tyson, G. W. (2015). CheckM: assessing the quality of microbial genomes recovered from isolates, single cells, and metagenomes. *Genome Research*, *25*(7), 1043-1055.

Petit III, R. A., & Read, T. D. (2020). Bactopia: a flexible pipeline for complete analysis of bacterial genomes. *Msystems*, *5*(4), 10.1128/msystems. 00190-00120.

Poimenidou, S. V., Chrysadakou, M., Tzakoniati, A., Bikouli, V. C., Nychas, G. J., & Skandamis, P. N. (2016). Variability of *Listeria monocytogenes* strains in biofilm formation on stainless steel and polystyrene materials and resistance to peracetic acid and quaternary ammonium compounds. *International Journal of Food Microbiology*, *237*, 164-171. https://doi.org/10.1016/j.ijfoodmicro.2016.08.029

Quan, Y., Choi, K. D., Chung, D., & Shin, I. S. (2010). Evaluation of bactericidal activity of weakly acidic electrolyzed water (WAEW) against *Vibrio vulnificus* and *Vibrio parahaemolyticus*. *International Journal of Food Microbiology*, *136*(3), 255-260. https://doi.org/10.1016/j.ijfoodmicro.2009.11.005

Rodgers, S. L., Cash, J. N., Siddiq, M., & Ryser, E. T. (2004). A comparison of different chemical sanitizers for inactivating *Escherichia coli* O157:H7 and *Listeria monocytogenes* in solution and on apples, lettuce, strawberries, and cantaloupe. *Journal of Food Production*, *67*(4), 721-731. https://doi.org/10.4315/0362-028x-67.4.721

Rosa, J. V., Conceição, N. V., Conceição, R. C. S., & Timm, C. (2018). Biofilm formation by *Vibrio parahaemolyticus* on different surfaces and its resistance to sodium hypochlorite. *Ciência Rural*, *48*.

Roy, P. K., Mizan, M. F. R., Hossain, M. I., Han, N., Nahar, S., Ashrafudoulla, M., Toushik, S. H., Shim, W.-B., Kim, Y.-M., & Ha, S.-D. (2021). Elimination of *Vibrio parahaemolyticus* biofilms on crab and shrimp surfaces using ultraviolet C irradiation coupled with sodium hypochlorite and slightly acidic electrolyzed water. *Food Control*, *128*, 108179. https://doi.org/10.1016/j.foodcont.2021.108179

Sharma, V. K., Johnson, N., Cizmas, L., McDonald, T. J., & Kim, H. (2016). A review of the influence of treatment strategies on antibiotic resistant bacteria and antibiotic resistance genes. *Chemosphere*, *150*, 702-714. https://doi.org/10.1016/j.chemosphere.2015.12.084

Shikongo-Nambabi, M. N. N. N., Kachigunda, B., & Venter, S. N. (2010). Evaluation of oxidising disinfectants to control *Vibrio* biofilms in treated seawater used for fish processing. *Water SA*, *36*, 215-220. http://www.scielo.org.za/scielo.php?script=sci_arttext&pid=S1816-79502010000300003&nrm=iso

Thi, A. N. T., Sampers, I., Van Haute, S., Samapundo, S., Nguyen, B. L., Heyndrickx, M., & Devlieghere, F. (2015). Decontamination of Pangasius fish (*Pangasius hypophthalmus*) with chlorine or peracetic acid in the laboratory and in a Vietnamese processing company. *International Journal of Food Microbiology*, *208*, 93-101.

United States Environmental Protection Agency EPA 832-F-12-030. Alternative Disinfection Methods Fact Sheet: Peracetic Acid.

Vázquez-Sánchez, D., Cabo, M. L., Ibusquiza, P. S., & Rodríguez-Herrera, J. J. (2014). Biofilm-forming ability and resistance to industrial disinfectants of *Staphylococcus aureus* isolated from fishery products. *Food Control*, *39*, 8-16. https://doi.org/10.1016/j.foodcont.2013.09.029

Wang, D., Flint, S. H., Palmer, J. S., Gagic, D., Fletcher, G. C., & On, S. L. (2022). Global expansion of *Vibrio parahaemolyticus* threatens the seafood industry: Perspective on controlling its biofilm formation. *LWT*, 113182.

Wang, D., Yamaki, S., Kawai, Y., & Yamazaki, K. (2020). Sanitizing efficacy and antimicrobial mechanism of peracetic acid against histamine-producing bacterium,

Morganella psychrotolerans. *LWT*, *126*, 109263. https://doi.org/10.1016/j.lwt.2020.109263

Wang, Y., Chen, Z., Zhao, F., & Yang, H. (2023). Metabolome shifts triggered by chlorine sanitisation induce *Escherichia coli* on fresh produce into the viable but nonculturable state. *Food Research International*, *171*, 113084. https://doi.org/10.1016/j.foodres.2023.113084

Wong, H. C., Liao, R., Hsu, P., & Tang, C. T. (2018). Molecular response of *Vibrio parahaemolyticus* to the sanitizer peracetic acid. *International Journal of Food Microbiology*, *286*, 139-147. https://doi.org/10.1016/j.ijfoodmicro.2018.08.008

Yang, X., Wang, H., Hrycauk, S., & Klassen, M. D. (2021). Effects of Peroxyacetic Acid Spray and Storage Temperature on the Microbiota and Sensory Properties of Vacuum-Packed Subprimal Cuts of Meat. *Applied and Environmental Microbiology*, *87*(11), e03143-03120. https://doi.org/10.1128/AEM.03143-20

Yuan, L., Sadiq, F. A., Wang, N., Yang, Z., & He, G. (2021). Recent advances in understanding the control of disinfectant-resistant biofilms by hurdle technology in the food industry. *Critical Reviews in Food Science and Nutrition*, *61*(22), 3876-3891. https://doi.org/10.1080/10408398.2020.1809345

Zerbino, D. R., & Birney, E. (2008). Velvet: algorithms for de novo short read assembly using de Bruijn graphs. *Genome Research*, *18*(5), 821-829.

Zhao, L., Poh, C. N., Wu, J., Zhao, X., He, Y., & Yang, H. (2022). Effects of electrolysed water combined with ultrasound on inactivation kinetics and metabolite profiles of *Escherichia coli* biofilms on food contact surface. *Innovative Food Science & Emerging Technologies*, *76*, 102917. https://doi.org/10.1016/j.ifset.2022.102917

Zheng, S., & Brook, M. A. (2021). Elastomeric Silicone Sponges for Bleach Delivery. *ACS Applied Polymer Materials*, *3*(4), 2045-2053. https://doi.org/10.1021/acsapm.1c00101

Chapter 5. Comparative genome identification of accessory genes associated with strong biofilm formation in *V. parahaemolyticus*

This chapter is an adaptation of material that was published (published article reproduced in Appendix IX) as a peer-reviewed article:

Wang, D., Fletcher, G. C., Gagic, D., On, S. L., Palmer, J. S., & Flint, S. H. (2023). Comparative genome identification of accessory genes associated with strong biofilm formation in *Vibrio parahaemolyticus*. *Food Research International*, 166, 112605.

5.1 Introduction

Microbial cells can colonize different surfaces including biotic (e.g., shellfish), equipment (e.g., conveyor belts, stainless steel processing bench, pipes), or packaging materials (e.g., glass, polystyrene), forming complex community matrices covered by EPS (Lianou et al., 2020). Biofilms enable increased resistance by shielding pathogens and spoilage bacteria from environmental stresses, acting as hot spots for horizontal gene transfer (HGT) of virulence genes, and transforming previously benign strains into pathogens (Stalder & Top, 2016). The enhanced resistance of biofilms poses challenges for hygienic treatments in the food industry, thereby increasing the risks of cross-contamination and foodborne illness outbreaks (Gkana et al., 2017; Yuan et al., 2018). Sanitizers at recommended concentrations that are effective against *V. parahaemolyticus* planktonic cells, are ineffective to control biofilms therefore normal hygienic treatment cannot eradicate biofilm. Investigating key molecular mechanisms responsible for biofilm formation may help in devise novel control measures for biofilm.

Flagella and pili are often associated with the first stage of biofilm formation. *V. parahaemolyticus* uses polar and lateral flagella for motility. Polar flagella (driven by sodium ions) are used for swimming, and lateral flagella (driven by protons) for swarming (Kim & McCarter, 2000; McCarter, 2001). The polar flagella function as a mechano-sensor, resulting in a reduction in flagellar rotation and activation of the lateral flagella expression (Verstraeten et al., 2008). Mature *V. parahaemolyticus* biofilm formation requires mannose-sensitive hemagglutinin (MSHA) pili, virulence-associated toxin co-regulated pili (TCP) and chitin-regulated pili (ChiRP) to aggregate, attach and promote EPS synthesis (Yildiz & Visick, 2009). *cpsA-J* (*vpa1403-vpa1412*) is required for the synthesis of capsular polysaccharide A (CPSA), a major component of the *V. parahaemolyticus* biofilm (Yildiz & Visick, 2009). *vp1476-vp1458* is a conserved ortholog of the *syp* locus in *V. fischeri* which is responsible for

wrinkled colonies, pellicle formation and matrix production (Yildiz & Visick, 2009). *vp0190-vp0214* regulates the synthesis of lipid A, the core components of lipopolysaccharide (LPS) (Chen et al., 2010). However, it has not been determined which of these or other genotypes are responsible for strong biofilm formation in this bacterium.

The current study demonstrated genomic features of *V. parahaemolyticus* with weak, intermediate, and strong biofilm forming abilities, and the comparative genome analysis deciphered the exclusively molecular mechanisms of persistent *V. parahaemolyticus* on seafood contact surfaces, thereby providing insights for the design of novel biofilm control strategies.

5.2 Methods

5.2.1 Strains and growth conditions

Ten *V. parahaemolyticus* strains were chosen for this investigation (Table 3.1), seven of them were isolated from seafood processing plant wastewater by Plant and Food Research Ltd. New Zealand. Two were pathogens provided by the Institute of Environmental Science and Research Ltd. (ESR), New Zealand. The *V. parahaemolyticus* reference strain RIMD2210633 was kindly provided by Dr. Tetsuya Iida from Osaka University, Japan. According to previous studies, two strains, PFR30J09 and PFR34B02, were putative strong biofilm formers, whereas PFR21C03 and PFR37D08 were weak biofilm forming strains (Wang, 2022). Isolates from -80 ℃ bead storage system were recovered by shaking incubation at 37 ℃, 120 rpm using 3% NaCl TSB. Cells were centrifuged (8427 × *g*, 5 min) to obtain a cell pellet, that was washed and suspend in sterile saline to adjust the cell concentration to 7 $\log_{10}$ CFU/mL.

5.2.2 Genome assembly and annotation

Raw reads were kindly offered by Plant and Food Research Ltd. (New Zealand), for which sequencing was conducted by the Centre for Fisheries, Environment and Aquaculture Science (CEFAS, UK) using MiSeq with a coverage of 40-120X. Raw reads were processed to clean low-quality reads, low-quality sequences, trim adapters, estimate genome size and quality control using Bactopia (version 2.1.0, involving built-in tools of BBTools, fastq-scan, Lighter, Mash, and fastQC) (Petit III & Read, 2020). Cur-offs for reads quality check are minimum sequencing coverage of 20, per read sequencing quality of Q12, minimum mean read length of 49 bp. Sequencing data for continued steps used standard of maximum coverage per genome of 100 X, estimated genome size of between 100000 bp and 18040666 bp. *De novo* assembly using the assemblers SPAdes (version 3.15.2) and Velvet (version 1.2.10) were generated for each genome. SPAdes used k-mers (21, 33, 55) to build *de Brujin* graphs and generate contigs. The mismatch careful mode and error correction procedure were used to improve the assembly (Bankevich et al., 2012). *De novo* assembly was also performed via *de Brujin*-based Velvet and Velvet Optimizer, sizes of the k-mer (substrings of length k contained within a biological sequence) applied were of 31, 51, 71, 91, 121 (Zerbino & Birney, 2008) respectively. The quality of the draft assembly was evaluated using QUAST (version 5.0.2) and CheckM (version 1.1.3) (Gurevich et al., 2013; Parks et al., 2015), criteria to assess the assemblies involved contig numbers, N50, total length, misassembled contigs length, GC depth, genome completeness. Predicted coding sequences from bacterial genome assemblies were generated by Prokka (version 1.14.5) with default parameters, together with translated coding genes, genomic features and GFF version annotations were obtained (Seemann, 2014).

5.2.3 Average nucleotide identity (ANI) and phylogeny analysis

Average nucleotide identity (ANI) was analyzed using JSpecies (version 3.9.0) to measure the similarity among genomes by pairwise comparison based on nucleotide sequences (Richter et al., 2016). In this study, we also included the pathogen genomes of *E. coli* K-12 ER3413, *L. monocytogenes* ATCC 19117, *V. parahaemolyticus* RIMD2210633, *V. parahaemolyticus* BB22OP, *V. cholerae* ATCC 14035, *V. fischeri* ES114 and *V. vulnificus* ATCC 27562 to obtain a more complete view. To estimate the evolutionary relationship of *V. parahaemolyticus* genomes, phylogeny analysis was conducted based on 16s rRNA and ortholog clustering. DNA sequences were loaded into Barrnap (https://github.com/tseemann/barrnap) that applies HMMER 3.1 to search for ribosomal RNA genes. The 16s rRNA sequences were collected and aligned via MEGAX (version 10.2.6) software. A Maximum Likelihood phylogenetic tree was constructed using the nearest neighbor interchange model. Ortholog clustering analysis was performed via OrthoFinder2 (version: 2.5.4) using protein-coding genes. The orthogroups where species had single-copy genes were aligned via MAFFT. The phylogenetic tree was built by the IQ-TREE with 1000 bootstrap replications.

5.2.4 Homology clustering and pangenome analysis

Pangenome analysis to reveal core, dispensable and unique content was conducted using Roary and Anvi'o (Eren et al., 2015; Page et al., 2015). According to Roary (version 3.11.2), protein sequences with annotation were loaded and an all-against-all BLASTP was used to cluster proteins. The sequence identity of over 95% was set as the threshold for clustering protein homologues. Anvi'o clustered homologues based on the similarity of amino acid sequences and interactive visualization of results used the anvio-display-pan function. A circular graph contained information on gene numbers in gene clusters, maximum number of paralogs,

genomic homogeneity index, functional homogeneity index, combined homogeneity index, and single copy gene (SCG) clusters.

5.2.5 Comparative genome analysis

Four genomes, two from strong biofilm formers (PFR30J09 and PFR34B02) and two from weak biofilm formers (PFR21C03 and PFR37D08) were compared. Orthologous gene families and gene duplication events were analyzed via OrthoFinder2 and compared with a protein similarity search using DIAMOND (version 0.9.18). Another approach to predict orthologous gene clusters was performed using OrthoVenn2, which is based on all-to-all protein similarity comparisons and orthologous clusters using the Markov Cluster algorithm, the E-value and inflation value were set as 1e-5 and 1.5, respectively.

Functional assignment was conducted while examining functional domain distributions in Clusters of Orthologous Groups (COG) categories and looking for genes associated with strong biofilm formation. In addition, the DAVID database (https://david.ncifcrf.gov/) was used to annotate gene sets for Gene ontology (GO) terms. DAVID enables visualization of many-genes-to-many-terms relationships and clusters genes into groups. This was followed by a KEGG pathway analysis using BlastKOALA (https://www.kegg.jp/blastkoala/). A false discovery rate (FDR) value smaller than 0.05 was used as the cut-off for significance.

5.2.6 Identification of potential horizontal transfer genes

HGTector was used to predict the presence of horizontal gene transfer among genomes with BLASTP parameter thresholds of 60% identity, 60% coverage and an E-value of 1e-5. HGTector differentiates self (rank, genus; taxid: 662), close (rank, order; taxid: 135623) and distal gene groups by the gene hit bitscore (Zhu et al., 2014). Cut-offs were determined by taking the midpoint between the first peak and valley from the distribution of self, close and

distal groups. HGT genes were identified with a close weight smaller than the close cut-off but a distal weight greater than the distal cut-off (Yang et al., 2019).

5.2.7 Congo red indicator assay

Expression of extracellular polymeric cellulose was evaluated using the Congo red indicator method reported by Fang et al. (2022). Overnight culture was streaked onto agar plates and incubated at 37 ℃ for 48 h. The colony of red, brown, pink and white indicates the production of curli and cellulose, curli, cellulose, and none, respectively.

5.2.8 Anthrone absorbance assay

Cellulose determination was based on a previous study with minor modifications (Anriany et al., 2006). Briefly, 3 g cells (wet weight) of each sample were scratched from agar plates, mixed with 5 mL 8:2:1 acetic acid-nitric acid-distilled water and boiled for 30 min and centrifuged at 11000 rpm for 5 min. The pellet was washed with 1 mL distilled water and 1 mL acetone separately and left to dry overnight. The dried sample was dissolved in 1 mL H_2SO_4 (95%). Next, 0.1 mL was mixed with 0.5 mL anthrone solution (0.2 g in 100 mL H_2SO_4) and the absorbance determined at 620 nm. Crystalline cellulose (25 mg/mL, 50 mg/mL and 100mg/mL) was used as absorbance standards.

5.2.9 *In silico* cellulose synthase operon sequence analysis

The cellulose synthase operon genes of *V. parahaemolyticus* were BlastP searched against 138 *V. parahaemolyticus* reference genomes. The cellulose synthase genes of each genome were aligned using ClustalW. The accession numbers for nucleotide sequences of the genomes are attached in Table 5.4. The phylogeny of these cellulose synthase operons was analyzed using FastTree. The evolutional information was inferred using the Neighbor Joining method with a bootstrap consensus of 1000 replicates. The evolutionary distances were calculated using the

Maximum Likelihood Method and are in the units of the number of base substitutions per site. The amino acid sequences of *V. parahaemolyticus* RIMD2210633 were retrieved from the National Centre for Biotechnology Information (NCBI) Database and selected as the reference genome, followed by generating it into local database for BLASTP searching via diamond (Buchfink et al., 2021). Each sequenced *V. parahaemolyticus* genome was searched to identify the presence of genes (with > 70% identity and > 70% sequence coverage) (Fang et al., 2022).

5.2.10 Data availability

The sequence data determined in this work was deposited in the NCBI database under project accession No. PRJNA808748. The cellulose operon information for the strains used in this study are presented in Table 5.4.

5.3 Results and discussion

5.3.1 Genome assembly and annotation

The size of the *V. parahaemolyticus* genomes after trimming were from 5110607 bp to 5437835 bp, with an average value of 5290577 bp (Table 5.1). The GC contents of these genomes were not significantly different, ranging from 45.16% to 45.47%. Genome annotation was obtained from Prokka, which was to predict the coding DNA sequences (CDS) in the assemblies. The amount of CDS varied from 4591 to 4937. The variations in genome size and number could be due to gene diversity during evolution of *V. parahaemolyticus* isolates. The strain *V. parahaemolyticus* RIMD2210633 isolated from Japan was used as the reference genome for most of the molecular analysis. This genome consisted of chromosomes of 5165770bp, genes of 4832bp and a GC content of 45.4%. Overall, assembled genomes provided reasonable gene completeness and represented a reliable resource for analysis. In the present study, the largest genomes and highest gene numbers were observed in the environmental strain PFR30J09 and

PFR24B07. This was in accordance with reports by Pang et al. (2019) that there were 4718 genes on average from 19 *V. parahaemolyticus* environmental isolates compared with 4580 genes on average from 20 clinical isolates, suggesting higher genetic diversity and environmental adaptability in the environmental isolates. For the assembly of genome PFR30J09, it has highest number of contigs and total length, which shows oddity. Though the assemble was rational and the assembly met the assessment criteria of "Gold samples were defined as those having greater than 100 coverage, per-read mean quality greater than Q30, mean read length greater than 95 bp, and an assembly with fewer than 100 contigs. Silver samples were defined as those having greater than 50 coverage, per-read mean quality greater than Q20, mean read length greater than 75 bp, and an assembly with less than 200 contigs. Bronze samples were defined as those having greater than 20 coverage, per-read mean quality greater than Q12, mean read length greater than 49 bp, and an assembly with fewer than 500 contigs" (Petit III & Read, 2020), another study on a wider group of *V. parahaemolyticus* would be worth examining.

5.3.2 ANI analysis and phylogenetic tree

ANI provides the most commonly used criteria to define intra- or inter species relationships in prokaryotic genomes. ANI of > 95% represents the intraspecies boundaries (Jain et al., 2018). In this study, sequenced genomes revealed a high nucleotide identity (97.98-99.67%), indicating they belong to the same species, *V. parahaemolyticus* and PFR strains are from a common origin (Figure 5.1). *V. parahaemolyticus* nucleotide identity compared with other *Vibrio* spp. was 70.98-76.15%. The ANI across all *Vibrio* spp. ranges from 69.78% to 76.15%. The ANI results for *E. coli* K-12 ER3413 and *L. monocytogenes* ATCC 19117 are below 70%, demonstrating they are of different genera. Nucleotide acid sequences of 16S rRNA have been used for decades to assign phylogenetic relationships (Figure 5.1).

In this study, the phylogenetic relationship of *V. parahaemolyticus* species with other non-*Vibrio* species appears somewhat controversial. Among selected 16S rDNA sequences of *Escherichia coli* K-12 ER3413, *L. monocytogenes* ATCC 19117, *V. parahaemolyticus* RIMD2210633, *V. parahaemolyticus* BB22OP, *V. cholerae* ATCC 14035, *V. fischeri* ES114 and *V. vulnificus* ATCC 27562, the *V. parahaemolyticus* from the present study remained in

Table 5. 1 Summary of assemblies of *V. parahaemolyticus* genomes.

Assembly	PFR21C03	PFR24B07	PFR29A04	PFR30G02	PFR30J09	PFR34B02	PFR37C06	PFR37D08	PFR37E03
Contigs	93	133	129	99	329	104	95	85	110
Total length	5338398	5417990	5402653	5172378	5437835	5367801	5218301	5149233	5110607
GC (%)	45.27	45.16	45.19	45.27	45.47	45.19	45.25	45.24	45.27
CDS	4830	4937	4905	4659	4913	4857	4725	4639	4591
rRNA	7	8	8	7	5	8	9	8	7
tRNA	119	112	115	102	110	117	116	106	112
tmRNA	1	1	1	1	1	1	1	1	1

one subclade with *V. parahaemolyticus* RIMD2210633 and *V. parahaemolyticus* BB22OP, indicating that they are closely related. The most divergent species are *E. coli* K-12 ER3413 and *L. monocytogenes* ATCC 19117. Another method to assign the phylogenetic relationship is based on the orthologous groups, using 275 conserved single copy orthogroups, seen in Figure 5.1. The result was consistent with the phylogeny analysis based on 16S rDNA similarity that *V. parahaemolyticus* was located in the same clade with *V. parahaemolyticus* RIMD2210633 and *V. parahaemolyticus* BB22OP, and *E. coli* K-12 ER3413 and *L. monocytogenes* ATCC 19117. Among the subclade of *V. parahaemolyticus* species, PFR30J09 showed a lot of branching, suggesting some differences with other *V. parahaemolyticus* species. These data provide an evolutionary picture of sequenced *V. parahaemolyticus* genomes and reveal evolutionary distances among most studied food pathogens.

5.3.3 Pangenome analysis

The sizes of core and dispensable genomes were estimated using pangenome analysis via two distinct pipelines, Roary and Anvi'o. Roary analysis suggested there were 3253 core genes (33.20%, gene families shared by all genomes of a taxonomic unit), 2266 shell genes (23.13%, gene families shared by part of genomes), 4278 cloud genes (43.67%, gene families that are only present in certain genomes) out of 9797 genes in 9 sequenced *V. parahaemolyticus* genomes. The genome group is open, indicating that additional data input will alter the proportion of the core genome and that new orthogroups will be discovered. Despite both Roary and Anvi'o approaches use the MCL algorithm to identify clusters, the Anvi'o pangenomics workflow identified fewer gene clusters (6845), which may have led to a smaller number of core genes.

The differences might be due to their different ways to establish orthologs of protein clusters; Roary divides groups of homologous sequences into paralogs and orthologs using conserved

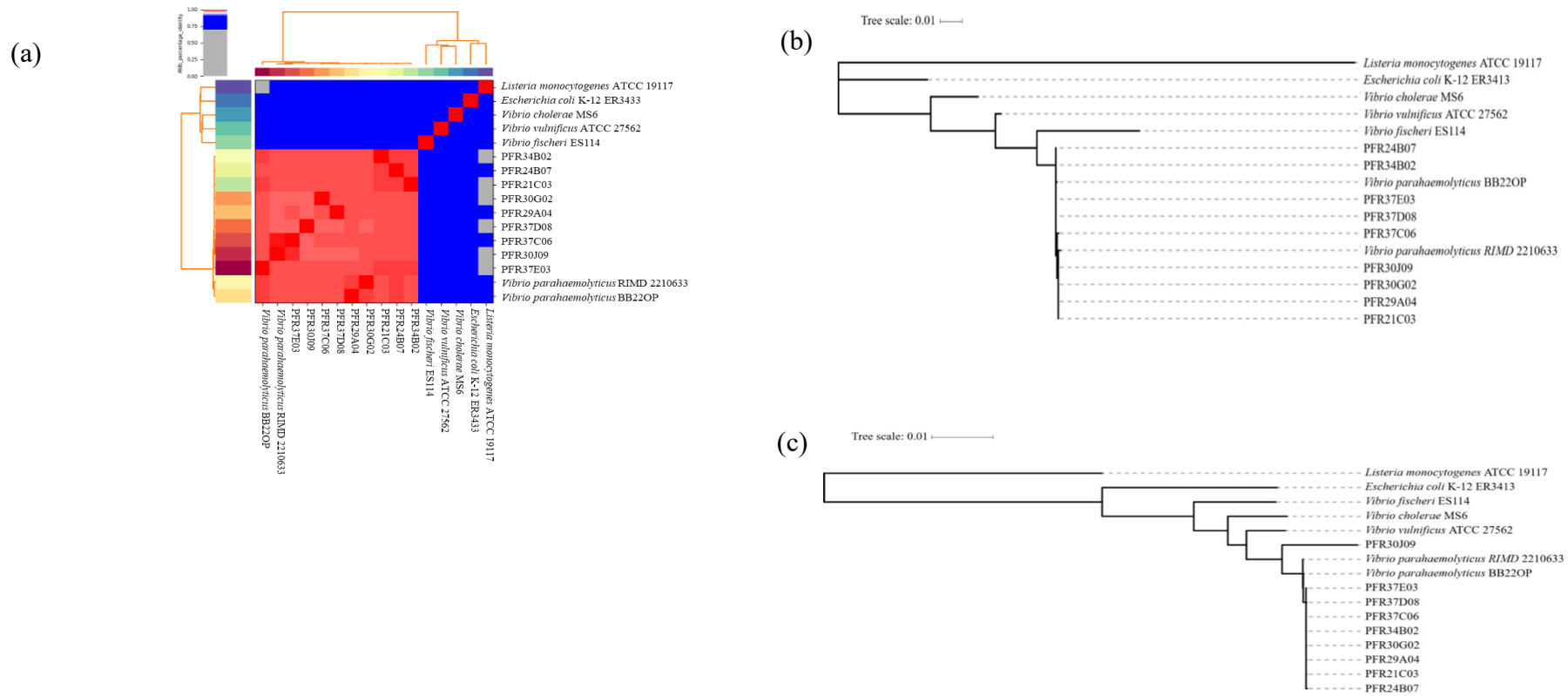

Figure 5. 1 Phylogenetic analysis and amino acid identities across genomes.

(a) Phylogeny based on a heatmap with row and column dendrograms from the average nucleotide identity (ANI) values. (b) The Maximum Likelihood phylogeny was constructed using the 16s rDNA sequences. (c) Maximum Composite Likelihood phylogeny was constructed based on single copy orthogroups.

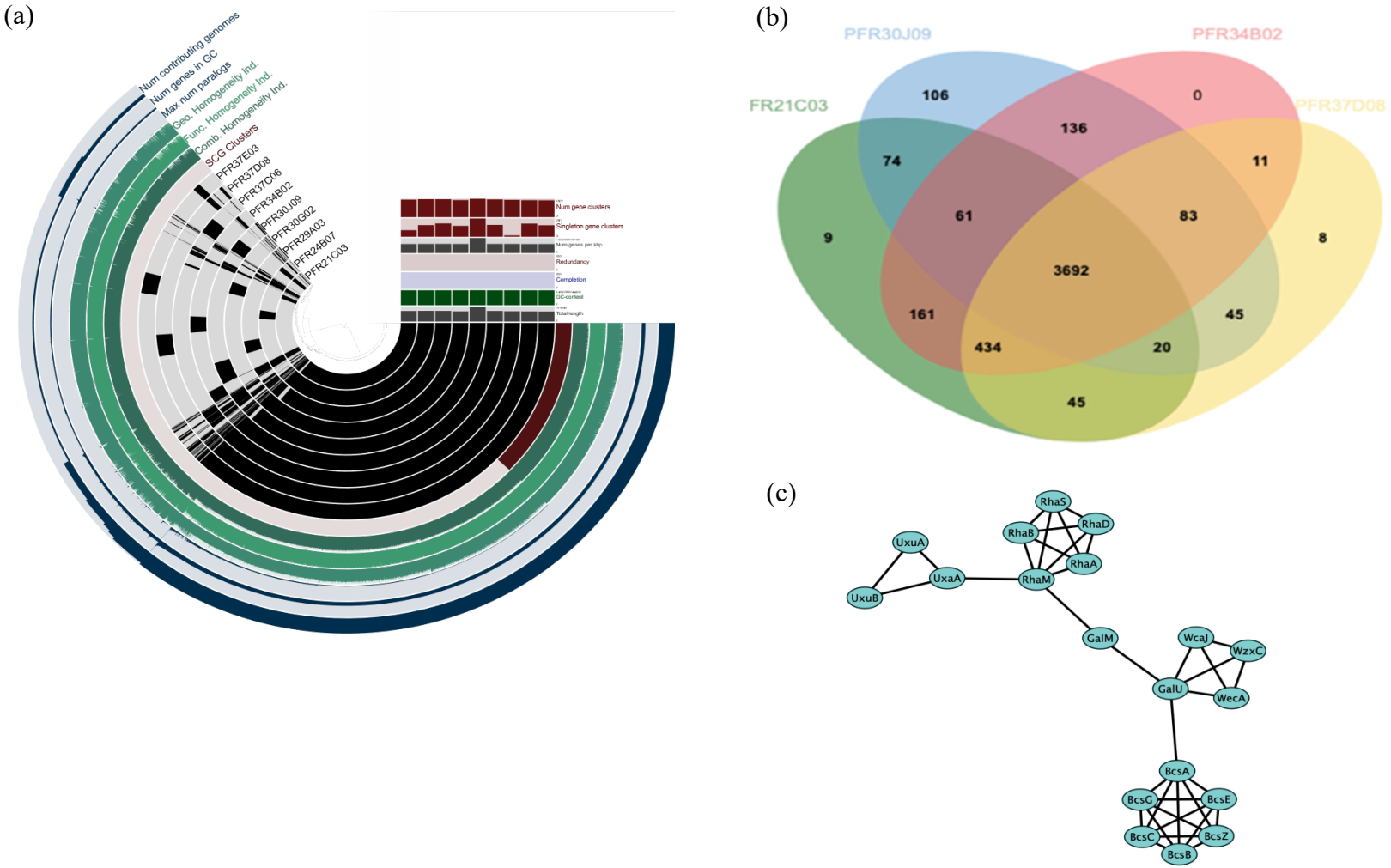

Figure 5. 2 Genomes of *V. parahaemolyticus* exhibit genetic diversity.

(a) Strain-specific gene families of nine *V. parahaemolyticus* genomes computed by the Anvi'o pangenome analysis pipeline employing the default setting. This figure present gene clusters across genomes, single-copy core gene (SCG) clusters, functional homogeneity (Fuc. Homogeneity Ind.), geometric homogeneity (Geo. Homogeneity Ind.), max number of paralogs (Max num paralogs), number of genes in gene caller (Num genes in GC), number of contributing genomes for gene clusters (num contributing genomes). (b) A comparison of protein orthologues in weak and strong biofilm-forming *V. parahaemolyticus*, generated by OrthoVenn2 with an E-value setting of 1e-5. (c) Protein-protein-interaction (PPI) network of 136 gene families exclusively present in strong biofilm-forming *V. parahaemolyticus*. Network was generated via STRING database (https://cn.string-db.org) based on 136 accessory gene families , network nodes represent proteins, edges represent protein-protein associations.

gene neighborhood information, while Anvi'o clusters orthologs based on the homology and synteny of genes (Maturana & Cárdenas, 2021). The low portion of core genome size (~ 33.20%) suggests that *V. parahaemolyticus* species may contain more accessory genes that are critical for adaptation to different environments and survival. A similar finding has been reported in a previous *V. parahaemolyticus* study by Pang et al. (2019) and Qin et al. (2021).

5.3.4 Comparative genome analysis

Genomes of strong biofilm formers (PFR30J09 and PFR34B02) and weak biofilm formers (PFR21C03 and PFR37D08) were collected for a comparative genome analysis to elucidate the common and different genomic features. OrthoVenn2 identified 136 gene families as being exclusively present in strong biofilm producers. The GO annotation was performed to assign the functional category of these 136 unique gene families. The significantly enriched GO terms include UDP-glucose metabolism (GO: 0006011), cellulose biosynthesis (GO: 0030244), rhamnose metabolism (GO: 0019299) and O antigen biosynthesis (GO: 0009243) (Table 5.2). Notably, cellulose synthesis, rhamnose catabolic and metabolic processes are absent in the *V. parahaemolyticus* reference strain RIMD2210633. These distinctive characteristics that may play crucial roles in robust biofilm formation. BlastKOALA was used to assign the amino acid sequences to KEGG functions, resulting in 24.3 percent (33/136) of them being successfully annotated, whereas the majority of them remain unidentified. The most frequently annotated pathways were metabolic pathways (ko01100), microbial metabolism in diverse environments (ko01120), pentose and glucuronate interconversions (ko00040), fructose and mannose metabolism (ko00051), biosynthesis of secondary metabolites (ko01110), galactose metabolism (ko00052) as well as starch and sucrose metabolism (ko00500). These pathways represent functions associated with the synthesis and metabolism of simple/complex sugars, which may aid in the utilization of diverse nutrient sources and adaptation to environmental

stress. Gene clusters associated with cellulose synthesis, rhamnose catabolism, and metabolic process were identified via KEGG gene annotation that was consistent with the result from GO enrichment (Table 5.3). Additionally, the CRISPR-Cas system was identified in the unique 136 gene families via KEGG annotation that has been reported to play critical roles in environmental stress defense, DNA repair and biofilm formation in microorganisms. In this study, the CRISPR-Cas system in *V. parahaemolyticus* was identified as the subtype I-F, encoded by *cas* gene *csy3*, consistent with previous studies (Liu et al., 2021; Makarova et al., 2011). However, whether and how the CRISPR-Cas system promotes biofilm formation in *V. parahaemolyticus* is not understood. The genome data also indicated that strong biofilm forming strains are more likely to have *mshA*, *mshC* and *mshD* genes that are lacking in the weak biofilm forming strains. MSHA is required for early attachment of *V. cholerae* to abiotic surfaces (Yildiz & Visick, 2009). Cells that are deficient in *mshA* cannot perform cell aggregation although they are involved in the formation of three-dimensional structures (Moorthy and Watnick, 2004). In *V. parahaemolyticus*, *mshA* mutants of *V. parahaemolyticus* show reduced adherence to surfaces (Shime-Hattori et al., 2006; Williams et al., 2014).

Table 5. 2 Gene ontology (GO) enrichment analysis of unique genes from strong biofilm forming strains. *

GO terms ID	Name	*p*-value
GO:0019301	rhamnose catabolic process	1.25E-06
GO:0006011	UDP-glucose metabolic process	4.96E-06
GO:0030244	cellulose biosynthetic process	0.000356
GO:0019299	rhamnose metabolic process	0.000704
GO:0009243	O antigen biosynthetic process	0.001724

*These pathways were assigned based on GO dataset GO enrichment analysis (https://geneontology.org/docs/go-enrichment-analysis/), this table lists significant shared GO terms by set of genes and *p* value (probability or chance of seeing at least x numbers of genes out of the total n genes in the list annotated to a particular GO term).

Table 5. 3 Enriched Kyoto Encyclopedia of Genes and Genomes (KEGG) functional assignment of unique genes from strong biofilm forming strains.

KO	Gene name	EC number	Pathways/associated functions
K02851	*wecA*, UDP-GlcNAc:undecaprenyl-phosphate/decaprenyl-phosphate GlcNAc-1-phosphate transferase	2.7.8.35	00542 O-Antigen repeat unit biosynthesis 00572 Arabinogalactan biosynthesis - Mycobacterium 01100 Metabolic pathways
K01785	*alM*, aldose 1-epimerase	5.1.3.3	00010 Glycolysis / Gluconeogenesis 00052 Galactose metabolism 01100 Metabolic pathways 01110 Biosynthesis of secondary metabolites 01120 Microbial metabolism in diverse environments
K00694	*bcsA*, cellulose synthase	2.4.1.12	00500 Starch and sucrose metabolism Cellulose biosynthesis
K01119	*cpdB*, 2',3'-cyclic-nucleotide 2'-phosphodiesterase / 3'-nucleotidase	3.1.4.16/3.1.3.6	00230 Purine metabolism 00240 Pyrimidine metabolism 01100 Metabolic pathways
K00008	*gutB*, L-iditol 2-dehydrogenase	1.1.1.14	00040 Pentose and glucuronate interconversions 00051 Fructose and mannose metabolism 01100 Metabolic pathways
K02554	*mhpD*, 2-keto-4-pentenoate hydratase	4.2.1.80	00360 Phenylalanine metabolism 00362 Benzoate degradation 00621 Dioxin degradation 00622 Xylene degradation 01100 Metabolic pathways 01120 Microbial metabolism in diverse environments 01220 Degradation of aromatic compounds
K01813	*rhaA*, L-rhamnose isomerase	5.3.1.14	00051 Fructose and mannose metabolism 01100 Metabolic pathways 01120 Microbial metabolism in diverse environments

K00848	*rhaB*, rhamnulokinase	2.7.1.5	00040 Pentose and glucuronate interconversions 00051 Fructose and mannose metabolism 01100 Metabolic pathways 01120 Microbial metabolism in diverse environments
K01629	*rhaD*, rhamnulose-1-phosphate aldolase	4.1.2.19	00040 Pentose and glucuronate interconversions 00051 Fructose and mannose metabolism 01100 Metabolic pathways 01120 Microbial metabolism in diverse environments
K00963	UTP glucose-1-phosphate uridylyltransferase	2.7.7.9	00040 Pentose and glucuronate interconversions 00052 Galactose metabolism 00500 Starch and sucrose metabolism 00520 Amino sugar and nucleotide sugar metabolism 00541 O-Antigen nucleotide sugar biosynthesis 01100 Metabolic pathways 01110 Biosynthesis of secondary metabolites 01240 Biosynthesis of cofactors 01250 Biosynthesis of nucleotide sugars
K00040	*uxuB*, fructuronate reductase	1.1.1.57	00040 Pentose and glucuronate interconversions 01100 Metabolic pathways
			Translation
K16694	*tuaB*; teichuronic acid exporter	-	Transporters
K08138	*xylE*; MFS transporter, SP family, xylose:H+ symportor	-	Transporters
K03765	*cadC*; transcriptional activator of cad operon	-	Transcription factors
K19130	*csy4*, CRISPR-associated endonuclease Csy4	3.1.-.-	Prokaryotic defense system
K19129	*csy3*, CRISPR-associated endonuclease Csy3	-	Prokaryotic defense system
K19128	*csy2*, CRISPR-associated endonuclease Csy2	-	Prokaryotic defense system
K19127	*csy1*, CRISPR-associated endonuclease Csy1	-	Prokaryotic defense system

K07012	*cas3*; CRISPR-associated endonuclease/helicase Cas3	3.1.-.- /5.6.2.4	Prokaryotic defense system
K15342	*cas1*; CRISP-associated protein Cas1	-	Prokaryotic defense system
K03534	*rhaM;* L-rhamnose mutarotase	5.1.3.32	Fructose and mannose metabolism Metabolic pathways Microbial metabolism in diverse environments
K02855	*rhaS*; AraC family transcriptional regulator, L-rhamnose operon regulatory protein RhaS	-	Fructose and mannose metabolism Metabolic pathways Microbial metabolism in diverse environments
K07733	*alpA*; prophage regulatory protein	-	Transcription factors
K03630	*radC*; DNA repair protein RadC	-	Replication and repair
K06877	DEAD/DEAH box helicase domain-containing protein	-	Poorly characterized
K03574	*mutT*, NUDT15, MTH2; 8-oxo-dGTP diphosphatase	3.6.1.55	DNA repair and recombination proteins
K20543	*bcsC*; cellulose synthase operon protein C	-	Cellulose biosynthesis
K20542	*bcsZ*; endoglucanase	3.2.1.4	Cellulose biosynthesis
K20541	*bcsB*; cellulose synthase operon protein B	-	Cellulose biosynthesis

V. parahaemolyticus employs multiple strategies to promote robust biofilm formation, and some of these strategies interact. The interaction between rhamnose metabolism, cellulose biosynthesis, and UDP-glucose metabolism was observed through protein-protein-interaction (PPI) analysis. GalU was connected with genes encoding capsular polysaccharide and those encoding cellulose synthesis. The ability to colonize and the altered core oligosaccharide of *galU*-deficient *V. cholerae* strains were approximately 50 to 100-fold diminished. Regmi and Boyd (2019) reported that the *rha* gene cluster, encoding rhamnose catabolic and metabolic processes, had limited distribution among *V. parahaemolyticus*. In the present study, the presence of rhamnose catabolic and metabolic processes may have contributed to substrate utilization and increased biofilm formation. UTP glucose-1-phosphate uridylyltransferase, catalysing the conversion of glucose-1-phosphate into UDP-glucose, is a crucial precursor for glycogen synthesis and was detected only in strong biofilm-forming strains. UDP-glucose is a precursor for the synthesis of the *Vibrio* polysaccharide synthesis (VPS) in *Vibrio cholerae*, and UTP glucose-1-phosphate uridylyltransferase may have aided *V. parahaemolyticus* in producing UDP-glucose and contributed to robust biofilm formation. ORFs are shown to encode a variety of glycotransferases that ulitize nucleotidylated sugars to add sugars to a growing repeat unit. In *E. coli*, the *wecA* gene is known to initiate the synthesis of enterobacterial common antigen, certain O polysaccharides, and biofilm by catalysing the transfer of N-acetylglucosamine to undecaprenol phosphate (Und-P), a lipid carrier (Greiner et al., 2004). WcaJ (WP_053807672.1) catalyses the first step in colanic acid synthesis by the attachment of glucose-1-phosphate onto undecaprenyl phosphate (Und-P), yielding the intermediate undecaprenyl-pyrophosphoryl-Glu (Patel et al. 2012), while WercA (WP_045605560.1) transfers the GlcNAc-1-phosphate moiety onto Und-P, yielding undecaprenyl-pyrophosphoryl-GlcNAc, which is the lipid intermediate involved in the synthesis of O-antigen and biofilm (Lehrer et al. 2007). WzxC is a colanic acid exporter and

an inner membrane protein that transfers polysaccharide units across the inner membrane. Colanic acid contributes to the intricate three-dimensional architecture of biofilms. However, colanic acid mutants of *E. coli* form biofilms with a significantly lower profile than wild-type cells (Danese et al., 2000; Verstraeten et al., 2008). In addition to the known virulence factors that aid in the colonisation and formation of biofilms, other factors involved in biofilm formation of *V. parahaemolyticus* are unknown. The presence of cellulose synthase operons in robust biofilm forming *V. parahaemolyticus* suggests that the cellulose component is one of the robust biofilm phenotypes, but for now, cellulose has only been reported in environmental isolates of *V. parahaemolyticus*. In other microorganisms, bacterial cellulose production is considered a virulence factor, and this could be the same in *V. parahaemolyticus*. It should be determined whether the presence of the cellulose synthesis gene cluster in *V. parahaemolyticus* is incidental or widespread.

5.3.5 Verification of cellulose production

Strong biofilm forming strains PFR30J09 and PFR34B02 produced red colonies on the Congo Red Assay, indicating the production of curli and cellulose (Figure 5.3). However, the weak biofilm forming strains, PFR21C03 and PFR37D08, only produced brown colonies, suggesting no cellulose was produced. The absence of cellulose biosynthesis in PFR21C03 and PFR37D08 is consistent with the results from the anthrone absorbance assay indicating no cellulose in PFR21C03 and PFR37D08 while cellulose was detected in PFR30J09 and PFR34B02 with OD_{620} of 0.234 ± 0.0356 and 0.185 ± 0.0546 (Figure 5.3), respectively. Crystalline cellulose was used as a control with 25 mg/mL producing an OD_{620} of 0.235 ± 0.0092.

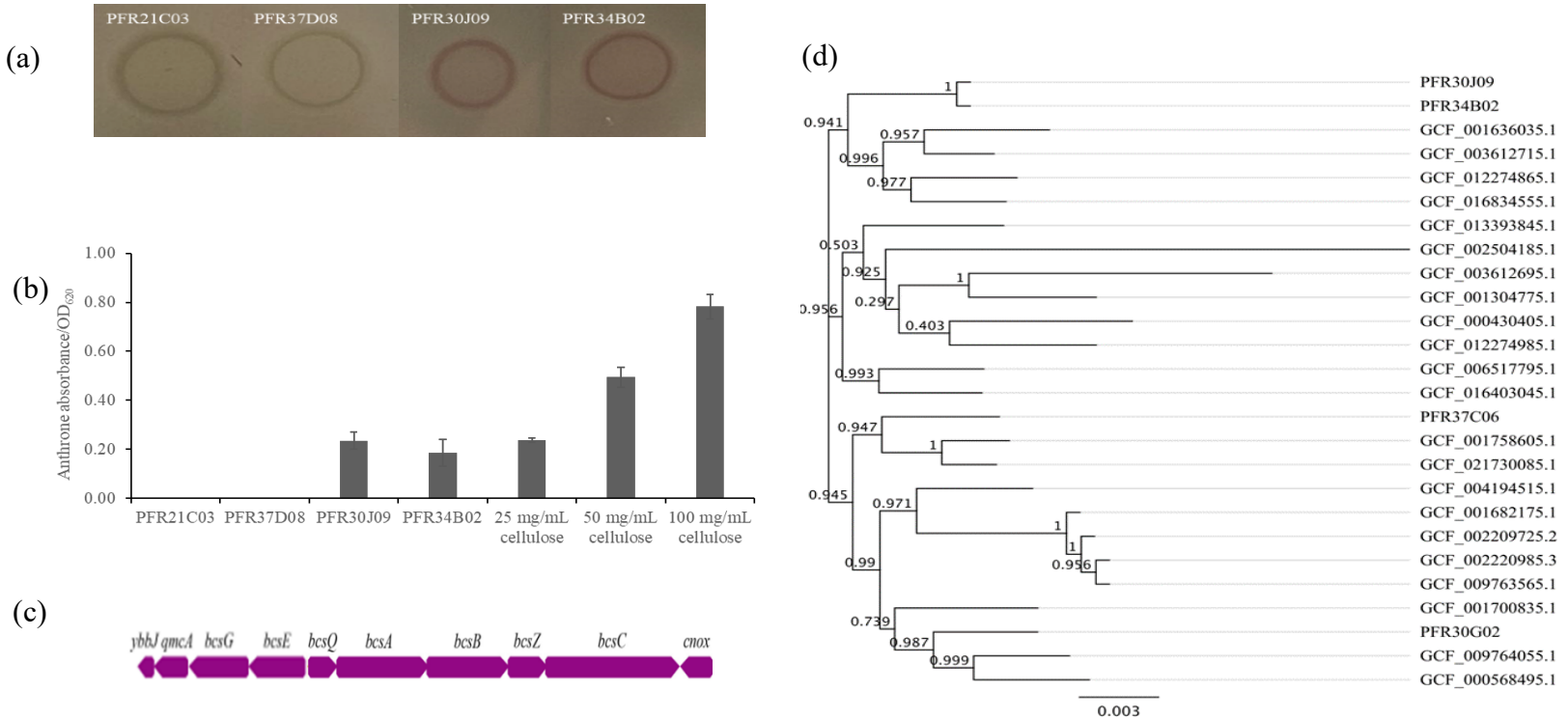

Figure 5. 3 Cellulose production at the phenotypic and genomic level in *V. parahaemolyticus*.

(a) Colony morphotypes on CRI agar plates indicating cellulose/curli production; (b) Anthrone absorbance assay to determine cellulose production in *V. parahaemolyticus*, crystalline cellulose (CC) chemical was assayed as the control. (c) Diagram of cellulose synthase operon in *V. parahaemolyticus*, consisting of *bcsG*, *bcsE*, *bcsQ*, *bcsA*, *bcsB*, *bcsZ*, and *bcsC*. (d) Evolutionary relationships between cellulose synthase operons

in *V. parahaemolyticus*. The cellulose synthase genes of selected genome were aligned using ClustalW, and the phylogenetic tree was inferred using the Neighbor-joining method through FastTree.

5.3.5 Putative horizontal gene transfer

Horizontal gene transfer is the major driver of genetic diversity, providing bacteria with properties that enable adaptation to various environments. An average of 126 ± 4.2 and 156 ± 45.3 potential HGT gene families were identified in weak and strong biofilm forming strains respectively as gene acquisition from outside *Vibrionales*. There were 123 and 129 predicted HGT events in PFR21C03 and PFR37D08 and 188 and 124 in PFR30J09 and PFR34B02 respectively. The results indicate that strong biofilm forming strains have more putative horizontal gene transfer than the weak biofilm forming strains. This may relate to better adaption to diverse environments through biofilm formation. The phylum of *Proteobacteria* (taxid: 1224) and *Gammaproteobacteria* (taxid: 1236) were suggested to be the main donor taxa, acquiring 39.5 ± 3.54 and 51 ± 21.21, 52.5 ± 0.71 and 60 ± 9.90 HGT genes among weak and strong biofilm forming strains, respectively. This observation is not surprising as the aquatic environments are preferred by *Proteobacteria* and *Gammaproteobacteria*, providing many opportunities for recombination. The unique gene clusters of rhamnose metabolism and the CRISPR-Cas system present in strong biofilm forming strains appear to be obtained by HGT events, that have resulted in gene diversity. Interestingly, the cellulose synthase operon was not included in the putative HGT event result, indicating the cellulose synthase function present in *V. parahaemolyticus* was from the order within *Vibrionales*. In this study, this *bcs* gene cluster was only presented in environmental isolates, and whether cellulose synthase operon only exists in environmental strains globally requires further study.

5.3.6 Prevalence of the cellulose synthase operon in *V. parahaemolyticus* genomes

The cellulose synthase operon was present in 22 out of 138 *V. parahaemolyticus* reference genomes from the NCBI dataset. The cellulose synthase operons of 22 *V. parahaemolyticus* genomes were aligned with one another, revealing a cellulose synthase operon conservatism.

Figure 5.4 depicts a diagram of the *bcs* locus and the transcription direction of cellulose synthase genes. The cellulose biosynthetic cluster was inserted on the chromosome 1 between the *ybbJ* and *cnoX* genes, except for strain *V. parahaemolyticus* HA2 that includes two genes, the helix-turn-helix (HTH) domain containing gene and the IS630 family gene (RefGenome: GCF_002504185.1).

Although the genomic analysis indicated that their cellulose synthase genes seem highly conserved in *V. parahaemolyticus*, the evolutionary analysis demonstrated these genes from each genome were not 100% identical, suggesting the *bcs* operon might be useful in distinguishing *V. parahaemolyticus* isolates. Interestingly in the present study, strong biofilm forming strains of PFR30J09 and PFR34B02 were clustered into a subgroup based on the cellulose operon. This section also examined whether the *bcs* gene cluster was restricted to environmental isolates. The results indicated that cellulose synthase operons were present in both environmental (73.08 percent, 19/26) and pathogenic (26.92 percent, 7/26) strains. Recent research analyzed the global population structure of unrelated clinical and environmental *V. parahaemolyticus* isolates and identified epistatic interaction between gene clusters for Type VI secretion system 1 (T6SS1) and cellulose biosynthesis in the flexible genome (Cui et al., 2015). However, in the present study, cellulose production may be associated with the presence of Type VI secretion system (T6SS) that is characterized by VgrG and Hcp (Table 5.4), regardless of whether the strains are clinical or environmental. This suggests different populations with distinct genomic characteristics. In this study, the gene co-occurrence analysis identified there were 468 co-occurring genes along with *bcsA*. These comprised the CRISPR-Cas system (*cas*, *cys* gene families), type II secretion system (*eps* gene family), rhamnose metabolic process (*rha* gene family) and capsular polysaccharide synthesis (*wec* gene family) co-occurring with *bcsA*, which was consistent with previous results from PPI analysis for two strong biofilm-forming *V. parahaemolyticus*.

Table 5. 4 Summary of the cellulose synthase operon in *V. parahaemolyticus*. *

Genome	Strain	Nation	BioSample ID	Source	TLH	TRH	TDH	VgrG_T6SS	Hcp_T6SS
GCF_001304775.1	FORC_006	South Korea: Gyeongnam	SAMN03140318	Environment: cutting board	+	-	-	+	+
GCF_006517795.1	Vb0624	China: Shenzhen	SAMN12123413	Environment: market	+	-	-	+	+
GCF_002504185.1	HA2	China:Tianjin	SAMN07680340	Environment: aquaculture	+	-	-	+	+
GCF_004194515.1	D3112	China	SAMN10591529	Environment: seawater	+	-	-	+	+
GCF_001758605.1	FORC_023	South Korea: Pusan	SAMN03701448	*Homo sapiens*	+	-	-	+	+
GCF_002209725.2	MAVP-Q	USA	SAMN05579852	*Homo sapiens*	+	+	+	+	+
GCF_016403045.1	81TDH2	India: Mangaluru	SAMN16844329	Seafood	+	-	-	+	+
GCF_013393845.1	LVP1	China	SAMN11579495	Seafood: crayfish	+	-	-	+	+
GCF_000430405.1	FDA_R31	USA:LA	SAMN02179882	Seafood: oyster	+	-	+	+	+
GCF_016834555.1	HP1	India: Kumta	SAMN16844529	Seafood: shrimp	+	-	-	+	+
GCF_021730085.1	VP157	China:Tianjin	SAMN17188296	Seafood: shrimp	+	-	-	+	+
GCF_001700835.1	CHN25	China	SAMN03325855	Seafood: shrimp	+	-	-	+	+
GCF_001636035.1	FORC_014	South Korea: Pusan	SAMN03457164	Seafood: toothfish	+	-	-	+	+
GCF_012274985.1	2012V-1165	USA	SAMN12648280	Stool	+	+	-	+	+

GCF_001682175.1	MAVP-Q	USA	SAMN03766034	Stool		+	+	+	+	+
GCF_002220985.3	MAVP-R	USA	SAMN06042545	Stool		+	+	-	+	+
GCF_009763565.1	2013V-1181	USA	SAMN12648285	Stool		+	+	+	+	+
GCF_000568495.1	UCM-V493	Unknown	SAMN03081521	Unknown		+	-	-	+	+
GCF_003612715.1	FORC_071	South Korea: Seoul	SAMN07629009	Unknown		+	-	-	+	+
GCF_012274865.1	AM51557	USA	SAMN12648303	Unknown		+	-	+	+	+
GCF_003612695.1	FORC_072	South Korea: Seoul	SAMN07629020	Unknown		+	-	-	+	+
GCF_009764055.1	2012AW-0224	USA	SAMN12648278	Unknown		+	-	-	+	+
PFR30G02	PFR30G02	New Zealand	-	Environment: seafood plant wastewater		+	-	-	+	+
PFR30J09	PFR30J09	New Zealand	-	Environment: seafood plant wastewater		+	-	-	+	+
PFR34B02	PFR34B02	New Zealand	-	Environment: seafood plant wastewater		+	-	-	+	+
PFR37C06	PFR37C06	New Zealand	-	*Homo sapiens*		+	-	-	+	+

*TLH stands for thermolabile hemolysin in *V. parahaemolyticus*, TDH stands for thermostable direct hemolysin, TRH stands for TDH-related hemolysin. T6SS stands for Type VI Secretion System in *V. parahaemolyticus*.

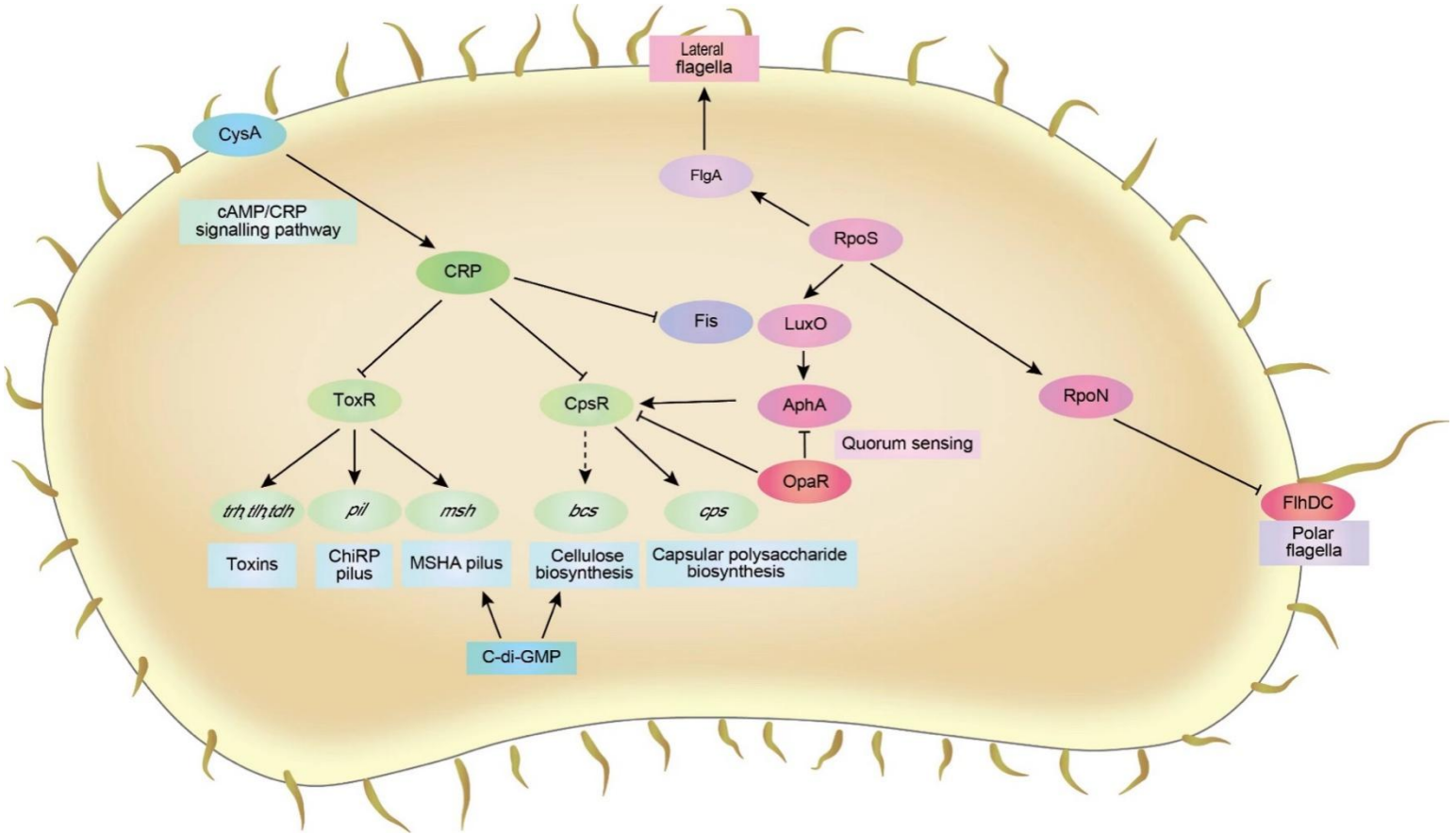

Figure 5. 4 Molecular mechanisms of biofilm formation in *V. parahaemolyticus*.

The known molecular mechanism was based on published studies (Abidi et al., 2022; Guo et al., 2020), presented using the solid line; the dash line represents the finding in this study.

5.4 Conclusion and perspectives

The expansion of gene families is a common strategy enabling bacteria to cope with diverse and changing environments. In this study, strong biofilm forming strains had high genetic diversity. In *V. parahaemolyticus*, the low percentage of the core genome (~ 33.20%) suggests more accessory genes that are critical for survival in diverse environments. This study identified that the phyla of *Proteobacteria* (taxid: 1224) and *Gammaproteobacteria* (taxid: 1236) were the main donor taxa for the genetic diversity in the strong biofilm forming strains. This observation is not surprising since aquatic environments are preferred by *Proteobacteria* and *Gammaproteobacteria*, providing many opportunities for recombination. Genes that are differentially abundant in strong biofilm forming genomes were associated with cellulose biosynthesis, rhamnose and other sugar metabolism, MSHA pili led attachment as well as the CRISPR-Cas system. Genes responsible for rhamnose metabolism and catalytic process, the CRISPR-Cas system as well as cellulose biosynthesis were believed to originate from HGT whereas cellulose biosynthesis was acquired within the order of *Vibrionales*.

This study is the first to show the correlation between cellulose secretion and robust biofilm formation in *V. parahaemolyticus.* The cellulose biosynthesis locus was initially assumed to be absent from other *Vibrio* species (Yildiz & Visick, 2009). The *bcs* operon responsible for cellulose production has been proposed for the classification and standardization of the nomenclature in *Proteobacteria* (Römling & Galperin, 2015). The distinctions of the *bcs* gene profiles from *Proteobacteria* are primarily from three areas: 1) the presence of the *bcsD* gene, 2) the presence of the *bcsE* and *bcsG* genes (and the absence of *bcsD*), 3) the absence of *bcsD*, *bcsE*, or *bcsG* (Römling & Galperin, 2015). A putative operon identified in *V. parahaemolyticus* has an organization similar to *E. coli*-like *bcs* operons, that have been found in *E. coli*, *Salmonella*, *Yersinia enterocolitica*, *V. fischeri* and *Pseudomonas* (Römling &

Galperin, 2015). Cellulose has been considered as one of the major causes of robust biofilm and strong resistance in *Salmonella*, *Cronobacter* and *E. coli* in the food industry (Hu et al., 2015; Kim et al., 2022; Sharma, 2012). Cellulose is an architectural element in biofilm matrices, providing advantages in water retention, porosity, mechanical resistance, low antigenicity and interaction with saccharidic and proteinaceous components of both bacteria and hosts. It enables biofilm with high sanitizer resistance. Solano et al. (2002) compared the effect of 30 ppm of sodium hypochlorite on the survival of biofilms of wild-type and cellulose mutants of *S*. Enteritidis formed on glass, 75% of the wild-type cells surviving a 20 min exposure to the disinfectant, while only 0.3% of the cellulose-deficient mutant cells survived, indicating the protective function of cellulose.

The interaction of the cellulose synthesis gene cluster and other genes in *V. parahaemolyticus* is unknown. A previous study identified epistatic interaction in the flexible genome between gene clusters for T6SS1 and cellulose biosynthesis, while clinical strains tend to depend on the antibacterial activity of T6SS1 proteins for survival in the aquatic milieu (Cui et al., 2020). The strains that lack T6SS depend on cellulose production (Cui et al., 2020). However, among the 138 *V. parahaemolyticus* genomes examined in the present study, the cellulose synthase operon was found to be present in both environmental (73.08%, 19/26) and pathogenic strains (26.92%, 7/26), and all cellulose synthase operons are not associated with the T6SS system. The reason for this discrepancy could be different clonal complexes of *V. parahaemolyticus* genomes used in the present study that differ those used in the earlier study. Symbiosis polysaccharide protein SypF has been identified in association with cellulose biosynthesis and production in *V. fischeri* via the polysaccharide biosynthesis protein VpsR, indicating that cellulose contributes to symbiotic initiation by promoting biofilm formation on the symbiotic organ surfaces (Darnell et al., 2008). In this study, the interaction between the VpsR homologue CpsR and cellulose

production was also identified in *V. parahaemolyticus*, reported for the first time, but whether cellulose plays roles in symbiosis in *V. parahaemolyticus* requires further investigation.

Although the present study demonstrated for the first-time cellulose is expressed and plays critical roles in persistence on abiotic surfaces in *V. parahaemolyticus*, the precise biochemical functions and chemical structures of cellulose component in biofilm matrices requires further identification. Indeed, the chemical elements of cellulose vary slightly between species with distinct *bcs* operon structures. For example, in *E. coli*, the cellulose in the biofilm matrix has been identified as phosphoethanolamined, whereas in *Pseudomonas*, the cellulose is amorphous. These differences have been comprehensively reviewed by (Abidi et al., 2022). Cellulase and enzymes may be opportunities in dismantling *V. parahaemolyticus* biofilms, additionally, inhibition of c-di-GMP signaling-dependent cellulose synthase have been reported as perspective approaches to control biofilm formation, for instance, Thongsomboon et al. (2018) reported that cellulose production in *E. coli* is controlled by c-di-GMP via regulating PilZ domain of BcsA and BcsE-BcsF-BcsG transmembrane signaling pathway, and BcsG is the potential target for inhibiting cellulose biosynthesis considering it is indispensable for the Bcs synthase functions in *E. coli*. Richter et al. (2020) pointed out c-di-GMP roles in the control of *E. coli* biofilm EPS cellulose production, revealed direct interaction of diguanylate cyclase DgcC and phosphodiesterase PdeK with cellulose synthase complex. However, limited is understood about mechanisms of bacterial cellulose synthase in *V. parahaemolyticus*, further study of inhibiting c-di-GMP dependent cellulose production is required to help on *V. parahaemolyticus* biofilm prevention and destruction.

5.5 Reference

Abidi, W., Torres-Sanchez, L., Siroy, A., & Krasteva, P. V. (2022). Weaving of bacterial cellulose by the Bcs secretion systems. *FEMS Microbiology Reviews*, *46*(2), fuab051. https://doi.org/10.1093/femsre/fuab051

Anriany, Y., Sahu, S. N., Wessels, K. R., McCann, L. M., & Joseph, S. W. (2006). Alteration of the rugose phenotype in *waaG* and *ddhC* mutants of *Salmonella enterica* serovar Typhimurium DT104 is associated with inverse production of curli and cellulose. *Applied and Environmental Microbiology*, *72*(7), 5002-5012.

Bankevich, A., Nurk, S., Antipov, D., Gurevich, A. A., Dvorkin, M., Kulikov, A. S., Lesin, V. M., Nikolenko, S. I., Pham, S., & Prjibelski, A. D. (2012). SPAdes: a new genome assembly algorithm and its applications to single-cell sequencing. *Journal of Computational Biology*, *19*(5), 455-477.

Buchfink, B., Reuter, K., & Drost, H. G. (2021). Sensitive protein alignments at tree-of-life scale using DIAMOND. *Nature Methods*, *18*(4), 366-368. https://doi.org/10.1038/s41592-021-01101-x

Chen, Y., Dai, J., Morris, J. G., & Johnson, J. A. (2010). Genetic analysis of the capsule polysaccharide (K antigen) and exopolysaccharide genes in pandemic *Vibrio parahaemolyticus* O3:K6. *BMC Microbiology*, *10*(1), 274. https://doi.org/10.1186/1471-2180-10-274

Cui, Y., Yang, C., Qiu, H., Wang, H., Yang, R., & Falush, D. (2020). The landscape of coadaptation in *Vibrio parahaemolyticus*. *Elife*, *9*, e54136.

Cui, Y., Yang, X., Didelot, X., Guo, C., Li, D., Yan, Y., Zhang, Y., Yuan, Y., Yang, H., Wang, J., Wang, J., Song, Y., Zhou, D., Falush, D., & Yang, R. (2015). Epidemic Clones,

Oceanic Gene Pools, and Eco-LD in the Free Living Marine Pathogen *Vibrio parahaemolyticus*. *Molecular Biology and Evolution*, *32*(6), 1396-1410. https://doi.org/10.1093/molbev/msv009

Danese, P. N., Pratt, L. A., & Kolter, R. (2000). Exopolysaccharide production is required for development of *Escherichia coli* K-12 biofilm architecture. *Journal of Bacteriology*, *182*(12), 3593-3596.

Darnell, C. L., Hussa, E. A., & Visick, K. L. (2008). The putative hybrid sensor kinase SypF coordinates biofilm formation in *Vibrio fischeri* by acting upstream of two response regulators, SypG and VpsR. *Journal of Bacteriology*, *190*(14), 4941-4950.

Eren, A. M., Esen, Ö. C., Quince, C., Vineis, J. H., Morrison, H. G., Sogin, M. L., & Delmont, T. O. (2015). Anvi'o: an advanced analysis and visualization platform for 'omics data. *PeerJ*, *3*, e1319.

Fang, Y., Visvalingam, J., Zhang, P., & Yang, X. (2022). Biofilm formation by Non-O157 Shiga toxin-producing *Escherichia coli* in monocultures and co-cultures with meat processing surface bacteria. *Food Microbiology*, *102*, 103902.

Gkana, E. N., Giaouris, E. D., Doulgeraki, A. I., Kathariou, S., & Nychas, G.-J. E. (2017). Biofilm formation by *Salmonella* Typhimurium and *Staphylococcus aureus* on stainless steel under either mono- or dual-species multi-strain conditions and resistance of sessile communities to sub-lethal chemical disinfection. *Food Control*, *73*, 838-846.

Greiner, L. L., Watanabe, H., Phillips, N. J., Shao, J., Morgan, A., Zaleski, A., Gibson, B. W., & Apicella, M. A. (2004). Nontypeable Haemophilus influenzae Strain 2019 Produces a Biofilm Containing *N*-Acetylneuraminic Acid That May Mimic Sialylated O-Linked Glycans. *Infection and Immunity*, *72*(7), 4249-4260.

Guo, L., Wang, J., Gou, Y., Tan, L., Liu, H., Pan, Y., & Zhao, Y. (2020). Comparative proteomics reveals stress responses of *Vibrio parahaemolyticus* biofilm on different surfaces: Internal adaptation and external adjustment. *Science of The Total Environment*, *731*, 138386.

Gurevich, A., Saveliev, V., Vyahhi, N., & Tesler, G. (2013). QUAST: quality assessment tool for genome assemblies. *Bioinformatics*, *29*(8), 1072-1075.

Hu, L., Grim, C. J., Franco, A. A., Jarvis, K. G., Sathyamoorthy, V., Kothary, M. H., McCardell, B. A., & Tall, B. D. (2015). Analysis of the cellulose synthase operon genes, *bcsA*, *bcsB*, and *bcsC* in Cronobacter species: Prevalence among species and their roles in biofilm formation and cell–cell aggregation. *Food Microbiology*, *52*, 97-105.

Jain, C., Rodriguez-R, L. M., Phillippy, A. M., Konstantinidis, K. T., & Aluru, S. (2018). High throughput ANI analysis of 90K prokaryotic genomes reveals clear species boundaries. *Nature Communications*, *9*(1), 1-8.

Kim, S.-H., Jyung, S., & Kang, D.-H. (2022). Comparative study of *Salmonella* Typhimurium biofilms and their resistance depending on cellulose secretion and maturation temperatures. *LWT*, *154*, 112700.

Kim, Y. K., & McCarter, L. L. (2000). Analysis of the polar flagellar gene system of *Vibrio parahaemolyticus*. *Journal of Bacteriology*, *182*(13), 3693-3704.

Lianou, A., Nychas, G.-J. E., & Koutsoumanis, K. P. (2020). Strain variability in biofilm formation: A food safety and quality perspective. *Food Research International*, *137*, 109424.

Liu, J., Qin, K., Wu, C., Fu, K., Yu, X., & Zhou, L. (2021). De Novo Sequencing Provides Insights Into the Pathogenicity of Foodborne *Vibrio parahaemolyticus* [Original

Research]. *Frontiers in Cellular and Infection Microbiology*, *11*. https://doi.org/10.3389/fcimb.2021.652957

Makarova, K. S., Haft, D. H., Barrangou, R., Brouns, S. J. J., Charpentier, E., Horvath, P., Moineau, S., Mojica, F. J. M., Wolf, Y. I., Yakunin, A. F., van der Oost, J., & Koonin, E. V. (2011). Evolution and classification of the CRISPR–Cas systems. *Nature Reviews Microbiology*, *9*(6), 467-477. https://doi.org/10.1038/nrmicro2577

Maturana, J. L., & Cárdenas, J. P. (2021). Insights on the Evolutionary Genomics of the Blautia Genus: Potential New Species and Genetic Content Among Lineages [Original Research]. *Frontiers in Microbiology*, *12*. https://doi.org/10.3389/fmicb.2021.660920

McCarter, L. L. (2001). Polar flagellar motility of the *Vibrionaceae*. *Microbiology and Molecular Biology Reviews*, *65*(3), 445-462.

Page, A. J., Cummins, C. A., Hunt, M., Wong, V. K., Reuter, S., Holden, M. T., Fookes, M., Falush, D., Keane, J. A., & Parkhill, J. (2015). Roary: rapid large-scale prokaryote pan genome analysis. *Bioinformatics*, *31*(22), 3691-3693.

Pang, R., Xie, T., Wu, Q., Li, Y., Lei, T., Zhang, J., Ding, Y., Wang, J., Xue, L., Chen, M., Wei, X., Zhang, Y., Zhang, S., & Yang, X. (2019). Comparative Genomic Analysis Reveals the Potential Risk of *Vibrio parahaemolyticus* Isolated From Ready-To-Eat Foods in China [Original Research]. *Frontiers in Microbiology*, *10*(186). https://doi.org/10.3389/fmicb.2019.00186

Parks, D. H., Imelfort, M., Skennerton, C. T., Hugenholtz, P., & Tyson, G. W. (2015). CheckM: assessing the quality of microbial genomes recovered from isolates, single cells, and metagenomes. *Genome Research*, *25*(7), 1043-1055.

Petit III, R. A., & Read, T. D. (2020). Bactopia: a flexible pipeline for complete analysis of bacterial genomes. *Msystems*, *5*(4), 10.1128/msystems. 00190-00120.

Qin, X., Wang, H., Miao, C., Yang, X., Zhang, Y., Feng, J., Forsythe, S. J., Man, C., & Jiang, Y. (2021). Comparative genomics reveals environmental adaptation differences between *Cronobacter* species. *Food Research International*, *147*, 110541.

Regmi, A., & Boyd, E. F. (2019). Carbohydrate metabolic systems present on genomic islands are lost and gained in *Vibrio parahaemolyticus*. *BMC Microbiology*, *19*(1), 112. https://doi.org/10.1186/s12866-019-1487-6

Richter, A. M., Possling, A., Malysheva, N., Yousef, K. P., Herbst, S., von Kleist, M., & Hengge, R. (2020). Local c-di-GMP Signaling in the Control of Synthesis of the *E. coli* Biofilm Exopolysaccharide pEtN-Cellulose. *Journal of Molecular Biology*, *432*(16), 4576-4595.

Richter, M., Rosselló-Móra, R., Oliver Glöckner, F., & Peplies, J. (2016). JSpeciesWS: a web server for prokaryotic species circumscription based on pairwise genome comparison. *Bioinformatics*, *32*(6), 929-931.

Römling, U., & Galperin, M. Y. (2015). Bacterial cellulose biosynthesis: diversity of operons, subunits, products, and functions. *Trends in Microbiology*, *23*(9), 545-557.

Seemann, T. (2014). Prokka: rapid prokaryotic genome annotation. *Bioinformatics*, *30*(14), 2068-2069.

Sharma, D. M. J. P. G. B. J. A. G. V. K. (2012). Role of Curli and Cellulose Expression in Adherence of *Escherichia coli* O157:H7 to Spinach Leaves. *Foodborne Pathogens and Disease*, *9*(2), 160-167. https://doi.org/10.1089/fpd.2011.1020

Solano, C., García, B., Valle, J., Berasain, C., Ghigo, J. M., Gamazo, C., & Lasa, I. (2002). Genetic analysis of *Salmonella enteritidis* biofilm formation: critical role of cellulose. *Molecular Microbiology*, *43*(3), 793-808.

Stalder, T., & Top, E. (2016). Plasmid transfer in biofilms: a perspective on limitations and opportunities. *npj Biofilms and Microbiomes*, *2*(1), 16022. https://doi.org/10.1038/npjbiofilms.2016.22

Thongsomboon, W., Serra, D. O., Possling, A., Hadjineophytou, C., Hengge, R., & Cegelski, L. (2018). Phosphoethanolamine cellulose: a naturally produced chemically modified cellulose. *Science*, *359*(6373), 334-338.

Verstraeten, N., Braeken, K., Debkumari, B., Fauvart, M., Fransaer, J., Vermant, J., & Michiels, J. (2008). Living on a surface: swarming and biofilm formation. *Trends in Microbiology*, *16*(10), 496-506. https://doi.org/10.1016/j.tim.2008.07.004

Wang, D. F., Steve; Palmer, Jon; Gagic, Dragana; Fletcher, Graham; On, Stephen;. (2022). Sodium Hypochlorite Susceptibility and Genetic Diversity of *Vibrio Parahaemolyticus*. *International Journal of Food Microbiology,* 385(2023), 110011.

Yang, Z., Wafula, E. K., Kim, G., Shahid, S., McNeal, J. R., Ralph, P. E., Timilsena, P. R., Yu, W.-b., Kelly, E. A., Zhang, H., Person, T. N., Altman, N. S., Axtell, M. J., Westwood, J. H., & dePamphilis, C. W. (2019). Convergent horizontal gene transfer and cross-talk of mobile nucleic acids in parasitic plants. *Nature Plants*, *5*(9), 991-1001. https://doi.org/10.1038/s41477-019-0458-0

Yildiz, F. H., & Visick, K. L. (2009). *Vibrio* biofilms: so much the same yet so different. *Trends in Microbiology*, *17*(3), 109-118. https://doi.org/10.1016/j.tim.2008.12.004

Yuan, L., Burmølle, M., Sadiq, F. A., Wang, N., & He, G. (2018). Interspecies variation in biofilm-forming capacity of psychrotrophic bacterial isolates from Chinese raw milk. *Food Control*, *91*, 47-57.

Zerbino, D. R., & Birney, E. (2008). Velvet: algorithms for de novo short read assembly using de Bruijn graphs. *Genome Research*, *18*(5), 821-829.

Zhu, Q., Kosoy, M., & Dittmar, K. (2014). HGTector: an automated method facilitating genome-wide discovery of putative horizontal gene transfers. *BMC Genomics*, *15*(1), 1-18.

Chapter 6. Transcriptome analysis of *V. parahaemolyticus* planktonic and biofilm cells using RNA sequencing (RNA-seq)

This study is in preparation and about to be submitted to journal.

6.1 Introduction

Comparative genomics has identified some sets of genes associated with biofilm formation in Chapter 4 and 5 (Wang et al., 2023). However, expression of these genes is necessary for their active involvement in biofilm formation. Comparative RNA analysis of planktonic and biofilm cells assists in understanding functional genes involved in biofilm formation. For instance, RNA-seq analysis identified 1292 (23.5%) genes were differentially expressed in biofilm cells and planktonic cells of *B. cereus* ATCC 14579 (Caro-Astorga et al., 2020). This study found that biofilm and planktonic populations were metabolically differentiated with rearranged metabolic pathways including the synthesis of the extracellular matrix, sporulation, reinforcement of the cell wall, activation of the ROS detoxification machinery and production of secondary metabolites in the biofilm cells. Chung et al. (2021) used RNA-seq to understand how *S. aureus* FORC_062 interacted with chicken breast, showing upregulation of carbohydrate metabolism, lipid metabolism, amino acid deamination, amino acid/dipeptide transporters, enterotoxin production, type VII secretion system and tetracycline resistance proteins as well as downregulation of amino acid biosynthesis. This demonstrated *S. aureus* FORC_062 utilized carbohydrates and lipids as nutrient sources and may import and utilize amino acids rather than synthesize them during colonization of chicken breast.

The present study compared the gene expression of planktonic and biofilm cells of *V. parahaemolyticus*, to understand the importance of specific genes expressed or repressed during biofilm formation.

6.2 Methods

6.2.1 Cell cultures

V. parahaemolyticus PFR21C03, selected as a representative strain isolated from a seafood environment in New Zealand, was used for this study. More information can be found in Section 3.2.1, Chapter 3.

6.2.2 Biofilm cell development and detachment

Coupon preparation, biofilm development and biofilm cell detachment are detailed in Sections 4.2.2 and Section 4.2.7, Chapter 4.

6.2.3 RNA extraction and sequencing

Total RNA was extracted using Trizol® Max™ Bacterial RNA Isolation Kit (Invitrogen™, Thermo Fisher Scientific, USA) as described by the product manual. *V. parahaemolyticus* culture (1.5 mL, containing 10^8~10^9 cells; biofilm cells were aseptically swabbed from stainless steel coupons using RNase free cotton swab, planktonic cells were collected according to Section 3.2.1) was transferred to a sterile prechilled tube, and centrifuged at 6000 × *g* for 5 min at 4 ℃. The supernatant was removed, the pellet of cells mixed with preheated Max™ Bacterial Enhancement Reagent (200 µL; Invitrogen™, Thermo Fisher Scientific, USA). Heated the tube to 95 ℃ for 4 min to lyse the cells. Trizol® reagent (1 mL; Invitrogen™ Thermo Fisher Scientific, USA) was added to the lysate and held at room temperature for 5 min. Cold chloroform (0.2 mL; Thermo Fisher Scientific, USA) was added and after 2-3 min, centrifuged the tube at 12000 × *g* for 15 min at 4 ℃. The upper, colorless phase was transferred to another tube, to which 0.5 mL of cold isopropanol (Thermo Fisher Scientific, USA) was added and held at room temperature for 10 min. The RNA pellet was collected after

centrifugation at 15000 × *g* for 10 min at 4 ℃, washed using 75% ethanol, and resuspended in 50 μL of prechilled RNase free water (Invitrogen™, Thermo Fisher Scientific, USA). This protocol was processed on ice. Triplicate was prepared for each sample of biofilm and planktonic cells.

RNA samples were sent to a contract laboratory to remove rRNA and prepare an RNA library for RNA-seq (AZENTA Life Sciences Ltd., USA). Total RNA of each sample was quantified and qualified by Agilent 2100 Bioanalyzer (Agilent Technologies, Palo Alto, CA, USA), NanoDrop (Thermo Fisher Scientific, USA) and 1% agrose gel. 1 μg total RNA with RIN value above 7 was used for following library preparation. Next generation sequencing library preparations were constructed according to the manufacturer's protocol (NEBNext® Ultra™ RNA Library Prep Kit for Illumina®; Illumina, San Diego, CA, USA). Then libraries with different indices were multiplexed and loaded on an Illumina HiSeq instrument according to manufacturer's instructions (Illumina, San Diego, CA, USA). Sequencing was carried out using a 2x150bp paired-end configuration; image analysis and base calling were conducted by the HiSeq Control Software + OLB + GAPipeline-1.6 on the HiSeq instrument.

6.2.4 RNA-seq data analysis

Raw data was assessed for quality and filtered to remove adapters, reads containing N < 5 % and reads of quality value Q < 15 using SOAPnuke (version 1.5.2) (Chen et al., 2017). Clean reads were aligned to reference genome of RIMD2210633 and assemble using HISAT2 (version 2.2.1) (Kim et al., 2019). The aligned reads were assembled using StringTie (version 2.2.1) (Pertea et al., 2015), and combined with Cuffmerge (version 2.2) (Trapnell et al., 2010). Quantitative expression analysis was conducted via Bowtie2 (version 2.4.5) and RSME (version 1.3.1) (Langmead & Salzberg, 2012; Li & Dewey, 2011), to align clean reads to the reference sequence, and calculate the expression of genes and transcripts. Reads were

normalized to transcripts per million (TPM), and differentially expressed genes (DEGs) were identified between the control group (planktonic cells) and the sample group (biofilm cells) using DESeq2 (https://github.com/thelovelab/DESeq2), cut-offs for the significant differential genes were Padj < 0.05 & Log2 Fold Change > |2| (Wang et al., 2010). Significantly differentiated genes were displayed using a Volcano Map and Scatter Plot in R. RNA-seq data analysis was completed by BGI Tech Solutions (Hongkong) Co. Ltd.

6.2.5 Functional enrichment analysis

mRNAs were aligned to KEGG database (https://www.genome.jp/kegg/) and uniprot database (https://www.uniprot.org) to obtain KEGG annotation and GO annotation using diamond (version 2.0.15.153) (Buchfink et al., 2021), enriched functional modules were generated based on annotations above and hypergeometric model, an FDR < 0.05 was used as the cut-off for significance.

6.3 Results and discussion

6.3.1 Differentially expressed genes (DEGs) between *V. parahaemolyticus* planktonic and biofilm cells

Clean reads were aligned to a reference genome RIMD2210633, the average mapping ratio of reads from the control group (planktonic cells) was 87.58% (uniquely mapping ratio was 86.16%). The mapping ratio of reads from the case group (biofilm cells) averaged 92.47% (uniquely mapping ratio was 90.33%). Known ORF/genes from the control group averaged 3872, while those from the case group averaged 3849. Information about the transcript expression level is in Supplemental Figure 1 according to the values of fragments per kilobase of transcript per million fragments mapped (FPKM <= 1 indicates a gene with a very low

expression level, FPKM > 1 & < 10 indicates a gene with a low expression level, FPKM > = 10 indicates a gene highly or moderately expressed).

DEGs were obtained based on comparing transcripts of *V. parahaemolyticus* planktonic cells and young biofilm cells (6-h old). The reason for collecting young biofilm cells was due to the routine sanitization protocol of 2-6 h on seafood processing surfaces. Transcriptome expression will help understand expression profiles of biofilm cells and highlight gene targets to design hygiene strategies to interfere with biofilm formation in 2-6 h. According to results from Section 3.3.2, PFR21C03 produced 6.63 $\log_{10}$ CFU/cm^2 cells in biofilm communities on stainless steel coupons after 6 h.

DEGs analysis based on DESeq2 revealed 74 significantly differentiated genes between planktonic cells and biofilm cells (Padj < 0.05 & Log2 Fold Change > |2|). A Volcano Map demonstrated the distribution of DEGs between planktonic and biofilm cells of *V. parahaemolyticus* (Figure 6.1). Annotation of DEGs is shown in Table 6.1, listing the lotus tag, reference protein ID, gene name, protein name and associated GO terms. The ratio of DEGs was 1.6% compared with the coding capacity of 4742 (ORFs in reference genome). This result suggests the biofilm population was at the initial stage of biofilm formation. Upregulated and downregulated DEGs are listed in Table 6.1, there were 11 upregulated and 65 downregulated genes among the DEGs.

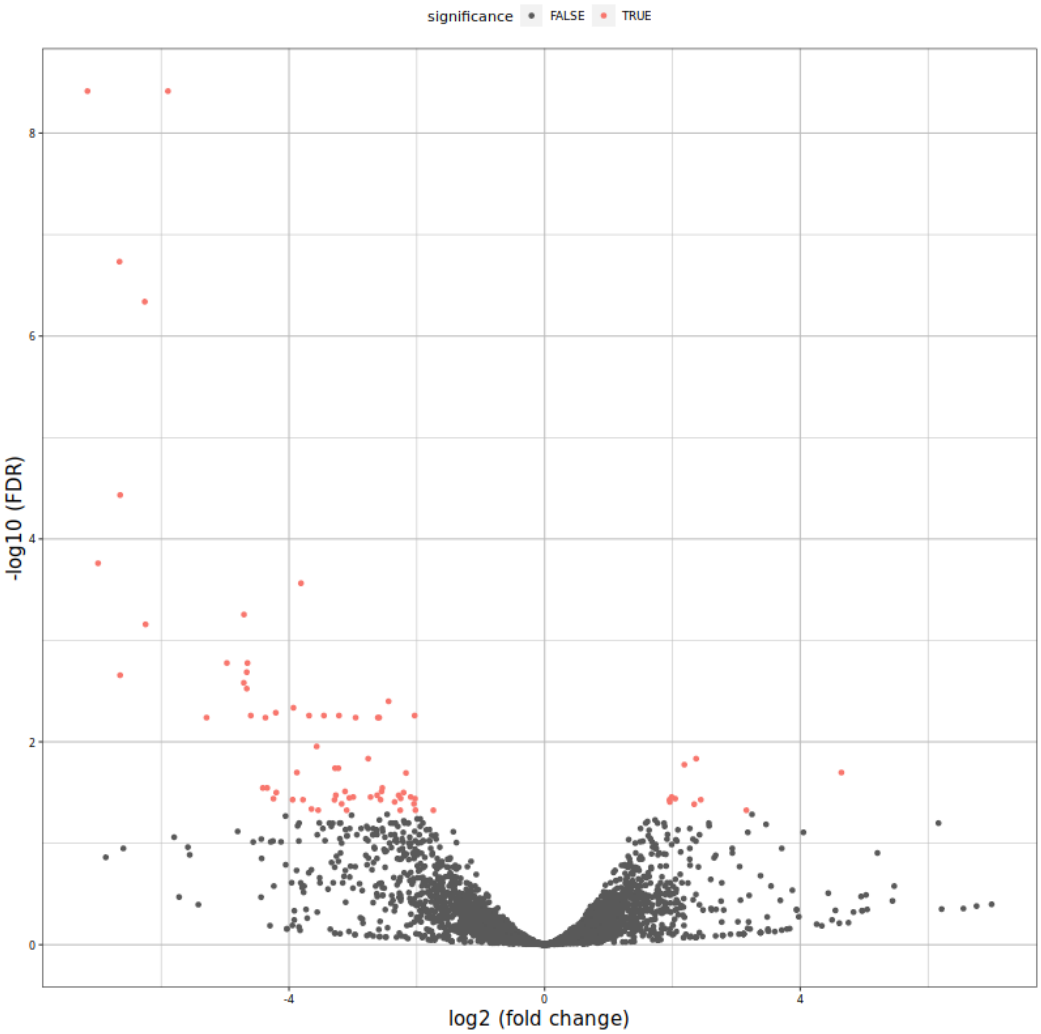

Figure 6. 1 Gene level volcano map of Planktonic-vs-Biofilm cells in *V. parahaemolyticus*. The x axis represents the fold change after conversion to log2, and the y axis represents the significance value after conversion to log10. Red indicates significantly different genes; grey indicates non-significantly different genes.

Table 6. 1 Annotations for Differentially Expressed Genes (DEGs) in Planktonic-vs-Biofilm cells.

Lotus tag	Ref protein	Gene/old lotus tag	Protein	Gene ontology (GO) terms	Up-/Down-regulated genes (Up/Dw in abbreviation)
VP_RS00075	WP_005458680.1	*VP0018*	Hsp20 family protein	-	Dw
VP_RS16645	WP_005463958.1	*VPA0287*	chaperonin GroEL	GO:0005515 - protein binding; GO:0016887 - ATP hydrolysis activity; GO:0006457 - protein folding	Dw
VP_RS17910	WP_005433302.1	*VPA0563*	Dps family protein	GO:0008199 - ferric iron binding, GO:0016491 - oxidoreductase activity	Dw
VP_RS15195	WP_005451019.1	*punC, VP3064*	purine nucleoside transporter PunC	GO:0016020 - membrane, GO:0042910 - xenobiotic transmembrane transporter activity, GO:1990961 - xenobiotic detoxification by transmembrane export across the plasma membrane	Dw
VP_RS12600	-				Dw
VP_RS17435	WP_010649632.1	*VPA0460*	PAS factor family protein	-	Dw
VP_RS22220	WP_000224891.1	*deoD, VPA1475*	purine-nucleoside phosphorylase	GO:0004731 - purine-nucleoside phosphorylase activity, GO:0043096 - purine nucleobase salvage	Dw
VP_RS16485	WP_005464033.1	*VPA0252*	hypothetical protein	-	Dw
VP_RS07960	WP_004416416.1	*VP1653*	tripartite tricarboxylate transporter permease	-	Dw
VP_RS08215	WP_005446094.1	*VP1706*	hypothetical protein		Dw
VP_RS18295	WP_017448113.1	*VPA0645*	dihydrolipoamide acetyltransferase family protein	GO:0006096 - glycolytic process	Dw

VP_RS18305	WP_005431459.1	*pdhA, VPA0647*	pyruvate dehydrogenase (acetyl-transferring) E1 component subunit alpha	GO:0045250 - cytosolic pyruvate dehydrogenase complex, GO:0004739 - pyruvate dehydrogenase (acetyl-transferring) activity, GO:0006086 - acetyl-CoA biosynthetic process from pyruvate	Dw
VP_RS07955	WP_005426618.1	*VP1652*	tripartite tricarboxylate transporter TctB family protein	GO:0005215 - transporter activity	Dw
VP_RS19270	WP_000035884.1	*VPA0857*	hypothetical protein	-	Dw
VP_RS18845	WP_020196304.1	*VPA0766*	YbaK/EbsC family protein	-	Dw
VP_RS16120	WP_007161257.1	*rimK, VPA0173*	L-glutamate ligase	GO:0005524 - ATP binding, GO:0046872 - metal ion binding, GO:0036211 - protein modification process	Dw
VP_RS21995	WP_005392455.1	*zau*	azurin	GO:0005507 - copper ion binding, GO:0009055 - electron transfer activity	Dw
VP_RS11590	WP_005436580.1	*glpD, VP2388*	glycerol-3-phosphate dehydrogenase	GO:0009331 - glycerol-3-phosphate dehydrogenase complex, GO:0004368 - glycerol-3-phosphate dehydrogenase (quinone) activity, GO:0006072 - glycerol-3-phosphate metabolic process	Dw
VP_RS04695	WP_005486978.1	*VP0958*	CBS domain-containing protein		Dw
VP_RS05440	WP_005459987.1	*htpX, VP1118*	protease HtpX	GO:0004222 - metalloendopeptidase activity, GO:0006508 - proteolysis	Dw
VP_RS16105	WP_011080224.1	*VPA0170*	arginine decarboxylase	GO:0008792 - arginine decarboxylase activity, GO:0008295 - spermidine biosynthetic process	Dw
VP_RS20705	WP_015313398.1	*VPA1156*	electron transfer flavoprotein subunit beta/FixA family protein	GO:0009055 - electron transfer activity	Dw

VP_RS23630	WP_017063012.1	-	hypothetical protein	-	Dw
VP_RS07000	WP_005451837.1	*VP1443*	TerB family tellurite resistance protein	-	Dw
VP_RS16650	WP_005395278.1	-	hypothetical protein	-	Dw
VP_RS18030	WP_012129104.1	*VPA0588*	hypothetical protein	-	Dw
VP_RS19250	WP_010649293.1	*VPA0853*	DUF1097 domain-containing protein	GO:0005886 - plasma membrane	Dw
VP_RS18385	WP_014234059.1	*VPA0666*	YgjV family protein	-	Dw
VP_RS06545	WP_017630977.1	*VP1349*	4-hydroxyphenylpyruvate dioxygenase	GO:0003868 - 4-hydroxyphenylpyruvate dioxygenase activity, GO:0006559 - L-phenylalanine catabolic process, GO:0006572 - tyrosine catabolic process	Dw
VP_RS15065	WP_005461432.1	*VP3037*	5-(carboxyamino)imidazole ribonucleotide synthase	GO:0004638 - phosphoribosylaminoimidazole carboxylase activity, GO:0005524 - ATP binding, GO:0046872 - metal ion binding, GO:0006189 - 'de novo' IMP biosynthetic process	Up
VP_RS18555	WP_009704179.1	*VPA0703*	hypothetical protein		Dw
VP_RS03190	WP_011078440.1	*purL*	hosphoribosylformylglycin amidine synthase	GO:0004642 - phosphoribosylformylglycinamidine synthase activity	Up
VP_RS14035	WP_009843368.1	*VP2852*	co-chaperone GroES	GO:0005524 - ATP binding, GO:0140662 - ATP-dependent protein folding chaperone	Dw
VP_RS22195	WP_001038492.1	*VPA1469*	Lpp/OprI family alanine-zipper lipoprotein	-	Dw

VP_RS02990	WP_010446203.1	*VP0622*	alanine/glycine: cation symporter family protein	GO:0016020 - membrane, GO:0005283 - amino acid: sodium symporter activity, GO:0006814 - sodium ion transport, GO:0006865 - amino acid transport	Dw
VP_RS08185	WP_005464548.1	*exsA, VP1699*	type III secretion system transcriptional regulator ExsA	-	Up
VP_RS11815	WP_010436196.1	*VP2436*	deoxyribose-phosphate aldolase	GO:0004139 - deoxyribose-phosphate aldolase activity, GO:0009264 - deoxyribonucleotide catabolic process	Dw
VP_RS06810	WP_005373381.1	*tssB, VP1402*	type VI secretion system contractile sheath small subunit	GO:0003674 - molecular_function, GO:0033103 - protein secretion by the type VI secretion system	Dw
VP_RS15460	WP_005428499.1	-	hypothetical protein	-	Dw
VP_RS19080	WP_014234292.1	*cra, VPA0814*	catabolite repressor/activator	GO:0003677 - DNA binding, GO:0006355 - regulation of DNA-templated transcription, GO:0009750 - response to fructose	Dw
VP_RS17005	WP_000846696.1	*VPA0367*	spermidine/putrescine ABC transporter substrate-binding protein	GO:0055052 - ATP-binding cassette (ABC) transporter complex, substrate-binding subunit-containing, GO:0019808 - polyamine binding	Dw
VP_RS22810	WP_012130061.1	*VPA1599*	patatin-like phospholipase family protein	-	Dw
VP_RS11810	WP_008218776.1	*VP2435*	thymidine phosphorylase	GO:0009032 - thymidine phosphorylase activity, GO:0006139 - nucleobase-containing compound metabolic process	Dw

VP_RS20540	WP_017634262.1	*VPA1121*	acyl-CoA dehydrogenase family protein	GO:0016627 - oxidoreductase activity, acting on the CH-CH group of donors	Dw
VP_RS11420	WP_012128724.1	*VP2352*	transcriptional regulator BolA	-	Dw
VP_RS14055	WP_009698897.1	*VP2857*	CpxP family protein	-	Dw
VP_RS16115	WP_005459284.1	*VPA0172*	RimK/LysX family protein	-	Dw
VP_RS04920	WP_005481867.1	*VP1008*	porin	GO:0016020 - membrane, GO:0015288 - porin activity	Up
VP_RS16100	WP_006741236.1	*VPA0169*	agmatinase	GO:0008783 - agmatinase activity, GO:0008295 - spermidine biosynthetic process	Dw
VP_RS21325	WP_009846872.1	*VPA1286*	MarR family transcriptional regulator	GO:0003677 - DNA binding, GO:0003700 - DNA-binding transcription factor activity	Dw
VP_RS22805	WP_005480168.1	*VPA1598*	N-acetylglucosamine-binding protein GbpA	-	Dw
VP_RS02075	WP_000749332.1	*VP0433*	Do family serine endopeptidase	GO:0030288 - outer membrane-bounded periplasmic space, GO:0004252 - serine-type endopeptidase activity, GO:0005515 - protein binding, GO:0006508 - proteolysis, GO:0006950 - response to stress	Dw
VP_RS00735	WP_000961392.1	*VP0149*	hypothetical protein	-	Dw
VP_RS06815	WP_005426840.1	*tssC, VP1403*	type VI secretion system contractile sheath large subunit	GO:0033104 - type VI protein secretion system complex, GO:0003674 - molecular_function, GO:0033103 - protein secretion by the type VI secretion system	Dw
VP_RS07815	WP_010448069.1	*VP1624*	Bax inhibitor-1/YccA family protein	-	Dw

VP_RS10165	WP_001907465.1	*oppB, VP2090*	oligopeptide ABC transporter permease OppB	GO:0016020 - membrane, GO:0055085 - transmembrane transport	Up
VP_RS04940	WP_005378407.1	*csgD, VP1012*	cold shock domain-containing protein CspD	GO:0008156 - negative regulation of DNA replication, GO:0009409 - response to cold	Dw
VP_RS10610	WP_017106165.1	*VP2185*	amidophosphoribosyltransferase	GO:0004044 - amidophosphoribosyltransferase activity, GO:0009152 - purine ribonucleotide biosynthetic process	Up
VP_RS14295	WP_017091565.1	*purH, VP2896*	bifunctional phosphoribosylaminoimidazolecarboxamide formyltransferase/IMP cyclohydrolase	GO:0003937 - IMP cyclohydrolase activity, GO:0004643- phosphoribosylaminoimidazolecarboxamide formyltransferase activity, GO:0009152 - purine ribonucleotide biosynthetic process	Up
VP_RS16780	WP_017447972.1	*VPA0314*	DMT family transporter	GO:0005215 - transporter activity, GO:0055085 - transmembrane	Dw
VP_RS19550	WP_005479370.1	*VPA0914*	hypothetical protein	-	Dw
VP_RS15795	WP_015312785.1	*VPA0113*	hypothetical protein	-	Dw
VP_RS17190	WP_005480191.1	*pyrC, VPA0408*	dihydroorotase	GO:0004151 - dihydroorotase activity, GO:0009220 - pyrimidine ribonucleotide biosynthetic process	Up
VP_RS20335	WP_017447449.1	*VPA1077*	DUF5666 domain-containing protein	-	Dw
VP_RS04575	WP_005384268.1	*VP0939*	Tim44 domain-containing protein	-	Dw
VP_RS05990	WP_004726370.1	*VP1233*	GrxA family glutaredoxin	-	Dw
VP_RS00770	WP_005384732.1	*VP0156*	uracil-xanthine permease family protein	GO:0016020 - membrane, GO:0015205 - nucleobase transmembrane transporter activity	Up

VP_RS15440	WP_010453583.1	*VPA0040*	DUF413 domain-containing protein	-	Dw
VP_RS00395	WP_005379165.1	*VP0076*	universal stress protein UspA	-	Dw
VP_RS21330	WP_005477256.1	*VPA1287*	CDF family Co(II)/Ni(II) efflux transporter DmeF	GO:0016020 - membrane, GO:0008324 - monoatomic cation transmembrane transporter activity, GO:0006812 - monoatomic cation transport, GO:0055085 - transmembrane transport	Dw
VP_RS09705	WP_005385782.1	*VP1997*	ABC transporter permease	GO:0042626 - ATPase-coupled transmembrane transporter activity, GO:0140359 - ABC-type transporter activity	Up
VP_RS14115	WP_005428788.1	*VP2869*	cation acetate symporter	-	Dw
VP_RS16715	WP_015312889.1	*VPA0300*	DUF1254 domain-containing protein	-	Dw
VP_RS21045	WP_004730049.1	*VPA1226*	DUF496 family protein	-	Dw

6.3.2 Kyoto Encyclopedia of Genes and Genomes (KEGG) pathway enrichment analysis of DEGs

To have a physiological screen of functions related to DEGs, functional KEGG pathway enrichment was performed. This identified 29 KEGG pathways, with 23 of them located in the metabolism (Supplemental Table 1). Within these 29 pathways, those containing most genes were representing metabolic pathways (KEGG: ko01100). They were biosynthesis of secondary metabolites (KEGG: ko01110), purine metabolism (KEGG: ko00230), propanoate metabolism (KEGG: ko00640), valine, leucine and isoleucine degradation (KEGG: ko00280), pyrimidine metabolism (KEGG: ko00240) and biofilm formation (KEGG: ko02025). These pathways indicated changes in global metabolism, amino acid metabolism, nucleotide metabolism, carbohydrate metabolism and cellular community in the biofilm cells of *V. parahaemolyticus* (Figure 6.2). In KEGG database, model microorganisms were used, such as *E. coli*, *P. aeruginosa*, and *V. parahaemolyticus* was not included as a model microorganism. Pathway of "Biofilm formation - *Pseudomonas aeruginosa*" was assigned by KEGG database based on DEGs, indicating *V. parahaemolyticus* DEGs have genes functioning similarly in the biofilm formation.

This result agrees with Caro-Astorga et al. (2020), where the biofilm population of *B. cereus* rearranged nucleotides and energy metabolism, changed the production of secondary metabolites and synthesis of extracellular matrix. The production of secondary metabolites was upregulated in the biofilm cells, contributing to colonization and protection against competitors. In the present study, there were 9 DEGs identified in the biosynthesis of secondary metabolites (KEGG: ko01110), the upregulated genes were *VP3037 (purK)*, *purH* and *VP2185 (purF)* and downregulated genes were *VPA0645*, *pdhA*, *glpD*, *VPA1121*, *deoD*. Upregulation of *pur* genes and downregulation of *deoD* contribute to nucleotide metabolism in the present study. Interplay

between nucleotide metabolism and biofilm formation is conserved in multiple bacteria, for example, *E. coli*, *P. aeruginosa* and *Vibrio cholerae* (Garavaglia et al., 2012). In the present study, *VPA0645*, *pdhA*, *glpD* and *VPA1121* modify metabolite flux to differentiate planktonic and biofilm cells via propanoate metabolism (KEGG: ko00640), valine, leucine and isoleucine degradation (KEGG: ko00280) and glycerophospholipid metabolism (KEGG: ko00564). In another study, *Bifidobacterium longum* co-culturing with *Bacteroides ovatus* (Case group A), *B. ovatus* co-culturing with *Enterococcus faecalis* (Case group B), *Bacteroides ovatus* co-culturing with *E. faecalis* and *Lactobacillus gasseri* (Case group C), all identified DEGs assigned to the biosynthesis of secondary metabolites (KEGG: ko01110), in comparison with the sole culture (control group) to form biofilms (Xu et al., 2023).

In the present study, genes of *VP3037* (*purK*), *purL*, *purH*, *VP2185* (*purF*) and *deoD* were assigned to purine metabolism (KEGG: ko00230), with *VP3037* (*purK*), *purl*, *purH* and *VP2185* (*purF*) upregulated and *deoD* downregulated. The expression of purine metabolism was highlighted using red colored rectangles (upregulated) and yellow rectangles (downregulated) (Figure 6.3). This figure was generated based on KEGG Module database for *V. parahaemolyticus* DEGs. The *pur* genes promote *de novo* purine biosynthesis (M00048). Downregulation of *deoD* associates with repressed adenine ribonucleotide degradation (M00958), guanine ribonucleotide degradation (M00959) and purine degradation (M00546).

In *E. coli*, deletion of *purH* using transposon mutagenesis induced *E. coli* biofilm dispersion (Hadjifrangiskou et al., 2012). The inactivation of *purH* via constructing a *purH* mutant influences adhesion factor expression (Garavaglia et al., 2012). In a Methicillin-Resistant *S. aureus*, the *purF* mutant had significantly lower ADP and ATP levels and less biofilm formation *in vitro* (Li et al., 2021). However, in another study of *E. coli*, sole deletion of *purF* did not influence the adherence *in vitro*, but led to that △*purF* mutant was unable to form

biofilms in yeast extract-Casamino Acids (YESCA) medium (Shaffer et al., 2017). In the present study, *VP2435* (*deoA*), *deoD* and *pyrC* were associated with pyrimidine metabolism (KEGG: ko00240) and nucleotide metabolism (KEGG: ko01232) in *V. parahaemolyticus*, which is likely to be associated with adhesion and EPS production. In *V. cholerae*, pyrimidines control EPS production and biofilm formation via the regulator CytR (Haugo & Watnick, 2002), suggesting a relationship between pyrimidine metabolism and biofilm formation. Intracellular nucleotide availability influences transcription of curli operons in *E. coli*, suggesting a link between curli production and pyrimidine metabolism (Garavaglia et al., 2012). In a study to investigate gene expression in early biofilm of *Streptococcus pneumoniae* using microarray, expression of purine and pyrimidine nucleotide metabolic pathways might be required for the growth of cells in biofilms and the initial stage of biofilm formation (Yadav et al., 2012).

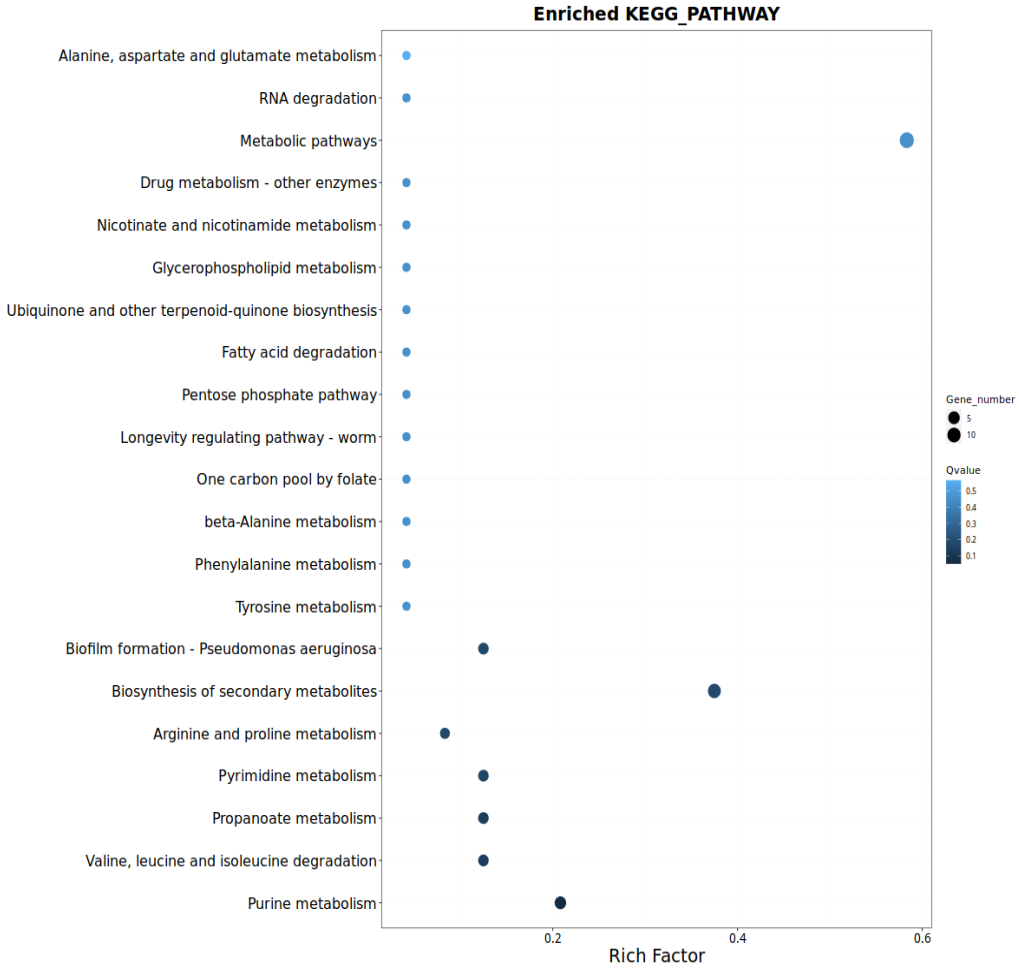

Figure 6. 2 Enriched Kyoto Encyclopedia of Genes and Genomes (KEGG) pathways by Differentially expressed genes (DEGs).

The x axis presents the enrichment ratio, the y axis presents class name of KEGG pathways, darkness of blue indicates the enriched significance, and size of round shape presents the number of genes annotated to this KEGG class.

(a)

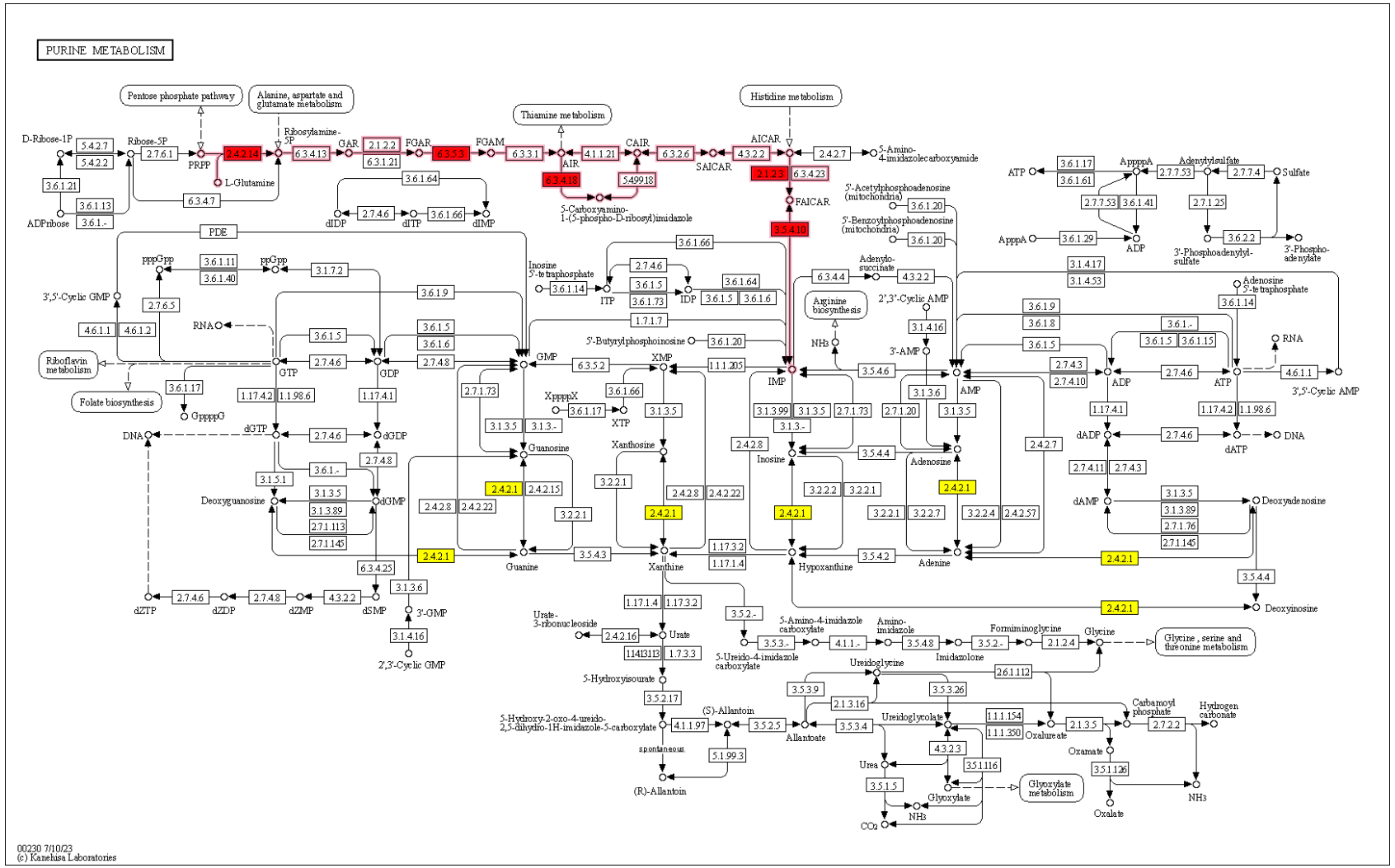
PURINE METABOLISM
Pentose phosphate pathway
Alanine, aspartate and glutamate metabolism
Thiamine metabolism
Histidine metabolism
Riboflavin metabolism
Folate biosynthesis
Arginine biosynthesis
Glycine , serine and threonine metabolism
Glyoxylate metabolism
D-Ribose-1P
Ribose-5P
PRPP
L-Glutamine
Ribosylamine-5P
GAR
FGAR
FGAM
AIR
CAIR
SAICAR
AICAR
5-Amino-4-imidazolecarboxyamide
FAICAR
5-Carboxyamino-1-(5-phospho-D-ribosyl)imidazole
ADPribose
dIDP
dITP
dIMP
PDE
pppGpp
ppGpp
3',5'-Cyclic GMP
RNA
GTP
GDP
GMP
IMP
XMP
ITP
IDP
Inosine 5'-triphosphate
5'-Butyrylphosphoinosine
GpppG
DNA
dGTP
dGDP
dGMP
Deoxyguanosine
dZTP
dZDP
dZMP
dSMP
3'-GMP
2',3'-Cyclic GMP
XpppX
XTP
Guanosine
Guanine
Xanthosine
Xanthine
Inosine
Hypoxanthine
Adenosine
Adenine
Deoxyinosine
Deoxyadenosine
AMP
ADP
ATP
dADP
dATP
dAMP
3'-AMP
2',3'-Cyclic AMP
3',5'-Cyclic AMP
NH3
Urate-3-ribonucleoside
Urate
5-Hydroxyisourate
5-Hydroxy-2-oxo-4-ureido-2,5-dihydro-1H-imidazole-5-carboxylate
(S)-Allantoin
(R)-Allantoin
spontaneous
Allantoate
Ureidoglycolate
Ureidoglycine
5-Amino-4-imidazole carboxylate
5-Ureido-4-imidazole carboxylate
Amino-imidazole
Imidazolone
Formiminoglycine
Glycine
Urea
Glyoxylate
Oxalureate
Oxamate
Oxalate
CO2
NH3
Carbamoyl phosphate
Hydrogen carbonate
ATP
AppppA
Adenylylsulfate
Sulfate
3'-Phosphoadenylyl-sulfate
3'-Phospho-adenylate
5'-Acetylphosphoadenosine (mitochondria)
5'-Benzoylphosphoadenosine (mitochondria)
Adenylo-succinate
Adenosine 5'-triphosphate
RNA
DNA
3',5'-Cyclic AMP
00230 7/10/23
(c) Kanehisa Laboratories

Figure 6. 3 Upregulated and downregulated genes in purine metabolism. (a) Upregulated *pur* genes in purine metabolism map and the influenced KEGG module. Red shapes represent upregulated genes and yellow represent downregulated genes. Red line in (a) indicates module of *de novo* purine biosynthesis (M00048), red line in (b) represents modules of adenine ribonucleotide degradation (M00958), guanine ribonucleotide degradation (M00959) and purine degradation. Colored shapes were generated based on KEGG Module database for *V. parahaemolyticus* DEGs.

(b)

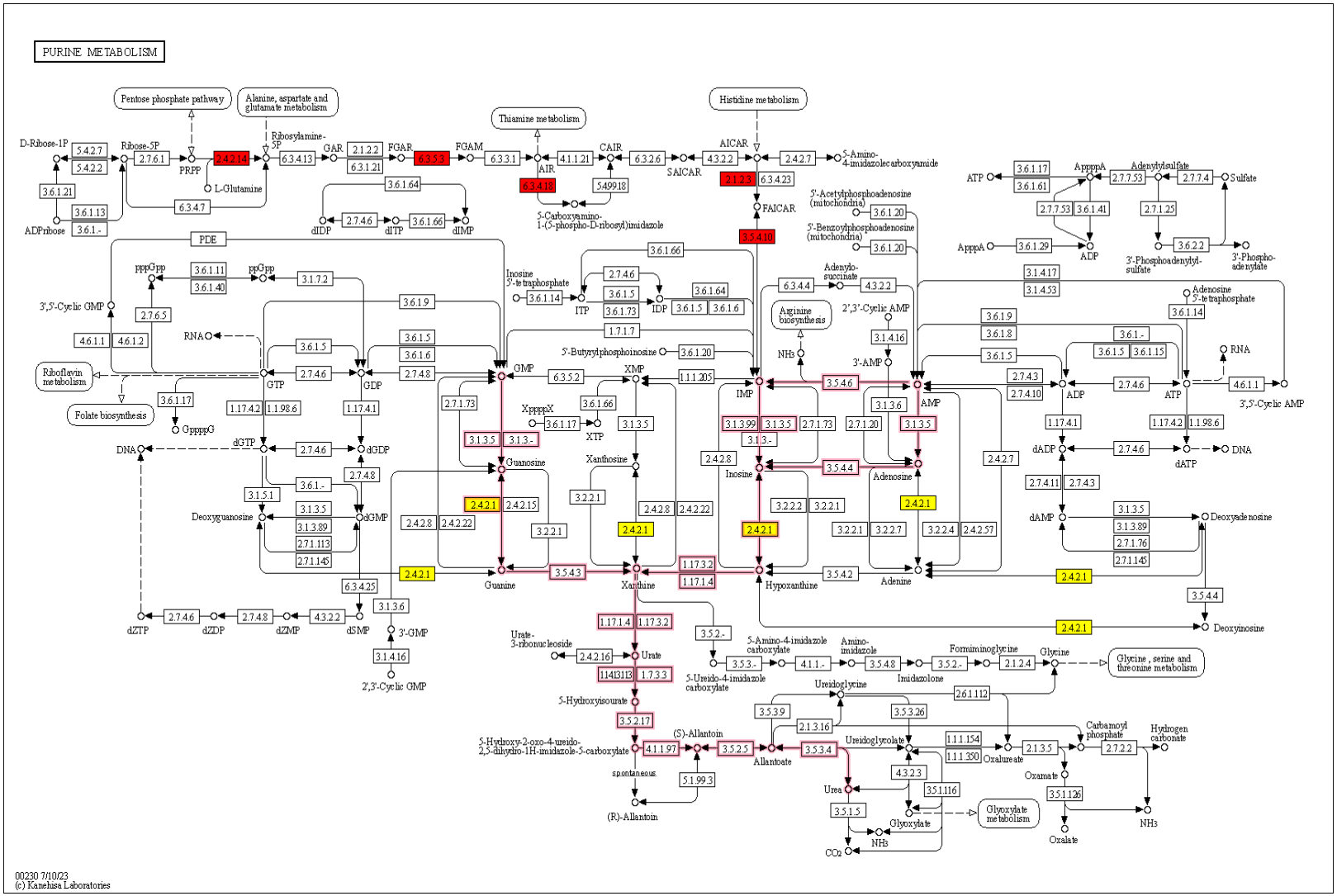
PURINE METABOLISM
Pentose phosphate pathway
Alanine, aspartate and glutamate metabolism
Thiamine metabolism
Histidine metabolism
Riboflavin metabolism
Folate biosynthesis
Arginine biosynthesis
Glycine, serine and threonine metabolism
PDE
D-Ribose-1P
Ribose-5P
PRPP
L-Glutamine
Ribosylamine-5P
GAR
FGAR
FGAM
AIR
CAIR
SAICAR
AICAR
5-Amino-4-imidazolecarboxyamide
FAICAR
5-Carboxyamino-1-(5-phospho-D-ribosyl)imidazole
dIDP
dITP
dIMP
ADPribose
ATP
ADP
Sulfate
Adenylylsulfate
3'-Phosphoadenylyl-sulfate
3'-Phospho-adenylate
5'-Acetylphosphoadenosine (mitochondria)
5'-Benzoylphosphoadenosine (mitochondria)
Adenylo-succinate
2',3'-Cyclic AMP
3'-AMP
Adenosine 5'-tetraphosphate
3',5'-Cyclic GMP
pppGpp
ppGpp
RNA
GTP
GDP
GMP
XMP
IMP
AMP
ITP
IDP
Inosine 5'-tetraphosphate
5'-Butyrylphosphoinosine
GpppG
DNA
dGTP
dGDP
dGMP
dZTP
dZDP
dZMP
dSMP
3'-GMP
2',3'-Cyclic GMP
Guanosine
Xanthosine
Inosine
Adenosine
Deoxyguanosine
Guanine
Xanthine
Hypoxanthine
Adenine
Deoxyadenosine
Deoxyinosine
XpppX
XTP
dADP
dATP
dAMP
Urate-3-ribonucleoside
Urate
5-Hydroxyisourate
5-Hydroxy-2-oxo-4-ureido-2,5-dihydro-1H-imidazole-5-carboxylate
(S)-Allantoin
(R)-Allantoin
spontaneous
Allantoate
Ureidoglycolate
Ureidoglycine
Urea
Glyoxylate
Oxamate
Oxalurate
Oxalate
Carbamoyl phosphate
Hydrogen carbonate
NH3
CO2
5-Amino-4-imidazole carboxylate
5-Ureido-4-imidazole carboxylate
Amino-imidazole
Imidazolone
Formiminoglycine
Glycine
Glyoxylate metabolism
00230 7/10/23
(c) Kanehisa Laboratories

Figure 6.3 Upregulated and downregulated genes in purine metabolism. (b) downregulated gene in purine metabolism map and the influenced KEGG modules. Red shapes represent upregulated genes and yellow represent downregulated genes. Red line in (a) indicates module of *de novo* purine biosynthesis (M00048), in (b) represents modules of adenine ribonucleotide degradation (M00958), guanine ribonucleotide degradation (M00959) and purine degradation. Colored shapes were generated based on KEGG Module database for *V. parahaemolyticus* DEGs.

In the present study, genes of *VPA0645*, *pdhA* and *VPA1211* were assigned to pathways of propanoate metabolism, and valine, leucine and isoleucine degradation. All these three genes were downregulated (Figure 6.4), colored shapes in the figure were generated based on KEGG Module database for *V. parahaemolyticus* DEGs. Similarly, Suyama et al. (2023) found downregulation of propanoate, valine, leucine and isoleucine metabolism in a model for *Bordetella pertussis* biofilm using proteomic expression. In the planktonic cell model, there was an increased conversion from pyruvate to acetyl-CoA which was fed back to the TCA cycle and upregulation of these pathways. According to annotation from the KEGG database, *VPA0645* is a putative dihydrolipoamide acetyltransferase. Downregulation of this gene indicates a slowdown of leucine degradation. In the present study, *pdhA*, encoding pyruvate dehydrogenase (acetyl-transferring) E1 component subunit alpha, is responsible for acetyl-CoA biosynthetic from pyruvate. The downregulation of *pdhA* might have slowed down the propanoate metabolism and influenced the TCA cycle. *glpD* encodes glycerol-3-phosphate dehydrogenase but little is known about the activity of this gene in *V. parahaemolyticus* except for the relationship between cold induced damage and *glpD*. In *P. aeruginosa*, the *glpD* gene is required for the production of a key virulence factor, and deregulation of glycerol metabolism (Scoffield & Silo-Suh, 2016). In *L. monocytogenes* incubation under aerobic and anaerobic conditions, *glpD* is upregulated in the presence of oxygen and downregulated in the absence of oxygen (Crespo Tapia et al., 2018).

6.3.3 Gene ontology (GO) term enrichment analysis of DEGs

The gene ontology database is another resource to investigate the functions of DEGs between biofilm cells and planktonic cells in *V. parahaemolyticus*. There were 33, 39 and 30 genes assigned to Cellular Components class (12 pathways involved), Molecular Function class (59 pathways involved) and Biological Processes class (48 pathways involved), respectively.

Pathways with more assigned DEGs included: membrane (GO:0016021), cytoplasm (GO:0005737), plasma membrane (GO:0005886) and metal ion binding (GO:0046872) (Figure 6.5, Supplemental Table 2).

In DEGs of biofilm (48-h old) and planktonic cells of *Brucella abortus*, Cellular Components class associated with the cell membrane (GO: 0016021), cytoplasm (GO: 0005737) and plasma membrane (GO: 0005886) (Tang et al., 2020), and this agrees with the present study. In another study, the pathway associating with the cell membrane (GO: 0016021) was related to DEGs after *Lactiplantibacillus pentosus* oils adapted to sunflower or olive oils (Alonso García et al., 2023). A similar result was reported by Xu et al. (2021), suggesting role of this pathway in environmental response and adaptation. Wang et al. (2023) suggested that the genes involved in the membrane and cytoplasm pathways might play a key role in spoilage of meat, seafood and milk.

In Figure 6.5b, the electron transfer activity (GO:0009055) was identified as one of the enriched GO terms for Molecular Function, involving genes of *glpD*, *VPA1156*, *zau*, and *VP1233*. The gene *zau* was assigned to another GO term of metal ion binding (GO:00046872). Metal ion binding supports enhancing ionic bridges in EPS and biofilm development (Chen et al., 2019). Ion binding is related to growth and maturation of biofilms with the ion metabolism enabling targets to prevent and control biofilm (Wang et al., 2015). *de novo* IMP biosynthesis (GO:0006189) appears to be related to DEG functions in *V. parahaemolyticus* biofilm cells. Genes of *purH*, *purL*, *VP3037* (*purK*) and *VP2185* (*purF*) were upregulated and are responsible for purine metabolism and the upregulation of these genes would improve IMP biosynthesis in *V. parahaemolyticus* biofilm cells. See Figure 6.3a and Figure 6.5 for more information.

(a)

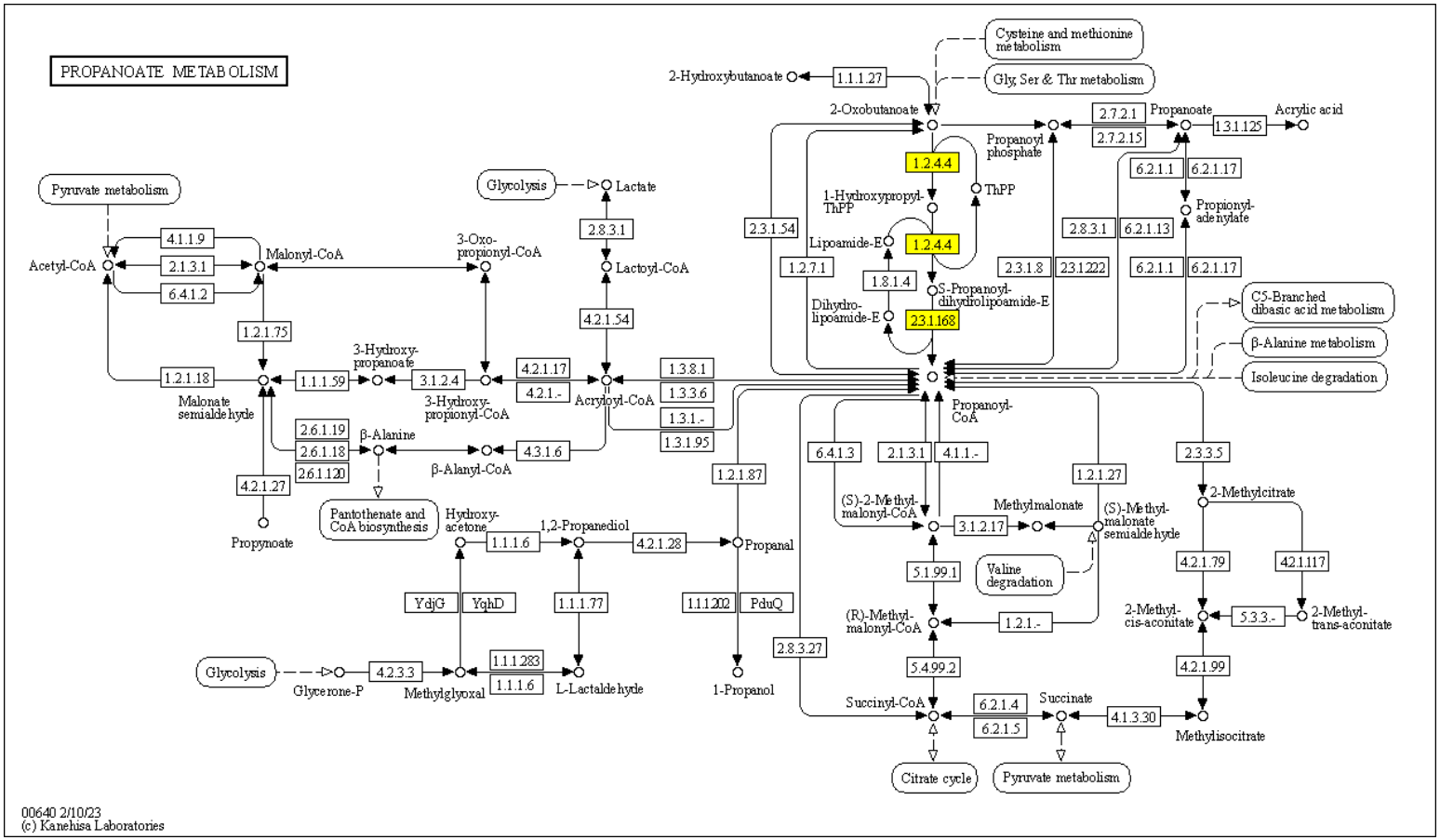

Figure 6. 4 DEGs in propanoate metabolism and valine, leucine and isoleucine degradation pathway.

(a) Downregulated genes in propanoate metabolism pathway. Yellow rectangular shapes represent downregulated genes. Colored shapes were generated based on KEGG Module database for *V. parahaemolyticus* DEGs.

(b)

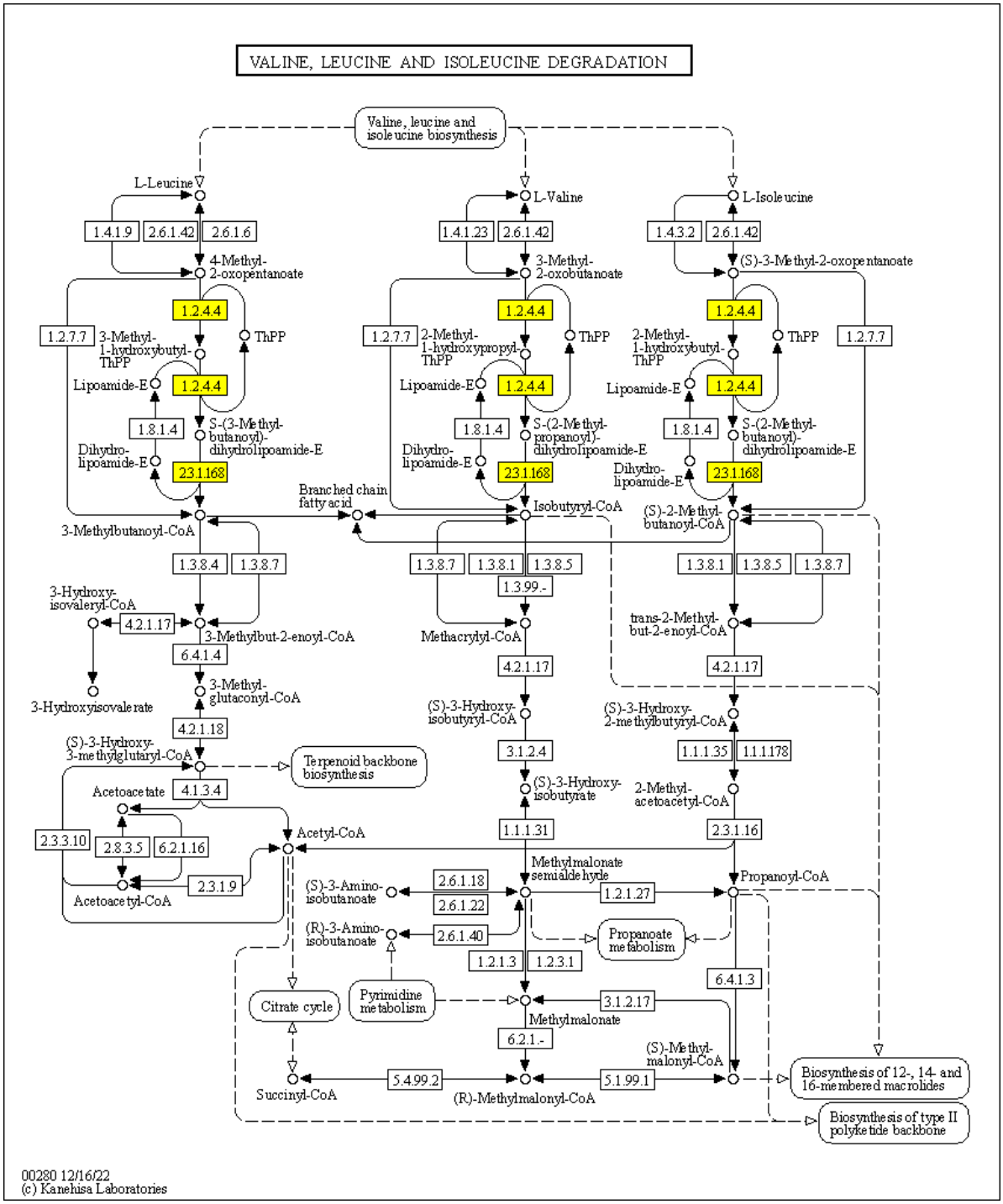

Figure 6. 4 DEGs in propanoate metabolism and valine, leucine and isoleucine degradation pathway. (b) Downregulated genes in valine, leucine and isoleucine degradation pathway. Yellow rectangular shapes represent downregulated genes. Colored shapes were generated based on KEGG Module database for *V. parahaemolyticus* DEGs.

6.3.4 Annotation of biofilm-forming related DEGs

T3SS1 consists of a basal body between in the inner and outer membrane of bacterial cells. A needle extends into the extracellular space, allowing delivery of bacterial effectors to the extracellular space (Zhang & Orth, 2013). T3SS1 exists in both environmental strains and clinical strains of *V. parahaemolyticus*, acting as a virulence factor (Zhang & Orth, 2013). ExsA is a type III secretion system transcriptional regulator in *V. parahaemolyticus*, positively regulating transcription of T3SS1 genes (Zhou et al., 2008). Upregulation of *exsA* indicates transcription of T3SS1 and effector production in the extracellular space. In addition, expression of *tssB* and *tssC* were observed, and these encode the T6SS system. T6SS is generally is used by Gram negative bacteria to deliver a toxic effector to attack adjacent cells (Toska et al., 2018).

Genes of *degP*, *VP1652* (*tctA*) and *VP1653* (*tctB*) were assigned to two component system pathways (Supplemental table 1). *tctA* and *tctB* are putative tricarboxylic transport membrane proteins. *tctA* encodes a key enzyme of carboxylic acids and is located in the periplasm of the cell wall and *tctB* is responsible for transporter activity. These two genes are responsible for downregulation of catabolite repression, suggesting a contribution to biofilm formation of *V. parahaemolyticus* (Franzino et al., 2022). *oppB* is an oligopeptide ABC transporter permease, functioning to transport oligopeptides. *oppB* is associated with quorum sensing, influences substrate transportation in and out of the cell, and affects *V. parahaemolyticus* biofilm formation (Wang et al., 2022). GbpA is an adhesin protein and contributes to colonization of *V. parahaemolyticus* on surfaces. According to results from Section 3.3.2 in the present study, *V. parahaemolyticus* biofilm cells reached a maximum cell number at 6^{th} hour followed by a decrease in cell numbers on stainless steel surfaces. This may explain the downregulation of

gbpA in 6-h old biofilm cells, as it is the initiation to modulate cells to reduce attachment and reach a balance of cell numbers on surfaces.

Proteins discussed above might be modified to adjust gene expression and influence biofilm formation in *V. parahaemolyticus*. For instance, VP0433 (*degP*) is a serine protease that functions in cell envelop protein folding and protein degradation according to the KEGG annotation. In *V. cholerae*, comparative proteomics revealed DegP roles in incorporation of nine proteins into outer membrane vesicles (OMV), including proteins functioning in chitin utilization, biofilm matrix formation and Type II Secretion System (Altindis et al., 2014). This study indicated DegP acted as a target for intestinal colonization and virulence blocking drugs, suggesting that small molecules to inhibit DegP functions, particularly targeting the PDZ2 domain, are perspective compounds against *V. cholerae*. In another study, azathioprine was identified being able to inhibit WspR-dependent c-di-GMP biosynthesis via interfering with PurH function and intracellular nucleotide pools in *P. aeruginosa*, therefore prevented its biofilm formation and virulence production (Antoniani et al., 2013). How to validate the homolog functions in *V. parahaemolyticus*, and how to apply these to control *V. parahaemolyticus* biofilm formation, require further study. Safe, green, and cost-effective biofilm control strategies own advances in the food industry to protect seafood safety and quality. Application of the designed, novel biofilm strategies in food commodities environments will be other steps to apply this in *V. parahaemolyticus* biofilm control in the food industry.

6.4 Conclusion

RNA-seq demonstrated *V. parahaemolyticus* encountered changes in gene expression and physiological changes when converting from planktonic to biofilm cells. Differential gene expression revealed biofilm cells rearranged nucleotide and energy metabolism. Biosynthesis

of secondary metabolites, purine and pyrimidine metabolism, propanoate metabolism, and valine, leucine and isoleucine degradation appear to be required in the young *V. parahaemolyticus* biofilms. DEGs show that these cells were in a developing biofilm. Genes of *purH*, *purF*, *pdhA* and *degP* are potential genetic targets for biofilm prevention and control of *V. parahaemolyticus*.

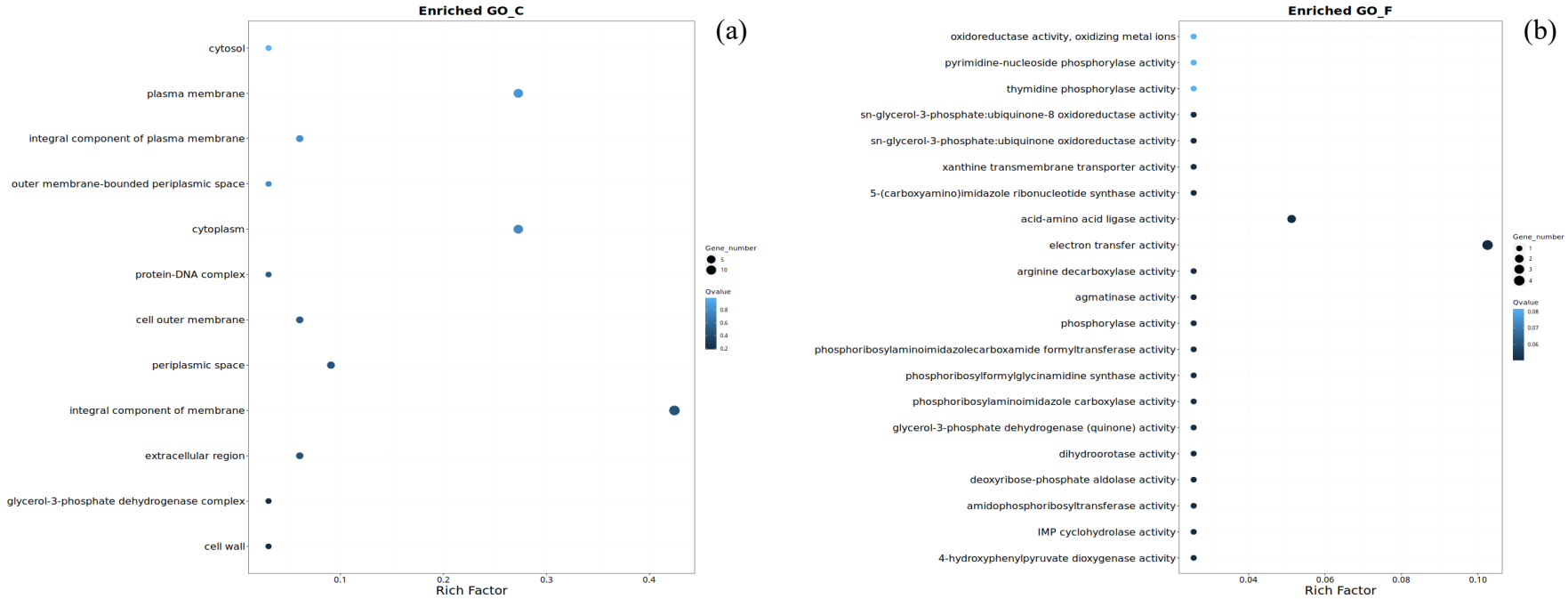

Figure 6. 5 Enriched Gene Ontology (GO) terms by DEGs in Planktonic-vs-Biofilm cells.

(a) Bubble chart of DEGs assigned to GO Cellular Component class; (b) bubble chart of DEGs assigned to GO Molecular Function class. x axis is the enrichment ratio, y axis is class name, color indicates the enriched significance, and size indicates the number of genes annotated to this class.

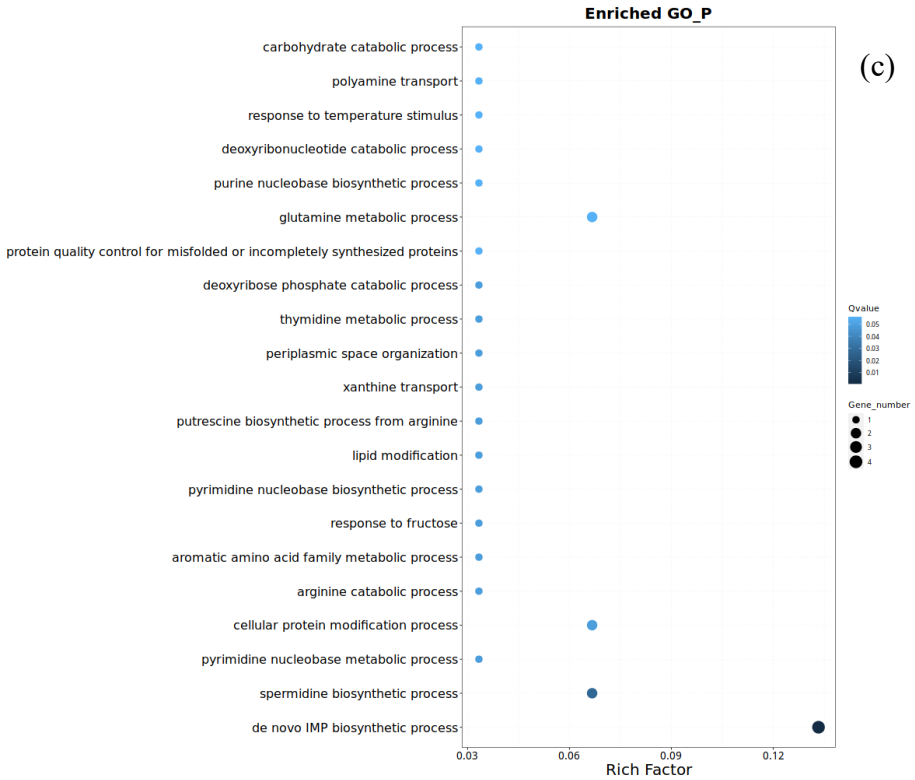

Figure 6. 5 Enriched GO terms by DEGs in Planktonic-vs-Biofilm cells. (a) Bubble chart of DEGs assigned to GO Cellular Component class; (b) bubble chart of DEGs assigned to GO Molecular Function class. x axis is the enrichment ratio, y axis is class name, color indicates the enriched significance, and size indicates the number of genes annotated to this class.

6.5 Reference

Alonso García, E., Benomar, N., Lavilla Lerma, L., de la Fuente Ordoñez, J. J., Knapp, C. W., & Abriouel, H. (2023). Changes in resistome profile of potential probiotic *Lactiplantibacillus pentosus* in response to edible oil adaptation. *Food Microbiology*, *109*, 104148.

Altindis, E., Fu, Y., & Mekalanos, J. J. (2014). Proteomic analysis of *Vibrio cholerae* outer membrane vesicles. *Proceedings of the National Academy of Sciences*, *111*(15), E1548-E1556.

Antoniani, D., Rossi, E., Rinaldo, S., Bocci, P., Lolicato, M., Paiardini, A., Raffaelli, N., Cutruzzolà, F., & Landini, P. (2013). The immunosuppressive drug azathioprine inhibits biosynthesis of the bacterial signal molecule cyclic-di-GMP by interfering with intracellular nucleotide pool availability. *Applied Microbiology and Biotechnology*, *97*(16), 7325-7336. https://doi.org/10.1007/s00253-013-4875-0

Buchfink, B., Reuter, K., & Drost, H.-G. (2021). Sensitive protein alignments at tree-of-life scale using DIAMOND. *Nature Methods*, *18*(4), 366-368. https://doi.org/10.1038/s41592-021-01101-x

Caro-Astorga, J., Frenzel, E., Perkins, J. R., Álvarez-Mena, A., de Vicente, A., Ranea, J. A. G., Kuipers, O. P., & Romero, D. (2020). Biofilm formation displays intrinsic offensive and defensive features of *Bacillus cereus*. *npj Biofilms and Microbiomes*, *6*(1), 3. https://doi.org/10.1038/s41522-019-0112-7

Chen, Y., Chen, Y., Shi, C., Huang, Z., Zhang, Y., Li, S., Li, Y., Ye, J., Yu, C., Li, Z., Zhang, X., Wang, J., Yang, H., Fang, L., & Chen, Q. (2017). SOAPnuke: a MapReduce acceleration-supported software for integrated quality control and preprocessing of

high-throughput sequencing data. *GigaScience*, *7*(1). https://doi.org/10.1093/gigascience/gix120

Chen, Z., Meng, Y., Sheng, B., Zhou, Z., Jin, C., & Meng, F. (2019). Linking Exoproteome Function and Structure to Anammox Biofilm Development. *Environmental Science & Technology*, *53*(3), 1490-1500. https://doi.org/10.1021/acs.est.8b04397

Chung, H. Y., Kim, Y.-T., Kwon, J.-G., Im, H. H., Ko, D., Lee, J.-H., & Choi, S. H. (2021). Molecular interaction between methicillin-resistant *Staphylococcus aureus* (MRSA) and chicken breast reveals enhancement of pathogenesis and toxicity for food-borne outbreak. *Food Microbiology*, *93*, 103602.

Crespo Tapia, N., den Besten, H. M. W., & Abee, T. (2018). Glycerol metabolism induces *Listeria monocytogenes* biofilm formation at the air-liquid interface. *International Journal of Food Microbiology*, *273*, 20-27.

Franzino, T., Boubakri, H., Cernava, T., Abrouk, D., Achouak, W., Reverchon, S., Nasser, W., & Haichar, F. e. Z. (2022). Implications of carbon catabolite repression for plant–microbe interactions. *Plant Communications*, *3*(2), 100272.

Garavaglia, M., Rossi, E., & Landini, P. (2012). The Pyrimidine Nucleotide Biosynthetic Pathway Modulates Production of Biofilm Determinants in *Escherichia coli*. *PLOS ONE*, *7*(2), e31252. https://doi.org/10.1371/journal.pone.0031252

Hadjifrangiskou, M., Gu, A. P., Pinkner, J. S., Kostakioti, M., Zhang, E. W., Greene, S. E., & Hultgren, S. J. (2012). Transposon Mutagenesis Identifies Uropathogenic *Escherichia coli* Biofilm Factors. *Journal of Bacteriology*, *194*(22), 6195-6205.

Haugo, A. J., & Watnick, P. I. (2002). *Vibrio cholerae* CytR is a repressor of biofilm development. *Molecular microbiology*, *45*(2), 471-483.

Kim, D., Paggi, J. M., Park, C., Bennett, C., & Salzberg, S. L. (2019). Graph-based genome alignment and genotyping with HISAT2 and HISAT-genotype. *Nature Biotechnology*, *37*(8), 907-915. https://doi.org/10.1038/s41587-019-0201-4

Langmead, B., & Salzberg, S. L. (2012). Fast gapped-read alignment with Bowtie 2. *Nature Methods*, *9*(4), 357-359. https://doi.org/10.1038/nmeth.1923

Li, B., & Dewey, C. N. (2011). RSEM: accurate transcript quantification from RNA-Seq data with or without a reference genome. *BMC Bioinformatics*, *12*(1), 323. https://doi.org/10.1186/1471-2105-12-323

Li, L., Li, Y., Zhu, F., Cheung, A. L., Wang, G., Bai, G., Proctor, R. A., Yeaman, M. R., Bayer, A. S., & Xiong, Y. Q. (2021). New Mechanistic Insights into Purine Biosynthesis with Second Messenger c-di-AMP in Relation to Biofilm-Related Persistent Methicillin-Resistant *Staphylococcus aureus Infections*. *mBio*, *12*(6), e02081-02021.

Pertea, M., Pertea, G. M., Antonescu, C. M., Chang, T.-C., Mendell, J. T., & Salzberg, S. L. (2015). StringTie enables improved reconstruction of a transcriptome from RNA-seq reads. *Nature Biotechnology*, *33*(3), 290-295. https://doi.org/10.1038/nbt.3122

Scoffield, J., & Silo-Suh, L. (2016). Glycerol metabolism promotes biofilm formation by *Pseudomonas aeruginosa*. *Canadian Journal of Microbiology*, *62*(8), 704-710.

Shaffer, C. L., Zhang, E. W., Dudley, A. G., Dixon, B. R. E. A., Guckes, K. R., Breland, E. J., Floyd, K. A., Casella, D. P., Algood, H. M. S., Clayton, D. B., & Hadjifrangiskou, M. (2017). Purine Biosynthesis Metabolically Constrains Intracellular Survival of Uropathogenic *Escherichia coli*. *Infection and Immunity*, *85*(1), 10.1128/iai.00471-00416.

Suyama, H., Luu, L. D. W., Zhong, L., Raftery, M. J., & Lan, R. (2023). Integrating proteomic data with metabolic modeling provides insight into key pathways of *Bordetella pertussis* biofilms. *Frontiers in Microbiology*, *14*, 1169870.

Tang, T., Chen, G., Guo, A., Xu, Y., Zhao, L., Wang, M., Lu, C., Jiang, Y., & Zhang, C. (2020). Comparative proteomic and genomic analyses of *Brucella abortus* biofilm and planktonic cells. *Molecular medicine reports*, *21*(2), 731-743.

Toska, J., Ho, B. T., & Mekalanos, J. J. (2018). Exopolysaccharide protects *Vibrio cholerae* from exogenous attacks by the type 6 secretion system. *Proceedings of the National Academy of Sciences*, *115*(31), 7997-8002.

Trapnell, C., Williams, B. A., Pertea, G., Mortazavi, A., Kwan, G., van Baren, M. J., Salzberg, S. L., Wold, B. J., & Pachter, L. (2010). Transcript assembly and quantification by RNA-Seq reveals unannotated transcripts and isoform switching during cell differentiation. *Nature Biotechnology*, *28*(5), 511-515. https://doi.org/10.1038/nbt.1621

Wang, D., Fletcher, G. C., Gagic, D., On, S. L. W., Palmer, J. S., & Flint, S. H. (2023). Comparative genome identification of accessory genes associated with strong biofilm formation in *Vibrio parahaemolyticus*. *Food Research International*, *166*, 112605.

Wang, H., Zhang, X., Dong, Y., Xu, X., & Zhou, G. (2015). Insights into the transcriptome profile of mature biofilm of *Salmonella* Typhimurium on stainless steels surface. *Food Research International*, *77*, 378-384.

Wang, L., Feng, Z., Wang, X., Wang, X., & Zhang, X. (2010). DEGseq: an R package for identifying differentially expressed genes from RNA-seq data. *Bioinformatics*, *26*(1), 136-138.

Wang, Q., Wang, P., Liu, P., & Ou, J. (2022). Comparative Transcriptome Analysis Reveals Regulatory Factors Involved in *Vibrio Parahaemolyticus* Biofilm Formation [Original Research]. *Frontiers in Cellular and Infection Microbiology*, *12*. https://doi.org/10.3389/fcimb.2022.917131

Wang, X.-Y., Yan, J., & Xie, J. (2023). Applications of Genomics, Metabolomics, Fourier Transform Infrared in the Evaluation of Spoilage Targets of *Shewanella putrefaciens* from Spoiled Bigeye Tuna. *Journal of Agricultural and Food Chemistry*, *71*(24), 9558-9568. https://doi.org/10.1021/acs.jafc.3c02113

Xu, D., Wei, M., Peng, S., Mo, H., Huang, L., Yao, L., & Hu, L. (2021). Cuminaldehyde in cumin essential oils prevents the growth and aflatoxin B1 biosynthesis of *Aspergillus flavus* in peanuts. *Food Control*, *125*, 107985.

Xu, T., Xiao, Y., Wang, H., Zhu, J., Lu, W., & Chen, W. (2023). Multiomics reveals the mechanism of *B. longum* in promoting the formation of mixed-species biofilms. *Food & Function*, *14*(18), 8276-8290.

Yadav, M. K., Kwon, S. K., Cho, C. G., Park, S. W., Chae, S. W., & Song, J. J. (2012). Gene expression profile of early in vitro biofilms of *Streptococcus pneumoniae*. *Microbiology and immunology*, *56*(9), 621-629.

Zhang, L., & Orth, K. (2013). Virulence determinants for *Vibrio parahaemolyticus* infection. *Current Opinion in Microbiology*, *16*(1), 70-77.

Zhou, X., Shah, D. H., Konkel, M. E., & Call, D. R. (2008). Type III secretion system 1 genes in *Vibrio parahaemolyticus* are positively regulated by ExsA and negatively regulated by ExsD. *Molecular microbiology*, *69*(3), 747-764.

6.6 Supplemental files

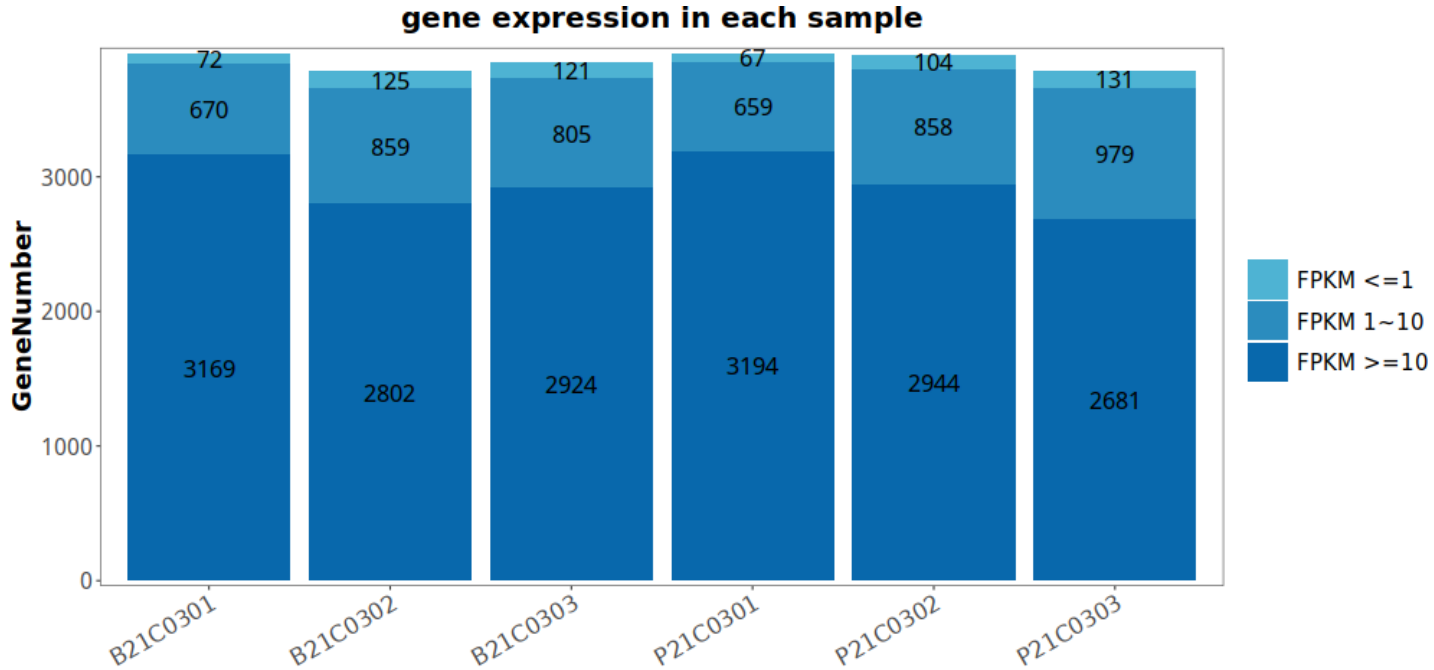

Supplemental Figure 1. Expression level of each replicate on gene level.

The X-axis indicates the sample name, the Y-axis indicates the number of genes, and the shades of color indicate different expression levels of transcript. B21C030x indicates results from sample of biofilm cells of PFR21C03, P21C030x indicates results from sample of planktonic cells of PFR21C03. Each cell sample (biofilm/planktonic cells) has three replicates included for sequencing and analysis.

Supplemental Table 1. KEGG pathway enrichment analysis based on DEGs.

kegg_pathway_term_candidate_gene_num	kegg_pathway_rich_ratio	kegg_pathway_pvalue	kegg_pathway_qvalue	kegg_pathway_term_name	kegg_pathway_term_level_1	kegg_pathway_term_level_2	term_candidate_gene_list
5	0.0746	0.0017	0.0506	Purine metabolism	Metabolism	Nucleotide metabolism	VP_RS03190,VP_RS10610,VP_RS14295,VP_RS15065,VP_RS22220
3	0.0909	0.0096	0.1270	Valine, leucine and isoleucine degradation	Metabolism	Amino acid metabolism	VP_RS18295,VP_RS18305,VP_RS20540
3	0.0811	0.0131	0.1270	Propanoate metabolism	Metabolism	Carbohydrate metabolism	VP_RS18295,VP_RS18305,VP_RS20540
3	0.0667	0.0223	0.1618	Pyrimidine metabolism	Metabolism	Nucleotide metabolism	VP_RS11810,VP_RS17190,VP_RS22220
2	0.0833	0.0418	0.1794	Arginine and proline metabolism	Metabolism	Amino acid metabolism	VP_RS16100,VP_RS16105
9	0.0249	0.0433	0.1794	Biosynthesis of secondary metabolites	Metabolism	Global and overview maps	VP_RS03190,VP_RS10610,VP_RS11590,VP_RS14295,VP_RS15065,VP_RS18295,VP_RS18305,VP_RS20540,VP_RS22220

3	0.0588	0.0310	0.1794	Biofilm formation - Pseudomonas aeruginosa	Cellular Processes	Cellular community - prokaryotes	VP_RS06810,VP_RS06815,VP_RS08185
1	0.0667	0.1886	0.4557	Tyrosine metabolism	Metabolism	Amino acid metabolism	VP_RS06545
1	0.0833	0.1538	0.4557	Phenylalanine metabolism	Metabolism	Amino acid metabolism	VP_RS06545
1	0.0909	0.1419	0.4557	beta-Alanine metabolism	Metabolism	Metabolism of other amino acids	VP_RS20540
1	0.0667	0.1886	0.4557	One carbon pool by folate	Metabolism	Metabolism of cofactors and vitamins	VP_RS14295
1	0.0769	0.1655	0.4557	Longevity regulating pathway - worm	Organismal Systems	Aging	VP_RS16645
1	0.0370	0.3144	0.4558	Pentose phosphate pathway	Metabolism	Carbohydrate metabolism	VP_RS11815
1	0.0385	0.3046	0.4558	Fatty acid degradation	Metabolism	Lipid metabolism	VP_RS20540

1	0.0500	0.2435	0.4558	Ubiquinone and other terpenoid-quinone biosynthesis	Metabolism	Metabolism of cofactors and vitamins	VP_RS06545
1	0.0400	0.2948	0.4558	Glycerophospholipid metabolism	Metabolism	Lipid metabolism	VP_RS11590
1	0.0370	0.3144	0.4558	Nicotinate and nicotinamide metabolism	Metabolism	Metabolism of cofactors and vitamins	VP_RS22220
1	0.0588	0.2110	0.4558	Drug metabolism - other enzymes	Metabolism	Xenobiotics biodegradation and metabolism	VP_RS11810
14	0.0159	0.2864	0.4558	Metabolic pathways	Metabolism	Global and overview maps	VP_RS03190,VP_RS06545,VP_RS10610,VP_RS11810,VP_RS11815,VP_RS14295,VP_RS15065,VP_RS16100,VP_RS16105,VP_RS17190,VP_RS18295,VP_RS18305,VP_RS20540,VP_RS22220
1	0.0385	0.3046	0.4558	RNA degradation	Genetic Information Processing	Folding, sorting and degradation	VP_RS16645

1	0.0263	0.4131	0.5662	Alanine, aspartate and glutamate metabolism	Metabolism	Amino acid metabolism	VP_RS10610
1	0.0250	0.4295	0.5662	Butanoate metabolism	Metabolism	Carbohydrate metabolism	VP_RS20540
1	0.0208	0.4909	0.6190	Fatty acid metabolism	Metabolism	Global and overview maps	VP_RS20540
3	0.0140	0.5841	0.7058	Two-component system	Environmental Information Processing	Signal transduction	VP_RS02075,VP_RS07955,VP_RS07960
2	0.0136	0.6147	0.7130	ABC transporters	Environmental Information Processing	Membrane transport	VP_RS10165,VP_RS17005
2	0.0114	0.7151	0.7977	Biosynthesis of cofactors	Metabolism	Global and overview maps	VP_RS06545,VP_RS17190
1	0.0103	0.7495	0.8051	Quorum sensing	Cellular Processes	Cellular community - prokaryotes	VP_RS10165
1	0.0088	0.8022	0.8309	Carbon metabolism	Metabolism	Global and overview maps	VP_RS20540

1	0.0043	0.9684	0.9684	Microbial metabolism in diverse environments	Metabolism	Global and overview maps	VP_RS20540	

Supplemental Table 2. GO terms enrichment analysis based on DEGs.

go_p_term_id	gene_num	go_p_rich_ratio	pvalue	qvalue	go_p_term_name	go_p_term_level_1	term_candidate_gene_list
GO:0016021	14	0.0199	0.1842	0.4421	integral component of membrane	cellular_component	VP_RS02990,VP_RS05440,VP_RS07815,VP_RS10165,VP_RS15195,VP_RS18385,VP_RS19250,VP_RS04575,VP_RS07955,VP_RS07960,VP_RS08215,VP_RS14115,VP_RS18030,VP_RS18555
GO:0005737	9	0.0157	0.5752	0.7669	cytoplasm	cellular_component	VP_RS00075,VP_RS00395,VP_RS03190,VP_RS04940,VP_RS05990,VP_RS10610,VP_RS11815,VP_RS14035,VP_RS16645
GO:0005886	9	0.0135	0.7771	0.8478	plasma membrane	cellular_component	VP_RS00770,VP_RS02075,VP_RS02990,VP_RS05440,VP_RS07815,VP_RS10165,VP_RS15195,VP_RS18385,VP_RS19250
GO:0046872	6	0.0179	0.4107	0.4751	metal ion binding	molecular_function	VP_RS03190,VP_RS06545,VP_RS15065,VP_RS16105,VP_RS16115,VP_RS16120
GO:0005524	6	0.0141	0.6583	0.6936	ATP binding	molecular_function	VP_RS03190,VP_RS14035,VP_RS15065,VP_RS16115,VP_RS16120,VP_RS16645
GO:0006189	4	0.3333	0.0000	0.0007	de novo' IMP biosynthetic process	biological_process	VP_RS03190,VP_RS10610,VP_RS14295,VP_RS15065
GO:0009055	4	0.0645	0.0138	0.0502	electron transfer activity	molecular_function	VP_RS05990,VP_RS11590,VP_RS20705,VP_RS21995
GO:0006355	3	0.0261	0.2185	0.2439	regulation of	biological_process	VP_RS04940,VP_RS08185,VP_RS19080

					transcription, DNA-templated		
GO:0042802	3	0.0341	0.1498	0.2250	identical protein binding	molecular_function	VP_RS02075,VP_RS10610,VP_RS19080
GO:0042597	3	0.0390	0.1190	0.4421	periplasmic space	cellular_component	VP_RS17005,VP_RS21995,VP_RS14055
GO:0008295	2	0.5000	0.0011	0.0272	spermidine biosynthetic process	biological_process	VP_RS16100,VP_RS16105
GO:0006464	2	0.1667	0.0116	0.0483	cellular protein modification process	biological_process	VP_RS16115,VP_RS16120
GO:0006541	2	0.1250	0.0204	0.0560	glutamine metabolic process	biological_process	VP_RS03190,VP_RS10610
GO:0006457	2	0.0741	0.0542	0.0855	protein folding	biological_process	VP_RS02075,VP_RS14035
GO:0006412	2	0.0299	0.2433	0.2595	translation	biological_process	VP_RS16115,VP_RS16120
GO:0016881	2	0.4000	0.0022	0.0502	acid-amino acid ligase activity	molecular_function	VP_RS16115,VP_RS16120
GO:0016887	2	0.0500	0.1239	0.2088	ATPase activity	molecular_function	VP_RS14035,VP_RS16645
GO:0000976	2	0.0476	0.1342	0.2140	transcription regulatory	molecular_function	VP_RS08185,VP_RS19080

					region sequence-specific DNA binding		
GO:0008270	2	0.0211	0.4307	0.4887	zinc ion binding	molecular_function	VP_RS05440,VP_RS17190
GO:0003700	2	0.0146	0.6295	0.6753	DNA-binding transcription factor activity	molecular_function	VP_RS19080,VP_RS21325
GO:0003677	2	0.0084	0.8937	0.8937	DNA binding	molecular_function	VP_RS04940,VP_RS11420
GO:0005576	2	0.0408	0.1798	0.4421	extracellular region	cellular_component	VP_RS22805,VP_RS22195
GO:0009279	2	0.0308	0.2737	0.4886	cell outer membrane	cellular_component	VP_RS04920,VP_RS22195
GO:0005887	2	0.0141	0.6677	0.8013	integral component of plasma membrane	cellular_component	VP_RS00770,VP_RS11590
GO:0006206	1	1.0000	0.0141	0.0483	pyrimidine nucleobase metabolic process	biological_process	VP_RS11810
GO:0006527	1	1.0000	0.0141	0.0483	arginine catabolic process	biological_process	VP_RS16105
GO:0009072	1	1.0000	0.0141	0.0483	aromatic amino acid	biological_process	VP_RS06545

					family metabolic process		
GO:0009750	1	1.0000	0.0141	0.0483	response to fructose	biological_process	VP_RS19080
GO:0019856	1	1.0000	0.0141	0.0483	pyrimidine nucleobase biosynthetic process	biological_process	VP_RS17190
GO:0030258	1	1.0000	0.0141	0.0483	lipid modification	biological_process	VP_RS22195
GO:0033388	1	1.0000	0.0141	0.0483	putrescine biosynthetic process from arginine	biological_process	VP_RS16100
GO:0042906	1	1.0000	0.0141	0.0483	xanthine transport	biological_process	VP_RS00770
GO:0043580	1	1.0000	0.0141	0.0483	periplasmic space organization	biological_process	VP_RS22195
GO:0046104	1	1.0000	0.0141	0.0483	thymidine metabolic process	biological_process	VP_RS11810
GO:0046386	1	1.0000	0.0141	0.0483	deoxyribose phosphate catabolic process	biological_process	VP_RS11815

GO:0006515	1	0.5000	0.0280	0.0560	protein quality control for misfolded or incompletely synthesized proteins	biological_process	VP_RS02075
GO:0009113	1	0.5000	0.0280	0.0560	purine nucleobase biosynthetic process	biological_process	VP_RS10610
GO:0009264	1	0.5000	0.0280	0.0560	deoxyribonucleotide catabolic process	biological_process	VP_RS11815
GO:0009266	1	0.5000	0.0280	0.0560	response to temperature stimulus	biological_process	VP_RS02075
GO:0015846	1	0.5000	0.0280	0.0560	polyamine transport	biological_process	VP_RS17005
GO:0016052	1	0.5000	0.0280	0.0560	carbohydrate catabolic process	biological_process	VP_RS11815
GO:0042278	1	0.5000	0.0280	0.0560	purine nucleoside metabolic process	biological_process	VP_RS22220

GO:0046168	1	0.5000	0.0280	0.0560	glycerol-3-phosphate catabolic process	biological_process	VP_RS11590
GO:0050709	1	0.5000	0.0280	0.0560	negative regulation of protein secretion	biological_process	VP_RS08185
GO:0006164	1	0.3333	0.0417	0.0742	purine nucleotide biosynthetic process	biological_process	VP_RS10610
GO:0050821	1	0.3333	0.0417	0.0742	protein stabilization	biological_process	VP_RS00075
GO:2000142	1	0.3333	0.0417	0.0742	regulation of DNA-templated transcription, initiation	biological_process	VP_RS19080
GO:0019563	1	0.2500	0.0552	0.0855	glycerol catabolic process	biological_process	VP_RS11590
GO:0019836	1	0.2500	0.0552	0.0855	hemolysis by symbiont of host erythrocytes	biological_process	VP_RS06545

GO:2000144	1	0.2500	0.0552	0.0855	positive regulation of DNA-templated transcription, initiation	biological_process	VP_RS08185
GO:0010468	1	0.2000	0.0686	0.1029	regulation of gene expression	biological_process	VP_RS04940
GO:0009409	1	0.1667	0.0818	0.1154	response to cold	biological_process	VP_RS04940
GO:0042026	1	0.1667	0.0818	0.1154	protein refolding	biological_process	VP_RS16645
GO:0009116	1	0.1429	0.0947	0.1263	nucleoside metabolic process	biological_process	VP_RS10610
GO:0044205	1	0.1429	0.0947	0.1263	'de novo' UMP biosynthetic process	biological_process	VP_RS17190
GO:1990961	1	0.1250	0.1075	0.1395	drug transmembrane export	biological_process	VP_RS15195
GO:0006635	1	0.1000	0.1326	0.1675	fatty acid beta-oxidation	biological_process	VP_RS20540
GO:0045454	1	0.0909	0.1449	0.1784	cell redox homeostasis	biological_process	VP_RS05990

GO:0006508	1	0.0833	0.1570	0.1884	proteolysis	biological_process	VP_RS02075
GO:0006629	1	0.0667	0.1924	0.2252	lipid metabolic process	biological_process	VP_RS22810
GO:0006096	1	0.0588	0.2152	0.2439	glycolytic process	biological_process	VP_RS18305
GO:0006979	1	0.0556	0.2263	0.2469	response to oxidative stress	biological_process	VP_RS02075
GO:0015031	1	0.0227	0.4680	0.4884	protein transport	biological_process	VP_RS10165
GO:0055085	1	0.0192	0.5264	0.5376	transmembrane transport	biological_process	VP_RS10165
GO:0009405	1	0.0182	0.5466	0.5466	pathogenesis	biological_process	VP_RS06545
GO:0003868	1	1.0000	0.0153	0.0502	4-hydroxyphenylpyruvate dioxygenase activity	molecular_function	VP_RS06545
GO:0003937	1	1.0000	0.0153	0.0502	IMP cyclohydrolase activity	molecular_function	VP_RS14295
GO:0004044	1	1.0000	0.0153	0.0502	amidophosphoribosyltransferase activity	molecular_function	VP_RS10610

GO:0004139	1	1.0000	0.0153	0.0502	deoxyribose-phosphate aldolase activity	molecular_function	VP_RS11815
GO:0004151	1	1.0000	0.0153	0.0502	dihydroorotase activity	molecular_function	VP_RS17190
GO:0004368	1	1.0000	0.0153	0.0502	glycerol-3-phosphate dehydrogenase (quinone) activity	molecular_function	VP_RS11590
GO:0004638	1	1.0000	0.0153	0.0502	phosphoribosylaminoimidazole carboxylase activity	molecular_function	VP_RS15065
GO:0004642	1	1.0000	0.0153	0.0502	phosphoribosylformylglycinamidine synthase activity	molecular_function	VP_RS03190
GO:0004643	1	1.0000	0.0153	0.0502	phosphoribosylaminoimidazolecarboxamide	molecular_function	VP_RS14295

					formyltransferase activity		
GO:0004645	1	1.0000	0.0153	0.0502	phosphorylase activity	molecular_function	VP_RS11810
GO:0008783	1	1.0000	0.0153	0.0502	agmatinase activity	molecular_function	VP_RS16100
GO:0008792	1	1.0000	0.0153	0.0502	arginine decarboxylase activity	molecular_function	VP_RS16105
GO:0034028	1	1.0000	0.0153	0.0502	5-(carboxyamino)imidazole ribonucleotide synthase activity	molecular_function	VP_RS15065
GO:0042907	1	1.0000	0.0153	0.0502	xanthine transmembrane transporter activity	molecular_function	VP_RS00770
GO:0052590	1	1.0000	0.0153	0.0502	sn-glycerol-3-phosphate: ubiquinone oxidoredu	molecular_function	VP_RS11590

					ctase activity sn-glycerol-3-phosphate: ubiquinone-8 oxidoreductase activity		
GO:0052591	1	1.0000	0.0153	0.0502		molecular_function	VP_RS11590
GO:0009032	1	0.5000	0.0304	0.0815	thymidine phosphorylase activity	molecular_function	VP_RS11810
GO:0016154	1	0.5000	0.0304	0.0815	pyrimidine-nucleoside phosphorylase activity	molecular_function	VP_RS11810
GO:0016722	1	0.5000	0.0304	0.0815	oxidoreductase activity, oxidizing metal ions	molecular_function	VP_RS17910
GO:0019808	1	0.5000	0.0304	0.0815	polyamine binding	molecular_function	VP_RS17005
GO:0004739	1	0.3333	0.0452	0.1068	pyruvate dehydrogenase (acetyl-	molecular_function	VP_RS18305

					transferring) activity		
GO:0008289	1	0.3333	0.0452	0.1068	lipid binding	molecular_function	VP_RS22195
GO:0015655	1	0.3333	0.0452	0.1068	alanine:sodium symporter activity	molecular_function	VP_RS02990
GO:0004731	1	0.2500	0.0599	0.1308	purine-nucleoside phosphorylase activity	molecular_function	VP_RS22220
GO:0004812	1	0.2500	0.0599	0.1308	aminoacyl-tRNA ligase activity	molecular_function	VP_RS18845
GO:0090729	1	0.2000	0.0743	0.1565	toxin activity	molecular_function	VP_RS06545
GO:0000986	1	0.1667	0.0885	0.1582	bacterial-type proximal promoter sequence-specific DNA binding	molecular_function	VP_RS19080
GO:0002161	1	0.1667	0.0885	0.1582	aminoacyl-tRNA editing activity	molecular_function	VP_RS18845

GO:0003995	1	0.1667	0.0885	0.1582	acyl-CoA dehydrogenase activity	molecular_function	VP_RS20540
GO:0008061	1	0.1667	0.0885	0.1582	chitin binding	molecular_function	VP_RS22805
GO:0008199	1	0.1667	0.0885	0.1582	ferric iron binding	molecular_function	VP_RS17910
GO:0008233	1	0.1250	0.1162	0.2017	peptidase activity	molecular_function	VP_RS00735
GO:0042834	1	0.1111	0.1298	0.2127	peptidoglycan binding	molecular_function	VP_RS22195
GO:0016757	1	0.1000	0.1432	0.2223	transferase activity, transferring glycosyl groups	molecular_function	VP_RS10610
GO:0005507	1	0.0909	0.1563	0.2250	copper ion binding	molecular_function	VP_RS21995
GO:0015035	1	0.0909	0.1563	0.2250	protein disulfide oxidoreductase activity	molecular_function	VP_RS05990
GO:0015288	1	0.0769	0.1821	0.2558	porin activity	molecular_function	VP_RS04920
GO:0051082	1	0.0714	0.1947	0.2671	unfolded protein binding	molecular_function	VP_RS16645
GO:0042910	1	0.0667	0.2071	0.2777	xenobiotic transmem	molecular_function	VP_RS15195

					brane transporter activity		
GO:0071949	1	0.0588	0.2313	0.3033	FAD binding	molecular_function	VP_RS11590
GO:0004222	1	0.0476	0.2776	0.3485	metalloendopeptidase activity	molecular_function	VP_RS05440
GO:0030145	1	0.0476	0.2776	0.3485	manganese ion binding	molecular_function	VP_RS16100
GO:0001216	1	0.0435	0.2997	0.3609	bacterial-type RNA polymerase transcriptional activator activity, sequence-specific DNA binding	molecular_function	VP_RS08185
GO:0004252	1	0.0435	0.2997	0.3609	serine-type endopeptidase activity	molecular_function	VP_RS02075
GO:0050660	1	0.0313	0.3914	0.4619	flavin adenine dinucleotide binding	molecular_function	VP_RS20540

GO:0003676	1	0.0263	0.4459	0.4964	nucleic acid binding	molecular_function	VP_RS04940
GO:0043565	1	0.0192	0.5553	0.6067	sequence-specific DNA binding	molecular_function	VP_RS08185
GO:0022857	1	0.0130	0.7006	0.7252	transmembrane transporter activity	molecular_function	VP_RS14115
GO:0000287	1	0.0099	0.7960	0.8097	magnesium ion binding	molecular_function	VP_RS10610
GO:0005618	1	1.0000	0.0158	0.1878	cell wall	cellular_component	VP_RS22195
GO:0009331	1	0.5000	0.0313	0.1878	glycerol-3-phosphate dehydrogenase complex	cellular_component	VP_RS11590
GO:0032993	1	0.0476	0.2850	0.4886	protein-DNA complex	cellular_component	VP_RS08185
GO:0030288	1	0.0189	0.5741	0.7669	outer membrane-bounded periplasmic space	cellular_component	VP_RS02075
GO:0005829	1	0.0038	0.9879	0.9879	cytosol	cellular_component	VP_RS10610

Chapter 7. Discussion

7.1 Final discussion

An increase in the number of cases of *V. parahaemolyticus* food poisonings across more locations in the world is associated with an increase in seawater temperatures due to global warming (FAO, 2021). *V. parahaemolyticus* is isolated from seafood, seafood markets and industry processing plants (Cruz et al., 2015; FAO, 2021; F. Han et al., 2017; Martinez-Urtaza et al., 2010; Odeyemi, 2016). In nature, most bacteria live in biofilms, which are self-secreted niches that provide protection from harsh environments, preventing the removal of pathogens and effectiveness of sanitizer treatment in the food industry. The increasing *V. parahaemolyticus* infection rates and biofilm-forming problems (Chapter 2) are causing concerns in the seafood industry in maintaining food safety. Biofilm formation of *V. parahaemolyticus* was evaluated on the surfaces of seafood processing plant (polystyrene, stainless steel) (Chapter 3). The efficacy of commercial sanitizers sodium hypochlorite and PAA were determined in Chapter 4, providing information of effective concentrations of sanitizers killing *V. parahaemolyticus* in the seafood industry. Comparative genome analysis between genomes of strong and weak biofilm forming strains found out 136 accessory genes responsible for strong biofilm formation in *V. parahaemolyticus* (Chapter 5). Gene expression was used to provide additional information on genomic characteristics involved in biofilm formation in *V. parahaemolyticus* (Chapter 6).

7.1.1 Biofilm formation of *V. parahaemolyticus* and its susceptibility to sanitizers

At 25 °C, *V. parahaemolyticus* isolates from the seafood industry formed biofilms on the stainless steel of over 7 $\log_{10}$ CFU/cm^2 after 6 h incubation, similar to previous studies (Chen et al., 2020; Guo et al., 2020; Han et al., 2016; Q. Han et al., 2017; Li et al., 2020; Mougin et al., 2019; Ning et al., 2021; Roy et al., 2021; Sun et al., 2019; Tan et al., 2021). In addition to bacterial numbers, biofilm formation was assessed using a crystal violet assay and BFI values

in microtiter plates (Figure 3.1, Chapter 3). Epifluorescence microscopy was used to visualize the biofilm to determine the approximate proportion of live and dead cells, the extent of EPS and an indication of the layers of cells in the biofilm (Figure 3.3, Chapter 3). There was some variation in the ability of different strains to form biofilm, according to the growth dynamics of biofilm cells, the results of the BFI, and fluorescence microscope screening.

When treating *V. parahaemolyticus* biofilms with free available chlorine at 1176 mg/L (pH 6.5-6.9, ambient temperature), the cell populations on stainless steel coupons were reduced by 1.74-2.28 $\log_{10}$ CFU/cm^2 (Figure 4.2, Chapter 4). Increasing concentrations of sodium hypochlorite inactivated more biofilm cells of *V. parahaemolyticus*. When biofilms were treated with 4704 mg/L chlorine, cell populations were reduced to undetectable levels (< 10 CFU/cm^2), except for biofilms formed by PFR30J09 and PFR34B02. The result also revealed ineffectiveness of sodium hypochlorite in removing *V. parahaemolyticus* biofilms from stainless steel surfaces at recommended concentrations.

PAA treatment of *V. parahaemolyticus* biofilm required 22.39 mg/L to inactivate 2.80 $\log_{10}$ CFU/cm^2 cells on stainless steel coupons (Figure 4.4, Chapter 4). It was consistent with the results for sodium hypochlorite. When treated with PAA at 89.56 mg/L, biofilm cells formed by weak and intermediate biofilm formers were reduced by > 5.00 $\log_{10}$ CFU/cm^2. However, this concentration cannot inactivate biofilm cells formed by the strong biofilm formers, PFR30J09 and PFR34B02 were reduced by 2.60 and 2.52 $\log_{10}$ CFU/cm^2, respectively. This shows the importance of the extent of biofilm formation and sanitizer resistance.

For all sanitizer trials on pre-formed biofilm, the biofilm preparation and cell numbers reached were the same with ~ 7 $\log_{10}$ CFU/cm^2 (Figure 4.2 & Figure 4.4). This suggests that the increased sanitizer resistance in the strong biofilm formers is not due to differences in cell numbers. Possible reasons are differences in the density of the biofilm or the nature of the EPS

matrix inhibiting the penetration of the biofilm by the sanitizers. Other possible explanations could be differences in the metabolic activity of the cells in the biofilm. Effect of sanitizer on biofilms is dependent on the microbial variants, the age of the biofilm, the structure of the biofilm matrix, the effective sanitizer concentrations, pH and treatment time.

7.1.2 Key genes for robust biofilm formation

Prospective genes for robust biofilm formation and sanitizer resistance was characterized via pangenome analysis and functional pathway analysis (Section 4.3.4, Chapter 4). PFR30J09 and PFR34B02 contain more genes in certain functional pathways when compared with the reference genome. These include genes in metabolic pathways in diverse environments. Presumably, these provide PFR30J09 and PFR34B02 the ability (e.g., in energy utilization, adaptation, etc.) to form more biofilms and resistance to environmental stress. Comparative genome analysis identified 136 accessory genes exclusively in strong biofilm forming strains. These genes may contribute to robust biofilm formation. Functional assignment of these genes to a Gene Ontology database, revealed an association with cellulose biosynthesis, rhamnose metabolic and catabolic processes, UDP-glucose processes, and O antigen biosynthesis ($p < 0.05$). Strategies of CRISPR-Cas system and MSHA pilus-led attachment in the strong biofilm-forming *V. parahaemolyticus* were implicated via KEGG annotation. Cellulose is a component in the robust biofilm matrix (See detail in Chapter 5). Its biosynthesis operon consists of *bcsG*, *bcsE*, *bcsQ*, *bcsA*, *bcsB*, *bcsZ*, *bcsC*.

7.2 Limitations

This study investigated biofilm formation of *V. parahaemolyticus* single species in static biofilm using 3% NaCl TSB as the media, however, in nature, biofilms are generally made of multiple species and survive in natural flowing and nutritious environments. Multiple

genes/pathways functioning to form biofilm and adapting to the environment, is the result of multiple genes as revealed in Chapters 4, 5 and 6. Gene expression may vary in the biofilm depending on the conditions, but there are no reports of this for *V. parahaemolyticus.*

Although the present study demonstrated cellulose has a role in robust biofilm formation in *V. parahaemolyticus*, precise biochemical functions and the chemical structures of cellulose require further exploration. Chemical elements of cellulose vary between species. For example, in *E. coli*, the cellulose in the biofilm matrix has been identified as phosphoethanolamined, whereas in *Pseudomonas*, the cellulose is amorphous. Interactions between cellulose and other components in extracellular matrix may be of interest to understand the biofilm matrix, as well as to develop novel and effective biofilm control measures, such as cellulase, c-di-GMP denpendent signaling roles in biofilm control. Perspective targets of *purH*, *purF*, *pdhA* and *degP* in *V. parahaemolyticus* biofilm formation, and their applications to control biofilms in the food industry require further study.

7.3 Further work

Biofilm formation includes multiple steps: attachment, microcolony formation, matrix formulation, and dispersion. Attachment has been reported as beginning of biofilm formation, with cells attaching to a surface and starting to form intercellular communication. Multiple factors influence cell attachment, including surface conditioning, surface charge, surface roughness, hydrophobicity, surface micro-topography, mass transport and growth medium (Flint et al., 1997; Flint et al., 2000; Palmer et al., 2007; Palmer et al., 2010). Signaling pathways, such as quorum sensing, c-di-GMP, participate in regulation of biofilm formation, influencing nutrient digestion, intracellular carbon flux and environment adaptation (Hengge, 2009; Kjelleberg & Molin, 2002). Other factors influence *V. parahaemolyticus* biofilm, include biofilms formed by Gram-negative/Gram-positive bacteria, biofilms formed by single

species/multiple species, communities formed on biotic surfaces/abiotic surfaces, and growth in static/flowing conditions, require further exploration.

Increasing seawater temperatures are believed to be associated with *V. parahaemolyticus* prevalence (Velez et al., 2023). *V. parahaemolyticus* cannot grow at < 5 °C, but grows well at 16-19 °C. The Optimal temperature for biofilm formation of *V. parahaemolyticus* is 25°C rather than 15°C and 30 °C (Song et al., 2017). Another study found 15-37 °C favored biofilm formulation and at 4 °C and 10 °C, *V. parahaemolyticus* formed monolayers (Han et al., 2016). Optimum pH for *V. parahaemolyticus* growth is 7.8-8.6, and it can survive when pH ranges from 4.8 to 11. Effects should be included to assess risks of *V. parahaemolyticus* biofilms (Velez et al., 2023).

V. parahaemolyticus demonstrated "biobrick" strategies to form biofilms, meaning that several pathways might have played roles in the robust biofilm formation. This has been indicated by results in Chapters 4 and 5. Genes/pathways contribute to robust biofilm formation by interplaying with each other, to assist *V. parahaemolyticus* in developing a robust biofilm formation. Sorting out hub gene(s) within "biobrick" strategies will help understand biofilm formation and narrow down genetic targets for developing novel control strategies against biofilms.

In the present study, cellulose was identified as important in developing robust biofilm and is associated with sanitizer resistance. This association could be confirmed through gene knock outs, chemical treatment to remove cellulose or altering the growth conditions to limit cellulose production. According to a study by Romling and Galperin (2015), chemical structures and components of cellulose can be different depending on the species, and this needs to be investigated for *V. parahaemolyticus* biofilms.

The O-antigen in *V. parahaemolyticus* is associated with biofilm formation (Chapter 4), but whether O-antigen is critical for robust biofilm formation is unknown. In *Xylella fastidiosa*, a rhamnose-rich O-antigen contributes to cell attachment, cell-cell aggregation and biofilm formulation, and the absence of this rhamnose-rich O-antigen compromised the ability to colonize host (Clifford et al., 2013). Kierek and Watnick (2003) reported that *V. cholerae* O139 O-antigen is critical for Ca^{2+} dependent biofilm development in sea water. However, in the present study, there was no further determination of the role of *V. parahaemolyticus* O-antigens, this is an opportunity for further research.

7.4 Reference

Chen, B., Huang, J., Li, H., Zeng, Q.-H., Wang, J. J., Liu, H., Pan, Y., & Zhao, Y. (2020). Eradication of planktonic *Vibrio parahaemolyticus* and its sessile biofilm by curcumin-mediated photodynamic inactivation. *Food Control*, *113*, 107181. https://doi.org/10.1016/j.foodcont.2020.107181

Clifford, J. C., Rapicavoli, J. N., & Roper, M. C. (2013). A rhamnose-rich O-antigen mediates adhesion, virulence, and host colonization for the xylem-limited phytopathogen *Xylella fastidiosa*. *Molecular Plant-Microbe Interactions* *26*(6), 676-685. https://doi.org/10.1094/MPMI-12-12-0283-R

Cruz, C. D., Hedderley, D., & Fletcher, G. C. (2015). Long-term study of *Vibrio parahaemolyticus* prevalence and distribution in New Zealand shellfish. *Applied and Environmental Microbiology*, *81*(7), 2320-2327. https://doi.org/10.1128/AEM.04020-14

FAO. (2021). *Advances in science and risk assessment tools for Vibrio parahaemolyticus and V. vulnificus associated with seafood*. https://www.fao.org/documents/card/fr/c/cb5834en/

Flint, S., Brooks, J., & Bremer, P. (1997). The influence of cell surface properties of thermophilic streptococci on attachment to stainlesssteel. *Journal of applied microbiology*, *83*(4), 508-517.

Flint, S. H., Brooks, J. D., & Bremer, P. J. (2000). Properties of the stainless steel substrate, influencing the adhesion of thermo-resistant streptococci. *Journal of Food Engineering*, *43*(4), 235-242. https://doi.org/10.1016/s0260-8774(99)00157-0

Guo, L., Wang, J., Gou, Y., Tan, L., Liu, H., Pan, Y., & Zhao, Y. (2020). Comparative proteomics reveals stress responses of *Vibrio parahaemolyticus* biofilm on different surfaces: Internal adaptation and external adjustment. *Science of the Total Environment*, *731*, 138386. https://doi.org/10.1016/j.scitotenv.2020.138386

Han, F., Gu, R. R., Shen, X. S., Chen, Y. G., Tian, L. L., Zhou, W. F., & Cai, Y. Q. (2017). Detection of Total and Pathogenic *Vibrio parahaemolyticus* in Shellfish Growing along the South Yellow Sea and the East China Sea. *Journal of Food Protection*, *80*(11), 1882-1889. https://doi.org/10.4315/0362-028X.JFP-17-080

Han, N., Mizan, M. F. R., Jahid, I. K., & Ha, S.-D. (2016). Biofilm formation by *Vibrio parahaemolyticus* on food and food contact surfaces increases with rise in temperature. *Food Control*, *70*, 161-166. https://doi.org/10.1016/j.foodcont.2016.05.054

Han, Q., Song, X., Zhang, Z., Fu, J., Wang, X., Malakar, P. K., Liu, H., Pan, Y., & Zhao, Y. (2017). Removal of Foodborne Pathogen Biofilms by Acidic Electrolyzed Water. *Frontiers in Microbiology*, *8*, 988. https://doi.org/10.3389/fmicb.2017.00988

Hengge, R. (2009). Principles of c-di-GMP signalling in bacteria. *Nature Reviews Microbiology*, *7*(4), 263-273. https://doi.org/10.1038/nrmicro2109

Kierek, K., & Watnick, P. I. (2003). The *Vibrio cholerae* O139 O-antigen polysaccharide is essential for Ca^{2+}-dependent biofilm development in sea water. *Proceedings of the National Academy of Sciences of the United States of America*, *100*(24), 14357-14362. https://doi.org/10.1073/pnas.2334614100

Kjelleberg, S., & Molin, S. (2002). Is there a role for quorum sensing signals in bacterial biofilms? *Current Opinion in Microbiology*, *5*(3), 254-258. https://doi.org/10.1016/s1369-5274(02)00325-9

Li, Y., Tan, L., Guo, L., Zhang, P., Malakar, P. K., Ahmed, F., Liu, H., Wang, J. J., & Zhao, Y. (2020). Acidic electrolyzed water more effectively breaks down mature *Vibrio parahaemolyticus* biofilm than DNase I. *Food Control*, *117*, 107312. https://doi.org/10.1016/j.foodcont.2020.107312

Martinez-Urtaza, J., Bowers, J. C., Trinanes, J., & DePaola, A. (2010). Climate anomalies and the increasing risk of *Vibrio parahaemolyticus* and *Vibrio vulnificus* illnesses. *Food Research International*, *43*(7), 1780-1790. https://doi.org/10.1016/j.foodres.2010.04.001

Mougin, J., Copin, S., Bojolly, D., Raguenet, V., Robert-Pillot, A., Quilici, M.-L., Midelet-Bourdin, G., Grard, T., & Bonnin-Jusserand, M. (2019). Adhesion to stainless steel surfaces and detection of viable but non cultivable cells of *Vibrio parahaemolyticus* and *Vibrio cholerae* isolated from shrimps in seafood processing environments: Stayin' alive? *Food Control*, *102*, 122-130. https://doi.org/10.1016/j.foodcont.2019.03.024

Ning, H. Q., Lin, H., & Wang, J. X. (2021). Synergistic effects of endolysin Lysqdvp001 and epsilon-poly-lysine in controlling *Vibrio parahaemolyticus* and its biofilms. *International Journal of Food Microbiology*, *343*, 109112. https://doi.org/10.1016/j.ijfoodmicro.2021.109112

Odeyemi, O. A. (2016). Incidence and prevalence of *Vibrio parahaemolyticus* in seafood: a systematic review and meta-analysis. *Springerplus*, *5*, 464. https://doi.org/10.1186/s40064-016-2115-7

Palmer, J., Flint, S., & Brooks, J. (2007). Bacterial cell attachment, the beginning of a biofilm. *Journal of Industrial Microbiology & Biotechnology*, *34*(9), 577-588. https://doi.org/10.1007/s10295-007-0234-4

Palmer, J. S., Flint, S. H., Schmid, J., & Brooks, J. D. (2010). The role of surface charge and hydrophobicity in the attachment of *Anoxybacillus flavithermus* isolated from milk powder. *Journal of Industrial Microbiology and Biotechnology*, *37*(11), 1111-1119. https://doi.org/10.1007/s10295-010-0758-x

Romling, U., & Galperin, M. Y. (2015). Bacterial cellulose biosynthesis: diversity of operons, subunits, products, and functions. *Trends in Microbiology*, *23*(9), 545-557. https://doi.org/10.1016/j.tim.2015.05.005

Roy, P. K., Mizan, M. F. R., Hossain, M. I., Han, N., Nahar, S., Ashrafudoulla, M., Toushik, S. H., Shim, W.-B., Kim, Y.-M., & Ha, S.-D. (2021). Elimination of *Vibrio parahaemolyticus* biofilms on crab and shrimp surfaces using ultraviolet C irradiation coupled with sodium hypochlorite and slightly acidic electrolyzed water. *Food Control*, *128*, 108179. https://doi.org/10.1016/j.foodcont.2021.108179

Song, X., Ma, Y., Fu, J., Zhao, A., Guo, Z., Malakar, P. K., Pan, Y., & Zhao, Y. (2017). Effect of temperature on pathogenic and non-pathogenic *Vibrio parahaemolyticus* biofilm formation. *Food Control*, *73*, 485-491. https://doi.org/10.1016/j.foodcont.2016.08.041

Sun, Y., Guo, D., Hua, Z., Sun, H., Zheng, Z., Xia, X., & Shi, C. (2019). Attenuation of Multiple *Vibrio parahaemolyticus* Virulence Factors by Citral. *Frontiers in Microbiology*, *10*, 894. https://doi.org/10.3389/fmicb.2019.00894

Tan, L., Li, H., Chen, B., Huang, J., Li, Y., Zheng, H., Liu, H., Zhao, Y., & Wang, J. J. (2021). Dual-species biofilms formation of *Vibrio parahaemolyticus* and *Shewanella putrefaciens* and their tolerance to photodynamic inactivation. *Food Control*, *125*, 107983. https://doi.org/10.1016/j.foodcont.2021.107983

Velez, K. E. C., Leighton, R. E., Decho, A. W., Pinckney, J. L., & Norman, R. S. (2023). Modeling pH and Temperature Effects as Climatic Hazards in *Vibrio Vulnificus* and

Vibrio Parahaemolyticus Planktonic Growth and Biofilm Formation. *GeoHealth*, *7*(4), e2022GH000769.

Appendices

Appendix I. Statement of contribution - Chapter 2

MASSEY UNIVERSITY
TE KUNENGA KI PŪREHUROA
UNIVERSITY OF NEW ZEALAND

GRADUATE RESEARCH SCHOOL

STATEMENT OF CONTRIBUTION
DOCTORATE WITH PUBLICATIONS/MANUSCRIPTS

We, the student and the student's main supervisor, certify that all co-authors have consented to their work being included in the thesis and they have accepted the student's contribution as indicated below in the Statement of Originality.

Student name:	Dan Wang
Name and title of main supervisor:	Steve Flint
In which chapter is the manuscript/published work?	Chapter 2

Describe the contribution that the student and members of the supervisory team have made to the manuscript/published work:[1]

Dan Wang: writing - original draft, review & editing;
Steve Flint, Jon Palmer, Dragana Gagic, Graham Fletcher and Stephen On: supervision, writing - review & editing.

Please select one of the following three options:

- (●) **The manuscript/published work is published or in press**
  Please provide the full reference of the research output:
  LWT - Food Science and Technology, 158 (2022), 113182
- ( ) **The manuscript is currently under review for publication**
  Please provide the name of the journal:
- ( ) **It is intended that the manuscript will be published, but it has not yet been submitted to a journal**

Student's signature:	Dan Wang — Digitally signed by Dan Wang Date: 2023.11.20 11:35:00 +13'00'	Main supervisor's signature:	Steve Flint — Digitally signed by Steve Flint Date: 2023.11.21 12:07:14 +13'00'

This form should be placed at the beginning of each relevant thesis chapter.

[1] Refer to the Massey University Publishing and Authorship guidelines (OneMassey for staff, Stream for students) and/ or Contributor Roles Taxonomy (CRediT) guidelines for guidance.

Appendix II. Statement of contribution - Chapter 3

MASSEY UNIVERSITY
TE KUNENGA KI PŪREHUROA
UNIVERSITY OF NEW ZEALAND

GRADUATE RESEARCH SCHOOL

STATEMENT OF CONTRIBUTION
DOCTORATE WITH PUBLICATIONS/MANUSCRIPTS

We, the student and the student's main supervisor, certify that all co-authors have consented to their work being included in the thesis and they have accepted the student's contribution as indicated below in the Statement of Originality.

Student name:	Dan Wang
Name and title of main supervisor:	Steve Flint
In which chapter is the manuscript/published work?	Chapter 3

Describe the contribution that the student and members of the supervisory team have made to the manuscript/published work:[1]

Dan Wang: Conceptualization, Methodology, Investigation, Formal analysis, Writing – original draft, Writing – review & editing. Graham C. Fletcher: Resources, Conceptualization, Methodology, Supervision, Writing – review & editing. Stephen L.W. On: Conceptualization, Methodology, Supervision, Writing – review & editing. Jon S. Palmer: Conceptualization, Methodology, Supervision, Writing – review & editing. Dragana Gagic: Conceptualization, Methodology, Supervision, Writing – review & editing. Steve H. Flint: Project administration, Resources, Supervision, Conceptualization, Methodology, Writing – review & editing.

Please select one of the following three options:

- (●) **The manuscript/published work is published or in press**
  Please provide the full reference of the research output:
  As part in International Journal of Food Microbiology, 385 (2023), 110011.
- ( ) **The manuscript is currently under review for publication**
  Please provide the name of the journal:
- ( ) **It is intended that the manuscript will be published, but it has not yet been submitted to a journal**

Student's signature:	Dan Wang — Digitally signed by Dan Wang Date: 2023.11.20 11:37:41 +13'00'	Main supervisor's signature:	Steve Flint — Digitally signed by Steve Flint Date: 2023.11.21 12:07:33 +13'00'

This form should be placed at the beginning of each relevant thesis chapter.

[1] Refer to the Massey University Publishing and Authorship guidelines (OneMassey for staff, Stream for students) and/ or Contributor Roles Taxonomy (CRediT) guidelines for guidance.

Appendix III. Statement of contribution - Chapter 4

MASSEY UNIVERSITY
TE KUNENGA KI PŪREHUROA
UNIVERSITY OF NEW ZEALAND

GRADUATE RESEARCH SCHOOL

STATEMENT OF CONTRIBUTION
DOCTORATE WITH PUBLICATIONS/MANUSCRIPTS

We, the student and the student's main supervisor, certify that all co-authors have consented to their work being included in the thesis and they have accepted the student's contribution as indicated below in the Statement of Originality.

Student name:	Wang Dan
Name and title of main supervisor:	Steve Flint
In which chapter is the manuscript/published work?	Chapter 4

Describe the contribution that the student and members of the supervisory team have made to the manuscript/published work:[1]

Dan Wang: Conceptualization, Methodology, Investigation, Formal analysis, Writing – original draft, review & editing; Steve Flint: Project administration, Resources, Supervision, Conceptualization, Methodology, Writing – review & editing. Graham Fletcher: Resources, Conceptualization, Methodology, Supervision, Writing – review & editing. Jon Palmer, Dragana Gagic & Stephen On: Conceptualization, Methodology, Supervision, Writing – review & editing.

Please select one of the following three options:

- (●) **The manuscript/published work is published or in press**
  Please provide the full reference of the research output:
  International Journal of Food Microbiology, 385 (2023), 110011.
  International Journal of Food Microbiology, 405 (2023), 110372.
- ( ) **The manuscript is currently under review for publication**
  Please provide the name of the journal:
- ( ) **It is intended that the manuscript will be published, but it has not yet been submitted to a journal**

Student's signature:	Dan Wang Digitally signed by Dan Wang Date: 2024.05.14 19:53:54 +12'00'	Main supervisor's signature:	Steve Flint Digitally signed by Steve Flint Date: 2024.05.15 14:06:17 +12'00'

This form should be placed at the beginning of each relevant thesis chapter.

[1] Refer to the Massey University Publishing and Authorship guidelines (OneMassey for staff, Stream for students) and/ or Contributor Roles Taxonomy (CRediT) guidelines for guidance.

Appendix IV. Statement of contribution - Chapter 5

MASSEY UNIVERSITY
TE KUNENGA KI PŪREHUROA
UNIVERSITY OF NEW ZEALAND

GRADUATE RESEARCH SCHOOL

STATEMENT OF CONTRIBUTION
DOCTORATE WITH PUBLICATIONS/MANUSCRIPTS

We, the student and the student's main supervisor, certify that all co-authors have consented to their work being included in the thesis and they have accepted the student's contribution as indicated below in the Statement of Originality.

Student name:	Dan Wang
Name and title of main supervisor:	Steve Flint
In which chapter is the manuscript/published work?	Chapter 5

Describe the contribution that the student and members of the supervisory team have made to the manuscript/published work:[1]
Dan Wang: Conceptualization, Methodology, Investigation, Formal analysis, Writing – original draft. Graham C. Fletcher: Resources, Conceptualization, Methodology, Supervision, Writing – review & editing. Dragana Gagic: Conceptualization, Methodology, Supervision, Writing – review & editing. Stephen L.W. On: Conceptualization, Methodology, Supervision, Writing – review & editing. Jon S. Palmer: Conceptualization, Methodology, Supervision, Writing – review & editing. Steve H. Flint: Project administration, Resources, Supervision, Conceptualization, Methodology, Writing – review & editing.

Please select one of the following three options:

- (●) **The manuscript/published work is published or in press**
  Please provide the full reference of the research output:
  Food Research International, 166 (2023), 112605.
- ( ) **The manuscript is currently under review for publication**
  Please provide the name of the journal:
- ( ) **It is intended that the manuscript will be published, but it has not yet been submitted to a journal**

Student's signature:	Dan Wang — Digitally signed by Dan Wang Date: 2024.05.14 19:54:36 +12'00'	Main supervisor's signature:	Steve Flint — Digitally signed by Steve Flint Date: 2024.05.15 14:07:18 +12'00'

This form should be placed at the beginning of each relevant thesis chapter.

[1] Refer to the Massey University Publishing and Authorship guidelines (OneMassey for staff, Stream for students) and/ or Contributor Roles Taxonomy (CRediT) guidelines for guidance.

Appendix V. Statement of contribution - Chapter 6

MASSEY UNIVERSITY
TE KUNENGA KI PŪREHUROA
UNIVERSITY OF NEW ZEALAND

GRADUATE RESEARCH SCHOOL

STATEMENT OF CONTRIBUTION
DOCTORATE WITH PUBLICATIONS/MANUSCRIPTS

We, the student and the student's main supervisor, certify that all co-authors have consented to their work being included in the thesis and they have accepted the student's contribution as indicated below in the Statement of Originality.

Student name:	Dan Wang
Name and title of main supervisor:	Steve Flint
In which chapter is the manuscript/published work?	Chapter 6

Describe the contribution that the student and members of the supervisory team have made to the manuscript/published work:[1]
Dan Wang: writing - original draft, review & editing; Steve Flint, Jon Palmer, Dragana Gagic, Graham Fletcher & Stephen On: supervision, conceptualization, writing.

Please select one of the following three options:

- ○ **The manuscript/published work is published or in press**
  Please provide the full reference of the research output:
- ○ **The manuscript is currently under review for publication**
  Please provide the name of the journal:
- ◉ **It is intended that the manuscript will be published, but it has not yet been submitted to a journal**

Student's signature:	Dan Wang — Digitally signed by Dan Wang Date: 2024.05.14 20:03:05 +12'00'	Main supervisor's signature:	Steve Flint — Digitally signed by Steve Flint Date: 2024.05.15 14:07:58 +12'00'

This form should be placed at the beginning of each relevant thesis chapter.

[1] Refer to the Massey University Publishing and Authorship guidelines (OneMassey for staff, Stream for students) and/ or Contributor Roles Taxonomy (CRediT) guidelines for guidance.

Appendix VI. Research output - Chapter 2

LWT - Food Science and Technology 158 (2022) 113182

Contents lists available at ScienceDirect

LWT

journal homepage: www.elsevier.com/locate/lwt

Global expansion of *Vibrio parahaemolyticus* threatens the seafood industry: Perspective on controlling its biofilm formation

Dan Wang [a,*], Steve H. Flint [a], Jon S. Palmer [a], Dragana Gagic [b], Graham C. Fletcher [c], Stephen L. W. On [d]

[a] School of Food and Advanced Technology, Massey University, Private Bag, 11222, Palmerston North, New Zealand
[b] School of Fundamental Sciences, Massey University, Private Bag, 11222, Palmerston North, New Zealand
[c] The New Zealand Institute for Plant & Food Research Limited, Private Bag, 92169, Auckland, 1142, New Zealand
[d] Faculty of Agriculture and Life Sciences, Lincoln University, Private Bag, 85084, Canterbury, New Zealand

ARTICLE INFO

Keywords:
Climate change
Biofilm
Life cycle
Molecular mechanisms
Control strategies

ABSTRACT

As global warming increases the geographical range and frequency of *Vibrio parahaemolyticus* infections, its formation of biofilms providing bacteria greater resistance to stress and contributing to the persistence of pathogens, is threatening the seafood industry. *V. parahaemolyticus* has a number of advantages leading to biofilm formation. This study reviews recent advances in understanding *V. parahaemolyticus* biofilm formation on biotic and abiotic surfaces, discusses research gaps in the mechanism of biofilm formation and examines promising biofilm control strategies to overcome current limitations of chemical disinfectant. This information will deepen our understanding of *V. parahaemolyticus* biofilm formation, as well as help design and optimize *V. parahaemolyticus* biofilm control strategies for the seafood industry.

1. Introduction

V. parahaemolyticus is a curved rod, Gram-negative bacterium that naturally exists in the marine environment. It can be prevalent in oysters, clams, fish, shrimps, mussels, scallop and periwinkle (Odeyemi, 2016), and infections involve the consumption of raw or undercooked seafood. *V. parahaemolyticus* survives at 5-45 °C and achieves substantial growth when seawater temperatures are over 14-19 °C. This explains why this pathogen is prevalent in summer and autumn seasons. Global warming has caused an increasing geographical range and frequency of *V. parahaemolyticus* infections. Repeated cases of infection and outbreaks have been reported in unexpected areas where there were previously no or only sporadic cases (Table 1).

V. parahaemolyticus has advantages enabling biofilm formation in seafood environments. *V. parahaemolyticus* forms biofilm assisted by a dual flagellar system - polar and lateral flagella (Kim & McCarter, 2000), which is not the case with *Escherichia coli*, *Salmonella* spp. and *Listeria monocytogenes* pathogens. This dual flagellar system allows *V. parahaemolyticus* to move under various conditions, thereby adjusting to different environments and attaching onto surfaces. *V. parahaemolyticus* can produce an active chitinase, enabling it to adsorb onto chitin- and copepod-surfaces (Makino et al., 2003). This helps *V. parahaemolyticus* initiate colonisation of seafood due to the capability to degrade and utilize chitinous materials of seafood surfaces. Biofilm communities are covered by extracellular polymeric substances (EPS) and show facilitated persistence within the seafood plant surfaces. Biofilms are posing challenges for hygienic treatments and risks of pathogen outbreaks.

Understanding *V. parahaemolyticus* biofilm formation will help develop biofilm decontamination techniques in seafood scenarios and reduce risks of *V. parahaemolyticus* infections. This study reviews new findings and conclusions about *V. parahaemolyticus* biofilm formation in seafood and processing plant environments, as well as describes recent advances in understanding the mechanisms of *V. parahaemolyticus* biofilm formation. It will contribute to overcoming the limitations of current chemical disinfectant treatments and help develop novel cost-effective control strategies to meet the requirements of achieving and maintaining product safety and quality in the seafood industry.

* Corresponding author.
E-mail address: d.wang3@massey.ac.nz (D. Wang).

https://doi.org/10.1016/j.lwt.2022.113182
Received 6 October 2021; Received in revised form 3 January 2022; Accepted 29 January 2022
Available online 3 February 2022

Table 1
Emerging *Vibrio* food poisoning in unexpected regions.

Region	Year	No. of cases	Infection route	Reference
France	2010–2019	91	Seafood	FAO (2021)
Canada	2020	21	Oysters	
Canada	2015	82	Oysters	
England	2010–2020	22	Seafood	
New Zealand	2019–2020	40	Mussels	

2. Overview of *V. parahaemolyticus* biofilm formation in seafood related environments

2.1. Fundamentals of V. parahaemolyticus biofilm formation in seafood related environments

V. parahaemolyticus forms biofilms on marine biotic surfaces and abiotic surfaces under appropriate incubation conditions, functioning as a source of pathogenic bacteria with 10-1000 times the resistance to hygiene treatments than planktonic counterparts. Table 2 summarises published methods for detecting *V. parahaemolyticus* biofilm. While these methods have contributed to a deeper understanding of *V. parahaemolyticus* biofilm, each method has limitations. Certain techniques may concentrate exclusively on a single or a few aspects of biomass, cell viability, VBNC population, matrix structure or biofilm composition. Therefore, researchers commonly employ a combination of methods to detect and describe biofilm characteristics.

Odeyemi (2016) examined the prevalence of *V. parahaemolyticus* based on 48 published studies and discovered its presence in oysters, clams, fish, shrimp, and mussels was 63.4 %, 52.9 %, 51.0 %, 48.3 %, and 28.0 %, respectively. *V. parahaemolyticus* can form biofilms on these surfaces (Table 3), especially uneven seafood surface areas where pits and edges provide protections for biofilm communities from biocidal treatments (Han, Mizan, Jahid, & Ha, 2016). *V. parahaemolyticus* biofilm was identified on crab and shrimp surfaces by Han et al. (2016), and on shrimp and mussel surfaces by Ashrafudoulla et al. (2019). However, Rosa, Conceição, Conceição, and Timm (2018) discovered that *V. parahaemolyticus* did not form biofilm on shrimp shells, the different results occurred which could be a result of different isolates examined.

Several studies have documented that *V. parahaemolyticus* forms biofilms on abiotic surfaces (Table 3). Stainless steel, polystyrene, fibreboard, polypropylene boxes, and glass are among materials that have the potential to support the biofilm production. *V. parahaemolyticus* can form biofilms on the internal pipe surfaces of water distribution networks in seafood processing plants, which may contaminate the entire processing plant when the water is used. Seawater is frequently utilised as the initial stage in washing seafood instead of freshwater, avoiding the depletion of restricted freshwater reserves. Many pathogens do not grow well in seawater, but *V. parahaemolyticus* is an exception. Notably, washing water is routinely recirculated, allowing *V. parahaemolyticus* to accumulate and potentially develop biofilms on interior pipe surfaces (Di Pippo, Di Gregorio, Congestri, Tandoi, & Rossetti, 2018). Although chlorine and ultraviolet (UV) treatments are commonly used to disinfect industrial water, they are ineffective at removing biofilms from the water distribution network and seafood processing facilities. Moreover, cells may detach from bacterial biofilms and enter the water distribution system as a result of these treatments (Shikongo-Nambabi, Kachigunda, & Venter, 2010).

2.2. Biofilm life cycle

2.2.1. Surface attachment

V. parahaemolyticus forms biofilms using polar and lateral flagella. Polar flagella (driven by sodium ions) are utilised for swimming, while lateral flagella (driven by protons) are used for swarming (Kim and McCarter, 2000). Polar flagella function via the *fla* gene system, which is

Table 2
Different methods to determine *V. parahaemolyticus* biofilm.

Method	Application	Limitations	References
Colony formation Units (CFU)	Enumeration of culturable cells in the biofilm matrix	Only detects culturable biofilm populations, but not dormant, viable but non culturable communities; Underestimates biofilm populations due to cell aggregation; Time consuming.	(Chen et al., 2020; Guo et al., 2020; Han et al., 2016, 2017; Li et al., 2020; Mougin et al., 2019; Ning et al., 2021; Roy et al., 2021; Sun et al., 2019; Tan et al., 2021)
Microtiter plate assay - crystal violet dye & biofilm formation index (BFI)	Quantification of biomass through crystal violet stain	Lack of sensitivity; Lack of consistency; Dead cells will be stained and included as the biomass volume.	
Microtiter plate assay - Calgary device	Quantification of biomass	Calgary device lid and bottom plate are needed; CFU assay to enumerate cell numbers inside biofilm matrix still needs to be performed.	
PMA-qPCR method	Quantification of viable cell numbers in the biofilm matrix	Expensive; Need to use CFU assay to enumerate cultivable cell population to obtain VBNC cell population.	
Fluorescence microscopy	Enumeration of living and dead cell numbers through living and dead cells stains	Expensive use of fluorescence dye; Cell number counts are limited by microscopic view scopes.	
Confocal laser scanning microscopy (CLSM) imaging	Biofilm matrix observation; Structural detection	High price of fluorescence dye; Interference of self-fluorescence from the matrix.	
Scanning electoral microscopy (SEM) imaging	Observe the biofilm morphology	General observation of biofilm morphology, not useful if used to compare biofilms with limited differences.	
XTT [2, 3-bis (2-methoxy-4-nitro-5-sulfophenyl)-2H-tetrazolium-5-carboxanilide] (Sigma Aldrich, UK) method	Determination of biofilm metabolic activity	Detection limit of 10^3–10^8 CFU/biofilm; Comparing the metabolic activity within the biofilm formed by same strain, strain variations may induce differences of metabolic activity.	
Phenol-sulphoacid method	Chemical method to quantify extracellular polymeric substance (EPS) production	Can only detect extracellular polysaccharides; Low accuracy; Quantification of EPS requires standard curves, or EPS production can	

(*continued on next page*)

Table 2 (*continued*)

Method	Application	Limitations	References
RT-qPCR	Quantifies expression levels of biofilm relative genes	only be compared by OD value. Expensive; Multiple steps to extract clean RNA.	

highly regulated and comprises three distinct types of gene clusters. The polar flagella function as a mechano-sensor, resulting in a reduction in flagellar rotation and activation of the *laf* gene-encoded lateral flagella expression (Kim and McCarter, 2000). Swarming via lateral flagella requires bacterial cells to reach certain numbers, and the morphology of *V. parahaemolyticus* becomes elongated as it transitions from swimming to swarming cells (Freitas, Glatter, & Ringgaard, 2020). *V. parahaemolyticus* swarms, twitches, and glides across surfaces through lateral flagella, pili and the secretion of slime surface adhesins, respectively. The motility facilitates cell interaction with the surface, biofilm formation as well as virulent infection of host cells (Rossi, Paroni, & Landini, 2018). However, it is unknown whether the flagellum is lost and/or degraded following surface attachment, or whether flagella serve as structural components of the biofilm, and little is understood about how the various forms of motility interact and initiate biofilm development in *V. parahaemolyticus*.

2.2.2. Microcolony formation and the matrix

Swarm motility promotes surface colonisation through a decrease in flagellar locomotion, adhesin protein secretion and exopolysaccharide synthesis. Microcolonies are aggregates of 50 or fewer cells that form as a forerunner to biofilm formation; small colony variants promote biofilm aggregate production and antimicrobial tolerance, acting as a survival strategy with a low reproduction rate (Steenackers, Parijs, Dubey, Foster, & Vanderleyden, 2016). Following microcolony development, the cells become stronger and more stable due to the secretion of structural components, exopolysaccharides, matrix proteins, and eDNA that work as a "molecular glue" to aid attachment. The mechanism by which individual cells transform into cell aggregates, on the other hand, is not completely understood.

Biofilm maturation results in cells buried deep within biopolymer layers with a variety of mature matrix structures, including: 1) monolayer biofilms - *V. parahaemolyticus* was reported to form this structure at 4 and 10 °C (Han et al., 2016); 2) multilayer biofilms with large aggregates of bacterial cells; 3) a matrix structure previously described for other species but not yet been observed for *V. parahaemolyticus*, consist of multi-layered biofilms with small aggregates at base and motile cells covering the surface, and associate with a late mature biofilm and dispersion (Houry et al., 2012). Chemical components contained within the *V. parahaemolyticus* biofilm matrix, such as polysaccharides, proteins and eDNA, shape the biofilm architecture by changing the biovolume, porosity and mean thickness of the three-dimensional matrix (Tan et al., 2018), but the mechanisms are poorly understood.

2.2.3. Dispersion

Dispersion is the final stage of the biofilm life cycle; cells inside the biofilm actively escape from the extracellular matrix, resulting in eroded biofilm matrices and bacterial cells that can migrate to new nutrition and resource-rich environments (Steenackers et al., 2016). While it is well established that dispersion is related with cell death and lysis, little is known about the information in *V. parahaemolyticus*.

2.3. Environmental factors influencing biofilm formation

Attachment and biofilm formation of *V. parahaemolyticus* to biotic and abiotic surfaces are complicated processes that are influenced by a variety of factors including temperature, composition of the attachment medium, contact surface, cell surface, strain variants and so on.

2.3.1. Temperature

Temperature has been claimed to play a key role in influencing *V. parahaemolyticus* biofilm formation. Song et al. (2017) reported that *V. parahaemolyticus* produced better biofilm at 25 °C than at 15 °C and

Table 3
Biofilm formulation of *V. parahaemolyticus* on biotic and abiotic surfaces.

Surface	Strain	Inoculum size	Incubation parameters	Biofilm formulation results	References
Biotic - crab - shrimp Abiotic - Stainless steel	Cocktail of *V. parahaemolyticus* KCTC 2471, KCTC 2729, ATCC 33844	Crab & shrimp: 1: 2500 dilution of OD 1.0 cell suspension SS: 1:50 dilution of OD 1.0 cell suspension	Time: 24 h Temperature: 4, 10, 15, 20, 25, 30, 35, and 37 °C	The higher CFU levels were observed on the crab surfaces (almost 8 log CFU/cm^2) than on the shrimp surfaces (7 log CFU/cm^2) at 25-37 °C. 30 °C was the optimum condition for biofilm formation (>8 log CFU/cm^2).	Han et al. (2016)
Biotic - shrimp - mussel	*V. parahaemolyticus* clinical isolates (ATCC17802, ATCC27969) and 8 other environmental isolates	10^5 CFU/mL, 10 mL	Time: 24 h Temperature: 30 °C	For shrimp surfaces, environmental isolates formed 6.21-6.89 $\log_{10}$ CFU/cm^2, clinical isolates formed 5.59-6.19 $\log_{10}$ CFU/cm^2. For mussel surfaces, environmental isolates formed 5.91-6.40 $\log_{10}$ CFU/cm^2, clinical isolates formed 5.29-5.72 $\log_{10}$ CFU/cm^2.	(Ashrafudoulla et al., 2019),
Biotic - shrimp - Fish, white mouth croaker	*8 V. parahaemolyticus* environmental isolates	Original concentration of overnight culture	Time: 240 h (replace inoculum broth each 48 h) Temperature: 37 °C	No biofilms on shrimp shells, but on operculum of fish (5-6 $\log_{10}$ CFU/cm^2).	Rosa et al. (2018)
Abiotic - Stainless steel	*V. parahaemolyticus* ANSES collection 14-B3PA-0046	10^8 CFU/mL, 11 mL	Time:3 h, 24 h, 48 h Temperature: 8 °C, 37 °C	No big difference of biofilm formation at 8 and 37 °C, ranging from 6 to 9 $\log_{10}$ CFU/cm^2.	Mougin et al. (2019)
Abiotic - Stainless steel - glass	*V. parahaemolyticus* ST55, 16 clinical and 12 environmental isolates	1:2 dilution of OD 1.5 cell suspension	Time: 1–8 h Temperature: 25 °C	Clinical strains attached better on stainless steel surface than did environmental strains. The cell density reached a peak at 6 or 8 h (6-8*10^5 CFU/mL) on stainless steel and glass surfaces and declined thereafter.	Wong (2002)
Abiotic - glass	*V. parahaemolyticus* VP-C7	1:100 dilution of OD 0.4 cell suspension	Time: 2 h, 8 h, 12 h, 24 h and 48 h Temperature: 15, 25 and 37 °C	When cultured at 15 °C, a mature biofilm only forms after 48 h (biofilm thickness of 19.73 μm), while a mature biofilm forms between 12 and 24 h at 25 C° (biofilm thickness of 18.94-19.80 μm).	Song et al. (2017)

37 °C. According to Han et al. (2016), *V. parahaemolyticus* develops multi-layered biofilms at 15 and 37 °C, but monolayers at 4 and 10 °C. It has been concluded that biofilm formation could be the main cause of food safety problems at higher temperature (25-37 °C) (Han et al., 2016).

2.3.2. Sodium chloride and glucose

Sodium chloride (NaCl) and glucose influence adhesion and maturation of *V. parahaemolyticus* biofilms. For example, the adsorption of *V. parahaemolyticus* onto plankton or chitin-containing materials was observed at salinities as low as 1.7 % in estuary waters while salinity in open ocean seawater is approximately 3.5 %. *V. parahaemolyticus* formed the best biofilm in tryptic soy broth (TSB) containing 2 % NaCl and the least biofilm in TSB containing 5 % NaCl. Glucose concentrations of 0.005-0.015 % in TSB promoted biofilm formation, whereas high glucose concentrations of 0.05 % inhibited the formation (Mizan, Ashrafudoulla, Sadekuzzaman, Kang, & Ha, 2018).

2.3.3. Contact surface (charge, hydrophobicity)

The charge on the cell surface varies under different physiological conditions, influencing bacterial attachment to surfaces. Cells of *V. parahaemolyticus* are frequently negatively charged, and thus prefer to attach to positively charged surfaces (Mizan et al., 2016). Besides, *V. parahaemolyticus* biofilm formation is positively correlated with cell surface hydrophobicity and is associated with the flagellar and proteins on the bacterial cell outer membrane (Mizan et al., 2016). The hydrophobicity of contact surface (stainless steel, polystyrene and glass) exhibited a negative correlation with the amount of eDNA, extracellular protein and biofilm biomass in *V. parahaemolyticus* biofilms (Guo et al., 2020). Instead of hydrophobic stainless steel, *V. parahaemolyticus* grows a better biofilm on surfaces such as polystyrene and glass; this phenotype was related with different survival adaptation mechanisms on these surfaces (Guo et al., 2020; Wong, 2002).

3. Molecular mechanisms of *V. parahaemolyticus* biofilm formation

3.1. Positive regulators

The mechanisms by which *V. parahaemolyticus* biofilms form are regulated by a systemic and integrated regulatory network. Though there are numerous genes responsible for EPS biosynthesis and production, the *cps* locus has been extensively studied and will be discussed in Positive regulators and Negative regulators (Fig. 1).

CpsQ can activate the expression of the capsular polysaccharide genes *cpsA-cpsJ* (*vpa1403-1412*) in *V. parahaemolyticus*, thereby regulating biofilm production. CpsQ is a c-di-GMP binding protein that is regulated by intracellular c-di-GMP concentrations, and has been demonstrated to be a positive, regulator of capsular polysaccharide CPSA expression. It was reported that quorum sensing regulators OpaR and AphA bind to the promoter region of the *mfpABC* operon to enhance and repress *mfpABC* transcription, as well as repress and enhance *cpsQ-mfpABC* operon expression, and influence biofilm development (Zhou et al., 2013). Due to their accumulation at high cell density, it was hypothesised that CpsQ and MfpABC might play a role in the middle/late stages of growth and pathogenesis. CpsQ contributes to capsule expression when c-di-GMP levels are elevated, but it is not solely responsible for biofilm formation; therefore, deletion of CpsQ does not eliminate biofilm formation (Kimbrough, Cribbs, & McCarter, 2020).

CpsR is another transcription regulator that regulates the formation of the biofilm matrix. CpsR is also not solely required for biofilm formation in *V. parahaemolyticus*, but it is critical for the increased CPSA

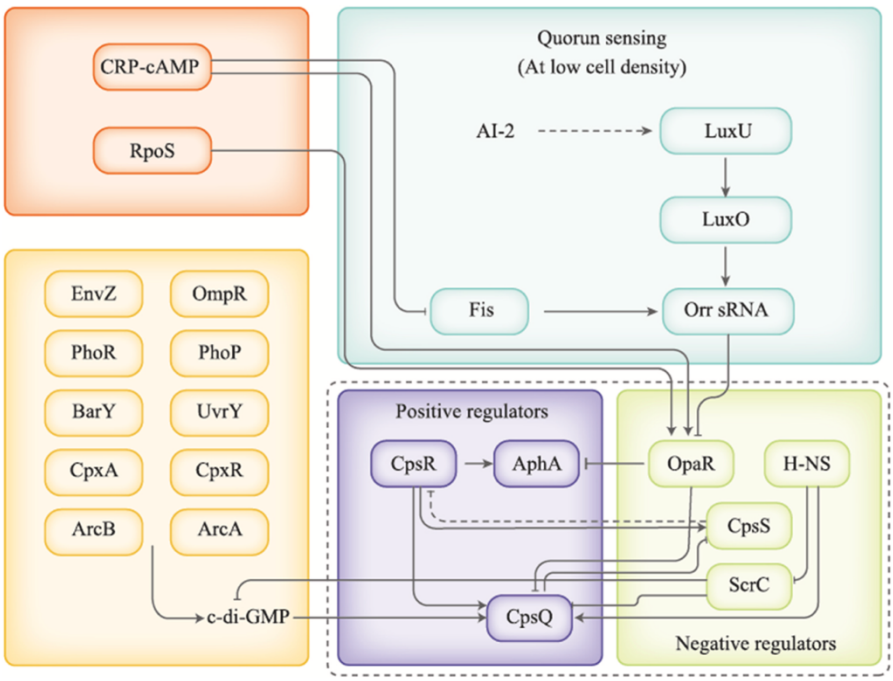

Fig. 1. The transcriptional network of *V. parahaemolyticus* biofilm formation.

expression elicited by c-di-GMP (Yildiz & Visick, 2009). It is required in the ScrABC-dependent pathway to regulate swarming and EPS production. Introduction of the *cpsR1*::Tn5 allele into the rugose *scrA* mutant resulted in the transformation of a rugose colony to smooth colony, the elimination of exopolysaccharide production, and a decreased capacity for biofilm formation (Guvener & McCarter, 2003). CpsR acts prior to CpsQ and can activate CpsQ and CpsS; the CpsS-CpsR-CpsQ regulatory cascade is responsible for the EPS production (Guvener & McCarter, 2003).

Quorum sensing governs sets of cellular pathways, including motility, virulence and biofilm formation through its master regulators-AphA and OpaR. AphA is a small PadR family expression regulator with an N-terminal winged-helix DNA-binding domain; AphA is activated at low cell density, to promote the transcription of virulence, flagella-mediated motility and biofilm formation (Zhou et al., 2013). In the presence of low cell density, redundant Qrr_{1-4} sRNAs regulated by LuxQ-LuxU-LuxO pathway inhibit *opaR* and *cpsQ-mfpABC* transcription, thereby influencing the formation of *V. parahaemolyticus* biofilms (Liu, Zhu, Zhang, & Zhao, 2021; Zhou et al., 2013).

3.2. Negative regulators

Signalling via chemotaxis ScrABC is involved in competitive colonisation and the development of the biofilm matrix. ScrA is found in the *scrABC* operon and promotes the expression of *laf* genes while repressing the transcription of *cps* genes in *V. parahaemolyticus* (Boles & McCarter, 2002). ScrC functions as a diguanylate cyclase (DGC), retains GGDEF and EAL domains and is regulated by ScrA and ScrB translation, it can promote CpsQ repression and c-di-GMP degradation (Kimbrough et al., 2020). A *scrABC* operon mutation has a profound effect on gene expression, resulting in decreased swarming activity, increased cellular c-di-GMP levels, overproduced CPSA, crinkly colonies and enhanced biofilm formation (Kimbrough et al., 2020).

CpsS is the dominant negative regulator in *V. parahaemolyticus* (Yildiz & Visick, 2009). It is another member of the CsgD family and contains a DNA-binding domain similar to that of CsgD. CpsS can inhibit *cpsR* expression, while *cpsR* activates *cpsQ*, and CpsQ inhibits *cpsS*. CpsS represses CpsQ, but it is unknown whether it directly or indirectly regulates CpsQ. Deletion of *cpsS* results in capsule overexpression and wrinkly colonies (Enos-Berlage, Guvener, Keenan, & McCarter, 2005).

OpaR governs biofilm formation through regulating CpsQ (Zhou et al., 2013). The histone-like nucleoid structuring protein H-NS is a "transcriptional silencer", it is involved in the transcription of genes and the folding of DNA and an expression activator of the *cpsA-cpsJ* operon (Enos-Berlage et al., 2005). Mutants of *hns* fail to trigger CPSA production and polar flagellar activity, thereby resulting in decreased biofilm formation in *V. parahaemolyticus* (Enos-Berlage et al., 2005).

3.3. EPS synthesis genes

Numerous gene loci/genes have been identified as being involved in the formation of the extracellular matrix of *V. parahaemolyticus* biofilms. *cpsA-J* (*vpa1403-1412*) is required for the synthesis of capsular polysaccharide A (CPSA), a major component of the *V. parahaemolyticus* biofilm (Yildiz & Visick, 2009). *cpsA-J* is also required for the formation of opaque colonies, rugose phase transmission of the colony and biofilm development (Enos-Berlage & McCarter, 2000). *vp1476-1458* is an ortholog of the *syp* locus that is conserved in *Vibrio fischeri*, this locus was reported to be responsible for wrinkled colonies, pellicle formation and matrix production in *V. fischeri* (Yildiz & Visick, 2009). *V. parahaemolyticus* shares 85.9 and 75.8 % similarities with the glycosyltransferase gene *sypQ* from *Vibrio alginolytious* 12G01 and *Vibrio harveyi* ATCC BAA-1116 (Ye, Zheng, & Zheng, 2014), indicating the relatedness with poly-N-acetylglucosamine (PNAG) biosynthesis and function as an intercellular adhesin. Cellulose is typically found in flagella or pili of Gram-negative bacteria; however, the cellulose synthase gene cluster is limited known in *V. parahaemolyticus*. Another locus involved in *V. parahaemolyticus* biofilm formation is *vp0214-0237*, which results in translucent colonies, decreased adherence to surfaces, inhibition of swarming motility and interruption of biofilm maturation (Enos-Berlage et al., 2005). Proteins and eDNA in the extracellular matrix contribute to the structure and stability, but they are poorly studied in *V. parahaemolyticus*.

3.4. Will pathogenicity influence biofilm formation?

Virulence factors are typically associated with bacterial pathogenicity. *V. parahaemolyticus* produces a variety of virulence factors, including thermostable direct hemolysin (TDH), TDH-related hemolysin (TRH) and two distinct type III secretion systems (T3SS1 and T3SS2) (Makino et al., 2003). The pathogenicity of a strain and its ability to form biofilms are related properties. Song et al. (2017) discovered that pathogenic *V. parahaemolyticus* accumulates more biofilm matrix than non-pathogenic strains. Similarly, Wong (2002) found that clinical strains adhered more readily to stainless steel than environmental strains, and that decreased c-di-GMP levels within cells can promote biofilm formation and pathogenicity in *V. parahaemolyticus*. Zhang et al. (2019) revealed that the transcription factor QsvR works in conjunction with QS system to regulate the expression of virulence genes, T3SS1 and pathogenicity island (PAI, T3SS2 and TDH), in *V. parahaemolyticus*. AphA has a role in the initial colonisation stage, it activates T3SS1 genes expression but inhibits the expression of PAI genes, thus boosting *V. parahaemolyticus* cytotoxicity, whereas OpaR and QsvR act at a higher cell density by activating PAI transcription, thereby enhancing enterotoxicity and causing severe gastroenteritis. QsvR can also maintain basal levels of T3SS1 expression despite OpaR negatively regulates it.

4. Limitation of chemical disinfectants and promising strategies to overcome

4.1. Limitation of chemical disinfectants

Chemical disinfectant treatment is a simple, cost-effective, and widely used strategy for pathogen contamination control in the food industry. Numerous studies to determine the efficacy of various chemical disinfectants against *V. parahaemolyticus* biofilms have been conducted (Table 4). While cleaning chemicals and disinfectants remove soils and inactivate biofilm cells from seafood and plant surfaces, using disinfectants alone at recommended concentrations makes it difficult to control biofilm effectively; what is worse, recurrence and recolonization of pathogen communities with increased acquired resistance may occur (Rosa et al., 2018). Increased disinfectant concentrations are discouraged, as they may corrode plant surfaces, influence seafood sensory attributes and produce chlorine and/or other by-products that are hazardous to human health. Additionally, routine exposure of biofilm populations to chemical disinfectants may also result in an increase in VBNC state cells, which aids in the persistence of biofilm communities on seafood processing plants. For instance, the routine use of chemical disinfectants in cleaning and sanitation in smoked salmon processing plants has resulted in the development of *L. monocytogenes* VBNC populations that are resistant to environmental stress and difficult to eradicate (Brauge et al., 2020).

4.2. Promising strategies

As chemical disinfectant treatments fail to remove *V. parahaemolyticus* biofilms effectively, alternative strategies for mitigating these risks are required (Fig. 2).

4.2.1. Plant surface modification

Processing plant surface modifications have been studied to inhibit biofilm colonisation and development. For example, it has been

Table 4
The effect of chemical disinfectant treatment on *V. parahaemolyticus* biofilm.

Disinfectants	Biofilm	Reduction	Reference
Sodium hypochlorite - 20 ppm chlorine (~20 mg/L chlorine), 10min	240 h old biofilms formed on biotic and abiotic surfaces	*V. parahaemolyticus* biofilm communities of 2-5 $\log_{10}$ CFU/cm^2 were remained after treatment (~6 $\log_{10}$ CFU/cm^2 biofilm as control).	Rosa et al. (2018)
Sodium hypochlorite - 4 mg/L chlorine, 1h	72 h old biofilm on glass slides	The bacterial density dropped from 7.90 to 3.97 $\log_{10}$ CFU/cm^2;	Shikongo-Nambabi et al. (2010)
Hydrogen peroxide (H_2O_2) - 0.08 %, 1h		Inactivated cells to non-detectable levels from over 7 $\log_{10}$ CFU/cm^2;	
Ozone - 1.6 mg/L, 1h		Reduced ~ 2 $\log_{10}$ CFU/cm^2 biofilm cell densities.	
Sodium hypochlorite - 50-300 ppm, 6 % w/v chlorine, 5min Strong acidic electrolyzed water (SAEW) - 30 ppm chlorine (~30 mg/L chlorine), 1–15 min	24 h old biofilm on shrimp and crab surfaces	Sodium hypochlorite rendered maximum reductions of 3.78 and 3.32 $\log_{10}$ CFU/cm^2 on shrimp and crab surfaces (6.87 and 7.37 $\log_{10}$ CFU/cm^2 as control); SAEW achieved reductions of 1.42-3.05 and 1.14 to 2.56 $\log_{10}$ CFU/cm^2 on shrimp and crab surfaces.	Roy et al. (2021)
Strong acidic electrolyzed water (SAEW) - pH 2.3, 136.33 mg/L chlorine, 30s	48 h old biofilm	Decreased viable *V. parahaemolyticus* from 6.90 to 3.33 $\log_{10}$ CFU/cm^2.	Han et al. (2017)
Acidic electrolyzed water - pH 2.28, 52.26 mg/mL chlorine, 10 min	48 h old biofilms on polystyrene surfaces	The biovolume, eDNA, protein and polysaccharide content of *V. parahaemolyticus* matrix was significantly reduced.	Li et al. (2020)

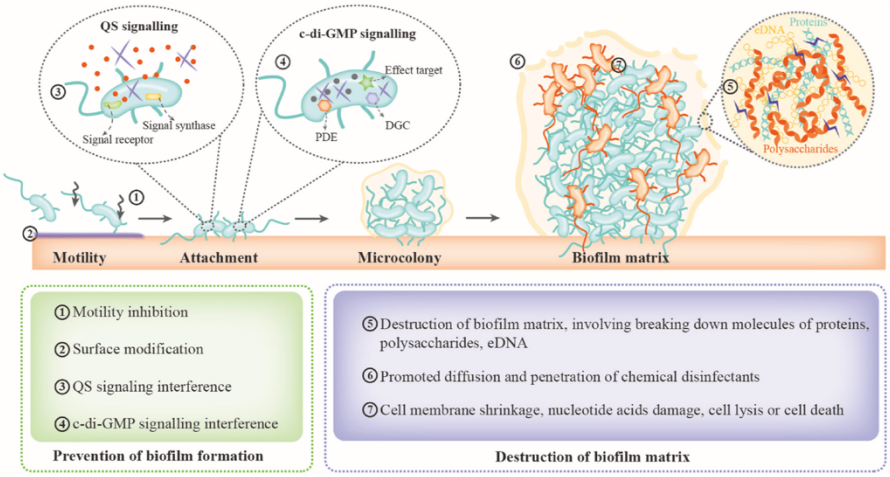

Fig. 2. Promising inactivation forms of *V. parahaemolyticus* biofilm communities.

demonstrated that sol-gel modification, in which the material is transformed from a liquid to a gel state, reached to reduce the average biomass weight attached. This was employed on milk processing plant surfaces to reduce biomass, and this investigation indicated that the biomass weight on stainless steel 316L and sol-gel-modified coupons in a benchtop plate heat exchanger was 19.21 mg/cm^2 and 0.37 mg/cm^2, respectively (Liu, Jindal, Amamcharla, Anand, & Metzger, 2017). Biosurfactants are surface-interactive molecules that exhibit both hydrophobic and hydrophilic properties, for instance, BS-SLSZ2, the biosurfactant derived from the marine bacterium *Staphylococcus lentus*, which has been shown to hinder bacterial attachment, impair bacteria-bacteria interactions, and prevent the formation of biofilms. At a dose of 20 μg, *V. harveyi* and *Pseudomonas aeruginosa* biofilm formation were inhibited by 80 % and 82 %, respectively (Hamza, Satpute, Banpurkar, Kumar, & Zinjarde, 2017).

4.2.2. Physical strategies

4.2.2.1. Bubbles. The bubble technique is being developed for anti-biofilm applications. Laser-induced vapour bubbles are used to enhance the distance between sessile cells. Millimetre-sized air bubbles in water significantly reduced the number of biofilm cells attached to stainless steel and polypropylene surfaces by 1.6 and 0.9 $\log_{10}$, respectively, and also removed the carbohydrate, protein and fat residues from stainless steel surfaces (Burfoot, Limburn, & Busby, 2017). Shiroodi, Schwarz, Nitin, and Ovissipour (2021) employed bubbles to treat *V. parahaemolyticus* biofilms on plastic and stainless-steel coupons, achieving reductions of 2.5 and 1.4 $\log_{10}$ CFU/cm^2 biofilm cells in 2 min, respectively, and cell elimination of >7 $\log_{10}$ CFU/cm^2 in 5 min.

4.2.2.2. Cold plasma. Cold plasma has received much attention for

biofilm controlling due to its non-thermal, rapid, green and waterless properties. The reactive species generated have been identified as the primary components for antibiofilm abilities, as they can destroy biofilm matrix, penetrate the structures and eventually lead the bacterial cells to death. High-voltage cold plasma (80 kV) treatment of 60 s reduced *L. monocytogenes*, *Salmonella enterica* and *Pseudomonas fluorescens* biofilm cells by 3.76, 4.14 and 2.6 $\log_{10}$ CFU/mL from initial cell concentrations of 5.4 ± 0.4 $\log_{10}$ CFU/mL, respectively (Patange et al., 2019). Dielectric barrier discharge plasma treatment (1.1 kV, 30 min) reduced *E. coli* in fresh oysters by 1.01 $\log_{10}$, while having no effect on the glycogen content or texture of oyster meat (Choi et al., 2022), demonstrating the potential for cold plasma application in seafood environments. However, the removal efficacy of *V. parahaemolyticus* biofilms is limited known and requires further investigations.

4.2.2.3. Low-frequency and high-intensity ultrasound treatment. The ultrasound with a low frequency and a high intensity has been proposed to be more effective at decontaminating biofilms, and the biofilm removal is based on mechanical oscillation, free radicals (H · and .OH) and hydrogen peroxide (H_2O_2) generated, as well as localized heating. 10 s treatment of 40 kHz flat ultrasonic transducer achieved to remove *E. coli* and *Staphylococcus aureus* dairy biofilms from stainless steel surfaces. The high-intensity ultrasound has been examined for its application on fish, involving salmon (*S. salar*), mackerel (*S. scombrus*), cod (*G. morhua*) and hake (*M. merluccius*) fillets. The microorganism on fish surfaces were significantly reduced, but no significant changes of lipid content, the moisture level remained stable except hake (Pedrós-Garrido et al., 2017). Additional research of low-frequency and high-intensity ultrasound treatment on *V. parahaemolyticus* biofilm cells should be conducted.

4.2.2.4. Ultraviolet-C (UV–C) treatment. UV-C spectrum (250-270 nm) is lethal to a wide range of microorganisms, including bacteria, yeasts and viruses. UV-C (5, 10 min) combined with 50-500 μg/mL peroxyacetic acid reduced *Salmonella* Enteritidis biofilm cells from stainless-steel and silicone rubber surfaces by 3.10-6.41 $\log_{10}$ CFU/mL, UV-C (5, 10 min) in combination with 0.5-2.0 % lactic acid reduced by 3.35-6.41 $\log_{10}$ CFU/mL (Byun et al., 2022). UV-C treatment of 5, 10 and 30 mW*s/cm^2 decreased *V. parahaemolyticus* biofilm communities by 1.37-2.53 and 0.75-1.94 $\log_{10}$ CFU/cm^2 on shrimp and crab surfaces, respectively; UV-C (60 mW*s/cm^2) along with sodium hypochlorite (300 ppm) reached decrease of biofilm cells by 3.78 and 3.32 $\log_{10}$ CFU/cm^2; UV-C (60 mW*s/cm^2) combined with slightly acidic electrolyzed water reduced *V. parahaemolyticus* biofilm cells by 4.41 and 4.06 $\log_{10}$ CFU/cm^2, respectively (Roy et al., 2021).

4.2.2.5. High hydrostatic pressure (HHP) treatment. HPP is another nonthermal approach that has been demonstrated to be effective at inactivating *V. parahaemolyticus* in the seafood industry. 400 MPa HHP (20 °C, 3 min) decreased *V. parahaemolyticus* in oysters to undetectable level from ~5 $\log_{10}$ CFU/g, and the characteristic taste of oyster meat can retain for up to 15 days if refrigerated at –20 °C (Liu et al., 2022). However, it is limited known about HPP efficacy on *V. parahaemolyticus* biofilm cells in seafood, despite reports of its use against other food pathogens. For example, *Enterobacter sakazakii* biofilm formation was significantly reduced by 45 % when incubated for 24 h with 400 MPa HHP (Liao, Tao, Li, Xu, & Wang, 2021).

4.2.2.6. Photodynamic inactivation (PDI). PDI involves the use of a photosensitizer (PDI) activated by visible light, leading to reactive oxygen species (ROS) production and consequently inactivation of microbial cells. Inactivation of microbes is caused by ROS which has potential to deconstruct EPS, proteins, lipids and nucleic acids in biofilm matrix (Tan et al., 2021). Chen et al. (2020) found that PDI treatment (5 min, 1.14 J/cm^2) with 1.0 μM curcumin as the photosensitizer (PS) decreased *V. parahaemolyticus* (~8 $\log_{10}$ CFU/mL) to non-detectable levels, it could downregulate virulence genes (*tdh* and *toxR*) and biofilm formation related genes (*oxyR*, *aphA*, *luxR* and *opaR*) thereby controlling *V. parahaemolyticus* biofilm contaminations, they also found that 20.0 μM curcumin PDI treatment (60 min, 13.68 J/cm^2) achieved to eradicate 48 h old *V. parahaemolyticus* biofilm on polystyrene surfaces.

4.2.3. Chemical strategies

4.2.3.1. Essential oils. Essential oils are plant-based extracts that contain a variety of antibacterial and antibiofilm components. Citrus peel essential oils inhibit *V. parahaemolyticus* biofilm formation by repressing flagella gene transcription, T3SS effector function and quorum sensing activities (Sun et al., 2019); at a concentration of 3.125 and 6.25 μg/mL, citral reduced 42 and 58 % autoinducer-2 (AI-2) quorum sensing activity, respectively; 6.25 and 12.5 μg/mL of citral decreased *V. parahaemolyticus* swimming and swarming by 20-47 % and 35-50 %, respectively; citral at a concentration of 12.5 g/mL was observed to disrupt the three-dimensional *V. parahaemolyticus* biofilm matrix with dispersed cells.

4.2.4. Biocontrol strategies

4.2.4.1. Small-molecule signal blocker. Interfering biofilm formation with small molecules is a novel strategy; these molecules are referred to as flagella inhibitors, quorum sensing inhibitors and c-di-GMP signalling blockers. For example, diguanylate cyclase (DGC) has been identified as a critical target for modulating the c-di-GMP process and biofilm formation phenotypes, Christen et al. (2019) demonstrated that 4-(2, 5-dimethylphenoxy)-N-(4-morpholin-4-ylphenyl) butanamide and six other small molecules in the low μM inhibited c-di-GMP signalling and biofilm formation via regulation of the DGC in a non-competitive manner. Similarly, 2,6-Di-*tert*-butyl-4-methylphenol (DTBMP) from *Chroococcus turgidus* was found to inhibit initial *V. parahaemolyticus* biofilm formation by interfering with hydrophobic activity, swarming motility and quorum sensing, 250 μg/mL of DTBMP reduced 74 % EPS production; DTBMP was also examined *in vivo* on pacific white shrimp, and demonstrated anti-adherence efficacy without causing fatal effects on the shrimp (Santhakumari et al., 2018).

4.2.4.2. Enzymes. Another alternative to biofilm contamination control in the food industry are non-toxic and disruptive enzymes. For example, endolysins are peptidoglycan hydrolases that can deconstruct biofilm matrix and hydrolyse bacterial cell wall peptidoglycan, the combination of endolysin Lysqdvp001 (60 U/g) and ε-PL (ε-poly-lysine, 0.20 mg/g) can significantly reduce *V. parahaemolyticus* in *Gadus macrocephalus*, *Penaeus orientalis* and oyster by 3.75, 4.16 and 2.50 $\log_{10}$ CFU/g, respectively. The sole usage of ε-PL reached elimination of *V. parahaemolyticus* biofilms by 28.67 %, 14.27 % and 12.67 %, respectively, from polystyrene, glass and stainless-steel surfaces, though Lysqdvp001 had no substantial effect; the cocktail of these two enzymes removed 55.13 %, 44.43 % and 68.00 % of the biofilms, indicating the synergistic effect of enzyme treatment may be due to the attack of different *V. parahaemolyticus* target sites (Ning, Lin, & Wang, 2021).

4.2.4.3. Bacteriophages. Bacteriophages can destroy biofilms by breaking down the biofilm matrix. For example, phage cocktails were prepared by mixing phage isolated from cattle faeces; the phage cocktails inhibited *E. coli* O177 biofilm formation at 25 °C within 24 h, and reduced pre-formed biofilms to undetectable levels within 5 h (Montso, Mlambo, & Ateba, 2021). Bacteriophage OMN was reported to kill 90 % and 99 % *V. parahaemolyticus* communities on oyster meat surfaces after 48 and 72 h of treatment, respectably, showing the viability of bacteriophage application in seafood contexts (Zhang et al., 2018). However, as much of the bacteriophage studies are limited to laboratory

conditions, additional work is required to apply in the industry.

5. Conclusions and perspectives

The persistence of the *V. parahaemolyticus* biofilm in the seafood plant may result in pathogen recurrence and complicate hygienic treatment. It is necessary to understand the mechanism by which *V. parahaemolyticus* biofilms form. Specific questions include the following: 1) Is the flagellum lost and/or degraded, or is flagella function structural in the biofilm following surface attachment? 2) Do various forms of motility collaborate, interact and trigger biofilm formation in *V. parahaemolyticus*? 3) What are the mechanisms underlying the formation of *V. parahaemolyticus* biofilm structures? 4) What are the polysaccharides and protein components of the matrix at various stages of biofilm development? 5) What is the mechanism behind biofilm dispersal? 6) What are the interactions of transcriptional regulators and biological pathways in biofilm formation and pathogenicity?

The most effective way to control *V. parahaemolyticus* biofilm contamination is to inhibit *V. parahaemolyticus* colonisation and biofilm formulation. In the seafood industry, biological-control, and safe and cost-effective strategies are preferred but require more investigation. Notably, while most novel biofilm decontamination strategies have been evaluated in the laboratory, it is necessary to consider their regulatory status and how they will be applied on an industrial scale.

Author contributions

Dan Wang: writing - original draft, review & editing; **Steve Flint, Jon Palmer**, **Dragana Gagic**, **Graham Fletcher** and **Stephen On**: supervision, writing - review & editing.

Funding

This study is funded by Massey University, the grant number is P963141222WangD.

Declaration of competing interest

The authors have no competing interests to declare.

Acknowledgement

Authors convey their appreciation to the support from School of Food and Advanced Technology (Massey University), School of Fundamental Sciences (Massey University), Plant & Food Research (New Zealand) and Faculty of Agriculture and Life Sciences (Lincoln University).

References

Ashrafudoulla, M., Mizan, M. F. R., Park, H., Byun, K. H., Lee, N., Park, S. H., et al. (2019). Genetic relationship, virulence factors, drug resistance profile and biofilm formation ability of *Vibrio parahaemolyticus* isolated from mussel. *Frontiers in Microbiology, 10*(513), 513. https://doi.org/10.3389/fmicb.2019.00513

Boles, B. R., & McCarter, L. L. (2002). *Vibrio parahaemolyticus scrABC*, a novel operon affecting swarming and capsular polysaccharide regulation. *Journal of Bacteriology, 184*(21), 5946–5954. https://doi.org/10.1128/JB.184.21.5946-5954.2002

Brauge, T., Faille, C., Leleu, G., Denis, C., Hanin, A., & Midelet, G. (2020). Treatment with disinfectants may induce an increase in viable but non culturable populations of *Listeria monocytogenes* in biofilms formed in smoked salmon processing environments. *Food Microbiology, 92*, 103548. https://doi.org/10.1016/j.fm.2020.103548

Burfoot, D., Limburn, R., & Busby, R. (2017). Assessing the effects of incorporating bubbles into the water used for cleaning operations relevant to the food industry. *International Journal of Food Science and Technology, 52*(8), 1894–1903. https://doi.org/10.1111/ijfs.13465

Byun, K.-H., Na, K. W., Ashrafudoulla, M., Choi, M. W., Han, S. H., Kang, I., … Ha, S.-D. (2022). Combination treatment of peroxyacetic acid or lactic acid with UV-C to control *Salmonella* Enteritidis biofilms on food contact surface and chicken skin. *Food Microbiology, 102*, 103906. https://doi.org/10.1016/j.fm.2021.103906

Chen, B., Huang, J., Li, H., Zeng, Q.-H., Wang, J. J., Liu, H., … Zhao, Y. (2020). Eradication of planktonic *Vibrio parahaemolyticus* and its sessile biofilm by curcumin-mediated photodynamic inactivation. *Food Control, 113*, 107181. https://doi.org/10.1016/j.foodcont.2020.107181

Choi, M.-S., Jeon, E. B., Kim, J. Y., Choi, E. H., Lim, J. S., Choi, J., & Park, S. Y. (2022). Application of dielectric barrier discharge plasma for the reduction of non-pathogenic *Escherichia coli* and *E. coli* O157: H7 and the quality stability of fresh oysters (*Crassostrea gigas*). *LWT, 154*, 112698. https://doi.org/10.1016/j.lwt.2021.112698

Christen, M., Kamischke, C., Kulasekara, H. D., Olivas, K. C., Kulasekara, B. R., Christen, B., … Miller, S. I. (2019). Identification of small-molecule modulators of diguanylate cyclase by FRET-based high-throughput screening. *ChemBioChem, 20*(3), 394–407. https://doi.org/10.1002/cbic.201800593

Di Pippo, F., Di Gregorio, L., Congestri, R., Tandoi, V., & Rossetti, S. (2018). Biofilm growth and control in cooling water industrial systems. *FEMS Microbiology Ecology, 94*(5). https://doi.org/10.1093/femsec/fiy044

Enos-Berlage, J. L., Guvener, Z. T., Keenan, C. E., & McCarter, L. L. (2005). Genetic determinants of biofilm development of opaque and translucent *Vibrio parahaemolyticus*. *Molecular Microbiology, 55*(4), 1160–1182. https://doi.org/10.1111/j.1365-2958.2004.04453.x

Enos-Berlage, J. L., & McCarter, L. L. (2000). Relation of capsular polysaccharide production and colonial cell organization to colony morphology in *Vibrio parahaemolyticus*. *Journal of Bacteriology, 182*(19), 5513–5520. https://doi.org/10.1128/JB.182.19.5513-5520.2000

FAO. (2021). Advances in science and risk assessment tools for *Vibrio parahaemolyticus* and *V. vulnificus* associated with seafood: Meeting report. Retrieved from https://www.who.int/publications/i/item/9789240024878. (Accessed August 2021).

Freitas, C., Glatter, T., & Ringgaard, S. (2020). The release of a distinct cell type from swarm colonies facilitates dissemination of *Vibrio parahaemolyticus* in the environment. *The ISME Journal, 14*(1), 230–244. https://doi.org/10.1038/s41396-019-0521-x

Guo, L., Wang, J., Gou, Y., Tan, L., Liu, H., Pan, Y., et al. (2020). Comparative proteomics reveals stress responses of *Vibrio parahaemolyticus* biofilm on different surfaces: Internal adaptation and external adjustment. *The Science of the Total Environment, 731*, 138386. https://doi.org/10.1016/j.scitotenv.2020.138386

Guvener, Z. T., & McCarter, L. L. (2003). Multiple regulators control capsular polysaccharide production in *Vibrio parahaemolyticus*. *Journal of Bacteriology, 185*(18), 5431–5441. https://doi.org/10.1128/JB.185.18.5431-5441.2003

Hamza, F., Satpute, S., Banpurkar, A., Kumar, A. R., & Zinjarde, S. (2017). Biosurfactant from a marine bacterium disrupts biofilms of pathogenic bacteria in a tropical aquaculture system. *FEMS Microbiology Ecology, 93*(11). https://doi.org/10.1093/femsec/fix140

Han, N., Mizan, M. F. R., Jahid, I. K., & Ha, S.-D. (2016). Biofilm formation by *Vibrio parahaemolyticus* on food and food contact surfaces increases with rise in temperature. *Food Control, 70*, 161–166. https://doi.org/10.1016/j.foodcont.2016.05.054

Han, Q., Song, X., Zhang, Z., Fu, J., Wang, X., Malakar, P. K., … Zhao, Y. (2017). Removal of foodborne pathogen biofilms by acidic electrolyzed water. *Frontiers in Microbiology, 8*, 988. https://doi.org/10.3389/fmicb.2017.00988

Houry, A., Gohar, M., Deschamps, J., Tischenko, E., Aymerich, S., Gruss, A., et al. (2012). Bacterial swimmers that infiltrate and take over the biofilm matrix. In *, Vol. 109. Proceedings of the National Academy of Sciences of the United States of America* (pp. 13088–13093). https://doi.org/10.1073/pnas.1200791109, 32.

Kimbrough, J. H., Cribbs, J. T., & McCarter, L. L. (2020). Homologous c-di-GMP-binding Scr transcription factors orchestrate biofilm development in *Vibrio parahaemolyticus*. *Journal of Bacteriology, 202*(6). https://doi.org/10.1128/JB.00723-19

Kim, Y. K., & McCarter, L. L. (2000). Analysis of the polar flagellar gene system of *Vibrio parahaemolyticus*. *Journal of Bacteriology, 182*(13), 3693–3704.

Liao, Q., Tao, H., Li, Y., Xu, Y., & Wang, H. L. (2021). Evaluation of structural changes and molecular mechanism induced by high hydrostatic pressure in *Enterobacter sakazakii*. [Original Research]. *Frontiers in Nutrition, 8*(669), 739863. https://doi.org/10.3389/fnut.2021.739863

Li, Y., Tan, L., Guo, L., Zhang, P., Malakar, P. K., Ahmed, F., … Zhao, Y. (2020). Acidic electrolyzed water more effectively breaks down mature *Vibrio parahaemolyticus* biofilm than DNAse I. *Food Control, 117*, 107312. https://doi.org/10.1016/j.foodcont.2020.107312

Liu, C., Gu, Z., Lin, X., Wang, Y., Wang, A., Sun, Y., et al. (2022). Effects of high hydrostatic pressure (HHP and storage temperature on bacterial counts, color change, fatty acids and non-volatile taste active compounds of oysters (*Crassostrea ariakensis*). *Food Chemistry, 372*, 131247. https://doi.org/10.1016/j.foodchem.2021.131247

Liu, D. Z., Jindal, S., Amamcharla, J., Anand, S., & Metzger, L. (2017). Short communication: Evaluation of a sol-gel-based stainless steel surface modification to reduce fouling and biofilm formation during pasteurization of milk. *Journal of Dairy Science, 100*(4), 2577–2581. https://doi.org/10.3168/jds.2016-12141

Liu, M., Zhu, X., Zhang, C., & Zhao, Z. (2021). LuxQ-LuxU-LuxO pathway regulates biofilm formation by *Vibrio parahaemolyticus*. *Microbiological Research, 250*, 126791. https://doi.org/10.1016/j.micres.2021.126791

Makino, K., Oshima, K., Kurokawa, K., Yokoyama, K., Uda, T., Tagomori, K., … Iida, T. (2003). Genome sequence of *Vibrio parahaemolyticus*: A pathogenic mechanism distinct from that of *V. cholerae*. *The Lancet, 361*(9359), 743–749. https://doi.org/10.1016/s0140-6736(03)12659-1

Mizan, M. F. R., Ashrafudoulla, M., Sadekuzzaman, M., Kang, I., & Ha, S.-D. (2018). Effects of NaCl, glucose, and their combinations on biofilm formation on black tiger shrimp (*Penaeus monodon*) surfaces by *Vibrio parahaemolyticus*. *Food Control, 89*, 203–209. https://doi.org/10.1016/j.foodcont.2017.12.004

Mizan, M. F., Jahid, I. K., Kim, M., Lee, K. H., Kim, T. J., & Ha, S. D. (2016). Variability in biofilm formation correlates with hydrophobicity and quorum sensing among *Vibrio parahaemolyticus* isolates from food contact surfaces and the distribution of the genes involved in biofilm formation. *Biofouling, 32*(4), 497–509. https://doi.org/10.1080/08927014.2016.1149571

Montso, P. K., Mlambo, V., & Ateba, C. N. (2021). Efficacy of novel phages for control of multi-drug resistant *Escherichia coli* O177 on artificially contaminated beef and their potential to disrupt biofilm formation. *Food Microbiology, 94*, 103647. https://doi.org/10.1016/j.fm.2020.103647

Mougin, J., Copin, S., Bojolly, D., Raguenet, V., Robert-Pillot, A., Quilici, M.-L., … Bonnin-Jusserand, M. (2019). Adhesion to stainless steel surfaces and detection of viable but non cultivable cells of *Vibrio parahaemolyticus* and *Vibrio cholerae* isolated from shrimps in seafood processing environments: Stayin' alive? *Food Control, 102*, 122–130. https://doi.org/10.1016/j.foodcont.2019.03.024

Ning, H. Q., Lin, H., & Wang, J. X. (2021). Synergistic effects of endolysin lysqdvp001 and epsilon-poly-lysine in controlling *Vibrio parahaemolyticus* and its biofilms. *International Journal of Food Microbiology, 343*, 109112. https://doi.org/10.1016/j.ijfoodmicro.2021.109112

Odeyemi, O. A. (2016). Incidence and prevalence of *Vibrio parahaemolyticus* in seafood: A systematic review and meta-analysis. *SpringerPlus, 5*(1), 464. https://doi.org/10.1186/s40064-016-2115-7

Patange, A., Boehm, D., Ziuzina, D., Cullen, P. J., Gilmore, B., & Bourke, P. (2019). High voltage atmospheric cold air plasma control of bacterial biofilms on fresh produce. *International Journal of Food Microbiology, 293*, 137–145. https://doi.org/10.1016/j.ijfoodmicro.2019.01.005

Pedrós-Garrido, S., Condón-Abanto, S., Beltrán, J. A., Lyng, J. G., Brunton, N. P., Bolton, D., et al. (2017). Assessment of high intensity ultrasound for surface decontamination of salmon (*S. salar*), mackerel (*S. scombrus*), cod (*G. morhua*) and hake (*M. merluccius*) fillets, and its impact on fish quality. *Innovative Food Science & Emerging Technologies, 41*, 64–70. https://doi.org/10.1016/j.ifset.2017.02.006

Rosa, J. V., Conceição, N. V., Conceição, R. C. S., & Timm, C. (2018). Biofilm formation by *Vibrio parahaemolyticus* on different surfaces and its resistance to sodium hypochlorite. *Ciência Rural, 48*.

Rossi, E., Paroni, M., & Landini, P. (2018). Biofilm and motility in response to environmental and host-related signals in Gram negative opportunistic pathogens. *Journal of Applied Microbiology, 125*(6), 1587–1602. https://doi.org/10.1111/jam.14089

Roy, P. K., Mizan, M. F. R., Hossain, M. I., Han, N., Nahar, S., Ashrafudoulla, M., … Ha, S.-D. (2021). Elimination of *Vibrio parahaemolyticus* biofilms on crab and shrimp surfaces using ultraviolet C irradiation coupled with sodium hypochlorite and slightly acidic electrolyzed water. *Food Control, 128*, 108179. https://doi.org/10.1016/j.foodcont.2021.108179

Santhakumari, S., Jayakumar, R., Logalakshmi, R., Prabhu, N. M., Abdul Nazar, A. K., Karutha Pandian, S., et al. (2018). *In vitro* and *in vivo* effect of 2,6-Di-tert-butyl-4-methylphenol as an antibiofilm agent against quorum sensing mediated biofilm formation of Vibrio spp. *International Journal of Food Microbiology, 281*, 60–71. https://doi.org/10.1016/j.ijfoodmicro.2018.05.024

Shikongo-Nambabi, M. N. N. N., Kachigunda, B., & Venter, S. N. (2010). Evaluation of oxidising disinfectants to control *Vibrio* biofilms in treated seawater used for fish processing. *SA Journal of Radiology, 36*, 215–220.

Shiroodi, S., Schwarz, M. H., Nitin, N., & Ovissipour, R. (2021). Efficacy of nanobubbles alone or in combination with neutral electrolyzed water in removing *Escherichia coli* O157:H7, *Vibrio parahaemolyticus*, and *Listeria innocua* biofilms. *Food and Bioprocess Technology, 14*(2), 287–297. https://doi.org/10.1007/s11947-020-02572-0

Song, X. Y., Ma, Y. J., Fu, J. J., Zhao, A. J., Guo, Z. R., Malakar, P. K., … Zhao, Y. (2017). Effect of temperature on pathogenic and non-pathogenic *Vibrio parahaemolyticus* biofilm formation. *Food Control, 73*, 485–491.

Steenackers, H. P., Parijs, I., Dubey, A., Foster, K. R., & Vanderleyden, J. (2016). Experimental evolution in biofilm populations. *FEMS Microbiology Reviews, 40*(3), 373–397. https://doi.org/10.1093/femsre/fuw002

Sun, Y., Guo, D., Hua, Z., Sun, H., Zheng, Z., Xia, X., et al. (2019). Attenuation of multiple *Vibrio parahaemolyticus* virulence factors by citral. *Frontiers in Microbiology, 10*, 894. https://doi.org/10.3389/fmicb.2019.00894

Tan, L., Li, H., Chen, B., Huang, J., Li, Y., Zheng, H., … Wang, J. J. (2021). Dual-species biofilms formation of *Vibrio parahaemolyticus* and *Shewanella putrefaciens* and their tolerance to photodynamic inactivation. *Food Control, 125*, 107983. https://doi.org/10.1016/j.foodcont.2021.107983

Tan, L., Zhao, F., Han, Q., Zhao, A. J., Malakar, P. K., Liu, H. Q., … Zhao, Y. (2018). High correlation between structure development and chemical variation during biofilm formation by *Vibrio parahaemolyticus*. *Frontiers in Microbiology, 9*, 1881.

Wong, H. (2002). Attachment and inactivation of *Vibrio parahaemolyticus* on stainless steel and glass surface. *Food Microbiology, 19*(4), 341–350. https://doi.org/10.1006/fmic.2002.0478

Ye, L., Zheng, X., & Zheng, H. (2014). Effect of *sypQ* gene on poly-N-acetylglucosamine biosynthesis in *Vibrio parahaemolyticus* and its role in infection process. *Glycobiology, 24*(4), 351–358. https://doi.org/10.1093/glycob/cwu001

Yildiz, F. H., & Visick, K. L. (2009). *Vibrio* biofilms: So much the same yet so different. *Trends in Microbiology, 17*(3), 109–118. https://doi.org/10.1016/j.tim.2008.12.004

Zhang, Y., Hu, L., Qiu, Y., Osei-Adjei, G., Tang, H., Zhang, Y., … Zhou, D. (2019). QsvR integrates into quorum sensing circuit to control *Vibrio parahaemolyticus* virulence. *Environmental Microbiology, 21*(3), 1054–1067. https://doi.org/10.1111/1462-2920.14524

Zhang, H., Yang, Z., Zhou, Y., Bao, H., Wang, R., Li, T., … Zhou, X. (2018). Application of a phage in decontaminating *Vibrio parahaemolyticus* in oysters. *International Journal of Food Microbiology, 275*, 24–31. https://doi.org/10.1016/j.ijfoodmicro.2018.03.027

Zhou, D., Yan, X., Qu, F., Wang, L., Zhang, Y., Hou, J., … Mao, P. (2013). Quorum sensing modulates transcription of *cpsQ-mfpABC* and *mfpABC* in *Vibrio parahaemolyticus*. *International Journal of Food Microbiology, 166*(3), 458–463. https://doi.org/10.1016/j.ijfoodmicro.2013.07.008

Appendix VII. Research output - Chapter 3 & Chapter 4

International Journal of Food Microbiology 385 (2023) 110011

Contents lists available at ScienceDirect

International Journal of Food Microbiology

journal homepage: www.elsevier.com/locate/ijfoodmicro

Biofilm formation, sodium hypochlorite susceptibility and genetic diversity of *Vibrio parahaemolyticus*

Dan Wang [a], Graham C. Fletcher [b], Stephen L.W. On [c], Jon S. Palmer [a], Dragana Gagic [d], Steve H. Flint [a,*]

[a] School of Food and Advanced Technology, Massey University, Private Bag 11222, Palmerston North, New Zealand
[b] The New Zealand Institute for Plant & Food Research Limited, Private Bag 92169, Auckland 1142, New Zealand
[c] Faculty of Agriculture and Life Sciences, Lincoln University, Private Bag 85084, Canterbury, New Zealand
[d] School of Fundamental Sciences, Massey University, Private Bag 11222, Palmerston North, New Zealand

ARTICLE INFO

Keywords:
Biofilm
Sodium hypochlorite
Whole genome sequencing (WGS)
Genomic feature
Multilocus sequence typing (MLST)

ABSTRACT

Vibrio parahaemolyticus is a marine oriented pathogen; and biofilm formation enables its survival and persistence on seafood processing plant, complicating the hygienic practice. The objectives of this study are to assess the ability of *V. parahaemolyticus* isolated from seafood related environments to form biofilms, to determine the effective sodium hypochlorite concentrations required to inactivate planktonic and biofilm cells, and to evaluate the genetic diversity required for strong biofilm formation. Among nine isolates, PFR30J09 and PFR34B02 isolates were identified as strong biofilm forming strains, with biofilm cell counts of 7.20, 7.08 $\log_{10}$ CFU/cm^2, respectively, on stainless steel coupons after incubation at 25 °C. Free available chlorine of 1176 mg/L and 4704 mg/L was required to eliminate biofilm cells of 1.74–2.28 $\log_{10}$ CFU/cm^2 and > 7 $\log_{10}$ CFU/cm^2, respectively, whereas 63 mg/L for planktonic cells, indicating the ineffectiveness of sodium hypochlorite in eliminating *V. parahaemolyticus* biofilm cells at recommended concentration in the food industry. These strong biofilm-forming isolates produced more polysaccharides and were less susceptible to sodium hypochlorite, implying a possible correlation between polysaccharide production and sodium hypochlorite susceptibility. Genetic diversity in *mshA*, *mshC* and *mshD* contributed to the observed variation in biofilm formation between isolates. This study identified strong biofilm-forming *V. parahaemolyticus* strains of new multilocus sequence typing (MLST) types, showed a relationship between polysaccharide production and sodium hypochlorite resistance.

1. Introduction

V. parahaemolyticus is a Gram-negative bacterium that naturally exists in aquatic environments and seafood, such as oyster, clam, mussel, octopus, shrimp, crab and fish. The infections are associated with consumption of raw or undercooked seafood. It grows substantially when temperatures exceed 14–19 °C and is prevalent during the summer and autumn seasons (Baker-Austin et al., 2010; Cruz et al., 2015). In the United States, the average annual number of *Vibrio* infections increased by 54 % between 2006 and 2017, and by 79 % in 2019 (Abanto et al., 2020). The Cholera and Other *Vibrio* Illness Surveillance System in the United States received 4116 reports of *V. parahaemolyticus* infections between 2010 and 2018 (CDC, 2021). In China, they experience an average of 523.5 cases each year during 2010 and 2020 (FAO, 2021). Climate change has been proposed as an explanation for the global spread of *V. parahaemolyticus* infections. Outbreaks have been regularly reported in countries with no or sporadic incidence in Canada, the United Kingdom, France, North Europe, New Zealand and Australia (Baker-Austin et al., 2020; Baker-Austin et al., 2018), raising concerns in the food industry.

There have been 5149 *V. parahaemolyticus* isolates submitted to the Molecular Typing and Microbial Genome Diversity (PubMLST) Database by February 2022 (Jolley et al., 2018). Some pandemic clones are more virulent than others and have been implicated in several previous outbreaks. Sequencing type 3 (ST3) emerged in Asia in the mid-1990s and spread throughout the world, becoming the most common pandemic clone by 2012 (Nair et al., 2007). Sequencing type 36 (ST 36) strains were restricted to the Pacific Northwest and Canada (Daniels et al., 2000), but have spread further into Europe, involving the largest known food-borne *Vibrio* outbreak reported in Spain in 2012 (Martinez-Urtaza

* Corresponding author.
E-mail address: s.h.flint@massey.ac.nz (S.H. Flint).

https://doi.org/10.1016/j.ijfoodmicro.2022.110011
Received 28 August 2022; Received in revised form 19 October 2022; Accepted 3 November 2022
Available online 8 November 2022

et al., 2018). ST 36, according to Abanto et al. (2020), can disperse intercontinentally due to its highly pathogenic and persistent nature, posing a threat to the safety of seafood products and human health. The epidemiology of *V. parahaemolyticus* infections has shifted from the dominance of domestically redistricted strains to the transcontinental spread of new clones. However, the relationship between ST and biofilm-forming ability of *V. parahaemolyticus* is unknown.

Biofilm formation is a dynamic life cycle involving motility, attachment, biofilm production and dispersal; once biofilm develops, the endurance and environmental adaptability enable cells to survive environmental stress. *V. parahaemolyticus* as a biofilm have advantages in seafood environments. *V. parahaemolyticus* biofilm is assisted by a dual flagellar system - polar and lateral flagella (Kim and McCarter, 2000), which is not the case with *Escherichia coli*, *Salmonella* spp. and *Listeria monocytogenes* pathogens. *V. parahaemolyticus* can produce an active chitinase, enabling it to adsorb onto chitin- and copepod- surfaces (e.g. oysters, clams, fish, shrimp, and mussels, etc.) (Kaneko and Colwell, 1975). This helps *V. parahaemolyticus* initiate colonization of seafood due to the capability to degrade and utilize chitinous materials of seafood surfaces. *V. parahaemolyticus* biofilms form on stainless steel, polystyrene, glass, and other abiotic surfaces in food processing equipment and packaging materials, showing a higher resistance than their planktonic counterparts, to cleaning and sanitation that may lead to recurring contamination.

Chlorine-based disinfectants, such as sodium hypochlorite, are oxidizing agents widely used for cleaning and disinfection in the food industry due to low cost, easy-use and broad-spectrum bactericidal activities. Although the concentrations of disinfectants required to eliminate biofilm cells have been determined in many species such as L. *monocytogenes* (Cruz and Fletcher, 2012) and *Pseudomonas fluorescens* (Cai et al., 2019), information gaps remain in the response of *V. parahaemolyticus* biofilm cells to sodium hypochlorite that may be used in the seafood processing environment (Wang et al., 2022). Sodium hypochlorite at recommended concentrations is inadequate to inactivate *V. parahaemolyticus* so optimisation of treatment with sodium hypochlorite is required. Shikongo-Nambabi et al. (2010) found that when exposing mature *V. parahaemolyticus* biofilms for 1 h with sodium hypochlorite (4 mg/L free available chlorine pH not specified), the bacterial density decreased from 7.90 to 3.97 $\log_{10}$ CFU/cm^2. Another study examined the efficacy of sodium hypochlorite in reducing the bacterial population of *V. parahaemolyticus* in mature biofilms formed on stainless steel, glass, and polystyrene, and discovered that a 10-min treatment with sodium hypochlorite (20 mg/L available chlorine, pH not specified) could reduce cell populations by as much as 3.0 $\log_{10}$ CFU/cm^2 from 5.5 $\log_{10}$ CFU/cm^2 (Rosa et al., 2018). However, information gaps remain in these studies, in particular with reference to the pH and temperatures used. Firstly, sodium hypochlorite dissolved in water will raise the pH and reduce antimicrobial efficacy. In the food industry, it has been recommended to adjust pH of sodium hypochlorite solution to 6.5–7.0 before the use on food contact surfaces. However, pH of sodium hypochlorite solution was overlooked when killing biofilm cells in the above studies. Additionally, sodium hypochlorite efficacy for removing biofilm cells will depend on amount and nature of biofilm formation of *V. parahaemolyticus*.

Despite widespread awareness of *V. parahaemolyticus* control in seafood, there is a lack of understanding around *V. parahaemolyticus* biofilm development and its resistance to sodium hypochlorite, particularly regarding the relationship between the phenotype and genotype. Thus, the objectives of this study are to: (1) assess the ability of *V. parahaemolyticus* isolates from different clones to form biofilms; (2) determine the susceptibility of *V. parahaemolyticus* biofilm cells to sodium hypochlorite; and (3) decipher the genotype profiles of strong biofilm formers using whole genome sequencing (WGS).

2. Material and methods

2.1. Bacterial isolates and culture conditions

Nine *V. parahaemolyticus* strains were used in this study, seven of them were isolated from New Zealand shellfish (isolation using alkaline peptone water of pH 8.6–9.0) and were kindly provided by The New Zealand Institute for Plant and Food Research Ltd. Another two strains are clinical isolates, PFR37D08 (National Health Index (NHI) No. 75/0294) and PFR37E03 (NHI No. CHE2822), provided by the Institute of Environmental Science and Research (ESR), New Zealand.

Strains were stored at −80 °C using the low temperature bead storage system (Protect; Thermo Fisher Scientific, USA). To recover, a bead was picked using a needle aseptically, transformed into tryptic soy broth (TSB) broth with 3 % NaCl and incubated at 37 °C with shaking at 120 rpm till cells enter stationary-phase (5–8 h). Cultures were centrifuged (10,000 rpm, 5 min) and washed for three times using sterile PBS buffer, the harvested cells were ready for use.

2.2. Motility assay

Swimming and swarming motility of *V. parahaemolyticus* were measured as described previously by Sybiya Vasantha Packiavathy et al. (2012) with minor modifications. Briefly, swimming motility was characterized on agar plates containing 0.3 % agar, 1 % tryptone and 1 % NaCl; and swarming motility was on agar plates containing 0.5 % agar, 0.8 % tryptone, 1 % NaCl and 0.5 % glucose. Cell suspension (5 μL) of *V. parahaemolyticus* ($OD_{595} = 0.4 \pm 0.05$) was stabbed into the centre of media plates, and the motility was evaluated by determining the migration of *V. parahaemolyticus* from the centre to the periphery of the plate after incubation at 37 °C for 18 h.

2.3. Crystal violet assay

A cell suspension was diluted to obtain an OD_{595} (Absorbance measurements at 595 nm) of 0.15 ± 0.05 using a microplate reader (Varioskan Lux 3020–1333, Thermo Fisher, USA), and each 200 μL of cell culture was added into the well of a 96-well flat-bottom microtiter plate. The plate was incubated at 37 °C for 72 h, then the OD_{595} was examined. The plate was inverted to remove the cultures, and each well was washed three times using 230 μL of distilled water, followed by 230 μL of ethanol to fix the cells for 10 min. The ethanol was removed, and the plate was allowed to dry. Then, each well was stained with 230 μL of 2 % crystal violet (CV) for 10 min, washed three times using distilled water, followed by 210 μL of 33 % acetic acid added into each well to dissolve the CV stain. The absorbance of resulting solution in each well was measured at 570 nm, and the biofilm forming index (BFI) of each strain was evaluated using the following equation:

$$BFI = \frac{(OD_{570} - OD_{570con})}{(OD_{595} - OD_{595con})}$$

OD_{570} and OD_{595} represent the absorbance value of sample wells at 570 nm and 595 nm, respectively. OD_{570con} and OD_{595con} represent the absorbance value of wells with only TSB with 3 % NaCl as a blank. The degree of biofilm formation was classified according to Naves et al. (2008): strong (BFI ≥ 1.10), moderate (1.09 ≥ BFI ≥ 0.70), weak (0.69 ≥ BFI ≥ 0.35) and none (BFI < 0.35).

2.4. Biofilm development on stainless steel surface and cells enumeration

Prepared cell culture (1 mL, ~ 4 $\log_{10}$ CFU/mL) was pipetted into each well of 48-well flat-bottom polystyrene plates, along with one precleaned and sanitised stainless-steel coupon (304 stainless steel, 1 × 1 cm). The number of culturable cells in the biofilm matrix was determined using a bead vortex mixing method reported previously with minor modifications (Hayrapetyan et al., 2015). In short, each coupon

was rinsed three times using sterile distilled water to remove the planktonic cells and transferred into a 25 mL glass bottle filled with 10 mL of 0.1 % peptone buffered water and 5 g of glass beads (5–8 mm), followed by 1 min vortex mixing to disrupt the biofilm matrix from the stainless steel surface and obtain individual cells. 10-fold serial dilutions of biofilm cell solution were prepared and colony forming unit (CFU) enumeration was examined on 3 % NaCl tryptic soy agar (TSA) plates.

2.5. Susceptibility to sodium hypochlorite

Sodium hypochlorite solution was prepared aseptically and used within 20 min. In brief, commercial concentrated sodium hypochlorite (XY-12, ECOLAB, New Zealand) containing around 140 g/L available chlorine (147 g/L sodium hypochlorite) was diluted in distilled water and the pH was adjusted to a range of 6.7 to 6.9 using 1 M HCl. The amount of free chlorine in the sodium hypochlorite solution was determined using titration (Zheng and Brook, 2021).

To determine the sodium hypochlorite susceptibility of planktonic *V. parahaemolyticus* cells, each well of 96-well polystyrene plates were loaded with 180 μL cell suspension (~ 8 $\log_{10}$ CFU/mL) and 20 μL sodium hypochlorite solution. The reaction was neutralised with 50 μL of 1 % sodium thiosulfate after 5 min cells exposure to sodium hypochlorite. Each set of experiments included a positive control (180 μL of inoculum and 20 μL distilled water) as well as a negative control (180 μL of saline and 20 μL of sodium hypochlorite). 10-fold serial dilutions of cells were prepared and colony forming unit (CFU) enumeration was examined on 3 % NaCl TSA plates. To determine the sodium hypochlorite susceptibility of *V. parahaemolyticus* biofilm cells, coupons containing pre-formed biofilm were placed into 48-well flat-bottom polystyrene plates. 1 mL of sodium hypochlorite solution was pipetted into each well, containing a coupon for 5 min, and then the coupon was transferred to another well containing 1 % sodium thiosulfate to neutralise the sodium hypochlorite. Cells on stainless steel coupons were detached and counted as described earlier.

2.6. Fluorescence microscopy

To visualise the biofilm, coupons with cultured biofilms were rinsed with sterile distilled water three times and allowed to half dry on a glass microscope slide. To stain, 1 drop of calcofluor white stain was placed on each coupon and left for 1 min before washing with sterile distilled water and allowing to partially dry. The stained samples were examined using an epifluorescent microscope (BX53; Olympus Corp., Japan) equipped with a DAPI filter (excitation at 340–360 nm, emission at 410 nm), the images were captured by the cellSense Dimension programme.

2.7. Detection of biofilm forming related genes

The Centre for Environment, Fisheries, and Aquaculture Science (CEFAS) did the DNA extraction, library construction and whole genome sequencing of *V. parahaemolyticus* using MiSeq with a coverage of 40-120× (Baker-Austin et al., 2020). Clean reads were used for de novo assembly and annotation via the Bactopia pipeline using Velvet and SPADES as the assembler (Petit and Read, 2020). The quality of assembled contigs was assessed using QUAST and CheckM (Gurevich et al., 2013; Parks et al., 2015). Genes related with colonization, toxin production, EPS biosynthesis and Type II secretion system were selected to detect the genetic diversity in *V. parahaemolyticus* (Table 2). The amino acid sequences of *V. parahaemolyticus* RIMD 2210633 were retrieved from the National Centre for Biotechnology Information (NCBI) Database and selected as the reference genome, followed by copying into a local database for BLASTP searching via diamond (Buchfink et al., 2021). Each sequenced *V. parahaemolyticus* genome was searched to identify the presence of genes (with >70 % identity and > 70 % sequence coverage) (Fang et al., 2022). The draft genomes were submitted to GenBank under the BioProject PRJNA808748 https://dataview.ncbi.nlm.nih.gov/object/PRJNA808748?reviewer=26p271csjvbj6lm07mvgldooc.

2.8. Statistical analysis

All experiments were performed with two or three biological replicates and three technical replicates. One-way variance analysis (ANOVA) was generated to evaluate the significant differences among experimental results with a p value below 0.05 considered as statistically significant.

3. Results

3.1. Ability of V. parahaemolyticus to swim and swarm

The diameter of the migration on the agar plate reflected the ability of *V. parahaemolyticus* to swim and swarm (Table 3). Each of the nine strains demonstrated swimming ability, with the top three measuring 71.00 ± 15.56 mm (strain PFR30G02), 69.33 ± 17.48 mm (strain PFR21C03) and 58.58 ± 30.50 mm (strain PFR30J09). With a diameter of 10.33 ± 0.76 mm, strain PFR34B02 exhibited the least capacity to swim. In the swarming motility assay, strain PFR29A04 had the lowest value of 22.83 ± 5.97 mm and strain PFR30J09 had the highest value of 60.33 ± 8.25 mm.

3.2. Ability of V. parahaemolyticus to form biofilm

The CV assay and the BFI value revealed that PFR30J09 and PFR34B02 formed the best biofilms, with BFI values of 1.214 and 1.060, respectively (Fig. 1). Biofilm formation varies and a comparison between the good and poor biofilm formers may reveal the important factors in biofilm formation. For other strains, the crystal violet staining and BFI values were high in PFR29A04 and PFR37D08, and low for PFR21C03, PFR24B07 and PFR37C06. Significant differences ($p < 0.05$) were observed between means of the good and poor biofilm isolates.

Biofilm formation by *V. parahaemolyticus* on stainless steel coupons is shown in Fig. 2. The detectable populations of *V. parahaemolyticus* in the biofilm matrix increased from ~4 $\log_{10}$ CFU/cm^2 to ~7 $\log_{10}$ CFU/cm^2 at 25 °C within 24 h. Strains PFR30J09 and PFR34B02 formed the best biofilms based on cell numbers with most reaching a maximum of 7.08–7.20 $\log_{10}$ CFU/cm^2. The PFR30J09 population increased from 3.83 $\log_{10}$ CFU/cm^2 at the first hour to 7.20 $\log_{10}$ CFU/cm^2 by the 6th hour. The cell numbers of PFR34B02 increased from 3.46 $\log_{10}$ CFU/cm^2 at the first hour to 7.08 $\log_{10}$ CFU/cm^2 6th hour. For PFR37D08 and PFR37E03, an apparent delay in the onset of biofilm formation was detected (growth curve peaked at 11th hour), indicating a long lag phase in biofilm growth. PFR37D08, PFR37E03 and PFR21C03 produced the lowest number of biofilm cells.

The polysaccharide content and the biofilm matrix were visualized using epifluorescence microscopy following calcofluor white staining. *V. parahaemolyticus* on stainless-steel coupons was stained after 6 h incubation at 25 °C. The most biomass was produced by PFR30J09 and PFR34B02 with dense and strong blue fluorescence (Fig. 3). Other strains had a flat and loose sessile cell distribution with fewer cell clusters. The microscopic result was consistent with other biofilm assays.

3.3. Susceptibility of planktonic and biofilm cultures to sodium hypochlorite

Planktonic cells were reduced by approximately 0.9 $\log_{10}$ CFU/mL with 16 mg/L chlorine and they were reduced by 1.49–2.79 $\log_{10}$ CFU/mL with 35 mg/L chlorine (Fig. 4). There was variation in the chlorine sensitivity of different strains with 35 mg/L chlorine, with PFR30J09 and PFR37E03 producing low reductions of 1.76 and 1.49 $\log_{10}$ CFU/mL, respectively, whereas PFR21C03, PFR37C06, and PFR37D08

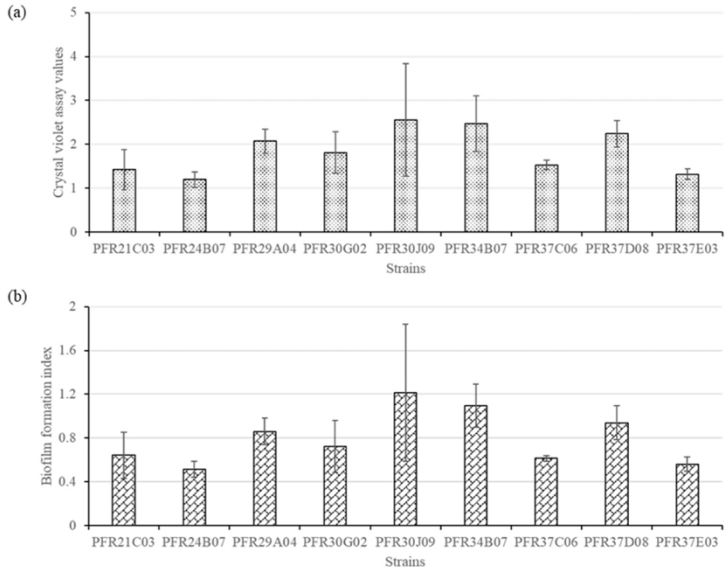

Fig. 1. Biofilm forming ability of *V. parahaemolyticus* strains. (a) presented the crystal violet values within 9 *V. parahaemolyticus* isolates. (b) shows their biofilm formation index (BFI) results (Mean ± SD).

reduced by 2.33, 1.81, and 2.24 $\log_{10}$ CFU/mL, respectively. Following exposure to 63 mg/L chlorine, all *V. parahaemolyticus* planktonic cells decreased to undetectable levels on agar plates, a reduction of >7 $\log_{10}$ CFU/mL.

Biofilms of *V. parahaemolyticus* required a chlorine concentration roughly 75 times greater than that needed for planktonic cells, to decrease the culturable cells to undetectable levels using the CFU counting method (Fig. 5). A concentration of 1176 mg/L chlorine was required to lower the *V. parahaemolyticus* culturable cell populations on stainless steel coupons by 1.74–2.28 $\log_{10}$ CFU/cm^2. The smallest declines were observed in the PFR30J09 and PFR34B02 biofilms, with cell populations decreasing by 1.78 and 1.91 $\log_{10}$ CFU/cm^2, respectively. When biofilms were treated with 4704 mg/L chlorine, the cell population of all strains except PFR30J09 and PFR34B02 was reduced to undetectable levels.

3.4. Analysis of genetic diversity

The clinical isolates PFR37D08 and PFR37E03 had the *tdh* gene that encodes thermostable direct hemolysin (TDH) toxins whereas other stains did not, while all nine isolates had the *tlh* gene encoding thermolabile hemolysin (TLH). Genes common among the isolates were those responsible for CPS polysaccharide biosynthesis, *syp*-like polysaccharide biosynthesis, chitin-regulated pili assembly, Type II secretion system and colonization factor GbpA There were differences among sequenced genomes located in genes of *mshA*, *mshC* and *mshD* that contribute to attachment and biofilm formation in *V. parahaemolyticus* (Fig. 6). Strain PFR21C03, PFR30G02, PFR37D08 and PFR37E03 lacked these three genes, among which, PFR21C03 and PFR37E03 were identified as weak biofilm forming strains. The strong biofilm-forming strain PFR30J09 and an intermediate one PFR37C06 possessed all these three genes, meanwhile, intermediate biofilm-forming strain PFR24B07 and strong biofilm former PFR34B02 had *mshC* and *mshD*. Strain PFR29A03 had the sole gene of *mshA*.

Combining information from Table 1, PFR37D08 of ST36 was identified as a weak biofilm former though it is the most prevalent environmental pathogen. Strain PFR30J09 and PFR37C06 shared the same nearest ST type of 2650, however, PFR30J09 was identified as the strong biofilm former whereas PFR37C06 was not. Strain PFR34B02 of potential ST 2648 was another strong biofilm forming strain.

4. Discussion

The persistence of the *V. parahaemolyticus* biofilm in seafood processing plants may result in pathogen recurrence and complicate hygienic treatment. In the present study, *V. parahaemolyticus* biofilms required 75 times higher disinfectant concentrations than planktonic cells, which raises concerns about developing and optimising biofilm control strategies. This study advances our understanding of the phenotypic and genetic interactions underlying *V. parahaemolyticus* biofilm development, meanwhile demonstrated promising ways to inhibit attachment of *V. parahaemolyticus* to surfaces via interfering with the Mannose-sensitive hemagglutinin (MSHA) type IV pilus. This study also identified two strains of novel MLST ST types that showed strong biofilm on stainless steel, but whether they will remain strong on other surfaces requires further investigation.

V. parahaemolyticus possesses dual flagella, polar flagella for swimming and lateral flagella for swarming. The extent to which bacteria swim and swarm contributes to the initial attachment and development of biofilm structures (Wadhwa and Berg, 2022). However, in our study, no strong links between swimming, swarming motility, and ability to form biofilms were seen in our study ($r = 0.063$ and 0.016, respectively; Table 3), implying swimming and swarming contribute to but did not play essential roles in biofilm formation. Other motility modes, other than swimming and swarming, for instance, twitching and gliding motility may be present in *V. parahaemolyticus* but were not examined in our study. This result is consistent with prior findings demonstrating that motility is not strongly associated with the ability to produce biofilms. Mizan et al. (2016) reported a weak negative correlation (−0.124) between swarming motility and biofilm formation in *V. parahaemolyticus*

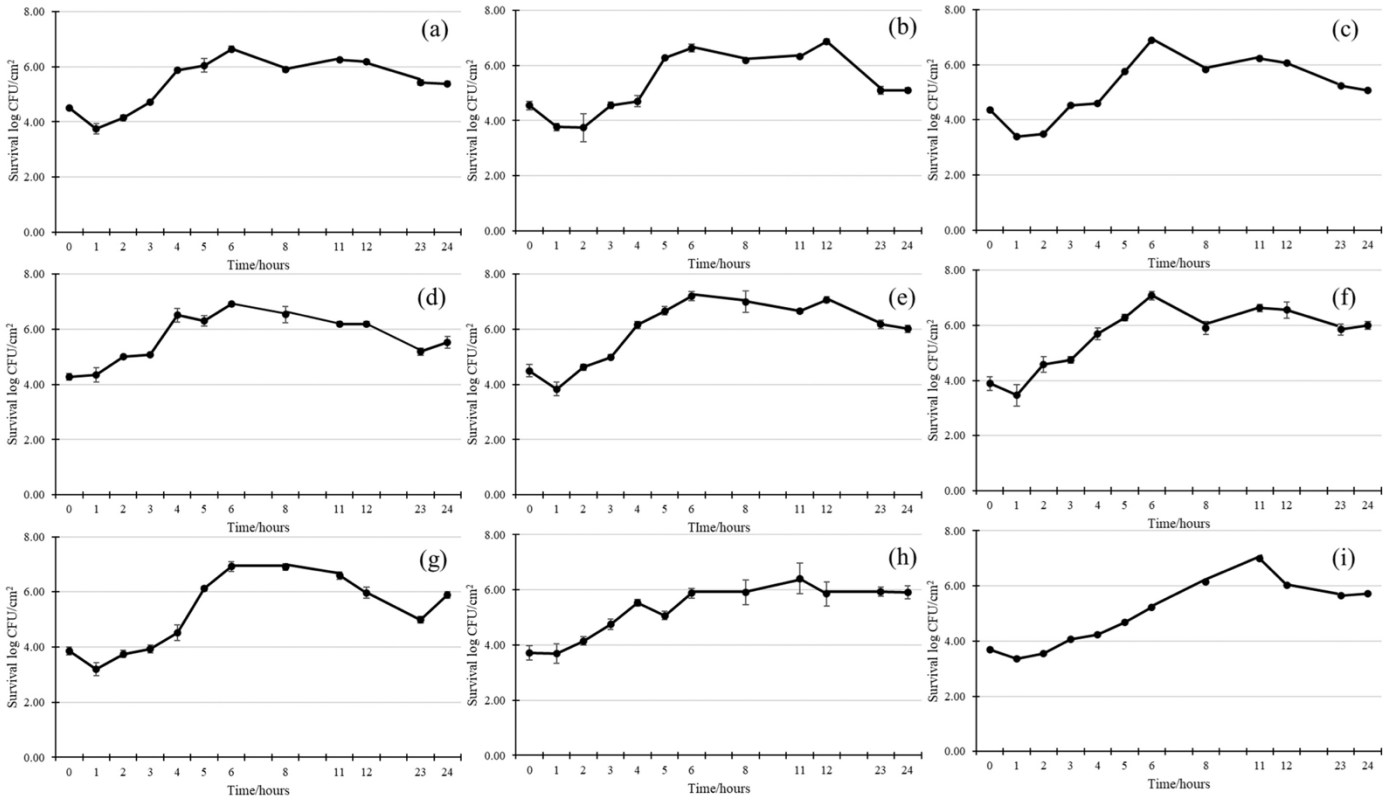

Fig. 2. *Vibrio parahaemolyticus* growth on stainless steel coupons within 24 h at 25 °C (Mean +/− SD). The indications for strains are as follows: (a) PFR21C03, (b) PFR24B07, (c) PFR29A04, (d) PFR30G02, (e) PFR30J09, (f) PFR34B02, (g) PFR37C06, (h) PFR37D08 and (i) PFR37E03.

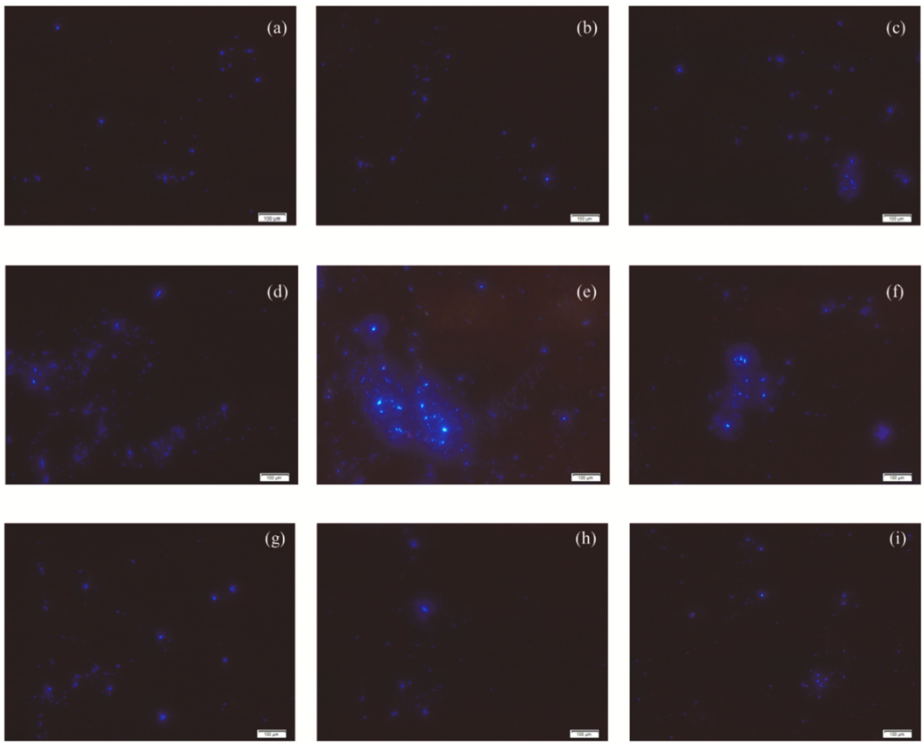

Fig. 3. Epifluorescence microscope screen of sessile *V. parahaemolyticus* (6-hour old, 25 °C) on stainless steel. Blue fluorescence was emitted from calcofluor white stain when binding with polysaccharides in biofilms. The indications for strains are as follows: (a) PFR21C03, (b) PFR24B07, (c) PFR29A04, (d) PFR30G02, (e) PFR30J09, (f) PFR34B02, (g) PFR37C06, (h) PFR37D08 and (i) PFR37E03.

isolates, as well as a moderate positive association between swimming motility and biofilm formation. No correlation was concluded between motility and biofilm production in L. *monocytogenes* as reported by Di Bonaventura et al. (2008), regardless of multiple temperatures tested. Sheikh et al. (2001) suggested that the absence of motility in *Escherichia coli* did not impair the ability to produce biofilms.

The BFI is normally determined to demonstrate biofilm-forming ability using the microtiter plate assay (Lucero-Mejia et al., 2020). In this study, BFI results suggested that PFR30J09 and PFR34B02 produce strong biofilm, whereas PFR21C03, PFR37C06 and PFR37E03 produce weak biofilm. PFR37D08 produced weak cell growth on stainless steel but showed a relatively high crystal violet value on polystyrene. This may be a result of the surface used with polystyrene favouring PFR37D08 rather than stainless steel. As the crystal violet stain will stain dead and live cells the standard test on polystyrene may simply reflect the difference between live sells (on stainless steel) compared with dead and live cells (on polystyrene) (Chiba et al., 1998). Ideally a crystal violet test should also be done on the stainless steel surfaces to determine if the observation is due to the nature of the substrate or the difference in test methods.

Stainless steel is one of the most frequently used surfaces in the food industry. In this study, CFU enumeration was used to detect viable and countable *V. parahaemolyticus* cells living in biofilms on stainless steel coupons. PFR30J09 and PFR34B02 formed the most biofilms. The population in PFR30J09 biofilm rose from 3.83 to 7.20 $\log_{10}$ CFU/cm^2 and the population of PFR34B02 increased from 3.46 to 7.08 $\log_{10}$ CFU/cm^2 within 6 h. The weak biofilm formers, such as PFR37D08, had growth curves with a delay in the rise of cell counts. Calcofluor white stain can bind to β-linked polysaccharides and emit blue fluorescence. Epifluorescence microscopy provided a direct, visual approach to define microbial biofilm forming ability. PFR30J09 and PFR34B02 were confirmed as strong biofilm forming strains under epifluorescence microscopy, with dense cell clusters and a structured matrix, whereas others showed flat and loose cell clusters. Using multiple assays for biofilm formation, the results were consistent for PFR30J09 and PFR34B02 therefore these were chosen as the strong biofilm formers for this study, PFR21C03 and PFR37D08 were selected as the weak biofilm strains for this study.

Studies on the inactivation of *V. parahaemolyticus* are limited. In this study, the effective chlorine concentration required to kill biofilm of *V. parahaemolyticus* was approximately 75-fold higher than that required to kill planktonic counterparts. In one published study, *V. parahaemolyticus* planktonic culture was reduced by 2.2 $\log_{10}$ CFU/mL from 7.6 $\log_{10}$ CFU/mL with 30s treatment of sodium hypochlorite (35 mg/L available chlorine concentration, pH not specified) (Quan et al., 2010). In another study, the planktonic cells were treated with sodium hypochlorite (81 mg/L available chlorine concentration, pH 10.8) for 3 min, with no cells detectable from an initial cell concentration of 7.85 $\log_{10}$ CFU/mL (Chen et al., 2016). For sodium hypochlorite efficacy for killing biofilm cells on biotic surfaces, Roy et al. (2021) assessed 5 min sodium hypochlorite treatment (50, 100, 200, and 300 mg/L, pH not specified) reduced *V. parahaemolyticus* biofilm cells from

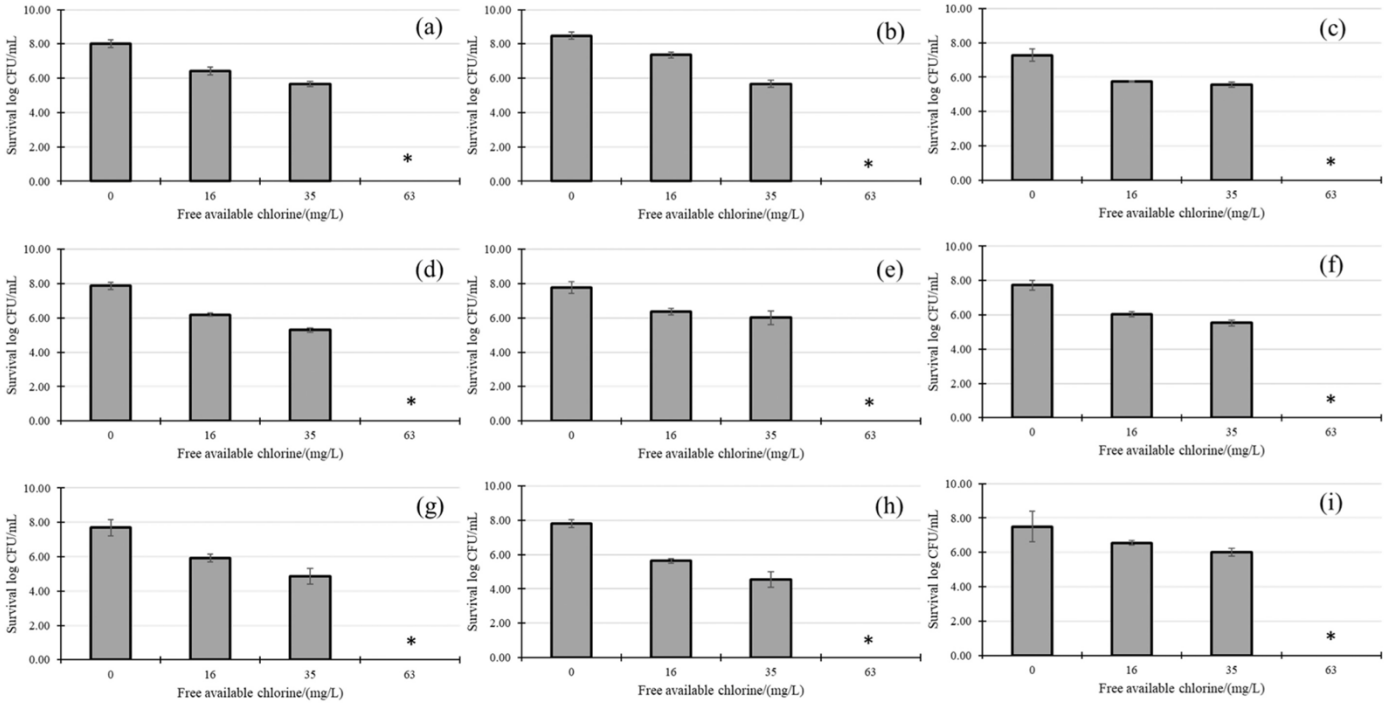

Fig. 4. Susceptibility of planktonic *V. parahaemolyticus* to sodium hypochlorite. The indications for strains are as follows: (a) PFR21C03, (b) PFR24B07, (c) PFR29A04, (d) PFR30G02, (e) PFR30J09, (f) PFR34B02, (g) PFR37C06, (h) PFR37D08 and (i) PFR37E03. * indicates the limit of CFU detection (< 10 CFU/mL). Data results presented as mean ± SD.

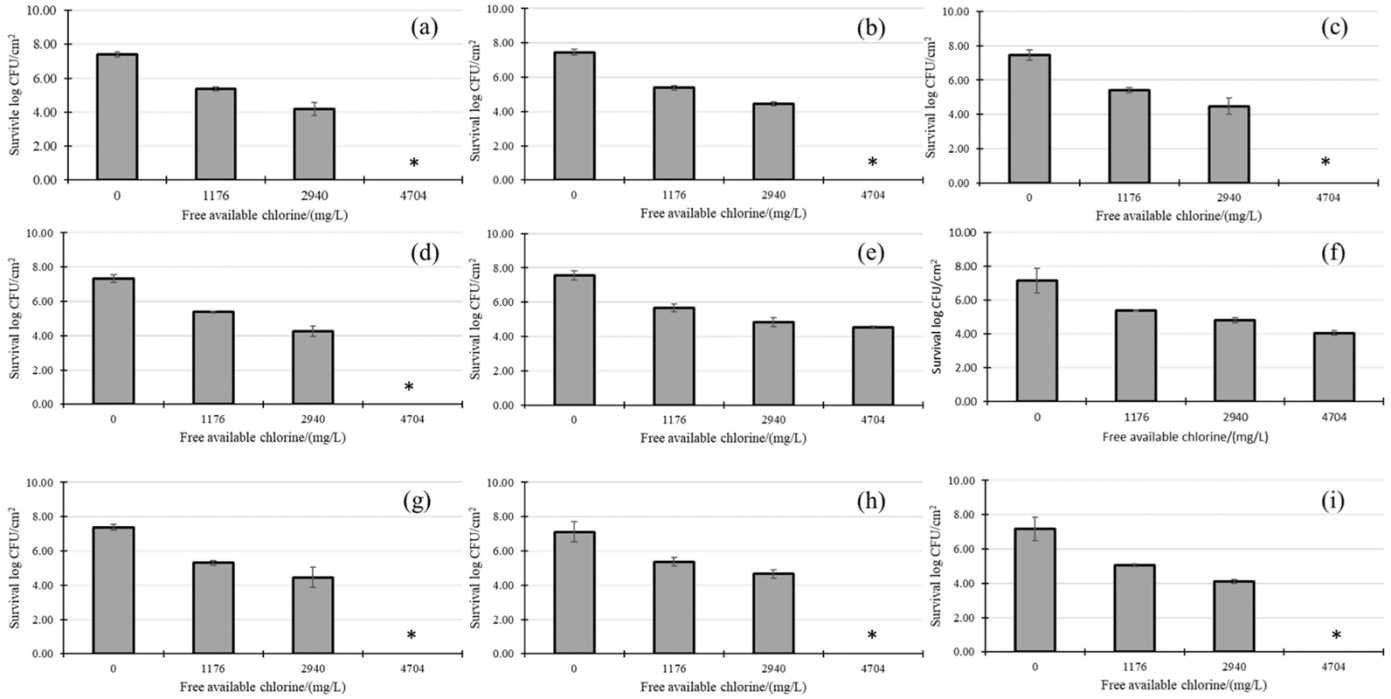

Fig. 5. Susceptibility of *V. parahaemolyticus* biofilms to sodium hypochlorite. The indications for strains are as follows: (a) PFR21C03, (b) PFR24B07, (c) PFR29A04, (d) PFR30G02, (e) PFR30J09, (f) PFR34B02, (g) PFR37C06, (h) PFR37D08 and (i) PFR37E03. * indicates the limit of CFU detection (< 10 CFU/mL). Data results presented as mean ± SD.

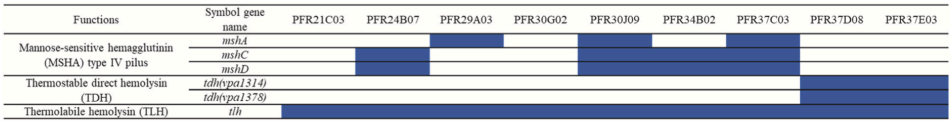

Fig. 6. Genetic diversity of biofilm-forming genes in *V. parahaemolyticus* isolates. The presence and absence of biofilm-forming related genes; the blue represents the presence of the gene, white represents the absence.

Table 1
Information of strains applied in this study.

Strains	MLST ST	Nearest ST match (loci hits)	*dnaE*	*gyrB*	*recA*	*dtdS*	*pntA*	*pyrC*	*tnaA*
PFR21C03	2632	–	*dnaE (226)*	*gyrB (25)*	*recA (97)*	*dtdS (19)*	*pntA (26)*	*pyrC (49)*	*tnaA (26)*
PFR24B07	New ST	2651(6)	*dnaE (175)*	*gyrB (235)*	*recA (3)*	*dtdS (85)*	*pntA (65)*	*pyrC (~68)*	*tnaA (23)*
PFR29A04	1357	–	*dnaE (162)*	*gyrB (399)*	*recA (80)*	*dtdS (150)*	*pntA (11)*	*pyrC (158)*	*tnaA (51)*
PFR30G02	1772	–	*dnaE (47)*	*gyrB (287)*	*recA (19)*	*dtdS (252)*	*pntA (245)*	*pyrC (18)*	*tnaA (217)*
PFR30J09	New ST	2650(3)	*dnaE (60)*	*gyrB (406)*	*recA (366)*	*dtdS (390)*	*pntA (18)*	*pyrC (94)*	*tnaA (47)*
PFR34B02	New ST	2648(6)	*dnaE (36)*	*gyrB (4)*	*recA (81)*	*dtdS (27)*	*pntA (26)*	*pyrC (82)*	*tnaA (225)*
PFR37C06	New ST	2650(5)	*dnaE (60)*	*gyrB (406)*	*recA (257)*	*dtdS (390)*	*pntA (~156)*	*pyrC (221)*	*tnaA (47)*
PFR37D08	36	–	*dnaE (21)*	*gyrB (15)*	*recA (1)*	*dtdS (23)*	*pntA (23)*	*pyrC (~21)*	*tnaA (16)*
PFR37E03	1140	–	*dnaE (19)*	*gyrB (295)*	*recA (295)*	*dtdS (223)*	*pntA (136)*	*pyrC (11)*	*tnaA (13)*

In this table, *dnaE*, *gyrB*, *recA*, *dtdS*, *pntA*, *pyrC* and *tnaA* are housekeeping genes in *V. parahaemolyticus*, and distinct parameters reflect their varied multilocus sequence typing (MLST) information. All 7 housekeeping loci matched with the PubMLST database otherwise, nearest match and loci hit numbers were shown above.

0.54 to 2.59 and 0.64 to 2.32 $\log_{10}$ CFU/cm^2 on shrimp and crab surfaces, respectively, from initial concentrations of 6.87 and 7.37 $\log_{10}$ CFU/cm^2.

The concentrations of sodium hypochlorite required to eliminate biofilm cells have been determined in many species. Corcoran et al. (2014) reported 500 mg/L sodium hypochlorite was not effective against *Salmonell*a biofilm, with a reduction of 1.11 $\log_{10}$ CFU/coupon after 90 min treatment. Cruz and Fletcher (2012) reported 3600 mg/L chlorine as the minimal effective concentration (99.999 % reduction) against L. *monocytogenes* biofilm cells. For *E. coli* O157:H7 attached to rind surfaces for 2 h, a > 5 $\log_{10}$ reduction occurred after treatment with 2000 mg/L of sodium hypochlorite. For 12 h old biofilms, 2000 mg/L could only achieve a 1.86 $\log_{10}$ reduction (Fu et al., 2017). The effect of sodium hypochlorite on biofilms is dependent on the variants, the age of the biofilm, the structure of the biofilm matrix, the chlorine concentrations, pH and treatment time (Yuan et al., 2021).

In the present trial on biofilm cells, the strong biofilm formers PFR30J09 and PFR34B02 required a greater chlorine concentration, possibly due to more polysaccharide production and a more organised matrix architecture. Similarly, Danese et al. (2000) reported the polysaccharide colonic acid is critical for the complex three-dimensional structure and depth of biofilms in *E. coli* K-12. In *Staphylococcus aureus*, the presence and expression of the gene *ica*, which encodes the polysaccharide poly-*N*-acetylglucosamine (PNAG), are credited with maintaining the integrity of the biofilm architecture and it's resistance to biocidal compounds (Schwartz et al., 2012). Brauge et al. (2018) identified the absence of *N*-acetylglucosamine in teichoic acids caused less adhesion onto surfaces and modified biofilm architecture in L. *monocytogenes*, thereby reducing tolerance to rinsing and cleaning procedures in seafood environments. A relationship between higher resistance and more polysaccharide production was suggested in this study. This could result from the effect on the structure of the matrix causing difficult in sodium hypochlorite to diffuse into or break down the biofilm.

Mature *V. parahaemolyticus* biofilm formation requires type IV pili (mannose-sensitive haemagglutinin type IV pili, MSHA and chitin-regulated pili, ChiRP), EPS biosynthesis and secretion as well as other regulatory factors. Based on the presence and absence of biofilm-forming related genes in this study, the differences among sequenced *V. parahaemolyticus* genomes were mainly located at the *msh* gene clusters that encode MSHA in *V. parahaemolyticus* and TLH toxin producing genes. MSHA has been reported to be required for early attachment to abiotic surfaces. In *V. cholerae*, the *mshA* deficient cells cannot perform cell aggregation though they form three dimensional structures (Moorthy and Watnick, 2004). In *V. parahaemolyticus*, *mshA* mutants of *V. parahaemolyticus* exhibited a lower ability to adhere to surfaces (Shime-Hattori et al., 2006; Williams et al., 2014). Similar results were found for *V. fisheries*, mutants of *mshA* or *mshN* genes in that they were defective for biofilm formation (Visick et al., 2013). Our study indicated that, PFR30J09, the strongest biofilm-forming strain, did not exhibit deficiencies in any of the following genes: *mshA*, *mshC* or *mshD*. In contrast, the weak biofilm forming strains, PFR21C03 and PFR37D08, showed an absence of these three genes. PFR34B02 showed stronger resistance against sodium hypochlorite but did not have the *mshA* gene, indicating that there were other factors responsible for the high EPS production and this requires further investigation. MSHA is modulated by *c*-di-GMP and MshE has as a high-affinity for the *c*-di-GMP receptor (Floyd et al., 2020), suggesting the possibility of using it to interfere with colonization and biofilm development of *V. parahaemolyticus*.

The TDH (encoded by the *tdh* gene) and the TDH-related hemolysin (TRH, encoded by *trh* gene) are primarily associated with pathogenicity, while TLH was reported to be associated with a cytotoxic effect in *V. parahaemolyticus* (Paria et al., 2021). The pathogenicity of *V. parahaemolyticus* may also influence biofilm production but this has not been proven. In the seafood industry, Song et al. (2017) discovered that pathogenic *V. parahaemolyticus* accumulates more biofilm matrix than non-pathogenic strains. Similarly, Wong et al. (2002) found that clinical strains adhered to stainless steel more readily than environmental strains. Though in our study, the pathogenic isolate PFR37D08 was categorized as a weak biofilm former, which might be due to the lack of a host signal/compound and thus the incompetency to incur the strong biofilm forming ability. This result was in consistent with those by Kadam et al. (2013) and Doijad et al. (2015).

Apart from capsular polysaccharide A (CPSA)-a major known component of the *V. parahaemolyticus* biofilm, *vp1476–1458* is an ortholog of the *syp* locus conserved in *V. fischeri*, which is responsible for *syp*-polysaccharide production however this has not been demonstrated for *V. parahaemolyticus* (Yildiz and Visick, 2009). However, the fluorescence microscopy result suggested other β-linked polysaccharides resulted in the biofilm differences among weak and strong biofilm-forming strains but have not this needs further examination.

Table 2
Biofilm-forming genes selected to examine in this study.

Subject_RIMD2210633	Gene locus	Symbol gene name	Functions
WP_005478391.1	*vpa1403*	*cpsA*	CPS polysaccharide
WP_005478164.1	*vpa1404*	*cpsB*	
WP_005463089.1	*vpa1405*	*cpsC*	
WP_005478193.1	*vpa1407*	*cpsE*	
WP_005478388.1	*vpa1408*	*cpsF*	
WP_005478236.1	*vpa1409*	*cpsG*	
WP_005478215.1	*vpa1410*	*cpsH*	
WP_005478165.1	*vpa1411*	*cpsI*	
WP_005478324.1	*vpa1412*	*cpsJ*	
WP_005465330.1	*vp0132*	*epsC*	Type II secretion system
WP_005478663.1	*vp0133*	*epsD*	
WP_005478662.1	*vp0134*	*epsE*	
WP_005465194.1	*vp0135*	*epsF*	
WP_005465191.1	*vpa0136*	*epsG*	
WP_005461161.1	*vp0137*	*epsH*	
WP_005478722.1	*vp0138*	*epsI*	
WP_005465187.1	*vp0139*	*epsJ*	
WP_005478666.1	*vp0140*	*epsK*	
WP_005458997.1	*vp0141*	*epsL*	
WP_005458943.1	*vp0142*	*epsM*	
WP_005459010.1	*vp0143*	*epsN*	
WP_005480168.1	*vpa1598*	*gbpA*	Colonization factor GbpA
WP_011106342.1	*vpa0747*	*mshA*	Mannose-sensitive
WP_005481001.1	*vp2696*	*mshC*	hemagglutinin (MSHA type
WP_005481015.1	*vp2695*	*mshD*	IV pilus)
WP_005456306.1	*vp2701*	*mshE*	
WP_005456302.1	*vp2699*	*mshF*	
WP_005456304.1	*vp2700*	*mshG*	
WP_011106082.1	*vp2708*	*mshH*	
WP_005481017.1	*vp2707*	*mshI*	
WP_005456325.1	*vp2706*	*mshJ*	
WP_005481006.1	*vp2705*	*mshK*	
WP_005456314.1	*vp2704*	*mshL*	
WP_005456312.1	*vp2703*	*mshM*	
WP_005480990.1	*vp2702*	*mshN*	
WP_005479695.1	*vp2524*	*pilB*	Type IV-A pilus
WP_005479682.1	*vp2525*	*pilC*	
WP_005490359.1	*vp2526*	*pilD*	
WP_005483463.1	*vp1463*	*sypN*	*syp*-like polysaccharide
WP_005454817.1	*vp1476*	*sypA*	
WP_005491469.1	*vp1475*	*sypB*	
WP_005483457.1	*vp1474*	*sypC*	
WP_005454821.1	*vp1473*	*sypD*	
WP_005454845.1	*vp1472*	*sypE*	
WP_005483461.1	*vp1469*	*sypH*	
WP_005483417.1	*vp1468*	*sypI*	
WP_005483478.1	*vp1467*	*sypJ*	
WP_005483470.1	*vp1466*	*sypK*	
WP_005483422.1	*vp1465*	*sypL*	
WP_005483419.1	*vp1464*	*sypM*	
WP_005483455.1	*vp1462*	*sypO*	
WP_005483418.1	*vp1461*	*sypP*	
WP_005483424.1	*vp1459*	*sypQ*	
WP_005483433.1	*vp1458*	*sypR*	
WP_005463268.1	*vpa1314*	*tdh*	Thermostable direct
WP_005478284.1	*vpa1378*	*tdh*	hemolysin
WP_005481504.1	*vpa0226*	*tlh*	Thermolabile hemolysin

5. Conclusion

In conclusion, the strong biofilm-forming strains identified in this study have novel MLST ST types, which will aid in understanding *V. parahaemolyticus* persistence in environmental conditions, shed light on underlying mechanisms of *V. parahaemolyticus* global spread, and aid in the development of effective pathogen control strategies in the food industry. This study also found that attachment contributed to strong biofilm formation in *V. parahaemolyticus*, suggesting additional genes that might have played roles in EPS production in *V. parahaemolyticus* requiring further investigation. *V. parahaemolyticus* biofilms, as with all microbial biofilms, are complex systems. Mono-specific biofilms formed in static high nutrient conditions were used in our study, nevertheless, multi-species biofilms are prevalent in nature and thrive in environments with flowing nutrients.

Table 3
Phenotypes of *V. parahaemolyticus* in motility.

Group	Swimming capacity (/mm)[a]	Swarming capacity (/mm)
PFR21C03	69.33 ± 17.48	38.25 ± 11.88
PFR24B07	15.17 ± 2.84	55.83 ± 5.58
PFR29A04	16.75 ± 1.06	22.83 ± 5.97
PFR30G02	71.00 ± 15.56	45.17 ± 22.41
PFR30J09	58.58 ± 30.50	60.33 ± 8.25
PFR34B02	10.33 ± 0.76	27.67 ± 4.07
PFR37C06	20.00 ± 6.08	28.67 ± 1.89
PFR37D08	20.67 ± 10.30	32.50 ± 12.28
PFR37E03	20.00 ± 2.18	38.83 ± 3.82
Correlation coefficient with BFI	0.0632	0.0161

[a] Data results presented as mean ± standard deviation (SD).

Funding

This study is funded by Massey University, the grant number is P963141222WangD.

CRediT authorship contribution statement

Dan Wang: Conceptualization, Methodology, Investigation, Formal analysis, Writing – original draft, Writing – review & editing. **Graham C. Fletcher:** Resources, Conceptualization, Methodology, Supervision, Writing – review & editing. **Stephen L.W. On:** Conceptualization, Methodology, Supervision, Writing – review & editing. **Jon S. Palmer:** Conceptualization, Methodology, Supervision, Writing – review & editing. **Dragana Gagic:** Conceptualization, Methodology, Supervision, Writing – review & editing. **Steve H. Flint:** Project administration, Resources, Supervision, Conceptualization, Methodology, Writing – review & editing.

Declaration of competing interest

The authors declare no competing conflicts of interest.

Data availability

Data will be made available on request.

Acknowledgements

The authors are grateful to Jaime Martinez-Urtaza and Andy Powell of Centre for Environment, Fisheries, and Aquaculture Science (CEFAS) who provided sequence data.

References

Abanto, M., Gavilan, R.G., Baker-Austin, C., Gonzalez-Escalona, N., Martinez-Urtaza, J., 2020. Global expansion of Pacific Northwest *Vibrio parahaemolyticus* sequence type 36. Emerg. Infect. Dis. 26, 323–326.

Baker-Austin, C., Stockley, L., Rangdale, R., Martinez-Urtaza, J., 2010. Environmental occurrence and clinical impact of *Vibrio vulnificus* and *Vibrio parahaemolyticus*: a European perspective. Environ. Microbiol. Rep. 2, 7–18.

Baker-Austin, C., Oliver, J.D., Alam, M., Ali, A., Waldor, M.K., Qadri, F., Martinez-Urtaza, J., 2018. *Vibrio spp.* infections. Nat. Rev. Dis. Primers. 4, 8.

Baker-Austin, C., Jenkins, C., Dadzie, J., Mestanza, O., Delgado, E., Powell, A., Bean, T., Martinez-Urtaza, J., 2020. Genomic epidemiology of domestic and travel-associated *Vibrio parahaemolyticus* infections in the UK, 2008–2018. Food Control 115, 107244.

Brauge, T., Faille, C., Sadovskaya, I., Charbit, A., Benezech, T., Shen, Y., Loessner, M.J., Bautista, J.R., Midelet-Bourdin, G., 2018. The absence of N-acetylglucosamine in wall teichoic acids of *Listeria monocytogenes* modifies biofilm architecture and tolerance to rinsing and cleaning procedures. PLoS One 13, e0190879.

Buchfink, B., Reuter, K., Drost, H.G., 2021. Sensitive protein alignments at tree-of-life scale using DIAMOND. Nat. Methods 18, 366–368.

Cai, L.L., Hu, H.J., Lu, Q., Wang, H.H., Xu, X.L., Zhou, G.H., Kang, Z.L., Ma, H.J., 2019. Morphophysiological responses of detached and adhered biofilms of *Pseudomonas fluorescens* to acidic electrolyzed water. Food Microbiol. 82, 89–98.
CDC, 2021. The Cholera and Other Vibrio Illness Surveillance (COVIS) System. US Department of Health and Human Services, CDC.
Chen, T.-Y., Kuo, S.-H., Chen, S.-T., Hwang, D.-F., 2016. Differential proteomics to explore the inhibitory effects of acidic, slightly acidic electrolysed water and sodium hypochlorite solution on *Vibrio parahaemolyticus*. Food Chem. 194, 529–537.
Chiba, K., Kawakami, K., Tohyama, K., 1998. Simultaneous evaluation of cell viability by neutral red, MTT and crystal violet staining assays of the same cells. Toxicol. in Vitro 12, 251–258.
Corcoran, M., Morris, D., De Lappe, N., O'Connor, J., Lalor, P., Dockery, P., Cormican, M., 2014. Commonly used disinfectants fail to eradicate *Salmonella enterica* biofilms from food contact surface materials. Appl. Environ. Microbiol. 80, 1507–1514.
Cruz, C.D., Fletcher, G.C., 2012. Assessing manufacturers' recommended concentrations of commercial sanitizers on inactivation of *Listeria monocytogenes*. Food Control 26, 194–199.
Cruz, C.D., Hedderley, D., Fletcher, G.C., 2015. Long-term study of *Vibrio parahaemolyticus* prevalence and distribution in New Zealand shellfish. Appl. Environ. Microbiol. 81, 2320–2327.
Danese, P.N., Pratt, L.A., Kolter, R., 2000. Exopolysaccharide production is required for development of *Escherichia coli* K-12 biofilm architecture. J. Bacteriol. 182, 3593–3596.
Daniels, N.A., Ray, B., Easton, A., Marano, N., Kahn, E., McShan II, A.L., Del Rosario, L., Baldwin, T., Kingsley, M.A., Puhr, N.D., Wells, J.G., Angulo, F.J., 2000. Emergence of a new *Vibrio parahaemolyticus* serotype in raw oysters: a prevention quandary. JAMA 284, 1541–1545.
Di Bonaventura, G., Piccolomini, R., Paludi, D., D'Orio, V., Vergara, A., Conter, M., Ianieri, A., 2008. Influence of temperature on biofilm formation by *Listeria monocytogenes* on various food-contact surfaces: relationship with motility and cell surface hydrophobicity. J. Appl. Microbiol. 104, 1552–1561.
Doijad, S.P., Barbuddhe, S.B., Garg, S., Poharkar, K.V., Kalorey, D.R., Kurkure, N.V., Rawool, D.B., Chakraborty, T., 2015. Biofilm-forming abilities of *Listeria monocytogenes* serotypes isolated from different sources. PLoS One 10, e0137046.
Fang, Y., Visvalingam, J., Zhang, P., Yang, X., 2022. Biofilm formation by Non-O157 Shiga toxin-producing *Escherichia coli* in monocultures and co-cultures with meat processing surface bacteria. Food Microbiol. 102, 103902.
FAO, 2021. Advances in science and risk assessment tools for *Vibrio parahaemolyticus* and *V. vulnificus* associated with seafood: meeting report. https://www.who.int/publications/i/item/9789240024878.
Floyd, K.A., Lee, C.K., Xian, W., Nametalla, M., Valentine, A., Crair, B., Zhu, S., Hughes, H.Q., Chlebek, J.L., Wu, D.C., Hwan Park, J., Farhat, A.M., Lomba, C.J., Ellison, C.K., Brun, Y.V., Campos-Gomez, J., Dalia, A.B., Liu, J., Biais, N., Wong, G.C. L., Yildiz, F.H., 2020. C-di-GMP modulates type IV MSHA pilus retraction and surface attachment in *Vibrio cholerae*. Nat. Commun. 11, 1549.
Fu, Y., Deering, A.J., Bhunia, A.K., Yao, Y., 2017. Biofilm of *Escherichia coli* O157:H7 on cantaloupe surface is resistant to lauroyl arginate ethyl and sodium hypochlorite. Int. J. Food Microbiol. 260, 11–16.
Gurevich, A., Saveliev, V., Vyahhi, N., Tesler, G., 2013. QUAST: quality assessment tool for genome assemblies. Bioinformatics 29, 1072–1075.
Hayrapetyan, H., Muller, L., Tempelaars, M., Abee, T., Nierop Groot, M., 2015. Comparative analysis of biofilm formation by *Bacillus cereus* reference strains and undomesticated food isolates and the effect of free iron. Int. J. Food Microbiol. 200, 72–79.
Jolley, K.A., Bray, J.E., Maiden, M.C.J., 2018. Open-access bacterial population genomics: BIGSdb software, the PubMLST.Org website and their applications. Wellcome Open Res. 3, 124.
Kadam, S.R., den Besten, H.M., van der Veen, S., Zwietering, M.H., Moezelaar, R., Abee, T., 2013. Diversity assessment of *Listeria monocytogenes* biofilm formation: impact of growth condition, serotype and strain origin. Int. J. Food Microbiol. 165, 259–264.
Kaneko, T., Colwell, R.R., 1975. Adsorption of *Vibrio parahaemolyticus* onto chitin and copepods. Appl. Microbiol. 29, 269–274.
Kim, Y.K., McCarter, L.L., 2000. Analysis of the polar flagellar gene system of *Vibrio parahaemolyticus*. J. Bacteriol. 182, 3693–3704.
Lucero-Mejia, J.E., Romero-Gomez, S.J., Hernandez-Iturriaga, M., 2020. A new classification criterion for the biofilm formation index: a study of the biofilm dynamics of pathogenic *Vibrio* species isolated from seafood and food contact surfaces. J. Food Sci. 85, 2491–2497.
Martinez-Urtaza, J., Trinanes, J., Abanto, M., Lozano-Leon, A., Llovo-Taboada, J., Garcia-Campello, M., Pousa, A., Powell, A., Baker-Austin, C., Gonzalez-Escalona, N., 2018. Epidemic dynamics of *Vibrio parahaemolyticus* illness in a hotspot of disease emergence, Galicia, Spain. Emerg. Infect. Dis. 24, 852–859.
Mizan, M.F., Jahid, I.K., Kim, M., Lee, K.H., Kim, T.J., Ha, S.D., 2016. Variability in biofilm formation correlates with hydrophobicity and quorum sensing among *Vibrio parahaemolyticus* isolates from food contact surfaces and the distribution of the genes involved in biofilm formation. Biofouling 32, 497–509.
Moorthy, S., Watnick, P.I., 2004. Genetic evidence that the *Vibrio cholerae* monolayer is a distinct stage in biofilm development. Mol. Microbiol. 52, 573–587.
Nair, G.B., Ramamurthy, T., Bhattacharya, S.K., Dutta, B., Takeda, Y., Sack, D.A., 2007. Global dissemination of *Vibrio parahaemolyticus* serotype O3:K6 and its serovariants. Clin. Microbiol. Rev. 20, 39–48.
Naves, P., del Prado, G., Huelves, L., Gracia, M., Ruiz, V., Blanco, J., Rodríguez-Cerrato, V., Ponte, M.C., Soriano, F., 2008. Measurement of biofilm formation by clinical isolates of *Escherichia coli* is method-dependent. J. Appl. Microbiol. 105, 585–590.
Paria, P., Behera, B.K., Mohapatra, P.K.D., Parida, P.K., 2021. Virulence factor genes and comparative pathogenicity study of *tdh*, *trh* and tlh positive *Vibrio parahaemolyticus* strains isolated from whiteleg shrimp, *Litopenaeus vannamei* (Boone, 1931) in India. Infect. Genet. Evol. 95, 105083.
Parks, D.H., Imelfort, M., Skennerton, C.T., Hugenholtz, P., Tyson, G.W., 2015. CheckM: assessing the quality of microbial genomes recovered from isolates, single cells, and metagenomes. Genome Res. 25, 1043–1055.
Petit III, R.A., Read, T.D., 2020. Bactopia: a flexible pipeline for complete analysis of bacterial genomes. mSystems 5 e00190-00120.
Quan, Y., Choi, K.-D., Chung, D., Shin, I.-S., 2010. Evaluation of bactericidal activity of weakly acidic electrolyzed water (WAEW) against *Vibrio vulnificus* and *Vibrio parahaemolyticus*. Int. J. Food Microbiol. 136, 255–260.
Rosa, J.V., Conceição, N.V., Conceição, R.C.S., Timm, C., 2018. Biofilm formation by *Vibrio parahaemolyticus* on different surfaces and its resistance to sodium hypochlorite. Cienc. Rural 48.
Roy, P.K., Mizan, M.F.R., Hossain, M.I., Han, N., Nahar, S., Ashrafudoulla, M., Toushik, S. H., Shim, W.B., Kim, Y.M., Ha, S.D., 2021. Elimination of *Vibrio parahaemolyticus* biofilms on crab and shrimp surfaces using ultraviolet C irradiation coupled with sodium hypochlorite and slightly acidic electrolyzed water. Food Control 128, 108179.
Schwartz, K., Syed, A.K., Stephenson, R.E., Rickard, A.H., Boles, B.R., 2012. Functional amyloids composed of phenol soluble modulins stabilize *Staphylococcus aureus* biofilms. PLoS Pathog. 8, e1002744.
Sheikh, J., Hicks, S., Dall'Agnol, M., Phillips, A.D., Nataro, J.P., 2001. Roles for fis and YafK in biofilm formation by enteroaggregative *Escherichia coli*. Mol. Microbiol. 41, 983–997.
Shikongo-Nambabi, M.N.N.N., Kachigunda, B., Venter, S.N., 2010. Evaluation of oxidising disinfectants to control *Vibrio* biofilms in treated seawater used for fish processing. Water SA 36, 215–220.
Shime-Hattori, A., Iida, T., Arita, M., Park, K.S., Kodama, T., Honda, T., 2006. Two type IV pili of *Vibrio parahaemolyticus* play different roles in biofilm formation. FEMS Microbiol. Lett. 264, 89–97.
Song, X., Ma, Y., Fu, J., Zhao, A., Guo, Z., Malakar, P., Yingjie, P., Zhao, Y., 2017. Effect of temperature on pathogenic and non-pathogenic *Vibrio parahaemolyticus* biofilm formation. Food Control 73, 485–491.
Sybiya Vasantha Packiavathy, I.A., Agilandeswari, P., Musthafa, K.S., Karutha Pandian, S., Veera Ravi, A., 2012. Antibiofilm and quorum sensing inhibitory potential of Cuminum cyminum and its secondary metabolite methyl eugenol against Gram negative bacterial pathogens. Food Res. Int. 45, 85–92.
Visick, K.L., Quirke, K.P., McEwen, S.M., 2013. Arabinose induces pellicle formation by *Vibrio fischeri*. Appl. Environ. Microbiol. 79, 2069–2080.
Wadhwa, N., Berg, H.C., 2022. Bacterial motility: machinery and mechanisms. Nat. Rev. Microbiol. 20, 161–173.
Wang, D., Flint, S.H., Palmer, J.S., Gagic, D., Fletcher, G.C., On, S.L., 2022. Global expansion of *Vibrio parahaemolyticus* threatens the seafood industry: perspective on controlling its biofilm formation. LWT 158, 113182.
Williams, T.C., Ayrapetyan, M., Oliver, J.D., 2014. Implications of chitin attachment for the environmental persistence and clinical nature of the human pathogen *Vibrio vulnificus*. Appl. Environ. Microbiol. 80, 1580–1587.
Wong, H.C., Chung, Y.C., Yu, J.A., 2002. Attachment and inactivation of *Vibrio parahaemolyticus* on stainless steel and glass surface. Food Microbiol. 19, 341–350.
Yildiz, F.H., Visick, K.L., 2009. *Vibrio* biofilms: so much the same yet so different. Trends Microbiol. 17, 109–118.
Yuan, L., Sadiq, F.A., Wang, N., Yang, Z., He, G., 2021. Recent advances in understanding the control of disinfectant-resistant biofilms by hurdle technology in the food industry. Crit. Rev. Food Sci. Nutr. 61, 3876–3891.
Zheng, S.J., Brook, M.A., 2021. Elastomeric silicone sponges for bleach delivery. ACS Appl. Polym. Mater. 3, 2045–2053.

Appendix VIII. Research output - Chapter 4

International Journal of Food Microbiology 405 (2023) 110372

Contents lists available at ScienceDirect

International Journal of Food Microbiology

journal homepage: www.elsevier.com/locate/ijfoodmicro

Efficacy of commercial peroxyacetic acid on *Vibrio parahaemolyticus* planktonic cells and biofilms on stainless steel and Greenshell™ mussel (*Perna canaliculus*) surfaces

Dan Wang [a,*], Jon S. Palmer [a], Graham C. Fletcher [b], Stephen L.W. On [c], Dragana Gagic [d], Steve H. Flint [a]

[a] School of Food and Advanced Technology, Massey University, Private Bag 11222, Palmerston North, New Zealand
[b] The New Zealand Institute for Plant & Food Research Limited, Private Bag 92169, Auckland 1142, New Zealand
[c] Faculty of Agriculture and Life Sciences, Lincoln University, Private Bag 85084, Canterbury, New Zealand
[d] School of Fundamental Sciences, Massey University, Private Bag 11222, Palmerston North, New Zealand

ARTICLE INFO

Keywords:
PAA
Vibrio parahaemolyticus
Sanitizer
Greenshell™ mussel
Seafood safety

ABSTRACT

The potential of using commercial peroxyacetic acid (PAA) for *Vibrio parahaemolyticus* sanitization was evaluated. Commercial PAA of 0.005 % (v/v, PAA: 2.24 mg/L, hydrogen peroxide: 11.79 mg/L) resulted in a planktonic cell reduction of >7.00 $\log_{10}$ CFU/mL when initial *V. parahaemolyticus* cells averaged 7.64 $\log_{10}$ CFU/mL. For cells on stainless steel coupons, treatment of 0.02 % PAA (v/v, PAA: 8.96 mg/L, hydrogen peroxide: 47.16 mg/L) achieved >5.00 $\log_{10}$ CFU/cm^2 reductions in biofilm cells for eight strains but not for the two strongest biofilm formers. PAA of 0.05 % (v/v, PAA: 22.39 mg/L, hydrogen peroxide: 117.91 mg/L) was required to inactivate >5.00 $\log_{10}$ CFU/cm^2 biofilm cells from mussel shell surfaces. The detection of PAA residues after biofilm treatment demonstrated that higher biofilm production resulted in higher PAA residues ($p < 0.05$), suggesting biofilm is acting as a barrier interfering with PAA diffusing into the matrices. Based on the comparative analysis of genomes, robust biofilm formation and metabolic heterogeneity within niches might have contributed to the variations in PAA resistance of *V. parahaemolyticus* biofilms.

1. Introduction

Vibrio parahaemolyticus is a Gram-negative marine-oriented microorganism, widely distributed in seafood such as shellfish, shrimp, and fish. It is a major seafood-borne pathogen, infecting humans via the consumption of raw or undercooked seafood. There are on average 34,664 *V. parahaemolyticus* infections each year in the USA, while 4116 cases have been reported due to cholera and other *Vibrio* illness reported in the Surveillance (COVIS) System during 2010 and 2018 (CDC, 2021; FAO, 2021). In China, they experienced an average of 523.5 reported cases each year during 2010 and 2020 (FAO, 2021). Large scale outbreaks have been reported in South America and Europe, including Chile (Gonzalez-Escalona et al., 2005), Peru (Martinez-Urtaza et al., 2008), and Spain (Baker-Austin et al., 2010). In recent years, *V. parahaemolyticus* outbreaks have been regularly reported in countries with little or no prior incidence including France, Canada, Australia and New Zealand, representing a global increase in *V. parahaemolyticus* as a food safety concern (FAO, 2021).

The bacteria existing as planktonic cells, attach to surfaces and present in the form of biofilm, which is more resistant to environmental stress, including disinfectant treatments, and posing threats to public health. Although novel alternative control strategies have been studied, chemical sanitisers remain the most common method for controlling pathogens in food manufacture as they are cost effective and easy to use. It is critical to evaluate the effectiveness of each disinfectant on biofilm cells in order to understand the potential risks in the food industry.

V. parahaemolyticus biofilms form on biotic surfaces (e.g., copepods, oysters, clams, fish, shrimps, and mussels) and abiotic surfaces (stainless steel, polystyrene, glass, etc.) in food processing equipment and packaging materials. Biofilms show a higher resistance than their planktonic counterparts (Ashrafudoulla, Mizan, Ha, et al., 2020). Chlorine, one of the most common disinfectants, cannot effectively kill *V. parahaemolyticus* biofilm cells on biotic/abiotic surfaces at recommended concentrations. Rosa et al. (2018) examined the efficacy of

* Corresponding author.
E-mail address: d.wang3@massey.ac.nz (D. Wang).

https://doi.org/10.1016/j.ijfoodmicro.2023.110372
Received 28 March 2023; Received in revised form 7 August 2023; Accepted 26 August 2023
Available online 29 August 2023

sodium hypochlorite in reducing the bacterial population of *V. parahaemolyticus* in mature biofilms formed on stainless steel, glass, and polystyrene; they discovered that a 10-min treatment with sodium hypochlorite (20 ppm free available chlorine) reduced cell populations by 3.0 $\log_{10}$ colony forming units (CFU)/cm^2 from 5.5 $\log_{10}$ CFU/cm^2. Roy et al. (2021) showed that 5-min treatment with 12 % w/v sodium hypochlorite containing 6 % free chlorine equivalent at concentrations of 50, 100, 200, and 300 ppm, reduced *V. parahaemolyticus* biofilm cells by 0.54 to 2.59 and 0.64 to 2.32 $\log_{10}$ CFU/cm^2 on shrimp and crab surfaces, respectively, from initial concentrations of 6.87 and 7.37 $\log_{10}$ CFU/cm^2. Additionally, the authors of the current study found that inactivating strong biofilm-forming strains of *V. parahaemolyticus* on stainless steel coupons required free available chlorine concentrations of over 1000 ppm (Wang et al., 2023b). Therefore, the investigation of other chemical disinfectant alternatives is required.

Peroxyacetic or peracetic acid (PAA) has been proposed as a green alternative to sodium hypochlorite because it does not produce disinfection by-products (DBPs) and imparts no taste or odour (Wang et al., 2020). Sodium hypochlorite dissociates into hypochlorite ions in water, while PAA exists in aqueous equilibrium as acetic acid and hydrogen peroxide, producing further oxidative effects (Sharma et al., 2016). Several PAA commercial formulations are available, for instance, Sani-Date® 5.0, VigorOx® 15 F&V, BioSide® HS-15 %, and Tsunami™ 100. PAA is approved for use as a sanitizer in the United States on food contact surfaces (Code of Federal Regulations 21 Part 178.1010) and for direct food contact with meat, poultry and seafood (Code of Federal Regulations 21 Part 173.310) at maximum concentrations of 80 and 110 ppm, respectively. In 2007, the U.S. Food and Drug Administration certified PAA for use as disinfectants in ice and wash water during the commercial preparation of fish and seafood, with a maximum allowed presence of PAA not exceeding 190 ppm (Food Contact Substance Notification FCN 000699). Since 2009, PAA has been legislatively restricted by Food Standards Australia New Zealand, with a limit of 0.7 mg/kg PAA allowed in food products (Australia New Zealand Food Standards F2009C00360). Followingly, the European Food Safety Agency (EFSA) accepts the use of PAA on poultry meat as effective against *Escherichia coli*, *Salmonella* and *Campylobacter* spp., with potential for use in seafood environments (EFSA, 2014).

Although PAA has the potential to control microorganisms in the seafood industry, there remain gaps. The objective of this study was to investigate the efficacy of PAA in reducing *V. parahaemolyticus* as planktonic cells and as biofilms grown on Greenshell™ mussels and food contact surfaces. Understanding the action of PAA on *V. parahaemolyticus* that may occur in the seafood processing environment will assist in the development of effective hygiene strategies.

2. Material & Methods

2.1. V. parahaemolyticus isolates

Ten *V. parahaemolyticus* strains were chosen for this investigation (Table 1). Seven of them were isolated from shellfish (mussels and oysters) by Plant and Food Research Ltd. (Cruz et al., 2015), two were provided by the Institute of Environmental Science and Research Ltd., as pathogens, and the *V. parahaemolyticus* reference strain RIMD2210633 was kindly offered by Dr. Tetsuya Iida from Research Institute for Microbial Diseases in Osaka, Japan. According to the previous study (Wang et al., 2023b), two strains, PFR30J09 and PFR34B02 were proven to be strong biofilm formers and least susceptible to chlorine treatment, whereas PFR21C03 and PFR37D08 were weak biofilm forming strains. Isolates from −80 °C bead storage (Protect™, Thermo Fisher Scientific, USA) were recovered by incubating in 3 % NaCl tryptic soy broth (TSB; Difco™, Becton, Dickson and Company, France) with shaking at 37 °C, 120 rpm. The cells were then centrifuged (8425 ×*g*, 5 min) to obtain a cell pellet, that was washed and suspended in sterile phosphate buffered saline (PBS) for further use.

2.2. Food contact surface inoculation and biofilm formation

Stainless steel coupons (10 mm^2, 1 mm thick, 304 grade with a 2B finish; Advanced Sheetmetals, New Zealand) were prepared by soaking in 99.5 % acetone for 12 h, rinsing with distilled water, followed by immersion in alkaline detergent 1 % NaOH (w/v, pH ~13.0; Merck KGaA, Darmstadt, Germany) for 1 h and rinsing again with distilled water. The coupons were cleaned using an ultrasonic cleaner (DT52; BANDELIN, Berlin, Germany) for 60 min, rinsed with distilled water, left to dry and sterilized by dry cycle autoclaving at 121 °C for 15 min. Coupons were freshly prepared for each set of experiments.

A coupon was placed in each well of a 24-well plate (FALCON®, Corning Incorporated, Durham, USA), containing 1 mL of 3 % NaCl TSB with *V. parahaemolyticus* inoculum at a concentration of ~4.00 $\log_{10}$ CFU/mL. The 24-well plates were placed in a static incubator for 6 h at 25 °C for biofilm growth.

2.3. Mussel shell surface inoculation and biofilm formation

Mussel shell surfaces were prepared according to a previous study with minor modifications (Fletcher and Statham, 1988). Briefly, the mussel shell surfaces were freshly cut into regular pieces (1.5 cm × 4 cm) using a disc grinder, washed with sodium carbonate (w/v, 2 %; LabServ™, Thermo Fisher Scientific, USA) to remove grime, slime and naturally formed biofilms, and then immersed in 70 % ethanol to sanitize for 1 h. The mussel shell surfaces were thoroughly washed with sterile saline (0.85 % NaCl) to remove residual ethanol. This treatment was applied for each set of experiments.

Each shell surface was placed upright in a 20 mL sterilized flask containing 5 mL of 3 % NaCl TSB with *V. parahaemolyticus* inoculum at a concentration of ~4.00 $\log_{10}$ CFU/mL (Determination of absorbance based on modelled linear relationship between absorbance of 595 nm and CFU plate counting). The flasks were placed in a static incubator for 6 h at 25 °C for biofilm growth.

Table 1
Vibrio parahaemolyticus strains examined in this study.

No.	Strain	Source	Pathogenicity	Collection date	Country	Reference
1	PFR21C03	Pacific oyster	Non-pathogenetic	16/02/2009	New Zealand	(Cruz et al., 2015)
2	PFR24B07	Greenshell™ mussel	Non-pathogenetic	2/03/2010	New Zealand	
3	PFR29A04	Pacific oyster	Non-pathogenetic	22/11/2010	New Zealand	
4	PFR30G02	Pacific oyster	Non-pathogenetic	8/03/2011	New Zealand	
5	PFR30J09	Pacific oyster	Non-pathogenetic	21/03/2011	New Zealand	
6	PFR34B02	Pacific oyster	Non-pathogenetic	27/03/2012	New Zealand	
7	PFR37C06	Pacific oyster	Non-pathogenetic	17/01/2013	New Zealand	
8	PFR37D08	Clinical	Pathogenetic	1/01/2013	New Zealand	
9	PFR37E03	Clinical NZRM 3391	Pathogenetic	1/01/1975	New Zealand	
10	RIMD2210633	Clinical	Pathogenetic	1996	Japan	(Makino et al., 2003)

2.4. Preparing PAA solutions and measuring their concentrations

Commercial PAA (ECOLAB, Hamilton, New Zealand), which contains hydrogen peroxide (10–30 %, CAS-No. 7722-84-1), acetic acid (5–10 %, CAS-No. 64-19-7) and peracetic acid (1–5 %, CAS-No. 79-21-0), was used in this study. The recommended dilution ranges from 0.2 % to 2.0 %. PAA solution were prepared and used within 20 min.

The actual PAA and H_2O_2 concentrations in the commercial preparation were determined using iodometric titrations. For PAA, hydrogen peroxide was first degraded with catalyse (Terminox®, Novozymes A/S, Denmark) followed by titration with sodium thiosulfate. Specifically, a 10 μL PAA sample was diluted with 10 mL of distilled water and kept at 4 °C. After adding 10 mL of Buffer solution A (5.014 g of $Na_2HPO_4{\cdot}12H_2O$, ScharLab®, Spain; 4.627 g of KH_2PO_4, Merck, Germany; 0.061 g of EDTA in 1000 mL H_2O) at pH 5.5, the sample was vortexed for 60s. Next, 15 mL of 12 N sulphuric acid (97 %; J.T. Baker®, Avantor, UK) and 15 mL of 166 g/L potassium iodide (Merck, Darmstadt, Germany) solution were added, and the solution was kept in the dark for 20 min. The solution was titrated with 1 % w/v sodium thiosulfate (AnalaR®, BDH, UK) using starch as an indicator, titrating until the blue colour disappeared. The consumption of sodium thiosulfate solution corresponds to the concentration of PAA according to the following equation.

$$C_{PAA} = \frac{N_{Na_2SO_3} \times V_{Na_2SO_3} \times EW_{PAA} \times 1000}{V_{PAA}}$$

where C_{PAA} is the PAA concentration in commercial products (mg/L); $N_{Na_2SO_3}$ is the normality of the thiosulfate solution; $V_{Na_2SO_3}$ is the titration volume of sodium thiosulfate solution required (Jonas et al.); EW_{PAA} is the PAA equivalent weight; and V_{PAA} is the volume of commercial PAA diluted solution (Jonas et al., 2010).

To determine the H_2O_2 concentrations, 10 mL of 10 % chilled sulphuric acid was added to 10 μL of the PAA sample and then diluted with 10 mL of distilled water. Next, 3 drops of 0.025 mol/L Ferroin solution were added to the mixture and titrated using a 0.1 mol/L Ce^{+4} sulfate (UNIVAR®, Ajax Finechem, Australia) solution until the colour turned from orange to blue.

The determination of residual PAA and H_2O_2 was based on the *N,N*-diethyl-*p*-phenylendiamine sulfate salt (DPD; BDH, UK) photometric method, as reported by Liu et al. (2015) with minor modifications. PAA (100 μL) was mixed with 50 μL of Buffer solution B (30.25 g of $Na_2HPO_4{\cdot}12H_2O$; 23 g of KH_2PO_4; 0.01 g of NaCl; and 0.5 g of KI, UNIVAR®, Ajax Finechem, Australia in 1000 mL of H_2O), and then 50 μL of DPD solution (1.6 g of DPD; 200 μL of 97 % H_2SO_4; and 0.02 g of EDTA in 100 mL of H_2O) was added. The absorption at 550 nm was measured after 30 s using a spectrophotometer (SpectrostarNano, BMG Labtech, Ortenberg, Germany). To measure residual H_2O_2, the same procedure was used, but Buffer solution C, with 5 mg of peroxidase from horseradish, was applied instead of Buffer solution B to determine total peroxide. The absorption at 550 nm was measured after 30 s using a spectrophotometer.

2.5. Disinfectant treatment

To determine the susceptibility of planktonic *V. parahaemolyticus* cells to PAA, sterilized 96-well polystyrene plates (FALCON®, Corning Incorporated, Durham, USA) were loaded with a cell suspension (~8.00 $\log_{10}$ CFU/mL, 100 μL) in saline (0.85 %), along with 100 μL of PAA solution. After a 5-min exposure, the solution was neutralised with 50 μL of 1 % sodium thiosulfate. To test the susceptibility of biofilms, stainless steel coupons or mussel shell surfaces containing pre-formed biofilm were placed into 1 mL of PAA solution. After 5 min, they were transferred to 1 % sodium thiosulfate to neutralise the disinfectant. Each experiment included positive and negative controls.

2.6. Detachment of biofilm populations

The number of viable cells in the biofilm was examined using a glass bead vortex mixing method (Hayrapetyan et al., 2015), with minor modifications. Coupons/surfaces with cultured biofilm cells were gently washed using sterile distilled water to remove planktonic cells and aseptically transferred to bottles with sterile glass beads (D = 3–5 mm; Sigma-Aldrich®, Merck, Darmstadt, Germany) and 0.1 % buffered peptone water which includes 1 % NaCl (Difco™, Becton, Dickson and Company, France), followed by 1 min of vortex mixing to detach biofilm cells from the surfaces. Serial 10-fold dilutions of the solution containing detached biofilm cells were prepared in 0.1 % buffered peptone water and spread-plated on 3 % NaCl tryptic soy agar (TSA; Difco™, Becton, Dickson and Company, France) plates, and then incubated at 37 °C for 18 h.

2.7. Identification of functional genes for strong biofilm formation

The Centre for Environment, Fisheries, and Aquaculture Science (CEFAS) did the DNA extraction, library construction and whole genome sequencing of *V. parahaemolyticus* using MiSeq with a coverage of 40–120× (Baker-Austin et al., 2020). Clean reads were used for de novo assembly and annotation via the Bactopia pipeline using Velvet and SPADES as the assembler (Petit 3rd and Read, 2020). The quality of assembled contigs were assessed using QUAST and CheckM (Gurevich et al., 2013; Parks et al., 2015). The draft genomes were submitted to NCBI GenBank under the BioProject PRJNA808748.

The amino acid sequences of all *V. parahaemolyticus* candidates were analysed using Roary version 3.13.0 with MAFFT as the alignment tool. Comparative analysis of these genomes was presented using a Flower plot. Kyoto Encyclopedia of Genes and Genomes (KEGG) pathway analysis was conducted using BlastKOALA (https://www.kegg.jp/blastkoala/). The variances in KEGG pathways across strong biofilm-forming strains (PFR30J09 and PFR34B02) and the reference strain (RIMD2210633) of *V. parahaemolyticus* were visualized using ggplot2 (version 3.4.0).

2.8. Data analysis

Viable colony counts of cells were enumerated and transformed as $\log_{10}$ CFU/mL or $\log_{10}$ CFU/cm^2. The mean and standard deviation (SD) for *V. parahaemolyticus* cell counting was based on three biological replicates and three technical replicates. One-way analysis of variance (ANOVA) with a *t*-test ($p < 0.05$) indicated significance of the results. Principle component analysis (PCA) was used to compare biofilm cell resistance against commercial PAA, the analysis was conducted using XLSTAT-Premium software (version 19.3).

3. Results and discussion

3.1. Efficacy of PAA against planktonic V. parahaemolyticus cells

Fig. 1 displays the effect of PAA on planktonic *V. parahaemolyticus*. The control cells of planktonic *V. parahaemolyticus* ranged from 7.27 $\log_{10}$ CFU/mL to 7.84 $\log_{10}$ CFU/mL. The concentrations of PAA ranged from 5 to 50 ppm. A concentration of 5 ppm produced a <2.00 $\log_{10}$ CFU/mL reduction. At 15 ppm, there was an average cell decrease of 2.70 ± 0.40 (mean ± SD) $\log_{10}$ CFU/mL. PAA of 35 ppm resulted in an average cell reduction of 4.76 ± 0.38 $\log_{10}$ CFU/mL. At 50 ppm PAA, there were no viable cells detected, indicating a cell reduction of >7.00 $\log_{10}$ CFU/mL (with a 1.00 $\log_{10}$ CFU/mL detection limit, Fig. 1).

3.2. Efficacy of PAA against V. parahaemolyticus on stainless steel coupons

Fig. 2 illustrates the effectiveness of PAA in reducing

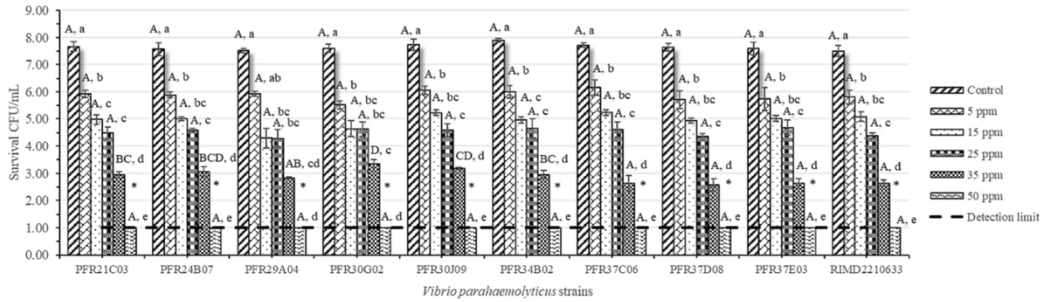

Fig. 1. The efficacy of peroxyacetic acid (PAA) for the inactivation of planktonic *V. parahaemolyticus* cells. The detection limit was 1.00 $\log_{10}$ colony forming units (CFU)/mL. * indicates no detectable cells after exposure of *V. parahaemolyticus* to 50 ppm PAA for 5 min. The means followed by different letters are significantly different ($p < 0.05$), the upper-case letters presented significant difference within species, the lower-case letters presented significant difference after treatment using PAA of different concentrations within the strain.

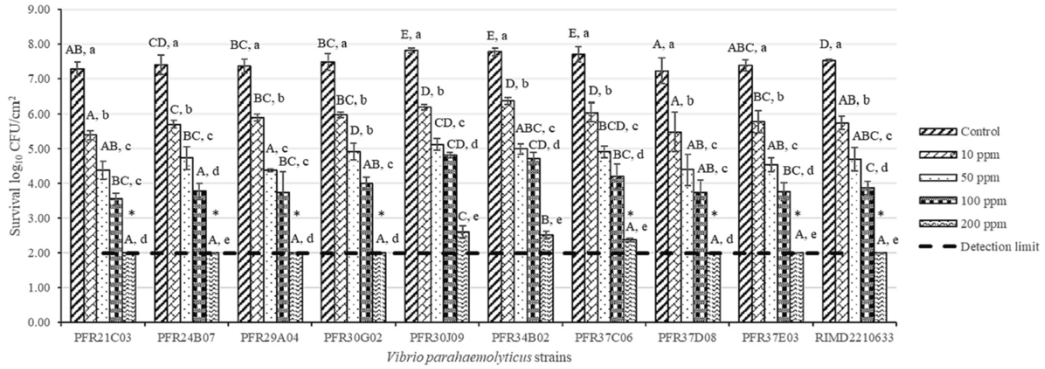

Fig. 2. The efficacy of PAA for the inactivation of *V. parahaemolyticus* on stainless steel coupons. The detection limit was 2.00 $\log_{10}$ colony forming units (CFU)/cm^2. The means followed by different letters are significantly different ($p < 0.05$), the upper-case letters presented significant difference within species, the lower-case letters presented significant difference after treatment using PAA of different concentrations within the strain.

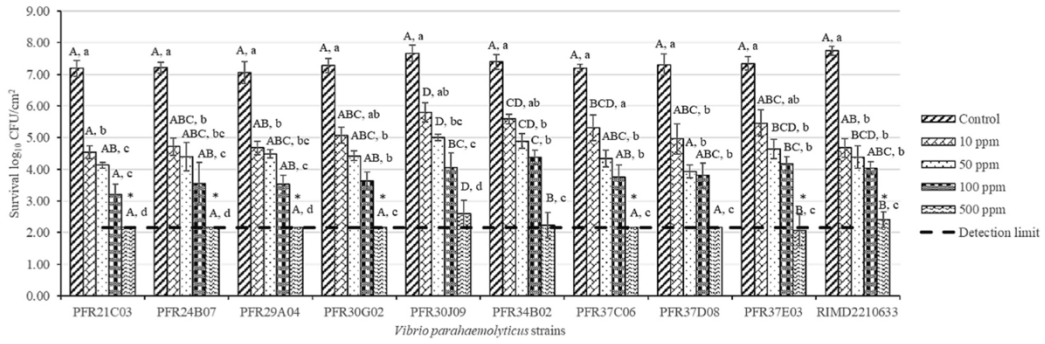

Fig. 3. The efficacy of PAA for the inactivation of *V. parahaemolyticus* on mussel shell surfaces. The detection limit was 2.17 $\log_{10}$ colony forming units (CFU)/cm^2. The means followed by different letters are significantly different ($p < 0.05$), the upper-case letters presented significant difference within species, the lower-case letters presented significant difference after treatment using PAA of different concentrations within the strain.

V. parahaemolyticus biofilms grown on stainless steel surfaces. *V. parahaemolyticus* biofilm cells averaged 7.50 ± 0.21 $\log_{10}$ CFU/cm^2 in the untreated control. PAA of 10 ppm, produced log reductions ranging from 1.86 to 2.06 $\log_{10}$ CFU/cm^2. The average cell numbers decreased by 2.80 ± 0.52 $\log_{10}$ CFU/cm^2 after treatment with 50 ppm PAA. High biofilm cell reduction was recorded for 100 ppm PAA treatment, averaging of 3.19 ± 0.44 $\log_{10}$ CFU/cm^2. Cell reductions after PAA treatment using 200 ppm, were over 5.00 $\log_{10}$ CFU/cm^2 (undetectable) for most strains. However, the two strongest biofilm formers (PFR30J09 and PFR34B02) still showed average cell numbers of 2.60 and 2.52 $\log_{10}$ CFU/cm^2, respectively, indicating that concentrations exceeding 200 ppm of PAA are required to inactivate their biofilm communities.

3.3. Efficacy of PAA against V. parahaemolyticus on mussel shell surfaces

Fig. 3 shows the effect of PAA on *V. parahaemolyticus* biofilm cells formed on mussel shell surfaces. The average cell number of biofilm formed on mussel shell surfaces was 7.34 ± 0.21 $\log_{10}$ CFU/cm^2. The removal of viable cells was 1.42 ± 0.29, 2.18 ± 0.32 and 2.54 ± 0.32 $\log_{10}$ CFU/cm^2 after PAA treatment with concentrations of 10, 50 and 100 ppm, respectively. Higher PAA concentrations were required to inactivate *V. parahaemolyticus* biofilms on mussel shell than on stainless steel surfaces; 500 ppm of PAA was required to inactivate >5.00 $\log_{10}$ CFU/cm^2 biofilm cells from mussel shell surfaces whereas 200 ppm was required to achieve a similar reduction on stainless steel coupons. Four biofilm formers (PFR30J09, PFR34B02, PFR37D08 and RIMD2210633) were still detected after treatment with 500 ppm of PAA. The pathogenic strains RIMD2210633 and PFR37E03 showed greater biofilm community viability on mussel surfaces rather than on stainless steel coupons, suggesting that additional protection may be associated with pathogenic *V. parahaemolyticus* biofilm cells.

3.4. PAA sanitizer residues following biofilm treatment

The original concentrations of peracetic acid and hydrogen peroxide in commercial PAA were titrated as 44.78 ± 6.01 g/L and 235.82 ± 6.37 g/L, respectively. Via absorbance screen of diluted commercial PAA, the linear relationship between peracetic acid concentration (x axis) and OD_{550} (y axis) was $y = 0.0373x + 0.0694$ ($R^2 = 0.9436$), the one between H_2O_2 (x axis) and OD_{550} (y axis) was $y = 0.1032x + 0.2655$ ($R^2 = 0.998$). The residues of peracetic acid and hydrogen peroxide in different dilutions of commercial PAA following biofilm treatment are listed in Tables 2 and 3. The residue concentrations were higher for the PAA treatment of robust biofilm communities of PFR30J09 and PFR34B02, indicating less diffusion into these biofilm matrices and lower effectiveness of the sanitizers.

3.5. Identification of functional genes for robust biofilm formation

PCA analysis revealed that PFR30J09 and PFR34B02 had distinct biofilm communities in terms of PAA resistance compared to the other strains (Fig. 4a). This is in accordance with the results from a previous study, that these two strains are strong biofilm forming strains of *V. parahaemolyticus*. According to comparative analysis of the genomes in Fig. 4b, there are 3854 core genes shared by these ten *V. parahaemolyticus* candidate strains, with PFR30J09 having 778 shell genes and 282 unique genes, while PFR34B02 had 765 shell genes and 239 unique genes, the reference strain RIMD2210633 had 481 shell genes and 240 unique genes. KEGG analysis was used to compare functional variances based on the shell genes and unique genes in *V. parahaemolyticus*. Fig. 4c and Supplemental Table 1 show that PFR30J09 and PFR34B02 had more genes in certain functional pathways, such as metabolic pathways, microbial metabolism in diverse environments, degradation of aromatic compounds, pentose and glucuronate interconversions, amino sugar and nucleotide sugar metabolism, fructose and mannose metabolism, benzoate degradation, xylene degradation, dioxin degradation and mismatch repair. RIMD2210633, being the pathogenetic strain, had more gene counts in the pathway of polyketide sugar unit biosynthesis, bacterial secretion system and flagellar assembly.

4. Discussion and conclusion

In this PAA trial, PAA of 50 ppm resulted in a planktonic cell reduction of >7.00 $\log_{10}$ CFU/mL when initial *V. parahaemolyticus* cells averaged 7.64 $\log_{10}$ CFU/mL. Wong et al. (2018) reported PAA at a concentration above 5 ppm (65.75 μM) was bactericidal to the wild-type *V. parahaemolyticus* strain, KX-V231, and using 5, 7.5 or 15 ppm of PAA resulted in the killing of about 1.00, 2.00 or 4.50 $\log_{10}$ CFU/mL of planktonic cells, respectively. However, the exposure time of PAA in this study was only 5 min, which is much shorter than the one-hour exposure time reported by Wong et al. (2018). This may explain why different effective PAA concentrations for killing planktonic *V. parahaemolyticus* strains were reported between the two studies. Little is known about PAA treatment to *V. parahaemolyticus* biofilm communities. In this study, the difference in sensitivity between planktonic and biofilm cells to PAA treatments demonstrated biofilm matrices lowered the cell susceptibility to the sanitization. Moreover, higher PAA concentrations were required to remove *V. parahaemolyticus* biofilm cells on biotic mussel shell surfaces compared to abiotic stainless steel in this study, with 500 ppm required to inactivate >5.00 $\log_{10}$ CFU/cm^2 biofilm cells on mussel shell surfaces and 200 ppm required for a similar log reduction on stainless steel coupons. This may be due to the chitin−/other nutrient sources in the mussel shell, the pits, edges, and the activation of genes responsible for promoting distinctive biofilm formation in seafood environments.

Table 2
Residues after treating biofilms formed on stainless steel coupons.

PAA dilution	PAA residue (mg/L)*				H_2O_2 residue (mg/L)*			
	200 ppm	100 ppm	50 ppm	10 ppm	200 ppm	100 ppm	50 ppm	10 ppm
PFR21C03	$1.88^{AB, a} \pm 0.16$	$1.77^{A, a} \pm 0.17$	$1.29^{AB, b} \pm 0.16$	$0.25^{ABC, c} \pm 0.16$	$18.27^{BC, a} \pm 0.37$	$17.9^{A, b} \pm 0.61$	$6.79^{A, c} \pm 0.08$	$1.7^{A, d} \pm 0.08$
PFR24B07	$2^{AB, a} \pm 0.17$	$1.8^{A, ab} \pm 0.18$	$1.61^{B, b} \pm 0.35$	$0.16^{ABC, c} \pm 0.17$	$21.6^{BC, a} \pm 0.62$	$18.93^{A, b} \pm 0.49$	$6.47^{AB, c} \pm 0.34$	$1.66^{AB, d} \pm 0.07$
PFR29A03	$2.75^{C, a} \pm 0.44$	$2.35^{B, ab} \pm 0.28$	$2.01^{C, b} \pm 0.2$	$0.09^{ABC, c} \pm 0.15$	$21.51^{D, a} \pm 0.61$	$18.74^{C, b} \pm 0.12$	$6.52^{AB, c} \pm 0.23$	$1.48^{ABC, d} \pm 0.06$
PFR30G02	$3.29^{D, a} \pm 0.17$	$2.8^{C, b} \pm 0.25$	$2.07^{C, c} \pm 0.16$	$0.3^{BC, d} \pm 0.15$	$21.1^{CD, a} \pm 1.9$	$18.49^{A, a} \pm 1.17$	$6.13^{BC, b} \pm 0.07$	$1.46^{BCD, d} \pm 0.17$
PFR30J09	$4.16^{E, a} \pm 0.33$	$3.36^{D, b} \pm 0.3$	$2.48^{D, c} \pm 0.22$	$0.4^{D, d} \pm 0.16$	$23.85^{AB, a} \pm 0.87$	$19.22^{B, b} \pm 4.53$	$6.12^{BC, c} \pm 0.15$	$1.22^{EF, d} \pm 0.05$
PFR34B02	$5.4^{F, a} \pm 0.21$	$5.33^{E, a} \pm 0.16$	$3.04^{E, b} \pm 0.4$	$0.71^{E, c} \pm 0.14$	$24.49^{A, a} \pm 0.98$	$19.09^{A, b} \pm 0.17$	$6.44^{AB, c} \pm 0.18$	$1.48^{ABC, d} \pm 0.05$
PFR37C06	$2.03^{AB, a} \pm 0.18$	$1.62^{A, b} \pm 0.15$	$1.23^{AB, c} \pm 0.15$	$0.38^{C, d} \pm 0.19$	$19.46^{CD, a} \pm 0.77$	$17.27^{B, b} \pm 0.15$	$5.23^{D, c} \pm 0.2$	$1.5^{ABC, d} \pm 0.06$
PFR37D08	$1.79^{A, a} \pm 0.13$	$1.63^{A, a} \pm 0.15$	$0.99^{A, b} \pm 0.14$	$0^{A, c} \pm 0.14$	$18.83^{CD, a} \pm 3.02$	$17.82^{A, a} \pm 1.18$	$5.99^{BC, b} \pm 0.4$	$1.06^{F, d} \pm 0.25$
PFR37E03	$2.21^{B, a} \pm 0.16$	$1.71^{A, b} \pm 0.14$	$1.23^{AB, c} \pm 0.14$	$0.13^{ABC, d} \pm 0.16$	$17.41^{D, a} \pm 0.96$	$18.09^{A, a} \pm 0.84$	$5.78^{CD, b} \pm 0.32$	$1.36^{CDE, d} \pm 0.06$
RIMD2210633	$2.11^{AB, a} \pm 0.16$	$1.53^{A, b} \pm 0.22$	$1.15^{A, c} \pm 0.19$	$0.03^{AB, d} \pm 0.21$	$17.33^{D, a} \pm 2.07$	$16.55^{AB, a} \pm 2.59$	$6.45^{AB, b} \pm 0.63$	$1.24^{DEF, d} \pm 0.14$

* Within the same examined strains, means not followed by the same letter are significantly different ($p < 0.05$). The upper-case letters presented significant difference within species, the lower-case letters presented significant difference after treatment using PAA of different concentrations within the strain.

Table 3
Residues after treating biofilms formed on Greenshell™ mussel shell surfaces.

PAA dilution	PAA residue (mg/L)*				H_2O_2 residue (mg/L)*			
	500 ppm	100 ppm	50 ppm	10 ppm	500 ppm	100 ppm	50 ppm	10 ppm
PFR21C03	$5.62^{A,\ a} \pm 0.55$	$2.13^{A,\ a} \pm 1.21$	$1.61^{A,\ a} \pm 2.32$	$0.46^{A,\ b} \pm 0.87$	$47.51^{AB,\ a} \pm 2.76$	$24.3^{C,\ b} \pm 0.86$	$15.52^{AB,\ c} \pm 0.34$	$1.49^{A,\ d} \pm 0.04$
PFR24B07	$5.86^{D,\ a} \pm 0.13$	$2.35^{D,\ b} \pm 0.07$	$1.1^{CD,\ b} \pm 0.14$	$0.82^{C,\ c} \pm 0.02$	$51.37^{AB,\ a} \pm 3.73$	$25.13^{C,\ b} \pm 0.74$	$16.01^{A,\ c} \pm 0.49$	$1.49^{A,\ d} \pm 0.04$
PFR29A03	$7.37^{D,\ a} \pm 0.09$	$3.19^{DE,\ b} \pm 0.03$	$0.92^{CD,\ c} \pm 0.02$	$0.55^{C,\ d} \pm 0.04$	$51.13^{AB,\ a} \pm 2.81$	$24.54^{C,\ b} \pm 0.83$	$15.36^{B,\ c} \pm 0.2$	$1^{B,\ d} \pm 0.02$
PFR30G02	$8.45^{B,\ a} \pm 1$	$3.73^{DE,\ b} \pm 0.07$	$2.85^{B,\ b} \pm 0.48$	$0.73^{A,\ a} \pm 3.74$	$51.72^{AB,\ a} \pm 3.64$	$29.54^{B,\ b} \pm 0.3$	$11.88^{C,\ c} \pm 0.15$	$1.63^{C,\ d} \pm 0.04$
PFR30J09	$10.18^{C,\ a} \pm 0.44$	$4.4^{B,\ b} \pm 0.24$	$3.35^{B,\ c} \pm 0.22$	$0.85^{B,\ c} \pm 0.16$	$53.63^{AB,\ a} \pm 1.51$	$29.79^{AB,\ b} \pm 0.53$	$11.72^{C,\ c} \pm 0.15$	$1.72^{C,\ d} \pm 0.04$
PFR34B02	$12.52^{D,\ a} \pm 0.17$	$6.86^{C,\ b} \pm 0.17$	$4.02^{BC,\ b} \pm 0.1$	$1.22^{BC,\ c} \pm 0.09$	$51.38^{AB,\ a} \pm 4.45$	$30.84^{A,\ b} \pm 0.28$	$12.03^{C,\ c} \pm 0.12$	$1.88^{D,\ d} \pm 0.03$
PFR37C06	$5.92^{E,\ a} \pm 0.11$	$2.31^{G,\ b} \pm 0.08$	$1.84^{D,\ b} \pm 0.1$	$0.82^{C,\ b} \pm 0.15$	$46.88^{B,\ a} \pm 3.36$	$17.92^{DE,\ b} \pm 0.3$	$11.53^{C,\ c} \pm 0.4$	$0.9^{E,\ d} \pm 0.05$
PFR37D08	$5.44^{EF,\ a} \pm 0.07$	$2.33^{FG,\ b} \pm 0.05$	$1.56^{D,\ b} \pm 0.18$	$0.35^{C,\ b} \pm 0.08$	$46.3^{B,\ a} \pm 2.03$	$18.89^{D,\ b} \pm 0.73$	$11.69^{C,\ b} \pm 0.19$	$1.06^{B,\ d} \pm 0.03$
PFR37E03	$6.29^{E,\ a} \pm 0.07$	$2.42^{DE,\ b} \pm 0.11$	$1.85^{CD,\ b} \pm 0.29$	$0.52^{C,\ c} \pm 0.11$	$48.6^{AB,\ a} \pm 0.8$	$17.71^{E,\ b} \pm 0.6$	$10.69^{D,\ b} \pm 0.08$	$0.58^{F,\ d} \pm 0.1$
RIMD2210633	$6.08^{F,\ a} \pm 0.41$	$2.2^{FG,\ b} \pm 0.1$	$1.75^{D,\ c} \pm 0.08$	$0.41^{C,\ d} \pm 0.1$	$46.62^{B,\ a} \pm 3.99$	$15.69^{E,\ b} \pm 0.54$	$6.68^{E,\ b} \pm 0.3$	$0.26^{G,\ d} \pm 0.09$

* Within the same examined strains, means not followed by the same letter are significantly different ($p < 0.05$). The upper-case letters presented significant difference within species, the lower-case letters presented significant difference after treatment using PAA of different concentrations within the strain.

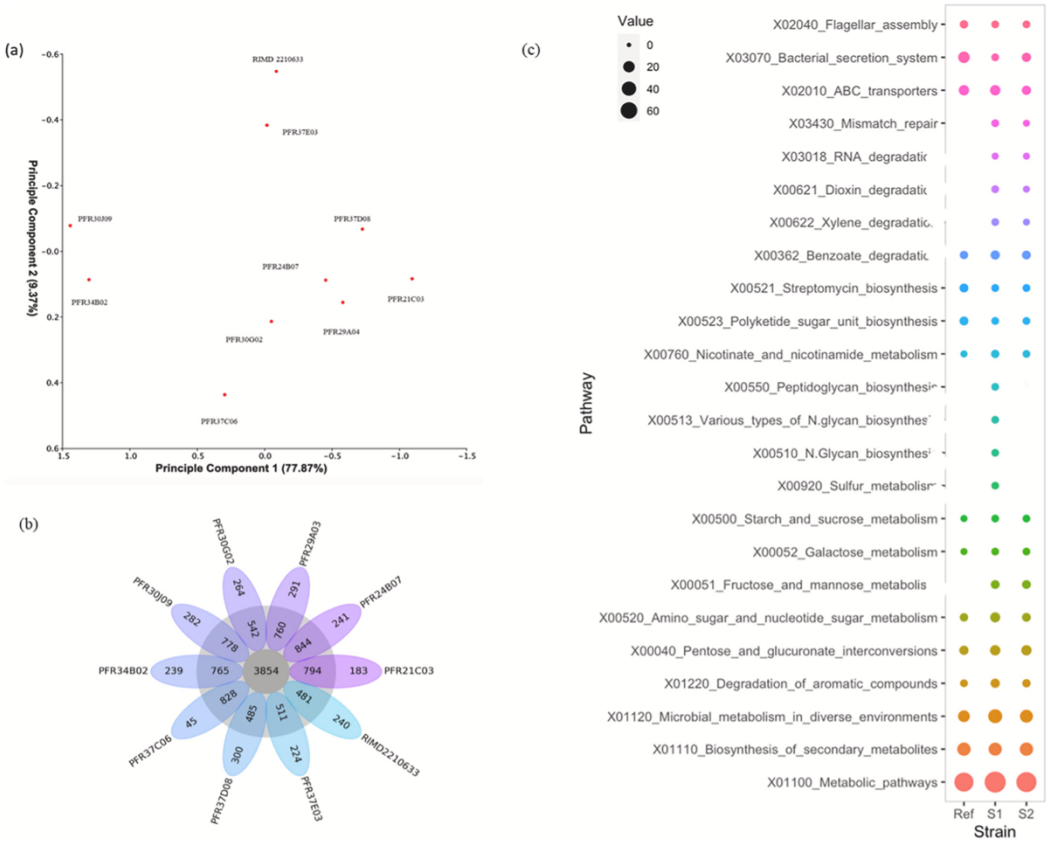

Fig. 4. Distinctive patterns of PAA resistance of *V. parahaemolyticus* biofilm cells and determination of the functional genes in these substrate-dependant resistance pathogens. (a) PCA analysis results of PAA resistance in various *V. parahaemolyticus* biofilm cells. (b) Pangenome analysis of *V. parahaemolyticus* candidate strains. (c) KEGG annotation for shell and unique genes from strong biofilm forming strains (S1: PFR30J09, S2: PFR34B02) and reference strain RIMD2210633, respectively. Multiple colours represent different KEGG pathways, round shape size represents gene count values.

Microorganisms of different species are known to vary in their sensitivity to sanitisers. Wang et al. (2020) reported that *Mycobacterium psychrotolerans* was reduced to undetectable levels (<1.70 $\log_{10}$ CFU/mL) with 20 ppm PAA treatment for 5 min, while 40 ppm for 1 min inactivated the cells to undetectable levels. In another study, 80 ppm of PAA exposure for 5 min was reported to inactivate *E. coli* O157:H7

(Rodgers et al., 2004). PAA at 90 ppm is the minimum inhibitory concentration for planktonic *Salmonella* Thompson (Nahar et al., 2022). Melchior et al. (2007) indicated inactivation of cells in a biofilm depends on the sensitivity of each strain in the biofilm. For *Listeria monocytogenes* biofilms formed on polystyrene and stainless steel, PAA of 2000 ppm reduced the biofilm cells by 2.80 $\log_{10}$ CFU/cm^2 and 3.50 $\log_{10}$ CFU/cm^2, respectively (Poimenidou et al., 2016). The use of a wide collection of strains for the assessment of the bactericidal activity of disinfectants seems to be necessary to ensure the optimal concentration is used, and the precise concentrations of PAA and H_2O_2 should be detailed.

PAA has shown potential for use in seafood or other meat related environments. For example, Thi et al. (2015) reported that 50 ppm of PAA (240 s exposure) decreased *E. coli* levels below the detection level (<1.00 $\log_{10}$ CFU/g) on *Pangasius* fillets. Wang et al. (2020) reported that 80 ppm PAA on saury (*Cololabis saira*) surfaces, for 1 min led to a 0.50 $\log_{10}$ CFU/cm^2 reduction in *M. psychrotolerans*, while a 5 min exposure time decreased the biofilm by 2.23 $\log_{10}$ CFU/cm^2. PAA treatment also has the potential to extend shelf life of stored fish at 4 °C (Wang et al., 2020). Similar results have been reported in poultry: the treatment of beef with 200 ppm PAA delayed the onset of spoilage by 7, 21, and 54 days at 4, 2, and −1 °C, respectively (Yang et al., 2021).

PAA has generally been found to be a more effective disinfectant than sodium hypochlorite against planktonic cells of various microorganisms (Vázquez-Sánchez et al., 2014). However, Alasri et al. (1992) investigated the biocidal activity of some disinfectants against *E. coli*, *Pseudomonas aeruginosa* and *Staphylococcus aureus*, and found that chlorine (sodium hypochlorite) was more effective than PAA, even when the latter was considered in combination with H_2O_2. Comparing the sodium hypochlorite effective concentration in inactivating *V. parahaemolyticus* biofilm cells with that reported in a previous study, PAA at 200 ppm was more effective in reducing cells to non-detectable levels for 80 % of strains from stainless steel coupons whereas sodium hypochlorite could not achieve this result (Wang et al., 2023b). In a similar research reported on biofilms of *E. coli*, *Salmonella Typhimurium* and *L. monocytogenes*, exposure to 100 ppm of sodium hypochlorite and PAA reduced biofilms cells by 0.50 to 3.63 and 2.83 to 5.78 $\log_{10}$ CFU/coupon (5 cm × 2 cm), respectively (Park et al., 2012).

Oxidizing disinfectants kill pathogens by oxidizing the cell wall and causing lysis, or by diffusing through the cell wall and oxidizing the intracellular material (United States Environmental Protection Agency EPA 832-F-12-030). PAA treatment of *M. psychrotolerans* cells was found to cause damage to the cell membrane and cell surface without damaging chromosomal DNA and protein profiles, suggesting a mechanism involving oxidative damage (Wang et al., 2020). Although the mechanisms of planktonic *V. parahaemolyticus* resistance to PAA are not fully understood, it is believed that the accumulation of reactive oxygen species and the presence of catalase genes *katE1* and *katE2* contribute to resistance (Wong et al., 2018). In this study, the resistance of robust biofilm matrices and physiological heterogeneity across strains may have contributed to variances in resistance. The identified variations in metabolic pathways within robust and weak biofilm-forming strains could explain mechanisms induced by sanitization in *V. parahaemolyticus*. Related results have been reported in recent studies. Wang et al. (2023a) identified that chlorine sanitization induced *E. coli* on pea sprouts into a VBNC state with differentiated metabolic pathways and metabolite contents (culturable counterparts as the control). The metabolic pathways of amino acid, organic acids, sugars, alcohol and nucleotide derivatives contributed to the dormancy and stronger resistance against sanitizers. Electrolyzed water acts as a sanitizer containing high oxidative and chlorine components. Electrolyzed water (4 mg/L free available chlorine) in addition with 50 °C heat treatment induced a reduction of *E. coli* by 2.31 $\log_{10}$ CFU/mL. Liu et al. (2020), through metabolomic analysis, demonstrated discriminative metabolic pathways of amino acid metabolism, nucleotide synthesis as well as lipid biosynthesis resulting in cell adaptation and stress response against the electrolyzed water and mild heat treatment in *E. coli* O157:H7. Another study showed the antimicrobial mechanisms of chlorine against *E. coli* biofilms (formed on stainless steel and high-density polyethylene surfaces) based on metabolomic investigation. The altered pathways were associated with amino acid metabolism, energy metabolism, and anti-chlorine metabolism in response to oxidative and osmotic stressors (Lin et al., 2022).

In accordance with published research, this study pointed out associations between metabolism of biofilm cells and sanitizer resistance. However, how metabolite patterns vary with sanitization treatment time is not clear. Inactivation kinetics is a predictable approach to determine the efficacy of sanitizers over time on biofilm cells. Zhao et al. (2022) reported the inactivation kinetics against electrolysed water combined with ultrasound treatment. A modified Weibull model (R^2: 0.81–0.97; RMSE: 0.04–0.71) was in a good fit, providing detailed information during the decontamination process. This study also screened metabolite profiles of *E. coli* biofilm cells, showing that the ultrasound treatment disrupted nucleotide metabolism and the electrolyzed water suppressed pathways of nucleotide biosynthesis, amino acid biosynthesis and energy-associated metabolism, suggesting a decreasing presence of nucleotide-related compounds (e.g., uridine, ATP, ADP) and most carbohydrates.

The present study revealed mechanisms of sanitization on *V. parahaemolyticus* biofilm cells based on whole genome sequencing. Integrated omics may provide more detailed information to understand antimicrobial and antibiofilm activities of various sanitizers (Lin et al., 2023; Liu et al., 2023; Mao et al., 2022). A combination of transcriptomics, proteomics, and metabolomics will help support the verification of results from whole genome sequencing, particularly demonstrating how sanitization influences phenotypic expression. Further exploration is needed to understand how these genes cooperate in *V. parahaemolyticus* and how they are quantitatively regulated.

5. Conclusion

This study evaluated the efficacy of using commercial PAA to sanitize *V. parahaemolyticus* planktonic cells and biofilm cells formed on stainless steel and Greenshell™ mussel shell surfaces, mimicking the scenarios in the seafood industry. PAA of 50 ppm resulted in total inactivation (>7.00 $\log_{10}$ CFU/mL) of planktonic cells. PAA of 200 ppm reduced >5.00 $\log_{10}$ CFU/cm^2 biofilm cells from stainless steel surfaces for 80 % of *V. parahaemolyticus* strains. However, strong biofilm-forming strains showed decreased efficacy, indicating that biofilm matrices interfere with PAA diffusion and highlighting the need to screen for persistent *V. parahaemolyticus* in the seafood industry. PAA of 500 ppm was required to inactivate >5.00 $\log_{10}$ CFU/cm^2 biofilm cells from mussel shell surfaces, indicating lower efficacy on biotic surfaces. Overall, PAA was found effective in reducing the burden of food safety and public health risks associated with *V. parahaemolyticus* contamination.

Supplementary data to this article can be found online at https://doi.org/10.1016/j.ijfoodmicro.2023.110372.

CRediT authorship contribution statement

Dan Wang: Conceptualization, Methodology, Investigation, Formal analysis, Writing – original draft, review & editing; Steve Flint: Project administration, Resources, Supervision, Conceptualization, Methodology, Writing – review & editing. Graham Fletcher: Resources, Conceptualization, Methodology, Supervision, Writing – review & editing. Jon Palmer, Dragana Gagic & Stephen On: Conceptualization, Methodology, Supervision, Writing – review & editing.

- 0.05 % commercial PAA was required to inactivate biofilm cells from mussel shell surfaces, whereas 0.02 % PAA for biofilm cells removal from stainless steel surfaces.

- Robust biofilm formation and metabolic heterogeneity within niches might have contributed to the variations in PAA resistance of *V. parahaemolyticus* biofilms.

Declaration of competing interest

The authors declare no competing financial interests or personal relationships.

Data availability

Data will be made available on request.

Acknowledgement

Dr. Tetsuya Iida (Research Institute for Microbial Diseases, Osaka, Japan) kindly supplied the culture of genome reference strain RIMD 2210633. The authors are grateful to Jaime Martinez-Urtaza and Andy Powell of Centre for Environment, Fisheries, and Aquaculture Science (Cefas) who provided sequence data.

References

Alasri, A., Roques, C., Michel, G., Cabassud, C., Aptel, P., 1992. Bactericidal properties of peracetic acid and hydrogen peroxide, alone and in combination, and chlorine and formaldehyde against bacterial water strains. Can. J. Microbiol. 38, 635–642.

Baker-Austin, C., Stockley, L., Rangdale, R., Martinez-Urtaza, J., 2010. Environmental occurrence and clinical impact of *Vibrio vulnificus* and *Vibrio parahaemolyticus*: a European perspective. Environ. Microbiol. Rep. 2, 7–18.

Australia New Zealand Food Standards F2009C00360. Processing aids. Retrieved from. https://www.legislation.gov.au/Details/F2009C00360/.

Baker-Austin, C., Jenkins, C., Dadzie, J., Mestanza, O., Delgado, E., Powell, A., Bean, T., Martinez-Urtaza, J., 2020. Genomic epidemiology of domestic and travel-associated *Vibrio parahaemolyticus* infections in the UK, 2008–2018. Food Control 115, 107244.

CDC, 2021. The Cholera and Other *Vibrio* Illness Surveillance (COVIS) System. US Department of Health and Human Services.

Code of Federal Regulations 21 Part 173.310. Secondary direct food additives permitted in food for human consumption: boiler water additives.. Retrieved from. https://www.accessdata.fda.gov/scripts/cdrh/cfdocs/cfcfr/cfrsearch.cfm?fr=173.310.

Code of Federal Regulations 21 Part 178.1010. Substances utilized to control the growth of microorganisms: sanitizing solutions. Retrieved from. https://www.accessdata.fda.gov/scripts/cdrh/cfdocs/cfcfr/CFRSearch.cfm?FR=178.1010.

Cruz, C.D., Hedderley, D., Fletcher, G.C., 2015. Long-term study of *Vibrio parahaemolyticus* prevalence and distribution in New Zealand shellfish. Appl. Environ. Microbiol. 81, 2320–2327.

EFSA, 2014. Scientific opinion on the evaluation of the safety and efficacy of peroxyacetic acid solutions for reduction of pathogens on poultry carcasses and meat. EFSA J. 12, 3599.

FAO, 2021. Advances in science and risk assessment tools for *Vibrio parahaemolyticus* and *V. vulnificus* associated with seafood: meeting report. Retrieved from https://www.who.int/publications/i/item/9789240024878.

Fletcher, G.C., Statham, J.A., 1988. Shelf-life of sterile yellow-eyed mullet (*Aldrichetta forsteri*) at 4 °C. J. Food Sci. 53, 1030–1035.

Food Contact Substance Notification FCN 000699. 190 ppm PAA in water and ice for seafood. Retrieved from. http://vm.cfsan.fda.gov/-dms/opa-fcn.html.

Gonzalez-Escalona, N., Cachicas, V., Acevedo, C., Rioseco, M.L., Vergara, J.A., Cabello, F., Romero, J., Espejo, R.T., 2005. *Vibrio parahaemolyticus* diarrhea, Chile, 1998 and 2004. Emerg. Infect. Dis. 11, 129–131.

Gurevich, A., Saveliev, V., Vyahhi, N., Tesler, G., 2013. QUAST: quality assessment tool for genome assemblies. Bioinformatics 29, 1072–1075.

Hayrapetyan, H., Muller, L., Tempelaars, M., Abee, T., Groot, M.N., 2015. Comparative analysis of biofilm formation by *Bacillus cereus* reference strains and undomesticated food isolates and the effect of free iron. Int. J. Food Microbiol. 200, 72–79.

Jonas, K., Edwards, A.N., Ahmad, I., Romeo, T., Römling, U., Melefors, O., 2010. Complex regulatory network encompassing the Csr, c-di-GMP and motility systems of *Salmonella* Typhimurium. Environ. Microbiol. 12, 524–540.

Lin, Z., Chen, T., Zhou, L., Yang, H., 2022. Effect of chlorine sanitizer on metabolic responses of *Escherichia coli* biofilms "big six" during cross-contamination from abiotic surface to sponge cake. Food Res. Int. 157, 111361.

Lin, Z., Wang, G., Zhang, K., Jiang, S., Li, S., Yang, H., 2023. Metabolomics investigation of global responses of *Cronobacter sakazakii* against common sanitizing in infant formula processing environments. Food Res. Int. 172, 113162.

Liu, D., Straus, D.L., Pedersen, L.F., Meinelt, T., 2015. Comparison of the toxicity of Wofasteril peracetic acid formulations E400, E250, and Lspez to Daphnia magna, with emphasis on the effect of hydrogen peroxide. N. Am. J. Aquac. 77, 128–135.

Liu, J., Zhao, H., Yin, Z., Dong, H., Chu, X., Meng, X., Li, Y., Ding, X., 2023. Application and prospect of metabolomics-related technologies in food inspection. Food Res. Int. 171, 113071.

Liu, Q., Chen, L., Laserna, A.K.C., He, Y., Feng, X., Yang, H., 2020. Synergistic action of electrolyzed water and mild heat for enhanced microbial inactivation of *Escherichia coli* O157:H7 revealed by metabolomics analysis. Food Control 110, 107026.

Makino, K., Oshima, K., Kurokawa, K., Yokoyama, K., Uda, T., Tagomori, K., Iijima, Y., Najima, M., Nakano, M., Yamashita, A., Kubota, Y., Kimura, S., Yasunaga, T., Honda, T., Shinagawa, H., Hattori, M., Iida, T., 2003. Genome sequence of *Vibrio parahaemolyticus*: a pathogenic mechanism distinct from that of *V. cholerae*. Lancet 361, 743–749.

Mao, X., Xia, L., Yang, L., You, Y., Luo, P., Li, Y., Wu, Y., Jiang, G., 2022. Data mining of natural hazard biomarkers and metabolites with integrated metabolomic tools. J. Hazard. Mater. 427, 127912.

Martinez-Urtaza, J., Huapaya, B., Gavilan, R.G., Blanco-Abad, V., Ansede-Bermejo, J., Cadarso-Suarez, C., Figueiras, A., Trinanes, J., 2008. Emergence of Asiatic *Vibrio* diseases in South America in phase with El Nino. Epidemiology 19, 829–837.

Melchior, M., Fink-Gremmels, J., Gaastra, W., 2007. Extended antimicrobial susceptibility assay for *Staphylococcus aureus* isolates from bovine mastitis growing in biofilms. Vet. Microbiol. 125, 141–149.

Nahar, S., Jeong, H.L., Cho, A.J., Park, J.-H., Han, S., Kim, Y., Park, S.-H., Ha, S.-D., 2022. Efficacy of ficin and peroxyacetic acid against *Salmonella enterica* serovar Thompson biofilm on plastic, eggshell, and chicken skin. Food Microbiol. 104, 103997.

Park, S.-H., Cheon, H.-L., Park, K.-H., Chung, M.-S., Choi, S.H., Ryu, S., Kang, D.-H., 2012. Inactivation of biofilm cells of foodborne pathogen by aerosolized sanitizers. Int. J. Food Microbiol. 154, 130–134.

Parks, D.H., Imelfort, M., Skennerton, C.T., Hugenholtz, P., Tyson, G.W., 2015. CheckM: assessing the quality of microbial genomes recovered from isolates, single cells, and metagenomes. Genome Res. 25, 1043–1055.

Petit 3rd, R.A., Read, T.D., 2020. Bactopia: a flexible pipeline for complete analysis of bacterial genomes. mSystems 5, e00190-00120.

Poimenidou, S.V., Chrysadakou, M., Tzakoniati, A., Bikouli, V.C., Nychas, G.-J., Skandamis, P.N., 2016. Variability of *Listeria monocytogenes* strains in biofilm formation on stainless steel and polystyrene materials and resistance to peracetic acid and quaternary ammonium compounds. Int. J. Food Microbiol. 237, 164–171.

Rodgers, S.L., Cash, J.N., Siddiq, M., Ryser, E.T., 2004. A comparison of different chemical sanitizers for inactivating *Escherichia coli* O157: H7 and *Listeria monocytogenes* in solution and on apples, lettuce, strawberries, and cantaloupe. J. Food Prot. 67, 721–731.

Rosa, J.V., Conceição, N.V., Conceição, R.C.S., Timm, C., 2018. Biofilm formation by *Vibrio parahaemolyticus* on different surfaces and its resistance to sodium hypochlorite. Cien. Rur. 48.

Roy, P.K., Mizan, M.F.R., Hossain, M.I., Han, N., Nahar, S., Ashrafudoulla, M., Toushik, S. H., Shim, W.B., Kim, Y.M., Ha, S.D., 2021. Elimination of *Vibrio parahaemolyticus* biofilms on crab and shrimp surfaces using ultraviolet C irradiation coupled with sodium hypochlorite and slightly acidic electrolyzed water. Food Control 128, 108179.

Sharma, V.K., Johnson, N., Cizmas, L., McDonald, T.J., Kim, H., 2016. A review of the influence of treatment strategies on antibiotic resistant bacteria and antibiotic resistance genes. Chemosphere 150, 702–714.

Thi, A.N.T., Sampers, I., Van Haute, S., Samapundo, S., Nguyen, B.L., Heyndrickx, M., Devlieghere, F., 2015. Decontamination of Pangasius fish (*Pangasius hypophthalmus*) with chlorine or peracetic acid in the laboratory and in a Vietnamese processing company. Int. J. Food Microbiol. 208, 93–101.

Vázquez-Sánchez, D., Cabo, M.L., Ibusquiza, P.S., Rodríguez-Herrera, J.J., 2014. Biofilm-forming ability and resistance to industrial disinfectants of *Staphylococcus aureus* isolated from fishery products. Food Control 39, 8–16.

Wang, D., Yamaki, S., Kawai, Y., Yamazaki, K., 2020. Sanitizing efficacy and antimicrobial mechanism of peracetic acid against histamine-producing bacterium, *Morganella psychrotolerans*. LWT 126, 109263.

Wang, D., Fletcher, G.C., On, S.L.W., Palmer, J.S., Gagic, D., Flint, S.H., 2023b. Biofilm formation, sodium hypochlorite susceptibility and genetic diversity of *Vibrio parahaemolyticus*. Int. J. Food Microbiol. 385, 110011.

Wang, Y., Chen, Z., Zhao, F., Yang, H., 2023a. Metabolome shifts triggered by chlorine sanitisation induce *Escherichia coli* on fresh produce into the viable but nonculturable state. Food Res. Int. 171, 113084.

Wong, H.-C., Liao, R., Hsu, P., Tang, C.-T., 2018. Molecular response of *Vibrio parahaemolyticus* to the sanitizer peracetic acid. Int. J. Food Microbiol. 286, 139–147.

Yang, X., Wang, H., Hrycauk, S., Klassen, M.D., Ercolini, D., 2021. Effects of peroxyacetic acid spray and storage temperature on the microbiota and sensory properties of vacuum-packed subprimal cuts of meat. Appl. Environ. Microbiol. 87 e03143-03120.

Zhao, L., Poh, C.N., Wu, J., Zhao, X., He, Y., Yang, H., 2022. Effects of electrolysed water combined with ultrasound on inactivation kinetics and metabolite profiles of *Escherichia coli* biofilms on food contact surface. Innovative Food Sci. Emerg. Technol. 76, 102917.

United States Environmental Protection Agency EPA 832-F-12-030, Alternative disinfection methods fact sheet: peracetic acid. Retrieved from https://www.epa.gov/sites/default/files/2019-08/documents/disinfection_-_paa_fact_sheet_-_2012.pdf.

Appendix IX. Research output - Chapter 5

Food Research International 166 (2023) 112605

Contents lists available at ScienceDirect

Food Research International

journal homepage: www.elsevier.com/locate/foodres

Comparative genome identification of accessory genes associated with strong biofilm formation in *Vibrio parahaemolyticus*

Dan Wang [a], Graham C. Fletcher [b], Dragana Gagic [c], Stephen L.W. On [d], Jon S. Palmer [a], Steve H. Flint [a,*]

[a] School of Food and Advanced Technology, Massey University, Private Bag 11222, Palmerston North, New Zealand
[b] The New Zealand Institute for Plant & Food Research Limited, Private Bag 92169, Auckland 1142, New Zealand
[c] School of Fundamental Sciences, Massey University, Private Bag 11222, Palmerston North, New Zealand
[d] Faculty of Agriculture and Life Sciences, Lincoln University, Private Bag 85084, Canterbury, New Zealand

ARTICLE INFO

Keywords:
whole genome sequencing (WGS)
Comparative genome
Cellulose
Horizontal gene transfer (HGT)
Seafood safety

ABSTRACT

Vibrio parahaemolyticus biofilms on the seafood processing plant surfaces are a potential source of seafood contamination and subsequent food poisoning. Strains differ in their ability to form biofilm, but little is known about the genetic characteristics responsible for biofilm development. In this study, pangenome and comparative genome analysis of *V. parahaemolyticus* strains reveals genetic attributes and gene repertoire that contribute to robust biofilm formation. The study identified 136 accessory genes that were exclusively present in strong biofilm forming strains and these were functionally assigned to the Gene Ontology (GO) pathways of cellulose biosynthesis, rhamnose metabolic and catabolic processes, UDP-glucose processes and O antigen biosynthesis ($p < 0.05$). Strategies of CRISPR-Cas defence and MSHA pilus-led attachment were implicated via Kyoto Encyclopedia of Genes and Genomes (KEGG) annotation. Higher levels of horizontal gene transfer (HGT) were inferred to confer more putatively novel properties on biofilm-forming *V. parahaemolyticus*. Furthermore, cellulose biosynthesis, a neglected potential virulence factor, was identified as being acquired from within the order *Vibrionales*. The cellulose synthase operons in *V. parahaemolyticus* were examined for their prevalence (22/138, 15.94 %) and were found to consist of the genes *bcsG*, *bcsE*, *bcsQ*, *bcsA*, *bcsB*, *bcsZ*, *bcsC*. This study provides insights into robust biofilm formation of *V. parahaemolyticus* at the genomic level and facilitates: identification of key attributes for robust biofilm formation, elucidation of biofilm formation mechanisms and development of potential targets for novel control strategies of persistent *V. parahaemolyticus*.

1. Introduction

Microbial cells can colonize biotic surfaces, equipment (e.g. conveyor belts, stainless steel processing bench, pipes), or packaging materials (e.g., glass, polystyrene), forming complex community matrices covered by extracellular polymeric substances (EPSs) (Lianou, Nychas, & Koutsoumanis, 2020). Biofilms enable increased resistance by shielding pathogens and spoilage bacteria from environmental stresses, acting as hot spots for horizontal gene transfer (HGT) of virulence genes, and transforming previously benign strains into pathogens (Stalder & Top, 2016). The enhanced resistance of biofilms poses challenges for hygienic treatments in the food industry, thereby increasing the risks of cross-contamination and foodborne illness outbreaks (Simões et al., 2010).

Vibrio parahaemolyticus is a marine oriented, gram-negative microorganism, that causes food poisoning through consumption of raw or undercooked seafood (Martinez-Urtaza et al., 2010). It is causing concerns across an expanding geographical range, with an increase in the frequency of infections and outbreaks in nations with no or limited prior occurrence (FAO, 2021). *V. parahaemolyticus* can enter and persist in seafood processing plants despite cleaning and sanitation (Lei et al., 2020; Roy et al., 2021; Wang et al., 2022). Sodium hypochlorite at concentrations that are effective against *V. parahaemolyticus* planktonic cells, can be ineffective at controlling biofilms. For instance, Chen et al. (2016) reported that 81 mg/L (pH 10.8, 3 min) of sodium hypochlorite eliminates 7.85 log CFU/mL of planktonic *V. parahaemolyticus* but 200 mg/L only reduced initial concentrations of 6.87 and 7.37 $\log_{10}$ CFU/cm^2 *V. parahaemolyticus* biofilm cells by 1.83 and 1.63 $\log_{10}$ CFU/cm^2 on

* Corresponding author.
E-mail address: s.h.flint@massey.ac.nz (S.H. Flint).

https://doi.org/10.1016/j.foodres.2023.112605
Received 30 October 2022; Received in revised form 4 February 2023; Accepted 14 February 2023
Available online 16 February 2023

shrimp and crab surfaces, respectively (Roy et al., 2021). The authors did not mention the pH or temperature of this treatment. Because normal hygienic treatment cannot eradicate *V. parahaemolyticus* biofilm, it is necessary to understand key molecular mechanisms and devise novel control strategies accordingly.

V. parahaemolyticus uses polar and lateral flagella for motility. Polar flagella (driven by sodium ions) are used for swimming, and lateral flagella (driven by protons) for swarming (Kim & McCarter, 2000; McCarter, 2001). The polar flagella function as a mechano-sensor, resulting in a reduction in flagellar rotation and activation of the lateral flagella expression in response to growth on a surface (Verstraeten et al., 2008). Mature *V. parahaemolyticus* biofilm formation requires mannose-sensitive hemagglutinin (MSHA) pili, virulence-associated toxin co-regulated pili (TCP) and chitin-regulated pili (ChiRP) to aggregate, attach and promote EPS synthesis. *cpsA-J* (*vpa1403-vpa1412*) is required for the synthesis of capsular polysaccharide A (CPSA), a major component of the *V. parahaemolyticus* biofilm (Güvener & McCarter, 2003). *vp1476-vp1458* is a conserved ortholog of the *syp* locus in *Vibrio fischeri* which is responsible for wrinkled colonies, pellicle formation and matrix production (Yildiz & Visick, 2009). *vp0190-vp0214* regulates the synthesis of lipid A, the core component of lipopolysaccharide (LPS) (Chen et al., 2010). *csrA* plays critical roles in carbohydrate metabolism and switching motility-sessility functions (Wang et al., 2021). However, it has not been determined which of these or other genotypes are responsible for significant biofilm formation and sodium hypochlorite resistance in this bacterium.

Therefore, the current study evaluated genomic features of *V. parahaemolyticus* with weak, intermediate, and strong biofilm forming abilities, conducted comparative genome analysis and deciphered the exclusive molecular mechanisms of persistent *V. parahaemolyticus* on seafood contact surface. This provides insights for the design of novel biofilm control strategies.

2. Methods

2.1. Strains and growth condition

Ten *V. parahaemolyticus* strains were chosen for this investigation (Table 1), seven of them were isolated from shellfish by Plant and Food Research ltd. (New Zealand), another two were clinical isolates provided by the Institute of Environmental Science and Research ltd. (ESR, New Zealand), and the *V. parahaemolyticus* genome reference strain RIMD 2210633 kindly donated by Dr. Tetsuya Iida was also included. According to previous studies, two strains (PFR30J09 and PFR34B02) were putative strong biofilm formers and least susceptible to chlorine treatment, whereas PFR21C03 and PFR37D08 were weak biofilm forming strains (Wang et al., 2023). Isolates from a −80 ℃ bead storage system were recovered by shaking incubation at 37 ℃, 120 rpm using 3 % NaCl tryptic soy broth (TSB). Cells were centrifuged (11200 × g, 5 min) to obtain the cell pellet. This was washed, suspended in sterile phosphate-buffered saline (PBS, pH 7.4) and the cell concentration adjusted to 7 log colony forming units (CFU)/mL.

2.2. Genome assembly and annotation

Sequencing of the PFR isolates (Table 1) was carried out by Cefas (Weymouth, U.K.). DNA was extracted from overnight grown cultures using the DNeasy Blood & Tissue Kit and the genomes were sequenced by MiSeq with a coverage of 40-120x. Raw reads were processed to trim adapters, as well as clean low-quality reads and low-quality sequences. *De novo* assembly using the assemblers SPAdes (version 3.15.2) and Velvet (version 1.2.10) were generated for each genome. SPAdes used k-mers (21, 33, 55) to build *de Brujin* graphs and generate contigs, the mismatch careful mode and error correction procedure was used to improve the assembly (Bankevich et al., 2012). *De novo* assembly was also performed via *de Brujin*-based Velvet and Velvet Optimizer, the k-mer sizes applied were of 31, 51, 71, 91, and 121 (Zerbino & Birney, 2008). The quality of the draft assembly was evaluated using QUAST and CheckM (Gurevich et al., 2013; Parks et al., 2015). The GC depth analysis was used to assess the potential contamination and the coverage of the assembly, and the completeness of genome assembly to examine the genome integrity. Predicted coding sequences from bacterial genome assemblies were generated by Prokka (version: 1.14.5) with default parameters, together with translated coding genes, genomic features and GFF version annotations (Seemann, 2014).

2.3. ANI and phylogeny analysis

Considering potentially bio-accumulated bacterium in molluscan shellfish and interfering seafood safety, published genomes of bacteria *Escherichia coli* K-12 ER3413, *Listeria monocytogenes* ATCC 19117, *V. parahaemolyticus* RIMD 2210633, *V. parahaemolyticus* BB22OP, *Vibrio cholerae* ATCC 14035, *Vibrio fischeri* ES114 and *Vibrio vulnificus* ATCC 27562 were included with those of our 9 isolates for ANI and phylogeny

Table 1
Strains used in this study.

No.	Strain	Source	Collection Date	Country	Biofilm formation abilities*	Sodium hypochlorite resistance (biofilms on stainless steel surfaces)**
1	PFR21C03	Pacific oyster	16/02/2009	New Zealand	W	+
2	PFR24B07	Greenshell™ mussel	2/03/2010	New Zealand	M	+
3	PFR29A04	Pacific oyster	22/11/2010	New Zealand	M	+
4	PFR30G02	Pacific oyster	8/03/2011	New Zealand	M	+
5	PFR30J09	Pacific oyster	21/03/2011	New Zealand	S	++
6	PFR34B02	Pacific oyster	27/03/2012	New Zealand	S	++
7	PFR37C06	Pacific oyster	17/01/2013	New Zealand	M	+
8	PFR37D08	Clinical	2013	New Zealand	W	+
9	PFR37E03	Clinical NZRM 3391	1975	New Zealand	M	+
10	RIMD2210633	Clinical	1996	Japan	M	+

* W indicated weak biofilm producer, M indicated moderate biofilm producer, S indicated strong biofilm producer.
** + indicated sodium hypochlorite resistance by *V. parahaemolyticus* biofilm cells, ++ indicated increased sodium hypochlorite resistance.

analysis, to obtain a more complete view. Average nucleotide identity (ANI) was analyzed using pyANI (version 0.2.12) to measure the similarity among genomes by pairwise comparison based on nucleotide sequences (Pritchard et al., 2016). To estimate the evolutionary relationship of *V. parahaemolyticus* genomes, phylogeny analysis was conducted based on 16 s rRNA and ortholog clustering. DNA sequences were loaded into Barrnap (https://github.com/tseemann/barrnap) that applies HMMER 3.1 to search for the locate ribosomal RNA genes. The 16 s rRNA sequences were collected and aligned via MEGAX (version 10.2.6) software. A Maximum Likelihood phylogenetic tree was constructed using the nearest neighbor interchange model. Ortholog clustering analysis was performed via OrthoFinder2 (version: 2.5.4) using protein-coding genes. The orthogroups had single-copy genes aligned via MAFFT. The phylogenetic tree based on ML of replicates was built by the IQ-TREE with 1000 bootstraps.

2.4. Homology clustering and pangenome analysis

Pangenome analysis to reveal core, dispensable and unique content was conducted using Roary and Anvi'o (Eren et al., 2015; Page et al., 2015). According to Roary (version 3.11.2), protein sequences with annotation were loaded and an all-against-all BLASTP was used to cluster proteins. The sequence identity of over 95 % was set as the threshold for clustering protein homologues. Anvi'o clustered homologues based on the similarity of amino acid sequences, the interactive visualization of results was generated by the anvio-display-pan function.

2.5. Comparative genome analysis

Four genomes, two from strong biofilm formers (PFR30J09 and PFR34B02) and two from weak biofilm formers (PFR21C03 and PFR37D08) were compared. Orthologous gene families and gene duplication events were analyzed via OrthoFinder2 and compared with a protein similarity search using DIAMOND (version 0.9.18). Another approach to predict orthologous gene clusters was performed using OrthoVenn2, which is based on all-to-all protein similarity comparisons and orthologous clusters using the Markov Cluster algorithm. The E-value and inflation values were set as 1e-5 and 1.5, respectively.

Functional assignment and the DAVID database (https://david.ncifcrf.gov/) was used to annotate gene sets for GO terms. DAVID enables visualization of many-genes-to-many-terms relationships and clusters genes into groups. This was followed by a Kyoto Encyclopedia of Genes and Genomes (KEGG) pathway analysis using BlastKOALA (https://www.kegg.jp/blastkoala/). A false discovery rate (FDR) value smaller than 0.05 was used as the cut-off for significance.

2.6. Identification of potential horizontal transfer genes

HGTector was used to predict the presence of horizontal gene transfer among genomes with BLASTP parameter thresholds of 60 % identity, 60 % coverage and an E-value of 1e-5. HGTector differentiates self (rank, genus; taxid: 662), close (rank, order; taxid: 135623) and distal gene groups by the gene hit bitscore (Zhu et al., 2014). Cut-offs were determined by taking the midpoint between the first peak and valley from the distribution of self, close and distal groups. HGT genes were identified with a close weight smaller than the close cut-off but a distal weight greater than the distal cut-off (Yang et al., 2019).

2.7. Congo red indicator assay

Expression of extracellular polymeric cellulose was evaluated using the Congo red indicator method reported by Fang et al. (2022) with minor modification. Overnight culture was streaked onto agar plates and incubated at 37 ℃ for 48 h. Colonies of red, brown, pink and white indicated the production of curli and cellulose, curli, cellulose, and none, respectively.

2.8. Anthrone absorbance assay

Cellulose determination was based on a previous study with minor modifications (Anriany et al., 2006). Briefly, 3 g cells (wet weight) of each sample were scratched from agar plates, mixed with 5 mL of an 8:2:1 acetic acid: nitric acid: distilled water mix, boiled for 30 min and centrifuged at 4480 × g for 5 min. The pellet was washed with 1 mL distilled water then 1 mL acetone and left to dry overnight. The dried sample was dissolved in 1 mL H_2SO_4 (95 %). Next, 0.1 mL was mixed with 0.5 mL anthrone solution (0.2 g in 100 mL H_2SO_4), and the absorbance was determined at 620 nm. Crystalline cellulose (25, 50 and 100 mg/mL) were used as absorbance standards.

2.9. In silico cellulose synthase operon sequence analysis

The cellulose synthase operon genes of *V. parahaemolyticus* were searched using BlastP against 138 *V. parahaemolyticus* reference genomes. The cellulose synthase genes of each genome were aligned using ClustalW. The accession numbers for nucleotide sequences of the genomes are attached in Table 4. The phylogeny of these cellulose synthase operons was analyzed using FastTree and was inferred using the Neighbour Joining method with a bootstrap consensus of 1000 replicates. The evolutionary distances were calculated using the Maximum Likelihood Method and are in the units of the number of base substitutions per site. The amino acid sequences of *V. parahaemolyticus* RIMD 2210633 were retrieved from the National Centre for Biotechnology Information (NCBI) Database and selected as the reference genome, followed by transferring into a local database for BLASTP searching via DIAMOND (Buchfink et al., 2021). Each sequenced *V. parahaemolyticus* genome was searched to identify the presence of genes (with > 70 % identity and > 70 % sequence coverage).

2.10. Gene co-occurrence analysis

Gene co-occurrence networks were computed using Coinfinder with a significance cut-off of 0.1 and gene presence/absence matrix from Roary. Networks were visualized using the R package igraph of Fruchterman Reingold.

2.11. Data availability

The sequence data determined in this work was deposited in the NCBI database under project accession No. PRJNA808748. The cellulose operon information for the strains used in this study are presented in Table 4.

3. Results and discussion

3.1. Genome assembly and annotation

The size of the *V. parahaemolyticus* genomes after trimming ranged from 5110607 bp to 7614640 bp, with an average value of 5532445 bp (Table 2). The GC contents of these genomes were not significantly different, ranging from 45.16 % to 45.47 %. Genome annotation was obtained from Prokka, which was to predict the coding of DNA sequences (CDS) in the assemblies. The number of CDS varied from 4591 to 4937. The variations in genome size and CDS number could be due to gene diversity during the evolution of *V. parahaemolyticus* isolates. The strain *V. parahaemolyticus* RIMD 2210633 isolated from Japan was used as the reference genome for most of our molecular analysis. This genome consisted of chromosomes of 5165770 bp, genes of 4832 bp and a GC content of 45.4 %. Overall, assembled genomes provided reasonable gene completeness and represented a reliable resource for analysis. In our study, the gene pools of the two clinical isolates were lower than the environmental (food) isolates; this was in accordance with reports by Pang et al. (2019) where there were 4718 genes on average from 19

Table 2
Summary of assemblies of *V. parahaemolyticus* genomes.

Assembly	PFR21C03	PFR24B07	PFR29A04	PFR30G02	PFR30J09	PFR34B02	PFR37C06	PFR37D08	PFR37E03	RIMD 2,210,633
Contigs (number)	93	133	129	99	329	104	95	85	110	–
Total length (bp)	5,338,398	5,417,990	5,402,653	5,172,378	7,816,420	5,367,801	5,218,301	5,149,233	5,110,607	5,165770
GC* (%)	45.27	45.16	45.19	45.27	45.47	45.19	45.25	45.24	45.27	45.4
CDS**	4830	4937	4905	4659	4913	4857	4725	4639	4591	4832
rRNA***	7	8	8	7	5	8	9	8	7	11
tRNA***	119	112	115	102	110	117	116	106	112	127
tmRNA***	1	1	1	1	1	1	1	1	1	1

* GC indicates Gunanine: Cytosine ratio.
** CDS indicates predicted coding sequences of DNA.
*** rRNA is ribosomal RNA, tRNA is transfer RNA and tmRNA is transfer-messenger RNA. - indicates not applicable, RIMD 2210633 is of scaffold assembled level.

V. parahaemolyticus environmental isolates compared with 4580 genes on average from 20 clinical isolates, suggesting higher genetic diversity and environmental adaptability in the environmental isolates.

3.2. ANI analysis and phylogenetic tree

ANI provides a commonly used metric to define intra- or inter-species relationships in prokaryotic genomes. An ANI of > 95 % has been proposed to represent the intra-species boundary (Jain et al., 2018). In this study, the dendrogram directly reflects the degree of identity between genomes; clustering across the dendrograms was based on ANI, forming one major clade of *V. parahaemolyticus* (Fig. 1a). The sequenced genomes revealed a high nucleotide identity (97.98–99.67 %), indicating they belong to the same species, *V. parahaemolyticus,* and are from a common origin. *V. parahaemolyticus* nucleotide identity compared with other *Vibrio* species was 70.98–76.15 %. The ANI across all *Vibrio spp*. ranges from 69.78 % to 76.15 %. The ANI result for *E. coli* K-12 ER3413 and *L. monocytogenes* ATCC 19117 is below 70 %, demonstrating they are of different genera.

Nucleotide acid sequences of 16 s rDNA have been used for decades to assign phylogenetic relationships (Fig. 1b). Among selected 16 s rDNA sequences of *E. coli* K-12 ER3413, *L. monocytogenes* ATCC 19117, *V. parahaemolyticus* RIMD 2210633, *V. parahaemolyticus* BB22OP, *Vibrio cholerae* ATCC 14035, *Vibrio fischeri* ES114 and *Vibrio vulnificus* ATCC 27562, our PFR species remained in one subclade with *V. parahaemolyticus* RIMD 2210633 and *V. parahaemolyticus* BB22OP, indicating that they are closely related. The most divergent species are *E. coli* K-12 ER3413 and *L. monocytogenes* ATCC 19117.

Another method to assign the phylogenetic relationship is based on the orthologous groups, using 275 conserved single copy orthogroups, seen in Fig. 1c. The result was consistent with the phylogeny analysis result based on 16 s rDNA similarity that *V. parahaemolyticus* was in the same clade with *V. parahaemolyticus* RIMD 2210633 and *V. parahaemolyticus* BB22OP, divergent from *E. coli* K-12 ER3413 and *L. monocytogenes* ATCC 19117. Among the subclade, PFR30J09 formed a different branch showing some deviation from the other isolates. These data provide an evolutionary picture of our sequenced *V. parahaemolyticus* genomes and reveal evolutionary distances from other studied seafood pathogens.

3.3. Pangenome analysis

The sizes of core and dispensable genomes were estimated using pangenome analysis via two distinct pipelines, Roary and Anvi'o. Roary analysis suggested there were 3253 core genes (33.20 %), 2266 shell genes (23.13 %), and 4278 cloud genes (43.67 %) out of 9797 genes in 9 sequenced *V. parahaemolyticus* genomes. The genome group is open, indicating that additional data input will alter the proportion of the core genome and that new orthogroups will be discovered (Supplemental Fig. 1). A circular graph was created via Anvi'o containing information on gene numbers in gene clusters, maximum number of paralogs, genomic homogeneity index, functional homogeneity index, combined homogeneity index, and single copy gene (SCG) clusters (Fig. 2a). Despite both Roary and Anvi'o approaches using the MCL algorithm to identify clusters, the Anvi'o pangenomics workflow identified fewer gene clusters (6845), which may have led to a smaller number of core genes. The differences might be due to different ways to establish orthologs of protein clusters. Roary divides groups of homologous sequences into paralogs and orthologs using conserved gene neighborhood information, while Anvi'o clusters orthologs based on the homology and synteny of genes (Maturana & Cárdenas, 2021). The core genome was a relatively low portion of the total (~33.20 %) which was revealed by Roary analysis, suggesting that the *V. parahaemolyticus* species may contain more accessory genes that are critical for adaptation to different environments and survival. A similar finding has been reported in previous *V. parahaemolyticus* studies by Pang et al. (2019) and Qin et al. (2021).

3.4. Comparative genome analysis

The strong biofilm-forming strains of *V. parahaemolyticus* (PFR30J09 and PFR34B02) both had more gene families than the weak biofilm-forming isolates (PFR21C03 and PFR37D08), but medium biofilm forming isolates covered the range of gene families (CDS, Table 2). Analysis of the amino acid sequences by OrthoVenn2 showed a total of 3692 gene families to be shared across the genomes of the four strong and weak biofilm forming isolates (Fig. 2b). OrthoVenn2 identified 136 gene families exclusively present in strong biofilm producers.

The GO annotation was performed to assign the functional category of these 136 unique gene families. The significantly enriched GO terms ($p < 0.05$) included UDP-glucose metabolism (GO: 0006011), cellulose biosynthesis (GO: 0030244), rhamnose metabolism (GO: 0019299) and O antigen biosynthesis (GO: 0009243) (Supplemental Table 1). Cellulose synthesis, rhamnose catabolic and metabolic processes are absent in the *V. parahaemolyticus* reference strain RIMD 2210633. These distinctive functions may play crucial roles in robust biofilm formation. BlastKOALA was used to assign the amino acid sequences to KEGG functions, resulting in 24.3 percent (33/136) of them being successfully annotated (Table 3), while many of them remained unidentified. The most frequently annotated pathways were metabolic pathways (path: ko01100), microbial metabolism in diverse environments (path: ko01120), pentose and glucuronate interconversions (path: ko00040), fructose and mannose metabolism (path: ko00051), biosynthesis of secondary metabolites (path: ko01110), galactose metabolism (path: ko00052) as well as starch and sucrose metabolism (path: ko00500). These pathways represent the synthesis and metabolism of simple/complex sugars, which may aid in the utilization of diverse nutrient sources and adaptation to environmental stress.

Gene clusters associated with cellulose synthesis, rhamnose catabolism, and metabolic process were identified via KEGG gene annotation (Table 3), that was consistent with the result from GO enrichment. Meanwhile, the clustered regularly interspaced short palindromic repeats (CRISPR)-Cas system was identified in the unique 136 gene families via KEGG annotation. This system has been reported to play critical

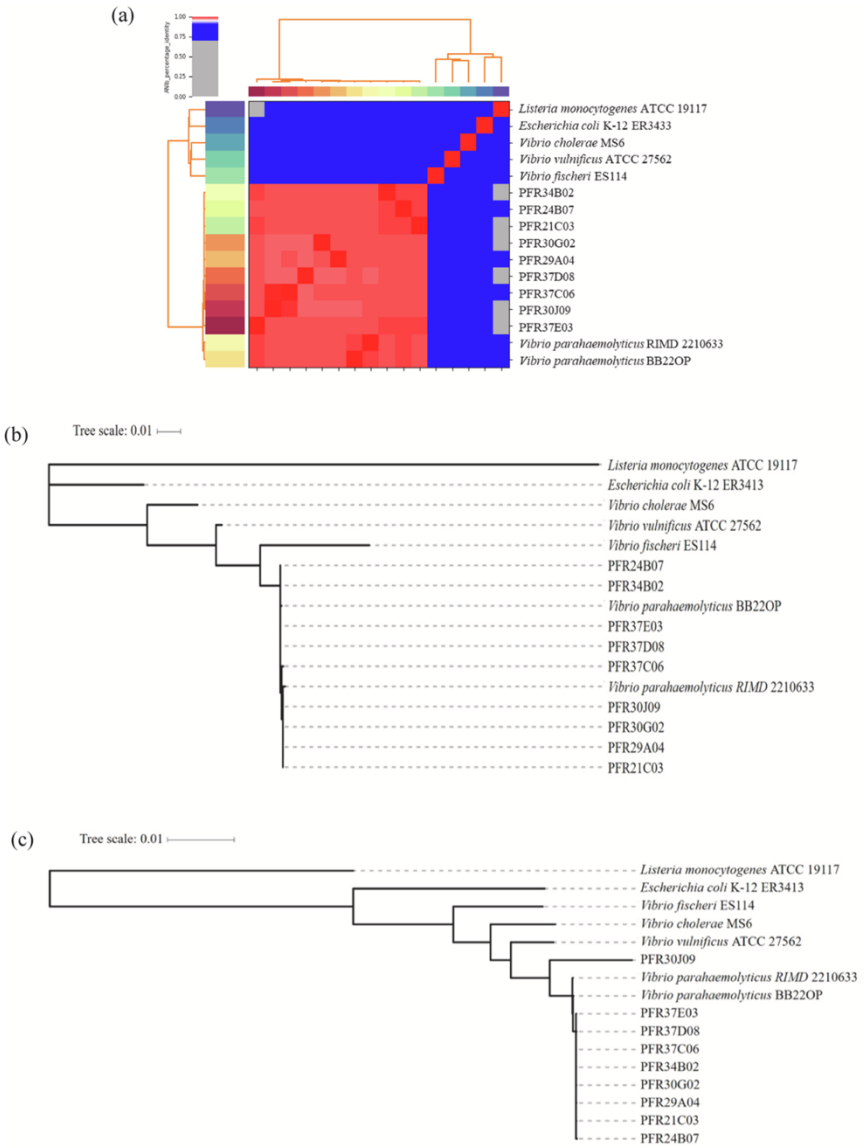

Fig. 1. Phylogenetic analysis and amino acid identities across genomes. (a) Phylogeny based on a heatmap with row and column dendrograms from the average nucleotide identity (ANI). (b) The Maximum Likelihood phylogeny was constructed using the 16 s rDNA sequences. (c) Maximum Composite Likelihood phylogeny was constructed based on single copy orthogroups.

roles in environmental stress defense, DNA repair and biofilm formation in microorganism cells. In this study, the CRISPR-Cas system in *V. parahaemolyticus* was identified as the subtype I-F, that is consistent with previous studies (Makarova et al., 2011). However, whether or how the CRISPR-Cas system promotes biofilm formation in *V. parahaemolyticus* is unknown. The genome data also indicated that strong biofilm forming strains are more likely to have *mshA*, *mshC* and *mshD* genes that are lacking in the weak biofilm forming strains. MSHA is required for early attachment of *V. cholerae* to abiotic surfaces. Cells that are deficient in *mshA* cannot perform cell aggregation although they are involved in the formation of three-dimensional structures (Moorthy and Watnick, 2004) and in *V. parahaemolyticus*, *mshA* mutants show reduced adherence to surfaces (Shime-Hattori et al., 2006).

Our study supports the hypothesis that *V. parahaemolyticus* employs

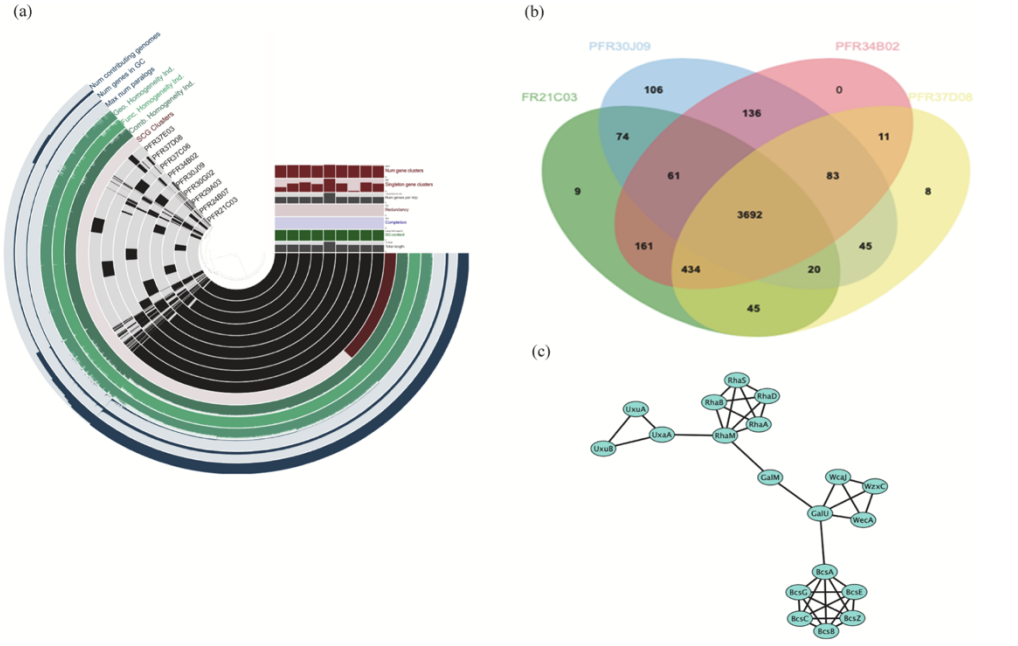

Fig. 2. Genomes of *Vibrio parahaemolyticus* exhibit genetic diversity. (a) Strain-specific gene families of nine *V. parahaemolyticus* genomes computed by the Anvi'o pangenome analysis pipeline employing the default setting. (b) A comparison of protein orthologues in weak and strong biofilm-forming *V. parahaemolyticus*, generated by OrthoVenn2 with an E-value setting of 1e-5. (c) PPI network of 136 gene families exclusively present in strong biofilm-forming *V. parahaemolyticus*.

multiple strategies to promote robust biofilm formation, and some of these strategies interact. In the PPI (protein–protein interaction) analysis of 136 gene families, an interaction between rhamnose metabolism, cellulose biosynthesis, as well as O-antigen and capsular biosynthesis were demonstrated (Fig. 2c). Regmi and Boyd (2019) reported that the *rha* gene cluster, encoding rhamnose catabolic and metabolic processes, had limited distribution among *V. parahaemolyticus* strains. Another study reported that the presence of the rhamnose operon is indispensable but not sufficient for biofilm formation in *Rhodobacteraceae* (Michael et al., 2016), but scenario varied here. In this study, the presence of the *rha* gene cluster might have played as one 'biobrick' for robust biofilm formation, but the absence did not interfere with the ability to form biofilms as presented in PFR21C03 and PFR37D08. The presence of cellulose synthase operons suggests that cellulose production is a phenotype of robust biofilm forming *V. parahaemolyticus* strains, but until now, cellulose has only been reported in environmental isolates of *V. parahaemolyticus* (Meparambu Prabhakaran et al., 2022). Given cellulose roles in virulence in other microorganisms (Arrebola et al., 2015; Heredia-Ponce et al., 2020), cellulose could be a neglected virulence factor that has previously been considered absent in *V. parahaemolyticus*. GalU is required to encode UDP-glucose pyrophosphorylase and produce a single substrate UDP-glucose for cellulose synthases. GalU is essential for cellulose secretion *in vivo* (Abidi et al., 2021; Valla et al., 1989). The subcluster encompassing WcaJ, WecA and WzxC was suggested to be responsible for the O antigen (Pang et al., 2019), as shown in Fig. 2. The PPI network revealed an indirect link between cellulose biosynthesis and O-antigen via GalU in strong biofilm forming strains of *V. parahaemolyticus*. L-Rhamnose is required for rhamnan O antigen synthesis (Broughton et al., 2006), which is to some extent in agreement with that *rha* gene cluster associated with O-antigen formation in this study. The variation in O-antigen can result in the structural diversity of O-antigen and linkages between monosaccharides, that in turn influence LPS and biofilm formation (Lerouge & Vanderleyden, 2002). Based on our study, cellulose production might relate to a specific type O-antigen in *V. parahaemolyticus* biofilms. However, whether cellulose biosynthesis is related with a specific O-antigen in other strong biofilm forming strains and how the O-antigen assist in the robust biofilm formation require further exploration in *V. parahaemolyticus*, although some evidence has been demonstrated by Lerouge and Vanderleyden (2002). To sum up, this is the first time that an interaction between rhamnose metabolic and catabolic processes, cellulose biosynthesis, and O-antigen biosynthesis pathways has been linked to robust biofilm formation. Biochemical studies are needed to determine whether this interaction is specific to the strains studied or more widespread in *V. parahaemolyticus* species.

3.5. Verification of cellulose production

Strong biofilm forming strains PFR30J09 and PFR34B02 produced red colonies in the Congo Red Assay, indicating the production of curli and cellulose (Fig. 3a). The weak biofilm forming strains, PFR21C03 and PFR37D08, only produced brown colonies, suggesting no cellulose was produced. The absence of cellulose biosynthesis in PFR21C03 and PFR37D08 is consistent with the results from the anthrone absorbance assay indicating no cellulose formation in PFR21C03 and PFR37D08 while cellulose was detected in PFR30J09 and PFR34B02 with OD_{620} of 0.234 ± 0.0356 and 0.185 ± 0.0546 (Fig. 3b), respectively. Crystalline cellulose was used as a control with 25 mg/mL producing an OD_{620} of 0.235 ± 0.0092.

Table 3
KEGG functional assignment of unique genes from strong biofilm forming strains.

KO	Gene name	EC number	Pathways/associated functions
K02851	*wecA*, UDP-GlcNAc: undecaprenyl-phosphate/ decaprenyl-phosphate GlcNAc-1-phosphate transferase	2.7.8.35	00542 O-Antigen repeat unit biosynthesis 00572 Arabinogalactan biosynthesis - Mycobacterium 01100 Metabolic pathways
K01785	*alM*, aldose 1-epimerase	5.1.3.3	00010 Glycolysis / Gluconeogenesis 00052 Galactose metabolism 01100 Metabolic pathways 01110 Biosynthesis of secondary metabolites 01120 Microbial metabolism in diverse environments
K00694	*bcsA*, cellulose synthase	2.4.1.12	00500 Starch and sucrose metabolism Cellulose biosynthesis
K01119	*cpdB*, 2′,3′-cyclic-nucleotide 2′-phosphodiesterase / 3′-nucleotidase	3.1.4.16/ 3.1.3.6	00230 Purine metabolism 00240 Pyrimidine metabolism 01100 Metabolic pathways
K00008	*gutB*, L-iditol 2-dehydrogenase	1.1.1.14	00040 Pentose and glucuronate interconversions 00051 Fructose and mannose metabolism 01100 Metabolic pathways
K02554	*mhpD*, 2-keto-4-pentenoate hydratase	4.2.1.80	00360 Phenylalanine metabolism 00362 Benzoate degradation 00621 Dioxin degradation 00622 Xylene degradation 01100 Metabolic pathways 01120 Microbial metabolism in diverse environments 01220 Degradation of aromatic compounds
K01813	*rhaA*, L-rhamnose isomerase	5.3.1.14	00051 Fructose and mannose metabolism 01100 Metabolic pathways 01120 Microbial metabolism in diverse environments
K00848	*rhaB*, rhamnulokinase	2.7.1.5	00040 Pentose and glucuronate interconversions 00051 Fructose and mannose metabolism 01100 Metabolic pathways 01120 Microbial metabolism in diverse environments
K01629	*rhaD*, rhamnulose-1-phosphate aldolase	4.1.2.19	00040 Pentose and glucuronate interconversions 00051 Fructose and mannose metabolism 01100 Metabolic pathways 01120 Microbial metabolism in diverse environments
K00963	UTP glucose-1-phosphate uridylyltransferase	2.7.7.9	00040 Pentose and glucuronate interconversions 00052 Galactose metabolism 00500 Starch and sucrose metabolism 00520 Amino sugar and nucleotide sugar metabolism 00541 O-Antigen nucleotide sugar biosynthesis 01100 Metabolic pathways 01110 Biosynthesis of secondary metabolites 01240 Biosynthesis of cofactors 01250 Biosynthesis of nucleotid8e sugars
K00040	*uxuB*, fructuronate reductase	1.1.1.57	00040 Pentose and glucuronate interconversions 01100 Metabolic pathways Translation
K16694	*tuaB*; teichuronic acid exporter	–	Transporters
K08138	*xylE*; MFS transporter, SP family, xylose:H + symportor	–	Transporters
K03765	*cadC*; transcriptional activator of cad operon	–	Transcription factors
K19130	*csy4*, CRISPR-associated endonuclease Csy4	3.1.-.-	Prokaryotic defense system
K19129	*csy3*, CRISPR-associated endonuclease Csy3	–	Prokaryotic defense system
K19128	*csy2*, CRISPR-associated endonuclease Csy2	–	Prokaryotic defense system
K19127	*csy1*, CRISPR-associated endonuclease Csy1	–	Prokaryotic defense system
K07012	*cas3*; CRISPR-associated endonuclease/helicase Cas3	3.1.-.- /5.6.2.4	Prokaryotic defense system
K15342	*cas1*; CRISP-associated protein Cas1	–	Prokaryotic defense system
K03534	*rhaM;* L-rhamnose mutarotase	5.1.3.32	Fructose and mannose metabolism Metabolic pathways Microbial metabolism in diverse environments
K02855	*rhaS*; AraC family transcriptional regulator, L-rhamnose operon regulatory protein RhaS	–	Fructose and mannose metabolism Metabolic pathways Microbial metabolism in diverse environments
K07733	*alpA*; prophage regulatory protein	–	Transcription factors
K03630	*radC*; DNA repair protein RadC	–	Replication and repair
K06877	DEAD/DEAH box helicase domain-containing protein	–	Poorly characterized
K03574	*mutT*, NUDT15, MTH2; 8-oxo-dGTP diphosphatase	3.6.1.55	DNA repair and recombination proteins
K20543	*bcsC*; cellulose synthase operon protein C	–	Cellulose biosynthesis
K20542	*bcsZ*; endoglucanase	3.2.1.4	Cellulose biosynthesis
K20541	*bcsB*; cellulose synthase operon protein B	–	Cellulose biosynthesis

3.6. Putative horizontal gene transfer

Horizontal gene transfer is the major driver of genetic diversity, providing bacteria with properties that enable adaption to various environments. An average of 126 ± 4.2 and 156 ± 45.3 potential HGT gene families providing gene acquisition from outside the *Vibrionales* were identified in weak and strong biofilm forming strains respectively. There were 123 and 129 predicted HGT events in PFR21C03 and PFR37D08 whereas 188 and 124 were predicted in PFR30J09 and PFR34B02. The results indicate that strong biofilm forming strains have

Table 4
Summary of the cellulose synthase operon in *V. parahaemolyticus*.

Genome	Strain	Nation	BioSample ID	Source	TLH	TRH	TDH	VgrG_T6SS	Hcp_T6SS
GCF_001304775.1	FORC_006	South Korea: Gyeongnam	SAMN03140318	Environment: cutting board	+	–	–	+	+
GCF_006517795.1	Vb0624	China: Shenzhen	SAMN12123413	Environment: market	+	–	–	+	+
GCF_002504185.1	HA2	China:Tianjin	SAMN07680340	Environment: aquaculture	+	–	–	+	+
GCF_004194515.1	D3112	China	SAMN10591529	Environment: seawater	+	–	–	+	+
GCF_001758605.1	FORC_023	South Korea: Pusan	SAMN03701448	Human	+	–	–	+	+
GCF_002209725.2	MAVP-Q	USA	SAMN05579852	Human	+	+	+	+	+
GCF_016403045.1	81TDH2	India: Mangaluru	SAMN16844329	Seafood	+	–	–	+	+
GCF_013393845.1	LVP1	China	SAMN11579495	Seafood: crayfish	+	–	–	+	+
GCF_000430405.1	FDA_R31	USA:LA	SAMN02179882	Seafood: oyster	+	–	+	+	+
GCF_016834555.1	HP1	India: Kumta	SAMN16844529	Seafood: shrimp	+	–	–	+	+
GCF_021730085.1	VP157	China:Tianjin	SAMN17188296	Seafood: shrimp	+	–	–	+	+
GCF_001700835.1	CHN25	China	SAMN03325855	Seafood: shrimp	+	–	–	+	+
GCF_001636035.1	FORC_014	South Korea: Pusan	SAMN03457164	Seafood: toothfish	+	–	–	+	+
GCF_012274985.1	2012 V-1165	USA	SAMN12648280	Stool	+	+	–	+	+
GCF_001682175.1	MAVP-Q	USA	SAMN03766034	Stool	+	+	+	+	+
GCF_002220985.3	MAVP-R	USA	SAMN06042545	Stool	+	+	–	+	+
GCF_009763565.1	2013 V-1181	USA	SAMN12648285	Stool	+	+	+	+	+
GCF_000568495.1	UCM-V493	Unknown	SAMN03081521	Unknown	+	–	–	+	+
GCF_003612715.1	FORC_071	South Korea: Seoul	SAMN07629009	Unknown	+	–	–	+	+
GCF_012274865.1	AM51557	USA	SAMN12648303	Unknown	+	–	+	+	+
GCF_003612695.1	FORC_072	South Korea: Seoul	SAMN07629020	Unknown	+	–	–	+	+
GCF_009764055.1	2012AW-0224	USA	SAMN12648278	Unknown	+	–	–	+	+
PFR30G02	PFR21C03	New Zealand	–	Seafood: oyster	+	–	–	+	+
PFR30J09	PFR30J09	New Zealand	–	Seafood: oyster	+	–	–	+	+
PFR34B02	PFR34B02	New Zealand	–	Seafood: oyster	+	–	–	+	+
PFR37C06	PFR37D08	New Zealand	–	Human	+	–	–	+	+

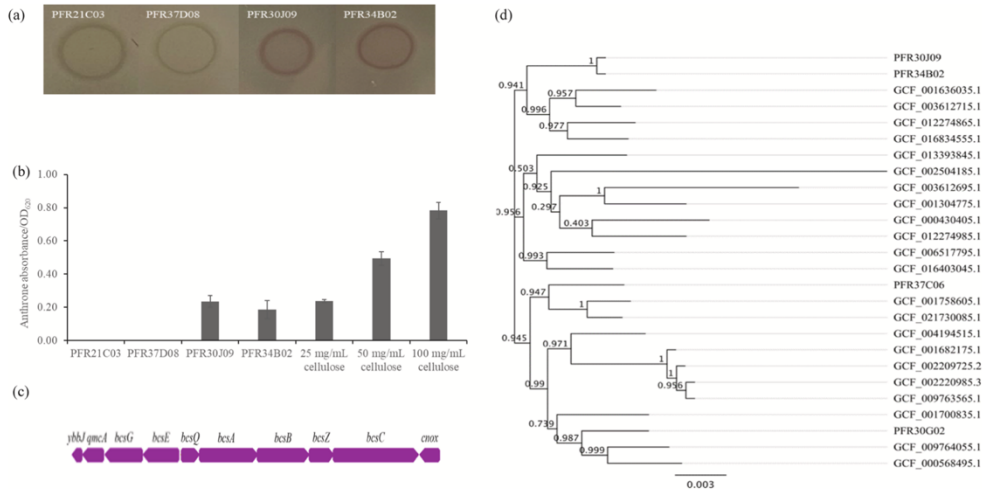

Fig. 3. Cellulose production at the phenotypic and genomic level in *V. parahaemolyticus*. (a) Colony morphotypes on CRI agar plates indicating cellulose/curli production. (b) Anthrone absorbance assay to determine cellulose production in *V. parahaemolyticus*, crystalline cellulose (CC) chemical was assayed as the control. (c) Diagram of cellulose synthase operon in *V. parahaemolyticus*, consisting of *bcsG*, *bcsE*, *bcsQ*, *bcsA*, *bcsB*, *bcsZ*, and *bcsC*. (d) Evolutionary relationships between cellulose synthase operons in *V. parahaemolyticus*. The phylogenetic tree was inferred using the Neighbor-joining method and FastTree.

more putative horizontal gene transfer events than the weak biofilm forming strains. This may relate to better adaption to diverse environments through biofilm formation. The phylum of *Proteobacteria* (taxid: 1224) and *Gammaproteobacteria* (taxid: 1236) were suggested to be the main donor taxa, providing 39.5 ± 3.54 and 51 ± 21.21, 52.5 ± 0.71 and 60 ± 9.90 HGT genes among weak and strong biofilm forming strains, respectively. This observation is not surprising as the aquatic environments are preferred by *Proteobacteria* and *Gammaproteobacteria*, providing many opportunities for recombination (Koblížek, 2015). The unique gene clusters of rhamnose metabolism and the CRISPR-Cas system present in strong biofilm forming strains appear to be obtained by HGT events resulting in the increased gene diversity in these strains.

Although these strategies were absent in weak biofilm-forming strains of *V. parahaemolyticus*, they are identified not only in strong biofilm-forming strains but also in part of the intermediate biofilm former (Data not shown). Interestingly, the cellulose synthase operon was not included in the putative HGT event results, indicating that the cellulose synthase function present in *V. parahaemolyticus* came from within the *Vibrionales* order. In our study, the *bcs* gene cluster was only present in environmental isolates, and whether cellulose only exists in environmental strains globally requires further study.

3.7. Prevalence of the cellulose synthase operon in V. Parahaemolyticus genomes

The cellulose synthase operon (*bsc*) was present in 22 out of 138 *V. parahaemolyticus* reference genomes from the NCBI dataset. The cellulose synthase operons of 22 *V. parahaemolyticus* genomes were aligned with one another, revealing a cellulose synthase operon conservatism. Fig. 3c is a diagram of the *bcs* locus and the transcription direction of cellulose synthase genes. The cellulose biosynthetic cluster was inserted on chromosome 1 between the *ybbJ* and *cnoX* genes, except for strain *V. parahaemolyticus* HA2 accommodating another two genes of the helix-turn-helix (HTH) domain containing gene and the IS630 family gene (RefGenome: GCF_002504185.1).

The cellulose biosynthesis locus was initially assumed to be absent from other *Vibrio* species (Yildiz & Visick, 2009). Although the genomic analysis indicated that the cellulose synthase genes were highly conserved in *V. parahaemolyticus*, the evolutionary analysis demonstrated that these genes were not 100 % identical, suggesting that the *bcs* operon might be useful in distinguishing *V. parahaemolyticus* isolates. Interestingly here, the strong biofilm forming strains of PFR30J09 and PFR34B02 were clustered into a subgroup based on the cellulose operon (Fig. 3d). We also examined whether the *bcs* gene cluster was restricted to environmental isolates in the reference genomes. The results indicated that cellulose synthase operons were present in both environmental (73.0 %, 19/26) and pathogenic (26.92 %, 7/26) strains.

The *bcs* operon responsible for cellulose production has been proposed as useful in the classification and standardized nomenclature in *Proteobacteria* (Römling & Galperin, 2015). The distinctions of the *bcs* gene profiles from *Proteobacteria* are primarily from three areas: 1) the presence of the *bcsD* gene, 2) the presence of the *bcsE* and *bcsG* genes (and the absence of *bcsD*) and 3) the absence of *bcsD*, *bcsE*, or *bcsG* (Abidi et al., 2021; Römling & Galperin, 2015). The putative operon identified in *V. parahaemolyticus* has an organization similar to *E. coli*-like -*bcs* operons, that have been found in *E. coli*, *Salmonella*, *Yersinia enterocolitica*, *V. fischeri* and *Pseudomonas*. Cellulose is considered as one of the major causes of robust biofilm and strong resistance in *Salmonella*, *Cronobacter* and *E. coli* in the food industry (Hu et al., 2015; Kim, Jyung, & Kang, 2022; Macarisin, Patel, Bauchan, Giron, & Sharma, 2012). Cellulose plays roles as an architectural element in biofilm matrices, providing advantages in water retention, porosity, mechanical resistance, low antigenicity, and interaction with saccharidic and proteinaceous components of both bacteria and hosts. This enables higher sanitizer resistance in biofilms. Solano et al. (2002) compared the influence of 30 ppm of sodium hypochlorite on the survival of biofilms of wild-type *Salmonella* Enteritidis and cellulose mutants formed on glass. Survival of 75 % of wild-type cells following 20 min exposure to the disinfectant contrasts with only 0.3 % survival of the cellulose-deficient mutant cells surviving, which clearly indicates the protective function of cellulose.

In *E. coli*-like *bcs* operon, BcsA and BcsB have been characterized as the enzymatic core of cellulose synthase, which is crucial for *in vitro* cellulose synthesis (Omadjela et al., 2013). BcsA provides glucosyltransferase activity that is allosterically triggered by the second messenger c-di-GMP and that, in conjunction with the BcsB subunit, produces a transmembrane channel for co-synthetic secretion of cellulose (Serra & Hengge, 2019). BcsE and BcsG subunits, produce a cytosolic c-di-GMP-binding protein and a membrane-anchored periplasmic pEtN transferase, respectively, and are the distinctive components of this type of *bcs* operon. The proteins mentioned above and c-di-GMP have been considered as molecular targets to interfere cellulose biosynthesis (Abidi et al., 2021), however, more exploration is required in *V. parahaemolyticus* species. Alternative carbon sources could be considered as an approach to inhibit cellulose production in food environments. Zhong et al. (2013) reported different carbon sources resulted in different bacterial cellulose production in *Gluconacetobacter xylinus*. Highest yields of cellulose were obtained when *G. xylinus* was cultured in glucose, fructose and glycerol, whereas lowest was obtained in those using inositol, sucrose and lactose as the medium. Carbon sources influence mechanical and microstructural characteristics of cellulose, as glycerol contributed to the highest cellulose yield in *G. xylinus*, as well as highest tensile strength of cellulose with thinner fibres and lower porosity.

A previous study identified epistatic interaction in the flexible genome between gene clusters for T6SS1 and cellulose biosynthesis, while clinical strains tend to depend on the antibacterial activity of T6SS1 proteins for competitive survival in the aquatic milieu and the strains that lack T6SS depend on cellulose production (Cui et al., 2020). However, in our genomic analysis, cellulose production appeared to be associated with the presence of T6SS that was characterized by both VgrG and Hcp (Table 4), regardless of whether the strains were clinical or environmental. The reason for this discrepancy could be that different clonal complexes of *V. parahaemolyticus* genomes used in the present study differ from those used in the earlier study. In our study, gene co-occurrence analysis identified that there were 468 co-occurring genes along with *bcsA*, notably, the CRISPR-Cas defense system (*cas*, *cys* gene families), the type II secretion system (*eps* gene family), the rhamnose metabolic process (*rha* gene family) and capsular polysaccharide synthesis (*wec* gene family). This was consistent with the results from PPI analysis for the two strong biofilm-forming *V. parahaemolyticus* (PFR30J09 and PFR34B02). Symbiosis polysaccharide protein SypF has been identified in association with cellulose biosynthesis and production in *V. fischeri* via the polysaccharide biosynthesis protein VpsR, indicating that cellulose contributes to symbiotic initiation by promoting biofilm formation on the symbiotic organ's surface (Darnell et al., 2008). Here, the interaction between the VpsR homologue CpsR and cellulose production was also identified in *V. parahaemolyticus*, reported for the first time in this study (Fig. 4). Whether cellulose is important in symbiosis in *V. parahaemolyticus* requires further investigation.

4. Conclusion and perspectives

The expansion of gene families is a common strategy whereby bacteria cope with diverse environments. In this study, strong biofilm forming strains appeared to have higher genetic diversity compared with the weak biofilm forming strains. In *V. parahaemolyticus*, the low portion of core genome size (~33.20 %) allows for more accessory genes that are critical for survival in multiple environments. We identified the phyla of *Proteobacteria* (taxid: 1224) and *Gammaproteobacteria* (taxid: 1236) act as the main donor taxa for the genetic diversity of strong biofilm forming strains. Genes that are more abundant in strong biofilm forming genomes were associated with cellulose biosynthesis, rhamnose and other sugar metabolism, O-antigen biosynthesis, MSHA pili led attachment as well as the CRISPR-Cas defence system. The genes of rhamnose metabolism and catabolismand the CRISPR-Cas defence system was most likely from HGT with cellulose biosynthesis being acquired within the order of *Vibrionales*. The PPI analysis demonstrated an interaction between rhamnose metabolism, cellulose production, and O-antigen biosynthesis. This study is limited to the contrast between high and low biofilm producers to highlight the key factors involved. This is a limitation of the study as it does not include the intermediate biofilm forming strains. Future studies will look at gene expression to provide some quantitative information that will cover the intermediate biofilm

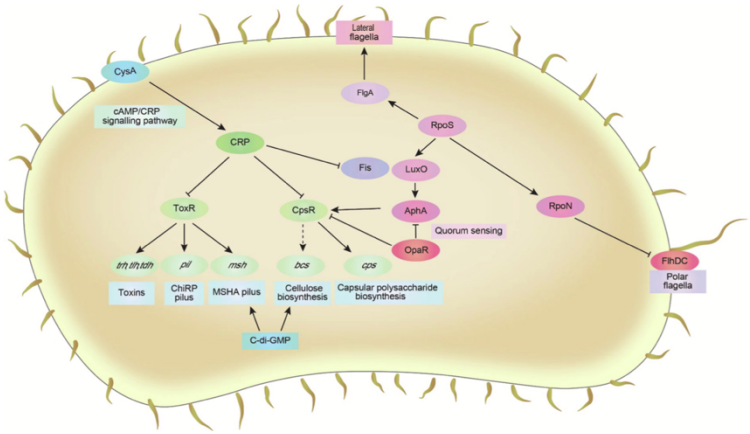

Fig. 4. Molecular mechanisms of biofilm formation in *V. parahaemolyticus*. The known molecular mechanism was based on Abidi et al., (2021) and Guo et al., (2020), presented using the solid line; the dash line represents the finding in this study.

forming strains.

We believe this study is the first to reveal the relationship between cellulose secretion and robust biofilm formation in *V. parahaemolyticus*. The cellulose synthase operons in *V. parahaemolyticus* were examined for their prevalence (22/138, 15.94 %) and were found to consist of the genes *bcsG*, *bcsE*, *bcsQ*, *bcsA*, *bcsB*, *bcsZ*, *bcsC*. The precise biochemical functions and chemical structures of the cellulose component in biofilm matrices require further identification. The chemical elements of cellulose vary slightly between species with distinct *bcs* operon structures. For example, in *E. coli*, the cellulose in the biofilm matrix has been identified as phosphoethanolamined, whereas in *Pseudomonas*, the cellulose is amorphous. The chemical structure of cellulose in *V. parahaemolyticus* and how it interacts with other biofilm matrix components is unknown. Robust biofilm formation is likely to protect the organism from sanitisers, creating higher risks of cross contamination and subsequent foodborne illness. Understanding cellulose in the biofilm matrix will help develop novel and effective biofilm control measures.

CRediT authorship contribution statement

Dan Wang: Conceptualization, Methodology, Investigation, Formal analysis, Writing – original draft. **Graham C. Fletcher:** Resources, Conceptualization, Methodology, Supervision, Writing – review & editing. **Dragana Gagic:** Conceptualization, Methodology, Supervision, Writing – review & editing. **Stephen L.W. On:** Conceptualization, Methodology, Supervision, Writing – review & editing. **Jon S. Palmer:** Conceptualization, Methodology, Supervision, Writing – review & editing. **Steve H. Flint:** Project administration, Resources, Supervision, Conceptualization, Methodology, Writing – review & editing.

Declaration of Competing Interest

The authors declare that they have no known competing financial interests or personal relationships that could have appeared to influence the work reported in this paper.

Data availability

Data will be made available on request.

Acknowledgements

Dr. Tetsuya Iida (Research Institute for Microbial Diseases, Osaka, Japan) kindly supplied the culture of genome reference strain RIMD 2210633. The authors are grateful to Jaime Martinez-Urtaza and Andy Powell of Centre for Environment, Fisheries, and Aquaculture Science (Cefas) who provided sequence data.

Funding

This study is funded by Massey University, the grant number is P963141222WangD.

Appendix A. Supplementary material

Supplementary data to this article can be found online at https://doi.org/10.1016/j.foodres.2023.112605.

References

Abidi, W., Torres-Sánchez, L., Siroy, A., & Krasteva, P. V. (2021). Weaving of bacterial cellulose by the Bcs secretion systems. *FEMS Microbiology Reviews, 46*(2). https://doi.org/10.1093/femsre/fuab051

Anriany, Y., Sahu, S. N., Wessels, K. R., McCann, L. M., & Joseph, S. W. (2006). Alteration of the rugose phenotype in *waaG* and *ddhC* mutants of *Salmonella enterica* serovar Typhimurium DT104 is associated with inverse production of curli and cellulose. *Applied and Environmental Microbiology, 72*(7), 5002–5012.

Arrebola, E., Carrión, V. J., Gutiérrez-Barranquero, J. A., Pérez-García, A., Rodríguez-Palenzuela, P., Cazorla, F. M., & de Vicente, A. (2015). Cellulose production in *Pseudomonas syringae* pv. *syringae*: A compromise between epiphytic and pathogenic lifestyles. *FEMS Microbiology Ecology, 91*(7). https://doi.org/10.1093/femsec/fiv071

Bankevich, A., Nurk, S., Antipov, D., Gurevich, A. A., Dvorkin, M., Kulikov, A. S., … Prjibelski, A. D. (2012). SPAdes: A new genome assembly algorithm and its applications to single-cell sequencing. *Journal of Computational Biology, 19*(5), 455–477.

Broughton, W., Hanin, M., Relic, B., Kopcińska, J., Golinowski, W., Simsek, S., … Kobayashi, H. (2006). Flavonoid-inducible modifications to rhamnan O antigens are necessary for *Rhizobium sp.* strain NGR234-legume symbioses. *Journal of Bacteriology, 188*(10), 3654–3663.

Buchfink, B., Reuter, K., & Drost, H. G. (2021). Sensitive protein alignments at tree-of-life scale using DIAMOND. *Nature Methods, 18*(4), 366–368. https://doi.org/10.1038/s41592-021-01101-x

Chen, T.-Y., Kuo, S.-H., Chen, S.-T., & Hwang, D.-F. (2016). Differential proteomics to explore the inhibitory effects of acidic, slightly acidic electrolysed water and sodium hypochlorite solution on *Vibrio parahaemolyticus*. *Food Chemistry, 194*, 529–537. https://doi.org/10.1016/j.foodchem.2015.08.019

Chen, Y., Dai, J., Morris, J. G., & Johnson, J. A. (2010). Genetic analysis of the capsule polysaccharide (K antigen) and exopolysaccharide genes in pandemic *Vibrio*

parahaemolyticus O3:K6. *BMC Microbiology, 10*(1), 274. https://doi.org/10.1186/1471-2180-10-274
Cui, Y., Yang, C., Qiu, H., Wang, H., Yang, R., & Falush, D. (2020). The landscape of coadaptation in *Vibrio parahaemolyticus*. *Elife, 9*, e54136.
Darnell, C. L., Hussa, E. A., & Visick, K. L. (2008). The putative hybrid sensor kinase SypF coordinates biofilm formation in *Vibrio fischeri* by acting upstream of two response regulators, SypG and VpsR. *Journal of Bacteriology, 190*(14), 4941–4950.
Eren, A. M., Esen, Ö. C., Quince, C., Vineis, J. H., Morrison, H. G., Sogin, M. L., & Delmont, T. O. (2015). Anvi'o: An advanced analysis and visualization platform for 'omics data. *PeerJ, 3*, e1319.
Fang, Y., Visvalingam, J., Zhang, P., & Yang, X. (2022). Biofilm formation by Non-O157 Shiga toxin-producing *Escherichia coli* in monocultures and co-cultures with meat processing surface bacteria. *Food Microbiology, 102*, Article 103902. https://doi.org/10.1016/j.fm.2021.103902
FAO. (2021). Advances in science and risk assessment tools for *Vibrio parahaemolyticus* and *V. vulnificus* associated with seafood: meeting report (9240024875). Retrieved from https://www.who.int/publications/i/item/9789240024878. Accessed October 6, 2022.
Güvener, Z. T., & McCarter, L. L. (2003). Multiple regulators control capsular polysaccharide production in *Vibrio parahaemolyticus*. *Journal of Bacteriology, 185*(18), 5431–5441.
Guo, L., Wang, J., Gou, Y., Tan, L., Liu, H., Pan, Y., & Zhao, Y. (2020). Comparative proteomics reveals stress responses of *Vibrio parahaemolyticus* biofilm on different surfaces: Internal adaptation and external adjustment. *Science of The Total Environment, 731*, Article 138386. https://doi.org/10.1016/j.scitotenv.2020.138386
Gurevich, A., Saveliev, V., Vyahhi, N., & Tesler, G. (2013). QUAST: Quality assessment tool for genome assemblies. *Bioinformatics, 29*(8), 1072–1075.
Heredia-Ponce, Z., Gutiérrez-Barranquero, J. A., Purtschert-Montenegro, G., Eberl, L., Cazorla, F. M., & de Vicente, A. (2020). Biological role of EPS from *Pseudomonas syringae* pv. *syringae* UMAF0158 extracellular matrix, focusing on a Psl-like polysaccharide. *npj Biofilms and Microbiomes, 6*(1), 1–13.
Hu, L., Grim, C. J., Franco, A. A., Jarvis, K. G., Sathyamoorthy, V., Kothary, M. H., … Tall, B. D. (2015). Analysis of the cellulose synthase operon genes, *bcsA*, *bcsB*, and *bcsC* in *Cronobacter* species: Prevalence among species and their roles in biofilm formation and cell–cell aggregation. *Food Microbiology, 52*, 97–105. https://doi.org/10.1016/j.fm.2015.07.007
Jain, C., Rodriguez-R, L. M., Phillippy, A. M., Konstantinidis, K. T., & Aluru, S. (2018). High throughput ANI analysis of 90K prokaryotic genomes reveals clear species boundaries. *Nature Communications, 9*(1), 1–8.
Kim, S. H., Jyung, S., & Kang, D. H. (2022). Comparative study of *Salmonella* Typhimurium biofilms and their resistance depending on cellulose secretion and maturation temperatures. *LWT, 154*, Article 112700. https://doi.org/10.1016/j.lwt.2021.112700
Kim, Y. K., & McCarter, L. L. (2000). Analysis of the polar flagellar gene system of *Vibrio parahaemolyticus*. *Journal of Bacteriology, 182*(13), 3693–3704.
Koblížek, M. (2015). Ecology of aerobic anoxygenic phototrophs in aquatic environments. *FEMS Microbiology Reviews, 39*(6), 854–870.
Lei, T., Jiang, F., He, M., Zhang, J., Zeng, H., Chen, M., … Wu, Q. (2020). Prevalence, virulence, antimicrobial resistance, and molecular characterization of fluoroquinolone resistance of *Vibrio parahaemolyticus* from different types of food samples in China. *International Journal of Food Microbiology, 317*, Article 108461. https://doi.org/10.1016/j.ijfoodmicro.2019.108461
Lerouge, I., & Vanderleyden, J. (2002). O-antigen structural variation: Mechanisms and possible roles in animal/plant–microbe interactions. *FEMS microbiology reviews, 26*(1), 17–47.
Lianou, A., Nychas, G. J. E., & Koutsoumanis, K. P. (2020). Strain variability in biofilm formation: A food safety and quality perspective. *Food Research International, 137*, Article 109424. https://doi.org/10.1016/j.foodres.2020.109424
Macarisin, D., Patel, J., Bauchan, G., Giron, J. A., & Sharma, V. K. (2012). Role of curli and cellulose expression in adherence of *Escherichia coli* O157: H7 to spinach leaves. *Foodborne pathogens and disease, 9*(2), 160–167. https://doi.org/10.1089/fpd.2011.1020
Makarova, K. S., Haft, D. H., Barrangou, R., Brouns, S. J. J., Charpentier, E., Horvath, P., … Koonin, E. V. (2011). Evolution and classification of the CRISPR–Cas systems. *Nature Reviews Microbiology, 9*(6), 467–477. https://doi.org/10.1038/nrmicro2577
Martinez-Urtaza, J., Bowers, J. C., Trinanes, J., & DePaola, A. (2010). Climate anomalies and the increasing risk of *Vibrio parahaemolyticus* and *Vibrio vulnificus* illnesses. *Food Research International, 43*(7), 1780–1790. https://doi.org/10.1016/j.foodres.2010.04.001
Maturana, J. L., & Cárdenas, J. P. (2021). Insights on the evolutionary genomics of the *Blautia* Genus: Potential new species and genetic content among lineages. *Frontiers in Microbiology, 12*. https://doi.org/10.3389/fmicb.2021.660920
McCarter, L. L. (2001). Polar flagellar motility of the *Vibrionaceae*. *Microbiology and Molecular Biology Reviews, 65*(3), 445–462.
Meparambu Prabhakaran, D., Patel, H. R., Chandrika, S. K., & S., & Thomas, S.. (2022). Genomic attributes differ between *Vibrio parahaemolyticus* environmental and clinical isolates including pathotypes. *Environmental Microbiology Reports, 14*(3), 365–375. https://doi.org/10.1111/1758-2229.13000
Michael, V., Frank, O., Bartling, P., Scheuner, C., Göker, M., Brinkmann, H., & Petersen, J. (2016). Biofilm plasmids with a rhamnose operon are widely distributed determinants of the 'swim-or-stick' lifestyle in roseobacters. *The ISME Journal, 10*(10), 2498–2513. https://doi.org/10.1038/ismej.2016.30
Omadjela, O., Narahari, A., Strumillo, J., Mélida, H., Mazur, O., Bulone, V., & Zimmer, J. (2013). BcsA and BcsB form the catalytically active core of bacterial cellulose synthase sufficient for *in vitro* cellulose synthesis. *Proceedings of the National Academy of Sciences, 110*(44), 17856–17861.
Moorthy, S., & Watnick, P. I. (2004). Genetic evidence that the *Vibrio cholerae* monolayer is a distinct stage in biofilm development. *Molecular Microbiology, 52*, 573–587.
Page, A. J., Cummins, C. A., Hunt, M., Wong, V. K., Reuter, S., Holden, M. T., … Parkhill, J. (2015). Roary: Rapid large-scale prokaryote pan genome analysis. *Bioinformatics, 31*(22), 3691–3693.
Pang, Y., Guo, X., Tian, X., Liu, F., Wang, L., Wu, J., … Liu, B. (2019). Developing a novel molecular serotyping system based on capsular polysaccharide synthesis gene clusters of *Vibrio parahaemolyticus*. *International Journal of Food Microbiology, 309*, Article 108332.
Parks, D. H., Imelfort, M., Skennerton, C. T., Hugenholtz, P., & Tyson, G. W. (2015). CheckM: Assessing the quality of microbial genomes recovered from isolates, single cells, and metagenomes. *Genome Research, 25*(7), 1043–1055.
Pritchard, L., Glover, R. H., Humphris, S., Elphinstone, J. G., & Toth, I. K. (2016). Genomics and taxonomy in diagnostics for food security: Soft-rotting enterobacterial plant pathogens. *Analytical Methods, 8*(1), 12–24. https://doi.org/10.1039/C5AY02550H
Qin, X., Wang, H., Miao, C., Yang, X., Zhang, Y., Feng, J., … Jiang, Y. (2021). Comparative genomics reveals environmental adaptation differences between *Cronobacter* species. *Food Research International, 147*, Article 110541. https://doi.org/10.1016/j.foodres.2021.110541
Regmi, A., & Boyd, E. F. (2019). Carbohydrate metabolic systems present on genomic islands are lost and gained in *Vibrio parahaemolyticus*. *BMC Microbiology, 19*(1), 112. https://doi.org/10.1186/s12866-019-1487-6
Römling, U., & Galperin, M. Y. (2015). Bacterial cellulose biosynthesis: Diversity of operons, subunits, products, and functions. *Trends in Microbiology, 23*(9), 545–557.
Roy, P. K., Mizan, M. F. R., Hossain, M. I., Han, N., Nahar, S., Ashrafudoulla, M., … Ha, S. D. (2021). Elimination of *Vibrio parahaemolyticus* biofilms on crab and shrimp surfaces using ultraviolet C irradiation coupled with sodium hypochlorite and slightly acidic electrolyzed water. *Food Control, 128*, Article 108179. https://doi.org/10.1016/j.foodcont.2021.108179
Seemann, T. (2014). Prokka: Rapid prokaryotic genome annotation. *Bioinformatics, 30*(14), 2068–2069.
Serra, D. O., & Hengge, R. (2019). Cellulose in Bacterial Biofilms. In E. Cohen, & H. Merzendorfer (Eds.), *Extracellular Sugar-Based Biopolymers Matrices* (pp. 355–392). Springer International Publishing. https://doi.org/10.1007/978-3-030-12919-4_8.
Shime-Hattori, A., Iida, T., Arita, M., Park, K. S., Kodama, T., & Honda, T. (2006). Two type IV pili of *Vibrio parahaemolyticus* play different roles in biofilm formation. *FEMS microbiology letters, 264*(1), 89–97.
Simões, M., Simões, L. C., & Vieira, M. J. (2010). A review of current and emergent biofilm control strategies. *LWT, 43*(4), 573–583. https://doi.org/10.1016/j.lwt.2009.12.008
Solano, C., García, B., Valle, J., Berasain, C., Ghigo, J. M., Gamazo, C., & Lasa, I. (2002). Genetic analysis of *Salmonella enteritidis* biofilm formation: Critical role of cellulose. *Molecular Microbiology, 43*(3), 793–808.
Stalder, T., & Top, E. (2016). Plasmid transfer in biofilms: A perspective on limitations and opportunities. *npj Biofilms and Microbiomes, 2*(1), 16022. https://doi.org/10.1038/npjbiofilms.2016.22
Valla, S., Coucheron, D. H., Fjærvik, E., Kjosbakken, J., Weinhouse, H., Ross, P., … Benziman, M. (1989). Cloning of a gene involved in cellulose biosynthesis in *Acetobacter xylinum*: Complementation of cellulose-negative mutants by the UDPG pyrophosphorylase structural gene. *Molecular and General Genetics MGG, 217*, 26–30.
Verstraeten, N., Braeken, K., Debkumari, B., Fauvart, M., Fransaer, J., Vermant, J., & Michiels, J. (2008). Living on a surface: Swarming and biofilm formation. *Trends in Microbiology, 16*(10), 496–506. https://doi.org/10.1016/j.tim.2008.07.004
Wang, D., Fletcher, G. C., On, S. L. W., Palmer, J. S., Gagic, D., & Flint, S. H. (2023). Biofilm formation, sodium hypochlorite susceptibility and genetic diversity of *Vibrio parahaemolyticus*. *International Journal of Food Microbiology, 385*, Article 110011. https://doi.org/10.1016/j.ijfoodmicro.2022.110011
Wang, D., Flint, S. H., Gagic, D., Palmer, J. S., Fletcher, G. C., & On, S. L. W. (2021). *In silico* analysis revealing CsrA roles in motility-sessility switching and tuning VBNC cells in *Vibrio parahaemolyticus*. *Biofouling, 37*(6), 680–688. https://doi.org/10.1080/08927014.2021.1955357
Wang, D., Flint, S. H., Palmer, J. S., Gagic, D., Fletcher, G. C., & On, S. L. W. (2022). Global expansion of *Vibrio parahaemolyticus* threatens the seafood industry: Perspective on controlling its biofilm formation. *LWT, 158*, Article 113182. https://doi.org/10.1016/j.lwt.2022.113182
Yang, Z., Wafula, E. K., Kim, G., Shahid, S., McNeal, J. R., Ralph, P. E., … dePamphilis, C. W. (2019). Convergent horizontal gene transfer and cross-talk of mobile nucleic acids in parasitic plants. *Nature Plants, 5*(9), 991–1001. https://doi.org/10.1038/s41477-019-0458-0
Yildiz, F. H., & Visick, K. L. (2009). *Vibrio* biofilms: So much the same yet so different. *Trends in Microbiology, 17*(3), 109–118. https://doi.org/10.1016/j.tim.2008.12.004
Zerbino, D. R., & Birney, E. (2008). Velvet: Algorithms for de novo short read assembly using de Bruijn graphs. *Genome Research, 18*(5), 821–829.
Zhong, C., Zhang, G.-C., Liu, M., Zheng, X.-T., Han, P.-P., & Jia, S.-R. (2013). Metabolic flux analysis of *Gluconacetobacter xylinus* for bacterial cellulose production. *Applied Microbiology and Biotechnology, 97*(14), 6189–6199. https://doi.org/10.1007/s00253-013-4908-8
Zhu, Q., Kosoy, M., & Dittmar, K. (2014). HGTector: An automated method facilitating genome-wide discovery of putative horizontal gene transfers. *BMC Genomics, 15*(1), 1–18.